DEVELOPMENT AND CHARACTERISATION OF ELECTROPOLYMERISED POLYPYRROLE AND POLYPYRROLE-REDUCED GRAPHENE OXIDE COMPOSITE FILMS AS A POTENTIAL TREATMENT METHOD FOR AZO DYES

By
Md Mominul Haque

Master of Philosophy in Chemistry, Bangladesh University of Engineering and Technology, Dhaka, Bangladesh

A thesis submitted as a partial fulfilment for the degree of

Doctor of Philosophy

MACQUARIE University

Department of Chemistry and Biomolecular Sciences
Faculty of Science and Engineering
Macquarie University
Sydney, Australia

November 2015

ABSTRACT

In this thesis, we report the development and application of conducting polypyrrole films as a potential green technology for electrochemical treatment of the model azo dye, Acid Red 1. Synthetic dyes, for example azo dyes, are extensively used as colouring agents in various industries including textile, paper, printing, and pharmaceutical industries. As a result, discharge of dye-containing industrial effluents into the aquatic ecosystems will generate undesirable colours in the water, reducing sunlight and oxygen penetration, and resisting photochemical and biological attack. In some cases, their degradation products can also be toxic, carcinogenic or even mutagenic. In addition, the majority of these dyes are chemically stable and resistant to microbiological attack that often exhibits a low degradation efficiency due to their complex structure. Therefore, discharge of dye-containing effluent in the hydrosphere without proper treatment is a major environmental concern.

Several treatment methods for azo dyes have hitherto been reported. However, there are severe limitations associated with these methods. Notably, many treatment methods often produce toxic by-products and hazardous residues during operation. Therefore, there is a need for developing alternative treatments that are effective and environmentally friendly in removing dyes from textile effluents. Electropolymerised conducting polypyrrole films have been chosen to avoid such a problem in this study. The synthesis of polypyrrole usually involves electrochemical oxidation of its monomer, pyrrole, to yield a polymeric chain with a positive backbone. In order to neutralise this charge, a counter anion, for example that of Acid Red 1, is entrapped in the backbone structure. Many studies have shown that this entrapment process is electrochemically reversible, enabling polypyrrole to act as an anion exchanger, depending upon the mobility of the entrapped counter anion. This has then been exploited as the basis for developing an eco-friendly treatment for dye in textile effluents. The azo dye, Acid Red 1, was used as a model dye in this study.

This thesis will begin with Chapter 1 presenting a brief introduction of different dyes, risks associated with dye effluents and their degradation products in the environment, conventional dye effluent treatment techniques and limitations. This section will also cover the fundamental chemistry of such conducting polymers as polyaniline and polypyrrole and justification for their

applications to dye removal from dye containing effluents. The scope of this study will also be outlined in Chapter 1.

Chapter 2 will provide details of experimental techniques used in this research. Here, we will describe the synthesis and characterisation techniques of polypyrrole films, and method for the evaluation of Acid Red 1 entrapment-liberation in polypyrrole films. This chapter will also describe the methods used for experimental data analysis.

In Chapter 3, we report the optimised synthesis parameters of polypyrrole-Acid Red 1 films and characterisation of polypyrrole films. Polypyrrole films were synthesised by anodically polymerising pyrrole in the presence of Acid Red 1 as a supporting electrolyte. These Acid Red 1-entrapped polypyrrole films were characterised by electrochemistry, scanning electron microscopy, Fourier transform infrared spectroscopy and X-ray diffraction analysis. Based on a two-level factorial design, we have identified the solution pH, the Acid Red 1 concentration and the polymerisation duration as the significant experimental parameters affecting the entrapment efficiency. The entrapment process will potentially aid in decolourising an Acid Red 1-containing solution. Similarly, in a cathodic process, electrons are supplied to neutralise the polypyrrole backbone, liberating Acid Red 1 into the solution. This allows the recovery of Acid Red 1 for recycling purposes.

In Chapter 4, we focus on the kinetic models, isotherms and thermodynamics of the electrochemical entrapment of Acid Red 1, at conducting polypyrrole films. The Acid Red 1 entrapment kinetic data were found to follow a pseudosecond order model involving an intra-particle diffusion. However, the equilibrium data obtained for Acid Red 1 entrapment in polypyrrole film failed to obey any common adsorption models such as the Langmuir and Freundlich isotherms. Therefore, enhanced quantity of dye may then be achievable by entrapment, making it a more effective and efficient technique than those involving only adsorption. Similarly, dye leakage from polypyrrole film surface to a sample matrix will be easily prevented. Thermodynamically, a negative standard Gibbs free energy of entrapment range between -1.46±0.78 and -2.94±0.24 kJ mol^{-1} at the corresponding temperature range of 298 K – 318 K, and a standard enthalpy change of 20.5±2.5 kJ mol^{-1} indicate a spontaneous and endothermic entrapment process. Also, a positive entropy change (73.6±8.2 J mol^{-1} K^{-1}) reveals increased randomness of the interface and an affinity of Acid Red 1 towards polypyrrole films.

A low activation energy (7.67±0.80 kJ mol^{-1}) confirms a physical process for Acid Red 1 entrapment in polypyrrole films.

Unfortunately, problems were uncounted when the same polypyrrole films were used in repeated entrapment-liberation process of Acid Red 1 due to their poor stability during cycling. This is because of swelling and shrinkage of polypyrrole films that take place during the entrapment-liberation process of Acid Red 1. This leads to mechanical degradation of the polypyrrole films and weakening of their electrochemical performance. To minimise this effect, polypyrrole-reduced graphene oxide composite films were considered. Accordingly, Chapter 5 is devoted to synthesis, characterisation and evaluation of Acid Red 1 entrapment and liberation at mechanically stable polypyrrole-reduced graphene oxide composite films. Initially, we anodically synthesised polypyrrole-graphene oxide films by *in situ* electropolymerisation of pyrrole and graphene oxide. Next, a reduction potential was applied to obtain a polypyrrole-reduced graphene oxide film from a polypyrrole-graphene oxide composite film. The synthesised composite films were then characterised by Fourier transform infrared spectroscopy, X-ray photoelectron spectroscopy, surface analysis, thermogravimetric analysis and scanning electron microscopy. Brunauer, Emmett and Teller surface area analysis showed a 7.4-fold increase in surface area of a polypyrrole-reduced-graphene oxide film compared to that of a polypyrrole film. Also, mechanical testing results revealed that the tensile strength of polypyrrole-reduced graphene oxide films was enhanced by 12.7 folds compared to that of polypyrrole films. We evaluated the entrapment-liberation efficiency of Acid Red 1 entrapped polypyrrole composite films and estimated a 95 % entrapment of Acid Red 1 in polypyrrole-reduced graphene oxide films, which is significantly higher than 58% in polypyrrole films. Similarly, a 73% liberation efficiency at polypyrrole-reduced graphene oxide composite films was found to be higher than 36% at polypyrrole films. Finally, a preliminary study of Acid Red 1 entrapment in polypyrrole-reduced graphene oxide films in the presence of Indigo Carmine was also investigated to evaluate the selectivity towards Acid Red 1 of polypyrrole-reduced graphene oxide film. We observed that electropolymerised polypyrrole-reduced graphene oxide film showed excellent memory effect for selective entrapment of Acid Red 1.

Finally, in Chapter 6, some concluding remarks on the development and applicability of polypyrrole and polypyrrole-reduced graphene oxide composite films to electrochemical

entrapment and liberation of Acid Red 1 will be presented. To this end, limitations of this treatment will also discussed. Further, several suggestions will be proposed as feasible future work for this project.

ACKNOWLEDGEMENTS

Firstly, I wish to express my sincere gratitude to my supervisor, Dr Danny Wong, who has been a tremendous mentor for me. I would like to thank you for his enthusiastic supervision, encouragement and help during my research and for allowing me to grow as a research scientist. His advice on both research as well as on my career have been priceless. I would also like to thank my associate supervisor, Dr Christopher McRae, for his valuable guidance and help throughout the years. Special mention goes to my fellow members of the Electroanalytical Chemistry Research Group, Thomas Somerville, Shajahan Siraj and Benjamin Pendelton for their help in the early days and throughout my candidature. I would like to thank the chemistry laboratory technicians and administrative staff for their kind help during my study. I would especially like to thank Nicole Vella (Microscopy Unit), Dr Nicholas Tse (Department of Engineering) and Russell Field (Department of Environment and Geography) for their kind help during my research.

To all colleagues who assisted with this project including Wendy Loa-Kum-Cheung, Nirmal Chaudhary, Ketan Ahire, Kavita Ragini and Shalini Tirunagari, thank you for being there when I needed an alternative perspective, or equipment access, and for availing your time as and when required.

To the most important people in my life, my loving wife, Zakia Sultana, and my parents, who made the biggest sacrifices. This research could only be completed with your support foremost. You have endured the most but were always there for me. No measure of success can repay the toll it took on all of us.

I gratefully acknowledge the assistance of a scholarship from iMQRES during this work. Finally, I would like to thank my friends and family for their unconditional support and encouragement.

This thesis is dedicated my beloved parents, truly the most intelligent person I ever know.

DECLARATION

I hereby declared that this thesis represents my own work and efforts in its entirety, and has not been submitted for a higher degree or otherwise at any other university, or institution.

Haque

02 November, 2015

Md Mominul Haque | Date

LIST OF PUBLICATIONS

Refereed journal articles

1. **M. M. Haque**, W. T. Smith and D. K. Y. Wong, "Conducting Polyprrole Films as a Potential Tool for Electrochemical Treatment of Azo Dyes in Textile Wastewaters", Journal of Hazardous Materials, Vol. 283, pp. 164-170, 2015. **(Impact Factor 5.123)**
2. **M. M. Haque** and D. K. Y. Wong, "Kinetic Model and Thermodynamic Study of Acid Red 1 Entrapment at Electropolymerised Polypyrrole Films", Journal of Colloid and Interface Science (Accepted). **(Impact Factor 3.583)**
3. **M. M. Haque** and D. K. Y. Wong, "Evaluation of Acid Red 1 Removal Performance by Electrochemically Synthesised Polypyrrole-Reduced Graphene Oxide Composite Film", (Under preparation for ACS Nano).

Conference presentations

1. **M. M. Haque** and Danny K. Y. Wong, "Characteristics of a Dye-Entrapped Polypyrrole Film Prepared in the Presence of a Different Dye", ICMSE 2015: XIII International Conference on Materials Science and Engineering, 2015, pp. 1161, Paris, France (2015, January 23-24).
2. **M. M. Haque** and Danny K. Y. Wong, "Entrapment Behaviour of Acid Red 1 in The Presence of Indigo Carmine at Electropolymerised Polypyrrole Films", 22nd Annual RACI Research and Development Conference, 2014, pp.370, Adelaide, Australia (2014, December 13-15).
3. **M. M. Haque** and Danny K. Y. Wong, "Entrapment-liberation Behaviour of Two Azo Dyes at Conducting Polypyrrole Films", RACI National Congress 2014, pp. 95, Adelaide, Australia, (2014, December 7-12).
4. **M. M. Haque** and Danny K. Y. Wong, "Electrochemical Characteristics of Acid Red 1 at. A polypyrrole film", 21st Annual RACI Research and Development Conference 2013, pp. 84, Canberra, Australia (2013, December 11-13).

5. **M. M. Haque**, W. T. Smith and Danny K. Y. Wong, "Characterisation of Acid Red 1-Entrapped Polypyrrole Films", ISE Satellite Student Regional Symposium, "The Future of Australian and New Zealand Electrochemistry" and 19th Australia and New Zealand Electrochemistry Symposium 2013, pp.43, Melbourne, Australia (2013, November 25-26).
6. **M. M. Haque**, W. T. Smith and Danny K. Y. Wong, "Electrochemical Treatment of Acid Red 1 using Conducting Polypyrrole", What's New in Laboratory Technology 2013, pp. 14, Sydney, Australia (2013, July 16-17).

TABLE OF CONTENT

CHAPTER 1

GENERAL INTRODUCTION

1.1 Background

A dye or dyestuff is a coloured compound that can be applied on a substrate. Dyes can be obtained from natural sources or can be synthesised in a laboratory. Synthetic dyes are extensively used as colouring agents over the last few decades in various industries including textile, leather tanning, pulp and paper, paint, printing, cosmetics, pharmaceuticals, plastic and food industries. Dyes are also used as inks, photographic dyes, as indicators, biomedical applications, biological strainer, body arts, gasoline, etc. All these have led to the discharge of dye-containing industrial effluents into the soil and aquatic ecosystems. Their presence in the hydrosphere is of a major environmental concern due to both their visibility even at very low concentrations (<1 mg L^{-1}) [1, 2], giving undesirable colours to the water, reducing sunlight and oxygen penetration, and resisting photochemical and biological attack. In the worst scenario, their degradation products can be toxic, carcinogenic or even mutagenic [3, 4]. Synthetic dyes usually have a complex aromatic molecular structure that possibly comes from coaltar-based hydrocarbons such as benzene, naphthalene, anthracene, toluene and xylene, making them more stable and more difficult to biodegrade [5].

Over 100,000 commercially available dyes exist and more than 700,000 tonnes are produced annually [1, 6]. It is predicted that 1-2% of dyes in production and 1-10% in use (during the colouration process) are subsequently lost [7]. The main reason for dye loss during use is the incomplete exhaustion of dyes onto the substrates. For some dyes, this figure can be approximately 10-20% due to low fixation [8]. The exact data on the quantity of dyes discharged in the environment are not available. However, it is estimated that 2% of dyes that are produced are discharged directly as aqueous effluent [1, 6].

Due to large-scale production, extensive application, their good solubility, and such appealing properties as the ability to make a wide range of brilliant shades, synthetic dyes are common

water pollutants present in trace quantities in industrial wastewater. Nevertheless, they are known to cause considerable environmental pollution and contribute to serious health-risk factors [9].

Coloured wastewater is a consequence of batch processes both in the dye manufacturing industries and in the dye-consuming industries. Many industries, such as dyestuffs, textile, paper and plastics, use dyes in order to colour their products, consume substantial volumes of water and chemicals for wet-processing of their products. In the dyeing of textile materials, water is used firstly in the form of steam to heat the treatment baths, and secondly to enable the transfer of dyes to the fibres. At the end of the dyeing process, the various treatment baths are drained out, including the first dye bath, which has a very high salt concentration ($\geq$ 60 g L^{-1}), is heavily coloured and contains a substantial load of organic substances [10]. As a result, they generate a considerable amount of coloured wastewater during the dyeing and finishing processes. Cotton, which is the most widely used fibre in the world, is also the substrate that requires a huge quantity of water in its dying process. The dyeing and rinsing of 1 kg of cotton with reactive dyes demands from 70 to 150 L water, 0.6 to 0.8 kg NaCl and anywhere from 30 to 60 g dyestuff [10]. The wastewater produced by dyeing generally contains [10, 11] (i) hydrolysed dyes not fixed on the substrate, representing 20-30% of the dyes applied (on average 2 g L^{-1}) (this residual amount is responsible for the colouration of the effluents and cannot be recycled); (ii) dyeing auxiliaries or organic substances that are used for desiring, scouring, bleaching, dyeing, printing, and finishing, which are non-recyclable and responsible for the high biochemical oxygen demand / chemical oxygen demand of the effluents; (iii) textile fibres, and (iv) 60-100 g L^{-1} electrolyte, essentially NaCl and Na_2CO_3, which is responsible for the very high saline content of the wastewater. In addition, these effluents exhibit a pH of 10-11 and a high temperature (50-70 ºC). The removal of colours from wastewaters is often more important than the removal of the soluble colourless organic substances. Methods for the removal of organic substances from most effluents are fairly well established. Dyes, however, are more difficult to treat because their synthetic origin are mainly complex aromatic molecular structures, often synthesised to resist fading on exposure to sweat, soap, water, light or oxidising agents [12, 13]. This renders them more stable and less amenable to biodegradation [5].

Access to freshwater is globally becoming more critical every day. Without proper treatment, dye-containing effluents discharged into the hydrosphere will contribute a significant source of

water pollution. Many of these dyes are also toxic and even carcinogenic and pose a serious hazard to aquatic living organisms [14]. Therefore, stringent rules are imposed in many countries for controlling the discharge of industrial effluents. Due to increasingly stringent restrictions on the dye content of industrial effluents, it is necessary to remove dyes from wastewater before it is discharged. However, wastewater containing dyes is very difficult to treat, as the dyes are complex organic molecules, resistant to aerobic digestion, and are stable to light, heat and oxidising agents [15]. To minimise the risk of dye containing effluents on environment, there is a real need for proper treatment before being discharged into the hydrosphere.

1.2 Dyes

The first synthetic dye, Mauveine, was discovered by the Englishman, William Henry Perkin by chance in 1856. Since then, the dyestuff industry has matured [16]. With few exceptions, all synthetic dyes are aromatic organic compounds. A substrate is the material to which a colourant is applied by one of the various processes of dyeing, printing, surface coating, etc. Generally, the substrate can be textile fibres, polymers, foodstuffs, oils, leather, or many other similar materials [17]. Not all coloured compounds are dyestuffs because a coloured compound may not have a suitable application on a substrate. For example, a chemical such as copper sulfate, which is coloured, finds no application on any substrate. If it is applied on a substrate, it will not have retaining power on the substrate and for this reason, copper sulfate cannot be termed as a dye. On the other hand, Acid Red 1, a typical synthetic organic coloured compound, can retain its colour on cotton when it is applied to this natural fibre under suitable conditions [17].

1.3 Chemistry of dyes

Synthetic dyes are aromatic compounds produced by chemical syntheses. Accordingly, aromatic rings in dyes contain delocated electrons and also different functional groups. Their colour is due to the chromogene-chromophore structure (acceptor of electrons), and the dyeing capacity is due to the auxochrome groups (donor of electrons). The chromogene is constituted from an aromatic structure normally based on rings of benzene, naphthaline or anthracene, with which chromophores bind. Chromophores contain double conjugated bonds with delocated electrons. These unsaturated chromophore groups basically are responsible for the respective colours (“chroma” means colour and “phore” means bearer). The chromophore configurations

are represented by the azo group (-N=N-), ethylene group (=C=C=), methine group (-CH=), carbonyl group (=C=O), carbon-nitrogen (=C=NH; -CH=N-), carbon-sulfur (=C=S; ≡CS-S-C≡), nitro (-NO_2) and nitroso (-N=O) groups. The auxochrome ("auxo" means augment) groups are ionisable groups that confer to the dye binding capacity on the substrates [17]. An auxochrome is a functional group of atoms attached to a chromophore that provides electrons to the chromophore groups, modifies the ability of the chromophore to absorb light, and alters the wavelength or intensity of the absorption. The usual auxochrome groups are NH_2 (amino), -COOH (carboxyl), -SO_3H (sulfonate) and -OH (hydroxyl) [18, 19]. Some chromophore and auxocrome groups are presented in Table 1.1.

Table 1.1 Names of chromophore and auxochrome groups of dyes

Chromophore group	Name	Auxogroup	Name
-N=N-	Azo	-NH_2	Amino
-N=N^+-O^-	Azoxy	-$NHCH_3$	Methyl amino
-N=N-NH	Azoamino	-$N(CH_3)_2$	Dimethyl amino
-N=O, =N-OH	Nitroso	-SO_3H	Sulfonic acid
>C=O	Carbonyl	-OH	Hydroxy
>C=C<	Ethenyl	-COOH	Carboxylic acid
>C=S	Thio	-Cl	Chloro
-NO_2	Nitro	-CH_3	Methyl
>C=NH, >C=N-	Azomethine	-OCH_3	Methoxy
		-CN	Cyano
		-$COCH_3$	Acetyl
		-$CONH_2$	Amido

1.4 Classification of dyes

Hunger *et al*. [16] described that the textile dyes are mainly classified in two different ways, (1) based on the application characteristics (such as acid, basic, direct, disperse, mordant, reactive, sulfur dye, vat dye *etc*.), and (2) based on the chemical structure (such as nitro, azo, carotenoid, diphenylmethane, xanthene, acridine, quinoline, indamine, sulfur, anthraquinone, indigoid, phthalocyanine, *etc*.). The classification of dyes is outlined in Figure 1.1.

Considering only the general structure, textile dyes are also classified as anionic, nonionic and cationic dyes. The major anionic dyes are the direct, acid and reactive dyes [1], and the most problematic ones are the brightly coloured, water soluble reactive and acid dyes because they cannot be removed through conventional treatment systems. The major nonionic dyes are disperse dyes that do not ionise in the aqueous environment, and the major cationic dyes are the azo basic, anthraquinone disperse and reactive dyes, *etc*.

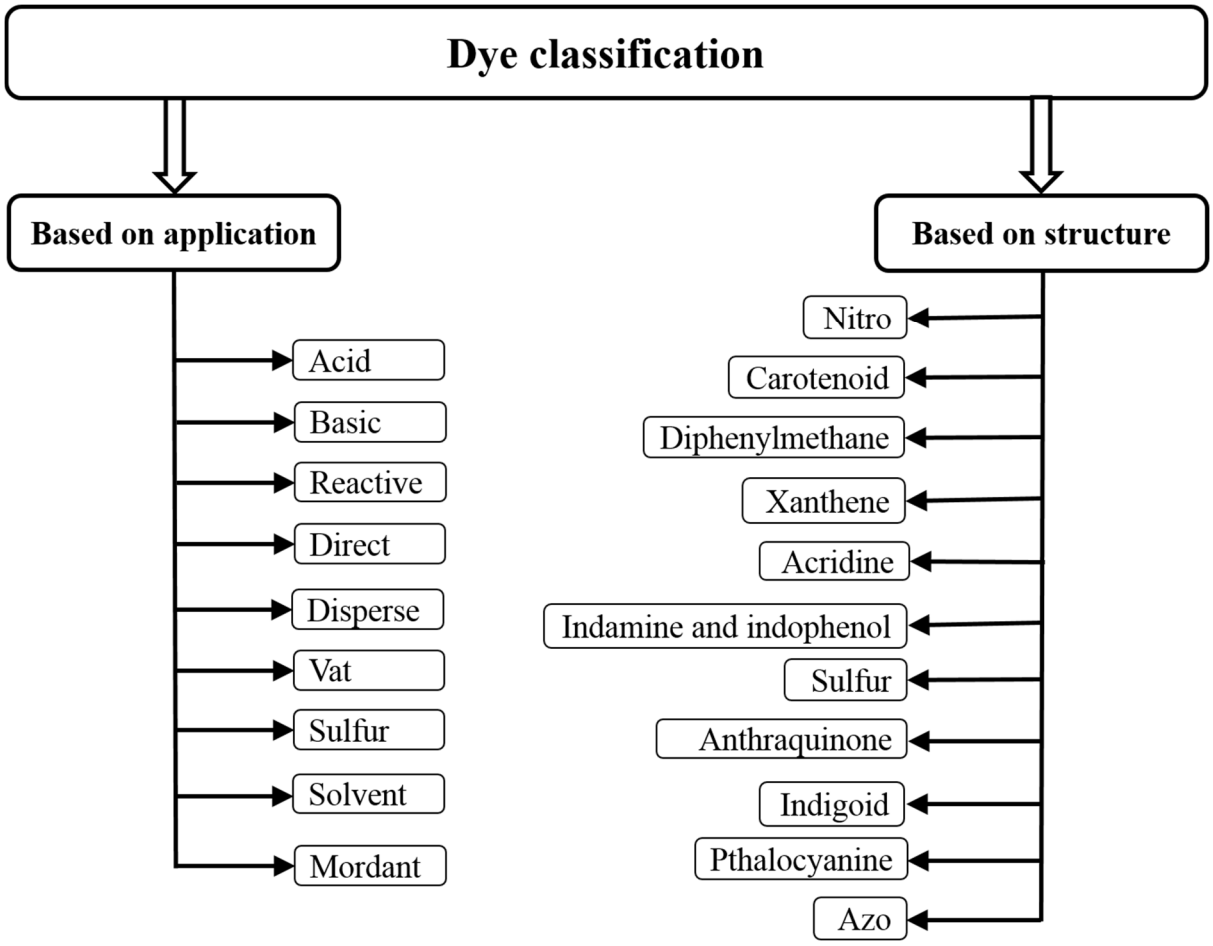

Figure 1.1 Classification of dyes

1.4.1 Application-based dyes

The classification of dyes by usage or application is the most important system adopted by the Colour Index (CI) [20]. Some of the common categories are detailed below.

1.4.1.1 Acid dyes

Acid dyes are water soluble anionic dyes and are applied on protein fibres, nylon, cotton, wool, silk, and modified acrylics. Moreover, they are used to dye paper, leather, inkjet printing, food, and cosmetics. Acid dyes produce bright colours that have excellent fastness, or the ability of the dye to stay on the fabric and not rub off or fade to dry cleaning, but not necessarily to washing or light and perspiration [16]. Commonly used acid dyes are the families of Acid Red, Acid Blue, Acid Orange, Acid Violet, and Acid Yellow.

1.4.1.2 Basic dyes

Basic dyes are cationic and water soluble. They produce bright colours that have excellent fastness to light, laundering, perspiration, and crocking on synthetic fibres, but poor fastness to washing and light on natural fibres. They are generally used for papers, acrylic, modified acrylic, polyacrylonitrile, modified nylons, modified polyesters, cellulosic, and protein fibres. In addition, they are often applied to silk, wool, and tannin–mordant cotton when brightness shade is more necessary than fastness to light and washing [16]. Examples of basic dyes are the Basic Blue, Basic Brown, Basic Green, Basic Red, Basic Violet, and Basic Yellow families.

1.4.1.3 Reactive dyes

Reactive dyes form a covalent chemical bond with fibre by an ether or ester linkage under suitable conditions. Majority of reactive dyes contain azo bonds that includes metallised azo, triphendioxazine, phthalocyanine, formazan, and anthraquinone. The molecular structures of these dyes are much simpler than direct dyes. They also produce brighter shades with excellent fastness in all areas, but are difficult to match shades [21]. Reactive dyes are primarily used for dyeing and printing of cotton fibres, but occasionally on protein fibres and nylon as well. Most widely used reactive dyes are the Reactive Black, Reactive Red, Reactive orange, and Reactive Yellow families.

1.4.1.4 Direct dyes

Direct dyes are anionic and soluble in aqueous solutions. They have a high affinity to cellulose fibres and have excellent fastness to perspiration and drycleaning, but poor fastness to washing and varied light fastness. Most direct dyes are polyazo compounds, along with some stilbenes, phthalocyanines, and oxazines. To improve wash fastness, frequently chelations with metal (such as copper and chromium) salts are applied to the dyestuff [16]. Commonly used direct

dyes in textile industries include the Direct Red, Direct Yellow, Direct Orange, and Direct Green families.

1.4.1.5 Disperse dyes

Disperse dyes are substantially water insoluble nonionic dyes, applied to hydrophobic fibres from microfine aqueous dispersion [16]. Disperse dyes are predominantly used for acetate, acrylic, modacrylic, nylon, polyester, polyamide, polypropylene and olefin fibres. The wash fastness with disperse dyes varies with the fibres, poor on acetate, excellent on polyester. The degree of fastness to light range from fair to good, but there is some gas fading on acetate. However, fastness to perspiration, crocking, and dry-cleaning is excellent [16]. Chemical structures of dyes are mainly consisted of azo and anthraquinonoid groups, having low molecular weight and containing groups which aid in forming stable aqueous dispersions. The Disperse Yellow, Disperse Red, and Disperse Orange families are some of the common disperse dye.

1.4.1.6 Vat dyes

Vat dyes are water insoluble and can be applied mainly to cellulose fibre by converting them to their leuco compounds. The latter was carried out by reduction and solubilisation with sodium hydrosulfite and sodium hydroxide solution, which is called a “vatting process” [16]. The main structural groups of vat dyes are anthraquinone and indigoid. Vat dyes have excellent fastness in all areas as well, especially to chlorine and bleach, however, if not properly applied, they may crock (release colour when rubbed) [16, 22]. Most widely used vat dyes are the Vat Black, Vat Blue, Vat Orange, Vat Red, Vat Yellow families.

1.4.1.7 Sulfur dyes

Sulfur dyes are water insoluble and are applied to cotton in the form of sodium salts by the reduction process using sodium sulfide as the reducing agent under alkaline conditions. The low cost and good wash fastness properties of dyeing make these dyes economic attractive [16]. Sulfur dyes are used on cellulosic fibres as well to form dull shades such as navy, black, and brown. They have excellent fastness in most areas, but are weak when exposed to chlorine. Some sulfur dyes that are most commonly used in textile industries are the Sulpfur Black, Sulfur Blue, Sulfur Green, Sulfur Yellow, and Sulfur Red families.

1.4.1.8 Solvent dyes

Solvent dyes are water insoluble, but organic solvent soluble, dyes having deficient polar solubility groups for example, sulfonic acid, carboxylic acid or quaternary ammonium [16]. They are used for colouring plastics, gasoline, oils, and waxes. Solvent dyes that are regularly used in textile industries are the Solvent Yellow, Solvent Red, Solvent Blue, Solvent Orange, Solvent Green, and Solvent Violet families.

1.4.1.9 Mordant dyes

Mordant dyes have dyeing properties with good quality in the presence of certain groups in the dye molecule. These groups are capable of holding metal residuals by formation of covalent and coordinate bonds involving a chelate compound [16]. The salts of aluminium, chromium, copper, cobalt, nickel, iron, and tin are used as mordant as their metallic salts [16]. Most commonly used mordant dyes are the Mordant Yellow, Mordant Orange, Mordant Red, Mordant Brown, Mordant Green, and Mordant Black families.

1.4.2 Chemical structure-based dyes

Following categories are based on their chemical structures.

1.4.2.1 Nitro dyes

As the name indicates, nitro dyes contain one or more nitro (-NO_2) groups. The N-O and N=O bonds of the nitro group are equivalent because of resonance, and they are conjugated with the resonating C-C and C=C bonds of the aromatic ring. If the compound is a phenol, the aromatic compound exists in equilibrium with a quinonoidone [16]. Examples include Picric Acid (CI 10305) and naphthol yellow S (CI 10316). Structures of several examples of nitro dyes are shown in scheme 1.

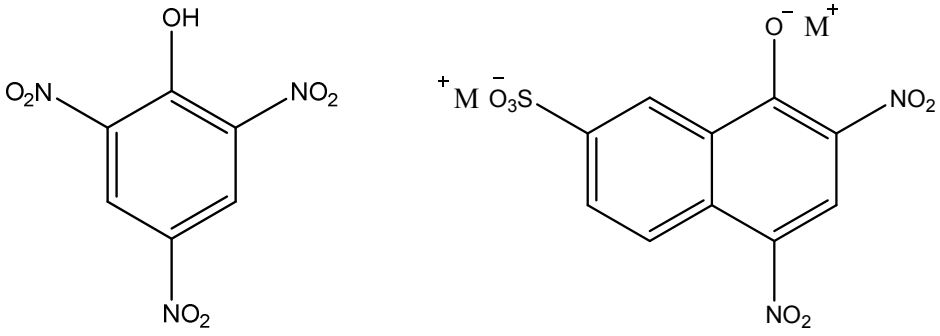

Scheme 1.1 structure of Picric acid and Naphthol yellow S

1.4.2.2 Carotenoid

Carotenoids are notable colourants for having no aromatic rings, but contain isoprene units (shown in Scheme 1.2) in their molecular structure [23]. More than 300 carotenoids occur in plants, and a few are synthesised industrially for colouring foodstuffs. The simplest member of the series is lycopene, named for its presence in *Lycopersicon* (tomato). Structure of lycopene is presented in Scheme 1.3.

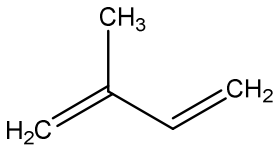

Scheme 1.2 An isoprene unit (2-methyl-1,3-butadiene)

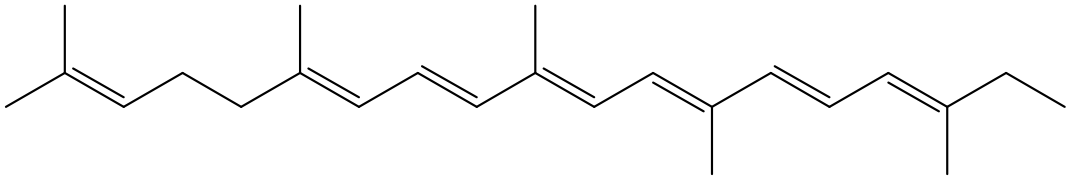

Scheme 1.3 Lycopene

This formula shows the carotenoid structure comprising eight isoprene units arranged so that there is a long conjugated chain in the middle part of the molecule. In other carotenoids, the ends of the chains are folded into rings, which may be alicyclic or quinonoid, and may bear such substituents as =O, -OH and -$OCOCH_3$.

1.4.2.3 Diphenylmethane

Diarylmethane is a small group of cationic dyes with the general structure shown in Scheme 1.4. Auramine O, CI 41000, is the only diarylmethane commonly used as a biological stain [24].

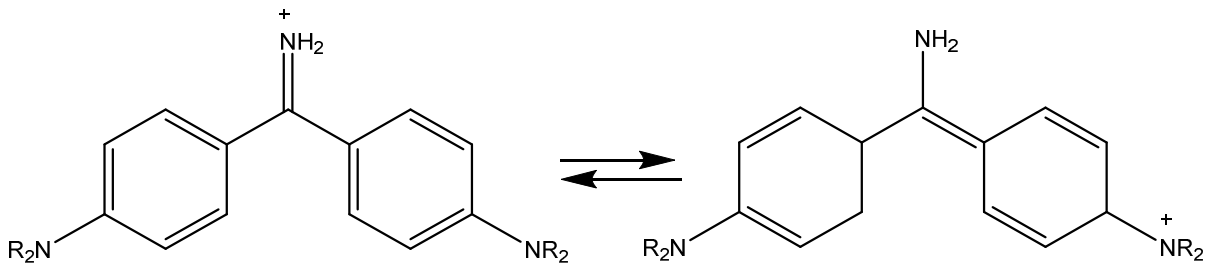

Scheme 1.4 Diarylmethane (R_2= any of H, CH_3 *etc*.)

1.4.2.4 Xanthene

The chromophore in xanthene contains the planar skeleton of the oxygen-containing heterocyclic compound xanthene [24] as shown in Scheme 1.5.

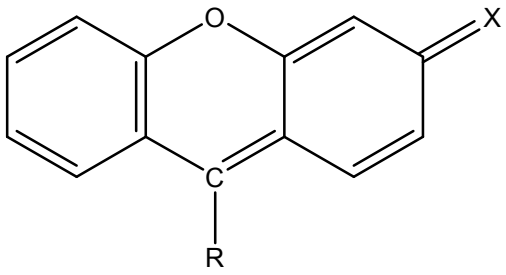

Scheme 1.5.Xanthene

In the general structure shown in Scheme 1.5, R may be a hydrogen atom or an aliphatic or aromatic group, and X is nitrogen in the aminoxanthenes or oxygen in the hydroxyxanthenes. The formula of an aminoxanthene dye is usually shown with a positively charged nitrogen attached to the *p*-quinoid ring, though resonance allows an alternative structure with a positive charge associated with the xanthene oxygen. Xanthene dyes used for biological staining are yellow or red, and many are also fluorescent. There are blue and violet xanthenes that are used as textile dyes. The pyronines and rhodamines are examples of aminoxanthene dyes; fluorescein and the eosins are well known hydroxyxanthenes.

1.4.2.5 Acridine

The structure of acridine (Scheme 16) resembles that of xanthene, except that the heteroatom is nitrogen instead of oxygen [25].

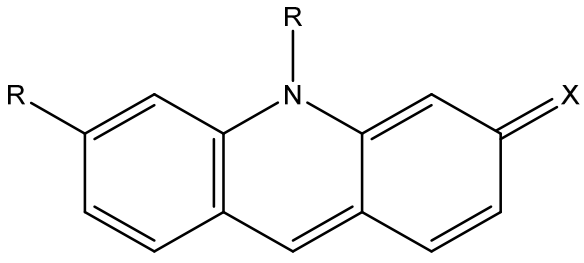

Scheme 1.6 Acridine

R is usually hydrogen, but may be an alkyl or aryl group. X is either nitrogen or oxygen. The acridines are strongly fluorescent yellow cationic dyes. Acridine orange, CI 46005, and acriflavine, CI 46000, are examples of dyes belonging to this class.

1.4.2.6 Quinophthalone dyes

Quinophthalone dyes, also known as quinoline dyes, have a quinoline joined to a phthalic anhydride [16]. An example of this type of dye is CI Lillie 1977 (Scheme 1.7).

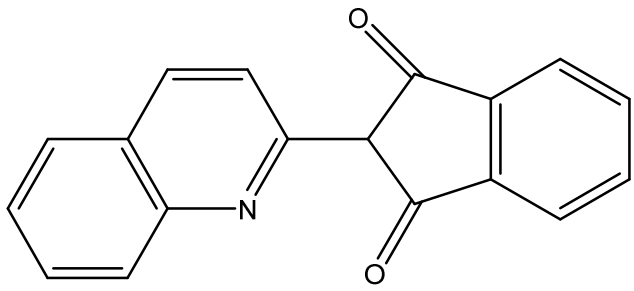

Scheme 1.7 CI Lillie 1977

1.4.2.7 Indamine and indophenol dyes

An indamine (-N=) group forms a bridge between an aromatic ring and a quinonoid ring. In indamine dyes, nitrogen atoms terminate the conjugated chain in both ring systems, whereas in an indophenol dye, the chain is terminated by phenolic hydroxyl or a quinonoid carbonyl group at one end [16]. These dyes are less important as biological stains [23], but some are used as analytical reagents. Coloured compounds with indamine and indophenol structures are the end products of some histochemical reactions. Example of indamine and indophenol dye is Indophenol Blue.

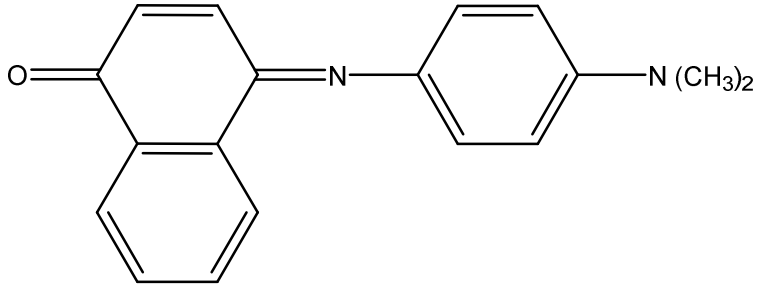

Scheme 1.8 Indophenol Blue

1.4.2.8 Sulfur dyes

Sulfur dyes are most commonly used dyes manufactured for cotton in terms of volume. They are cheap, generally have good wash-fastness, and are easy to apply. Sulfur dyes are predominantly black, brown, and dark blue. Red sulfur dyes are unknown, although a pink or lighter scarlet colour is available [16]. The most important sulfur dye is Sulfur Black 1 and its structure given in Scheme 1.9 [16, 26].

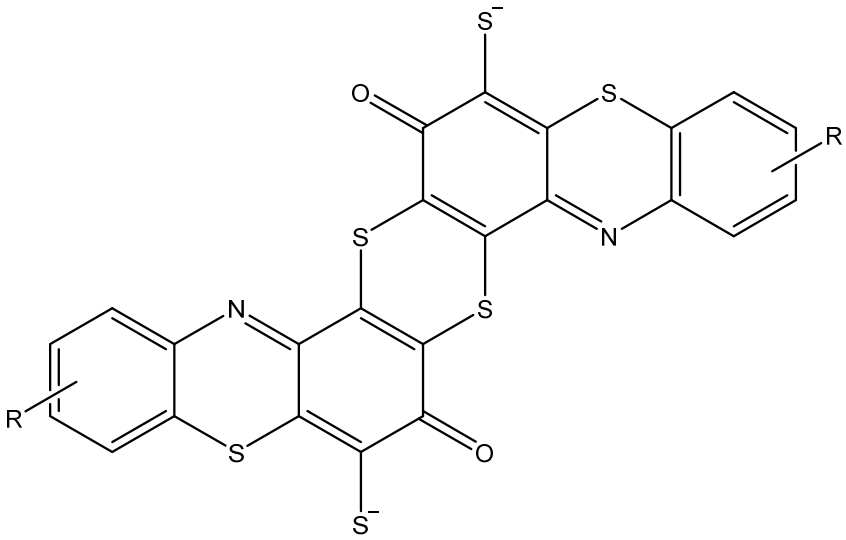

Scheme 1.9 Sulfur Black 1

1.4.2.9 Anthraquinone dyes

Anthraquinone dyes are built around the anthraquinone structure shown in Scheme 1.10. They can be many substitutions, including junctions with other fused ring systems. This is by far the largest group of carbonyl dyes including hundreds of compounds that are applied to textiles in many ways [23]. From an industrial standpoint, the most notable is the anthraquinone vat dyes for cotton.

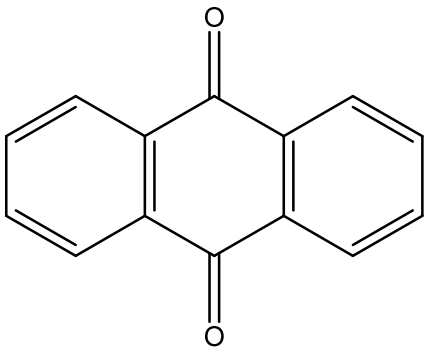

Scheme 1.10 Anthraquinone

1.4.2.10 Indigoid dyes

Similar to the anthraquinone dyes, benzodifuranone, and polycyclic aromatic carbonyl dyes, the indigoid dyes also contain carbonyl groups. They are also vat dyes. Indigoid dyes represent one of the oldest known classes of dyes. For example, 6,6'-dibromoindigo (structure shown in Scheme 1.11) is Tyrian Purple, the dye was made famous by the Romans [23]. Tyrian Purple was so expensive that only the very wealthy were able to afford garments dyed with it [23].

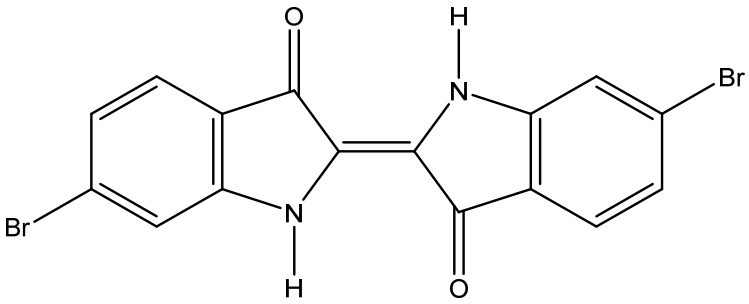

Scheme 1.11 6,6'-dibromoindigo

1.4.2.11 Phthalocyanine dyes

Phthalocyanine is an intensely blue-green-coloured aromatic macrocyclic compound that is widely used in dyeing. Phthalocyanines form coordination complexes with most elements of the periodic table. These complexes are also intensely coloured and are used as dyes or pigments [16]. The structure of copper phthalocyanine (Phthalocyanine Blue BN) is given in Scheme 1.12.

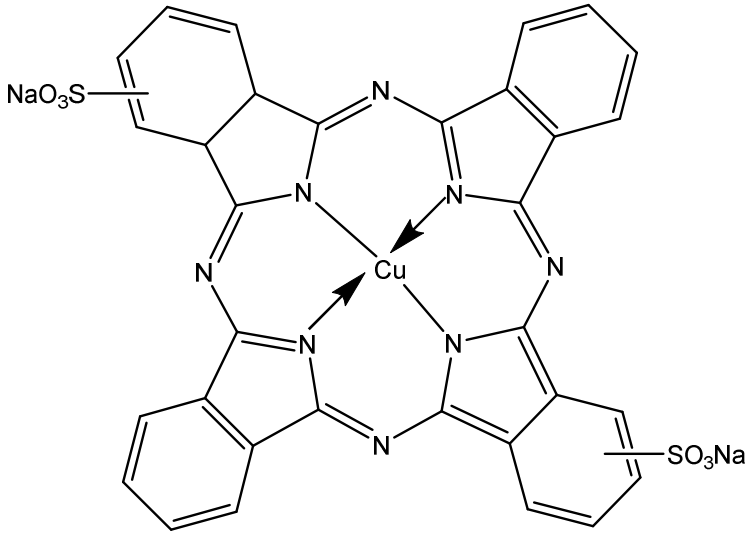

Scheme 1.12 Copper phthalocyanine

1.5 Azo dyes

Azo dyes are diazotised amines coupled to an amine or phenol, with one or more azo bonds (–N=N–). They are synthetic compounds and account for more than 50% of all the dyes produced annually, showing the largest spectrum of colours [16, 27-29]. Nearly all the dyestuffs used by the textile industry are azo dyes, and they are also widely used in the printing, food, papermaking and cosmetic industries [30, 31]. An estimate was made in the 1980's, that some 280,000 tonnes of textile dyes were annually discharged into industrial effluents worldwide [32, 33]. As the azo dyes represent about 70% by weight of the dyestuffs used in textile industries [34], they are the most common group of synthetic colorants released into the environment [33, 35]. The azo dyes show good fibre-fixation properties as compared to other synthetic dyes, showing up to 85% fixation, but nevertheless this explains why so much dye is released into the environment. An example of azo dyes is Acid Red 1, the structure of which is shown in Scheme 1.13). Due to its large scale production, extensive application, good solubility, and bright colours, it can frequently be found in the industrial wastewater. Moreover, azo dyes are the most problematic synthetic dyes that cannot be removed effectively by conventional dye effluent treatment methods.

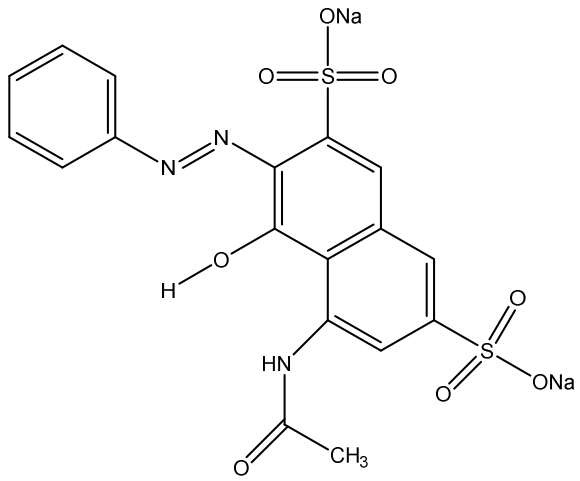

Scheme 1.13 Acid Red 1

1.5.1 Azo dyes and their effects on environment and human health

In addition to the effects caused by exposure to contaminated water and food, workers who deal with these dyes can be exposed to them in their place of work, and can suffer dermal absorption. Similarly, if dye-containing effluents enter into the water supply, possibly by contamination of

the ground water, the general population may be exposed to the dyes via the oral route and food chain. The latter point could be of great importance in places where the existent waste treatment systems are inefficient or where there is poor statutory regulation concerning industrial waste disposal [36].

1.5.1.1 Mutagenic effect

Various azo dyes have been shown to produce positive toxic results in different organisms from bacteria to human. Tsuboy *et al.* [37] analysed the mutagenic, cytotoxic and genotoxic effects of the azo dye CI Disperse Blue 291, and the results showed that this azo dye caused dose-dependent effects, inducing the formation of micronuclei, DNA fragmentation and increasing the apoptotic index in human hepatoma cells. A variety of azo dyes has shown mutagenic responses in *Salmonella* and mammalian assay systems, and it is apparent that their potencies depend on the nature and position of the aromatic rings, and the amino nitrogen atom. For instance, 2-methoxy-4-aminoazobenzene is an extremely weak mutagen, whereas under similar conditions, 3-methoxy-4-aminoazobenzene is a potent hepatocarcinogen in rats and a strong mutagen in *Escherichia coli* and *Salmonella typhimurium* [38-40].

Chung and Cerneglia [41] published a review of several azo dyes that were evaluated by the *Salmonella* / microsome assay. According to the authors, among the evaluated azo dyes, all nitro group containing azo dyes showed mutagenic activity. The Acid Alizarin Yellow R and Acid Alizarin GG showed this effect in the absence of metabolic activation [42]. The dyes, CI Basic Red 18 and Orasol Navy 2RB, which also contained nitro groups, were shown to be mutagenic both in the presence and absence of metabolic activation [43, 44]. The review also showed the results obtained in the *Salmonella* / microsomal test of azo dyes containing benzeneamines, and found that Chrysodin was mutagenic in the presence of a rat-liver preparation [41].

1.5.1.2 Effect of metabolites

The mutagenic, carcinogenic and toxic effects of azo dyes can be a result of direct action by the compound itself, or the formation of free radicals and aryl amine derivatives generated during the reductive biotransformation of the azo bond [36, 45], or even caused by the metabolites produced after oxidation via cytochrome P450 [46]. Sisley and Porscher carried out the earliest studies on the metabolism of azo compounds in mammals in 1911. They found that sulfanilic

acid in the urine of dogs fed with Orange I demonstrated, for the first time, that azo compounds could be metabolised by reductive cleavage of the azo group [47].

After an azo dye is orally ingested, it can be reduced to free aromatic amines by anaerobic intestinal microflora and possibly by a mammalian azo reductase in the intestinal wall or the liver [40, 47]. Such biotransformations can occur in a wide variety of mammalian species, including both *Rhesus* monkeys and humans [48]. Some of these aromatic amines are carcinogenic and can accumulate in food chains. For example, biphenylamines, such as benzidine and 4- biphenylamine, are present in the environment and constitute a threat to human health and to the ecosystems in general [49, 50]. Nitroanilines are another examples of aromatic amines that are commonly generated during the biodegradation of azo dyes under anaerobic conditions, formed by reductive cleavage of the azo bonds (–N=N–) by the action of microorganisms present in the wastewaters [4, 51, 52]. Depending on the individual compounds, many aromatic amine metabolites are considered to be non-biodegradable or only very slowly degradable [53], showing a wide range of toxic effects on aquatic life and higher organisms [51, 52, 54].

According to legislations passed by the European Community on 17th July 1994, the application of azo dyes in textiles is restricted to those colorants which cannot, under any circumstances, be converted to any of the following products: 4-aminodiphenyl; 4-amino-2',3-dimethylazobenzene (oaminoazo-toluene); 4-aminophenylether (4,4'-oxydianiline); 4-aminophenylthioether (4,4'-thiodianiline); benzidine; bis-(4-aminophenyl)-methane (4,4'-diaminodiphenylme-thane); 4-chloroaniline (*p*-chloroaniline); 4-chloro-2-methylaniline (4-chloro-o-toluidine); 2,4-diaminotoluene (2,4-toluenediamine); 3,3'-Dichlorobenzidine dihydrochloride; 3,3'-dimethoxybenzidine (*o*-dianisidine); 3,3'-dimethylbenzidine (*o*-toluidine); 3,3'-dimethyl- 4,4'-diamino-diphenyl methane; 2-methoxy-5-methylaniline (*p*-kresidine); 4-methoxy-1,3-phenylenediamine sulfate hydrate (2,4-diaminoanisole); 4,4'-methylene-bis (2-chloroaniline); 2-methyl-5-nitroaniline (2-amino-4-nitrotoluene); 2-naphthylamine; *o*- toluidine; 2,4,5-trimethylaniline [55].

1.6 Dye containing wastewater

Dye discharged wastewater by some industries under uncontrolled and unsuitable condition causes significant environmental problems. The importance of the environmental pollution

control and treatment is undoubtedly the key factor in the human future. If a textile industry discharges the wastewater into the local environment without proper treatment, it will have a serious impact on natural water bodies and land in the surrounding area.

The textile dyeing wastewater has a large amount of complex components with high concentrations of organic, inorganic, high-coloured compounds, which has a cumulative effect, and higher possibilities for entering into the food chain. Owing to their high biological oxygen demand / chemical oxygen demand, their colouration and their salt load, the wastewater resulting from dyeing fibres with reactive azo dyes are seriously polluted and dark in colour, which increases the turbidity of water body. As aquatic organisms need light to develop, any deficit in this respect caused by coloured water leads to an imbalance of the ecosystem [3, 4]. Moreover, the water of rivers that is used for drinking water must not be coloured, as otherwise the treatment costs will be increased. The governments of different countries have enacted strict rules controlling the discharge of wastewater into the water system. In order to minimise the pollution, manufacturers and government officials are seeking for solutions to reduce the problem in an efficient way. Thus, studies concerning the feasibility of treating dyeing wastewater are very important.

1.7 Wastewater treatment processes

In the past several decades, many techniques have been developed to seek an economical and efficient way for treating the textile dye wastewater, including physico-chemical, chemical, biological, combined treatment processes. None of the techniques is generally regarded acceptable because all of them offer both advantages and limitations, which are summarised in Table 1.2 on page 33. Because of the high cost and sludge disposal problems, many of these conventional methods for treating dye containing wastewater have not been widely applied at large scale in textile and paper industries.

There is no single process capable of adequate treatment, mainly due to the complex nature of the effluents [56, 57]. In practice, a combination of different processes is often applied to achieve the desired water quality in the most economical way. A literature survey by Crini [58] showed that research has been and continuing to be conducted in the areas of combined adsorption–biological treatments in order to improve the biodegradation of dyestuffs and to minimise the sludge production.

1.7.1 Physico-chemical treatment methods

Numerous studies were devoted to remove dyes from textile effluent, and have mainly concentrated on the development of an efficient and cost-effective removal process. These include physico-chemical methods such as adsorption, filtration, specific coagulation, chemical flocculation, *etc*. Dyes can also be removed from an industrial wastewater by other physico-chemical treatment technologies such as precipitation, ion exchange, and membrane processes (Kurniawan *et al*., 2006). Some of these methods are simple, cost effective, however, limitations including high cost, low efficiency, labour-intensive operation, lack of selectivity of the process and production of huge toxic solid sludge that required additional treatment before disposal have been encountered [59, 60].

1.7.1.1 Adsorption

Adsorption produces high quality product water by adsorbing the cationic, mordant and acid dyes from the textile wastewater. Adsorption techniques have gained favour recently due to their efficiency in the removal of pollutants that are too stable for conventional methods. This process is also economically feasible [61]. Decolourisation by adsorption is a result of two mechanisms, surface adsorption and ion exchange [62], and is influenced by many physio-chemical factors, such as dye / sorbent interaction, sorbent surface area, particle size, temperature, pH, and contact time [63]. In addition to activated carbon, a number of low-cost adsorbent materials, for example, peat, fly ash, wood chips, bentonite clay and fly ash have been investigated for colour removal [64].

Activated carbon. Activated carbon is the most commonly used method of dye removal by adsorption [65] and is very effective for adsorbing cationic, mordant, and acid dyes and, to a slightly lesser extent, dispersed, direct, vat, and reactive dyes [66, 67]. Performance is dependent on the type of carbon used and the characteristics of the wastewater. Due to its powdered nature, activated carbon has a large surface area, and hence has a good capacity for adsorption. Removal rates can be further improved by using massive doses, although regeneration or re-use results in a steep reduction in performance, and efficiency of dye removal becomes unpredictable and dependent on massive doses of carbon. Activated carbon, similar to many other dye-removal treatments, is well suited for one particular waste system and ineffective in another. Activated carbon is expensive. The carbon also has to be reactivated otherwise disposal of the concentrates has to be considered. Reactivation results in 10–15%

loss of the sorbent. Moreover the granular activated carbon can only maintain its adsorption capacity for a short time after the available adsorption sites are exhausted with adsorbed pollutants [68].

Peat. The cellular structure of peat makes it an ideal choice as an adsorbent. It has also the ability to adsorb transition metals and polar organic compounds from dye-containing effluents. Peat may be considered as a viable adsorbent in countries such as Ireland and United Kingdom, where it is widely available. Unlike activated carbon, (peat requires no activation) and is also cost effective [69].

Wood chips. Wood chips show a good adsorption capacity for acid dyes, but, due to their hardness, it is not as good as other available sorbents [70] and longer contact times are required [69]. Dye adsorbed wood chips are conventionally burnt to generate power, although there is potential of use for solid-state fermentation, which is a biomolecule manufacturing process used in the food, pharmaceutical, cosmetic, fuel and textile industries occurring in the absence or near absence of free water.

Fly ash and coal. Fly ash usually refers to ash produced during combustion of coal. A high fly ash concentration increases the adsorption rates of dyes due to larger surface area available for adsorption. This combination may be substituted for activated carbon, with a 1:1 mass ratio of fly ash : coal [71].

Silica gel. Silica gel is an effective material for removing basic dyes, although side reactions, such as air binding and air fouling with particulate matter, prevents it being used commercially.

Other materials. The use of such substrates as natural clay, corn cobs, and rice husks for dye removal is advantageous mainly due to their widespread availability and cost-effectiveness. They are economically attractive for dye removal, compared to activated carbon, with many comparing well in certain situations [70]. As these materials are non-expensive, regeneration is not necessary and the potential exists for dye-adsorbed materials to be used as substrates in solid state fermentation for protein enrichment.

1.7.1.2 Membrane filtration

Membrane filtration has the ability to clarify, concentrate and, most importantly, to separate dye continuously from effluents [72, 73]. It has several special features unrivalled by other methods, for example, resistance to temperature, an adverse chemical environment, and microbial attack. However, the concentrated residue remained after separation poses disposal problems, and high capital cost, the possibility of clogging, and membrane replacement are some of its disadvantages. This method is suitable for water recycling within a textile dye plant if the effluent contains low concentration of dyes, but it is unable to reduce the dissolved solid content, which makes water re-use a difficult task.

1.7.1.3 Reverse osmosis

Reverse osmosis membranes have a retention rate of at least 90% for most types of ionic compounds and produce a high quality of permeate. Decolourisation and elimination of chemical auxiliaries in dye house wastewater can be carried out in a single step by reverse osmosis. Reverse osmosis permits the removal of all mineral salts, hydrolysed reactive dyes, and chemical auxiliaries. Notably, the higher the concentration of dissolved salt, the more important the osmotic pressure becomes, therefore, the greater the energy required for the separation process [74].

1.7.1.4 Filtration

Filtration methods such as microfiltration, nanofiltration and ultrafiltration have been used for water recycling and chemical recovery. In textile industry, these filtration methods can be used for both filtering and recycling.of not only pigment rich wastewaters, but bleaching wastewaters. The specific temperature and chemical composition of the wastewater determine the type and porosity of the filter to be applied [75]. The major disadvantages of the filtration processes are the high investment costs and that they have a limited lifetime before membrane fouling occurs and the cost of periodic replacement must thus be included in any analysis of their economic. Moreover, the potential membrane fouling produces secondary waste streams which require further treatment [1, 58].

1.7.1.5 Ion exchange

Ion exchange was another effective treatment method. However, due to its high sludge producing properties and ineffective to diversity of dyes, it became economically unfeasible

hence not accepted widely [76]. Moreover, ion exchange has not been widely used for the treatment of dye-containing effluents, mainly due to the opinion that ion exchangers cannot accommodate a wide range of dyes [62]. Wastewater is passed over the ion exchange resin until the available exchange sites are saturated. Both cationic and anionic dyes can be removed from dye-containing effluent this way. Advantages of this method include no loss of adsorbent on regeneration, reclamation of solvent after use and the removal of soluble dyes. A major disadvantage is cost, organic solvents are expensive, and the ion exchange method is not very effective for disperse dyes [72].

1.7.1.6 Coagulation or flocculation

Coagulation or flocculation is an economically feasible method of dye removal. During coagulation or flocculation, the coagulant chemicals neutralise the electrical charges of the dye molecules in the water, allowing the particles to come close together and form large clumps. The coagulants, for example, ferrous sulfate and ferric chloride, allow excellent removal of direct dyes from wastewaters. Unfortunately, poor results with acid dyes, coupled with the high cost of the ferrous sulfate and ferric chloride, means that it is not a widely used method. The optimum coagulant concentration is dependent on the static charge of the dye in solution and difficulty in removing the sludge formed as part of the coagulation is a problem [72]. Production of large amounts of sludge occurs, and this results in high disposal costs [77].

1.7.1.7 Irradiation

Sufficient quantities of dissolved oxygen are required for organic substances to be broken down effectively by radiation. The dissolved oxygen is consumed very rapidly and so a constant and adequate supply is required. This has an effect on cost. Dye-containing effluent may be treated in a dual-tube bubbling reactor. This method showed that some dyes and phenolic molecules can be oxidised effectively at a laboratory scale only [78].

1.7.2 Chemical oxidation methods

Conventional oxidation methods by oxidising agents such as ozone (O_3), hydrogen peroxide (H_2O_2) and chlorite (ClO^-) have been used. These chemical techniques are often expensive, and although the dyes are removed, accumulation of concentrated sludge gives rise to a disposal problem. There is also the possibility that a secondary pollution problem will arise because of excessive chemical use. Modification in the chemical composition of a compound or a group

of compounds (for example, dyes) takes place in the presence of these oxidising agents, by which the dye molecule becomes susceptible to the degradation [79].

1.7.2.1 Ozonation

The use of ozone was first pioneered in the early 1970s, and it is a very good oxidising agent due to its high instability (oxidation potential 2.07 V) compared to other oxidising agent chlorine (1.36 V), and H_2O_2 (1.78 V) [80]. Oxidation by ozone is capable of degrading chlorinated hydrocarbons, phenols, pesticides and aromatic hydrocarbons [80]. The dosage applied to the dye-containing effluent is dependent on the total colour and residual chemical oxygen demand (which is a measure of the capacity of water to consume oxygen during the decomposition of organic matter and the oxidation of inorganic chemicals such as ammonia and nitrite) to be removed with no residue or sludge formation [81], and no toxic metabolites [77]. Ozonation leaves the effluent with no colour and low chemical oxygen demand suitable for discharge into environmental waterways. This method shows a preference for double-bonded dye molecules [62]. Ozonation was found to be effective in treating azo dye-containing wastewater due to its high reactivity with many azo dyes (by breaking azo -N=N- bond) [82]. One major advantage is that ozone can be applied in its gaseous state and therefore does not increase the reaction volume and sludge, and providing good colour removal efficiencies. However, it has limitation towards disperse dyes and those insoluble in water, low chemical oxygen demand removal, short half-life, typically approximately 20 min, therefore continuous ozonation is required, as well as the high cost of ozone [76, 83]. The half-life can be further shortened if dyes are present, with stability being affected by the presence of salts, pH, and temperature. Moreover in alkaline conditions, ozone decomposition is accelerated, and so careful monitoring of the effluent pH is required [62].

1.7.2.2 Sodium hypochloride (NaOCl)

This method involves attacking the amino group of the dye molecule by the Cl^+ group. It initiates and accelerates azo-bond cleavage. This method is unsuitable for disperse dyes. An increase in decolouration is observed with an increase in Cl concentration. The use of Cl for dye removal is becoming less frequent due to the negative effects it has when released into waterways [62] and the release of by-products, *e.g.*, aromatic amines which are carcinogenic, or otherwise toxic molecules [3].

1.7.2.3 Advanced oxidation process

Recently, other emerging techniques, known as advanced oxidation processes, which are based on the generation of very powerful oxidising agents such as hydroxyl radicals, have been successfully applied to pollutant degradation. Although these methods are efficient for the treatment of water contaminated with pollutants, they are very costly and commercially unattractive. The high electrical energy demand and the consumption of chemical reagents are common problems.

The use of the Fenton's reagent (a solution of hydrogen peroxide and ferrous iron catalyst) for the treatment of textile wastewater is one of the most used advanced oxidation processes [84]. The high removal efficiencies of Fenton's reagent is due to the formation of strong hydroxyl radical ($OH^{\bullet}$) in the presence of hydrogen peroxide, which is added in an acid solution (pH 2–3) containing Fe^{2+} ions. The oxidation of Fe^{2+} to Fe^{3+} leads to the formation of ferric hydro complexes, which then simultaneously acts as a coagulant and oxidant [85]. The $OH^{\bullet}/H_2O$ has a very strong oxidation potential of +2.73 V but it leaves a yellowish colour in the treated wastewater. This method was regarded as relatively cheap and it also represents high chemical oxygen demand removal and decolourisation efficiencies for both soluble and insoluble dyes. However, high sludge generation due to the flocculation of reagents and dye molecules still limit the application of this process [1].

Photocatalysis (H_2O_2/UV) is another effective advanced oxidation technology mainly because of achievable high colour removal (up to 95 %), no sludge formation and high chemical oxygen demand removal in a short retention time [86]. This method degrades dye molecules to CO_2 and H_2O [87, 88] by UV treatment in the presence of H_2O_2. Degradation is caused by the production of high concentrations of hydroxyl radicals. UV light is used to activate chemicals, such as H_2O_2, into two hydroxyl radicals ($OH^{\bullet}$) that initiate the chemical oxidation of organic material. The rate of dye removal is influenced by the intensity of the UV radiation, pH, dye structure and the dye bath composition [62]. This may be set-up in a batch or continuous column unit. Depending on initial materials and the extent of the decolourisation treatment, additional by-products, such as halides, metals, inorganic acids, organic aldehydes and organic acids may be produced [87]. There are several advantages of photochemical treatment of dye-containing effluent including no sludge generation and greatly reduced foul-odours. However, it was found to be less effective for disperse, vat dyes and highly coloured wastewater.

Formation of by products and inefficient use of UV light can increase the cost of the process [87].

1.7.3 Biological treatments

Biological treatments are often the most economical alternative compared to other physical and chemical processes. It is a clean-up approach and is on the front line and priority research area in environmental sciences. Biodegradation methods such as fungal decolourisation, microbial degradation, adsorption by (living or dead) microbial biomass and bioremediation systems are commonly applied to the treatment of industrial effluents because many microorganisms, for example bacteria, yeasts, algae and fungi are able to accumulate and degrade different pollutants [2, 89]. However, their application is often restricted because of technical constraints. Biological treatment requires a large land area and is constrained by sensitivity toward diurnal variation as well as toxicity of some chemicals, and less flexibility in design and operation [90]. Biological treatment is incapable of achieving satisfactory colour elimination with current conventional biodegradation processes [1]. Moreover, although many organic molecules are degraded, many others are also recalcitrant to biodegradation due to their complex chemical structure and synthetic organic origin [63]. In particular, due to their xenobiotic nature, azo dyes are not totally degraded [2, 89]. Another major limitation of this process is slow dye degradation rate [2, 89]. As biological treatment is insufficient to remove colour and to accomplish with current regulations, the application of specific treatments is required.

1.7.3.1 Decolourisation by white-rot fungi

White-rot fungi are organisms that are able to degrade lignin, the structural polymer found in woody plants [91]. The most widely studied white-rot fungus, in regards to xenobiotic degradation, is *Phanerochaete chrysosporium*. This fungus is capable of degrading dioxins, polychlorinated biphenyls and other chloro-organics [92, 93]. Davis *et al.* [94] showed the potential of using *P. sordida* to treat creosote contaminated soil. Kirby *et al.* [95] has shown that *P. chrysosporium* exhibited the ability to decolourise artificial textile effluent by up to 99% within 7 days.

White-rot fungi are able to degrade dyes using enzymes, such as lignin peroxidases, manganese dependent peroxidases [96]. Other enzymes used for this purpose include H_2O_2-producing

enzymes, such as, glucose-1-oxidase and glucose-2-oxidase, along with laccase, and a phenoloxidase enzyme [95, 97-99]. These are the same enzymes used for the lignin degradation [91, 93]. Azo dyes, the largest class of commercially produced dyes, are not readily degraded by micro-organisms but these can be degraded by *P. chrysosporium* [100]. Other fungi such as *Hirschioporus larincinus, Inonotus hispidus, Phlebia tremellosa and Coriolus versicolor* have also been shown to decolourise dye-containing effluent [2, 95].

Although white rot fungi are shown to non-specifically degrade a wide variety of poly aromatic compounds including azo dyes, the lignolytic oxidative enzyme production in liquid fermentations is known to be inconsistent [1]. This is mainly due to the unfamiliar environment of liquid fermentations for wood degrading fungi. The ability to utilise these fungi in their natural environment means that they are more likely to be more effective in solid state fermentation [101].

1.7.3.2 Other microbial cultures

Mixed bacterial cultures from a wide variety of habitats have also been shown to decolourise the diazo-linked chromophore of dye molecules in 15 days [102]. Nigam and Marchant [103], and Nigam *et al.* [21] demonstrated that a mixture of dyes was decolourised by anaerobic bacteria in 24–30 h using free growing cells or in the form of biofilms on various support materials. Ogawa and Yatome [104] demonstrated the use of bacteria for azo dye biodegradation. Unfortunately, these microbial systems exhibit the drawback of requiring a fermentation process, and are therefore unable to cope with large volumes of textile effluents.

The ability of bacteria to metabolise azo dyes has been investigated by a number of research groups [104-106]. Under anaerobic conditions, such as anoxic sediments, many bacteria gratuitously reduce azo dyes reportedly by the activity of unspecific, soluble, cytoplasmic reductases known as azo reductases. These enzymes are reported to result in the production of colourless aromatic amines, which may be toxic, mutagenic, and possibly carcinogenic to animals.

Increasingly, there is evidence suggesting that additional processes may also be involved in azo dye reduction. Many bacteria were reported to reduce a variety of sulfonated and non-sulfonated azo dyes under anaerobic conditions without specificity of any significance. In addition, many highly charged and high molecular-sized sulfonated and polymeric azo dyes are

unlikely to pass the cell membrane. Both pieces of evidence point to the existence of a reducing activity, which is not dependent on the intracellular availability of the azo dye [105]. This hypothesis was supported by the work reported by Keck *et al.* [105], in which they isolated a strain of *Sphingomonas* capable of using redox mediators generated during the aerobic metabolism of 2-naphthalenesulfonate to facilitate a 20-fold increase in its ability to reduce the sulfonated azo dye Amaranth [105]. These redox mediators were found to be decomposition products of 1,2-dihydroxynaphthalene and were able to anaerobically shuttle reduction equivalents from the bacterial cells to the extracellular azo dye. Subsequently this group found that the isolated *Sphingomonas sp*. strain BN6 possessed both cytoplasmic and membrane-bound azo-reductase activities [106].

Yeasts, such as *Klyveromyces marxianus*, are also capable of decolourising dyes. Banat *et al.* [2] showed that *K. marxianus* was capable of decolourising Remazol Black B by 78–98%. Zissi *et al.* [107] showed that *Bacillus subtilis* could be used to break down *p*-aminoazobenzene, a specific azo dye. Further research using mesophilic and thermophilic microbes have also shown these bacteria to degrade and decolourise dyes [21, 108].

1.7.3.3 Adsorption by living / dead microbial biomass

The uptake or accumulation of chemicals by microbial mass has been termed biosorption [63, 109]. Dead bacteria, yeast and fungi have all been used for the purpose of decolourising dye-containing effluents.

Textile dyes vary greatly in their chemistries, and therefore their interactions with micro-organisms depend on the chemistry of a particular dye and the specific chemistry of the microbial biomass [110]. Depending on the dye and the species of microorganism used, different binding rates and capacities will be observed. In general, a certain dye will exhibit a particular affinity for binding with microbial species.

Previously, biomass derived from the thermotolerant ethanol-producing yeast strain, *K. marxianus* IMB3, exhibited a relatively high affinity for heavy metals [111, 112]. Biosorption capacities supported that this type of biomass showed a significantly high affinity (98 mg g^{-1}) for dye removal, and so widened the spectrum of use for biomass [111].

Hu [109] demonstrated the ability of bacterial cells to adsorb reactive dyes. Zhou and Zimmerman [113] used actinomyces as an adsorbent for decolourisation of effluents containing anthroquinone, phalocyanine and azo dyes.

Biosorption tends to occur reasonably quickly, ranging from a few minutes in algae to a few hours in bacteria [109]. This is likely to be due to an increase in surface area caused by cell rupture during autoclaving [110].

The use of biomass has its advantages, especially if the dye-containing effluent is very toxic. Biomass adsorption is effective when conditions are not always favourable for the growth and maintenance of the microbial population [114]. Adsorption by biomass occurs mainly by ion exchange.

1.7.4 Electrochemical techniques

Generally, electrochemical processes have been used in metal recovery treatments. But more recently, a wide range of other applications involving electrochemical processes has been proposed to solve technical problems associated with several effluent treatments in textile industry.

Most electrochemical discoloration studies are focused on reactive dyes. Reactive dyes represent about 20–30% of the total market [115] because of their solidity and brilliant colours. Their structure generally consists on a reactive group (which reacts with a fibre), and a chromophore group (which gives the colour). The most used chromophore group is the “azo” (–N=N–), followed by the anthraquinone group [116]. Azo group constitutes more than half of worldwide production [20, 117-119]. In general, electrochemical methods are more economical than other methods. But, azo dyes produce toxic aromatic products in their electrochemical degradation. For example, the degradation of the azo dyes, azo benzene, *p*-methyl red and methyl orange in aqueous solution at room temperature has been studied by an advanced electrochemical oxidation process under potential-controlled electrolysis conditions using a Pt anode and a carbon felt cathode. In this process, degradation products including 1,4–benzoquinone, pyrocatechol, 4-nitrocatechol, 1,3,5-trihydroxynitrobenzene and *p*-nitrophenol were identified [120], all of which are highly toxic compounds [121, 122].

1.7.4.1 Electrocoagulation methods

Electrocoagulation is a process consisting of generating metallic hydroxides flocs within the wastewater by electrodissolution of soluble anodes, usually made of iron or aluminium. Electrocoagulation has been applied successfully to treatment of various kind of wastewater, for example, heavy metals, food and protein wastes, textile wastewater, fluoride containing water, restaurant wastewater and textile dye solutions [123] Electrocoagulation occurs via serial steps including electrolytic reactions at electrode surfaces, formation of coagulants in an aqueous phase, adsorption of soluble or colloidal pollutants on coagulants, which are removed by sedimentation or flotation.

The metal ion generation takes place at the anode, while hydrogen gas is released from the cathode. The hydrogen gas would also help to float the flocculated particles out of the water. The main reactions occurring at the electrode are as follows [123]:

$$\text{Anode: } Al(s) \rightarrow Al^{3+}(aq) + 3e- \quad (1)$$

$$\text{Cathode: } 3H_2O\,(l) + 3e- \rightarrow 3/2H_2(g) + 3OH^-(aq) \quad (2)$$

Al^{3+} and OH^- ions generated by electrode reaction (1) and (2) react to form various monomeric species such as $Al(OH)^{2+}$, $Al(OH)_2^+$, $Al_2(OH)_2^{4+}$, $Al(OH)_4^-$, and polymeric species such as $[Al_6(OH)_{15}]^{3+}$, $[Al_7(OH)_{17}]^{4+}$, $[Al_8(OH)_{20}]^{4+}$, $[Al_{13}O_4(OH)_{24}]^{7+}$, which transform finally into $Al(OH)_3(s)$ according to complex precipitation reaction as shown in reaction (3).

$$Al(aq)^{3+} + 3H_2O(l) \rightarrow Al(OH)_3(s) + 3H(aq)^+ \quad (3)$$

The inconvenience of electrocoagualtion in comparison to the other electrochemical methods is that it produces secondary residues (the complex formed with pollutant and hydroxide), which need to be further treated for proper disposal.

1.7.4.2 Electrochemical reduction methods

Electrochemical reduction methods have only been discussed in several publications because of poor degradation of pollutants in comparison to direct and indirect electro-oxidation methods [124]. Bechtold *et al*. [125] suggested that this method is particularly suitable for the treatment of highly coloured wastewaters such as the residual pad-batch dyeing bath with reactive dyes. The electrochemical reduction of azo dye produces amines, and its degradation steps are shown below [126].

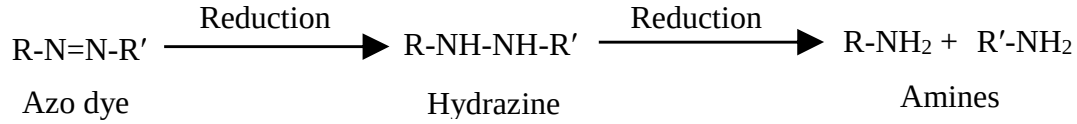

In another report, Vanerkova *et al.* [127] proposed a reduction mechanism for azo dye degradation at platinised titanium electrodes in the presence of NaCl. In their study, they reported that hypochlorite generated by oxidation of chloride reduces azo bonds of azo dye and produces amino products.

1.7.4.3 Electrochemical oxidation methods

Electrochemical oxidation is a process based on pollutant removal by direct anodic oxidation or by chemical reaction with electrogenerated metal hydroxyl radical (M [$OH^{\bullet}$]) or metal oxide ([MO]), as shown in Reactions (4) and (5) below [124]. In this process, the metal is initially electrochemically oxidised and produce (M [$OH^{\bullet}$]) in aqueous dye solution, which then oxidises dye molecule (R) and produces dye degradation product (RO).

$$H_2O + M \rightarrow M\,[OH^{\bullet}] + H^+ + e^- \quad (4)$$

$$R + M\,[OH^{\bullet}] \rightarrow M + RO + H^+ + e^- \quad (5)$$

Many studies have shown that the total mineralisation is possible with high efficiencies depending on the anode material, for example, SnO_2 [128], PbO_2 [129-131], boron-doped diamond [132-138], Ti/SnO_2/SbO_x/RuO_2, and Ti/TiO_2 [115]. However, the dye solution is not decolorised effectively at both glassy and reticulated vitreous carbon electrodes [115]. The boron-doped diamond thin-film electrodes have physical characteristics as an inert surface with low-adsorption properties, good corrosion stability, and a wide potential window (-1.25 to +2.3 V *versus* standard hydrogen electrode) without significant water decomposition in aqueous medium [138, 139]. In spite of its high cost, boron-doped diamond electrodes have much greater O_2 overvoltage (2 V) than conventional anodes, for example Pt, PbO_2, *etc.* (650 mV). Consequently, this electrode generates an increased amount of M [$OH^{\bullet}$], which implies a faster oxidation of the dye molecules [140].

In the same way, Martínez-Huitle and Brillas [124] compared different kinds of electrodes in two types of wastewaters (chloride-free dye wastewaters and effluents containing chloride).

They supported that most of the anodes tested could destroy the chromophore group (*e.g.*, –N=N–) producing its discoloration efficiently. In the presence of chloride, the destruction of dyes was accelerated by active chlorine species produced.

1.7.4.4 Indirect oxidation method

Indirect electro-oxidation occurs when strong oxidants are generated *in situ* during the electrolysis and react with the organic pollutants such as dyestuffs, resulting in either total or partial degradation.

There are mainly two methods used. Method (i) exploits the electro-oxidation with active chlorine [141, 142] which is the major oxidising agent. In this case, free-chlorine gaseous and or the generated chlorine-oxygen species such as hypochlorous acid (HClO) or hypochlorite ions (ClO^-) depending on the pH, oxidise the organic matter present in the effluents, according to the reactions presented below. Here, dye treatment occurs via several steps. Initially, active chlorine is oxidised to chlorine gas, which then reacts with water and produces hypochlorite ions. Finally, the hypochlorite ions oxidises and degrades dye molecules to dye intermediates and finally carbon dioxide.

$$2Cl^- \rightarrow Cl_{2(aq)} + 2e^- \quad (6)$$

$$Cl_{2(aq)} + H_2O \rightarrow ClO^- + Cl^- + H^+ \quad (7)$$

$$\text{Dye} + ClO^- \rightarrow \text{dye intermediates} \rightarrow CO_2 + H_2O + Cl^- \quad (8)$$

Method (ii) is concerned with the electro-Fenton process [143], where dye degradation occurs by hydroxyl radicals ($OH^\bullet$) formed from Fenton's reaction between catalytic Fe^{2+} and H_2O_2 electrogenerated from O_2 reduction. The overall dye degradation steps are shown in reactions below:

$$O_2\,(g) + 2H^+ + 2e^- \rightarrow H_2O_2 \quad (9)$$

$$H_2O_2\,(g) + Fe^{2+} + .H^+ \rightarrow Fe^{3+} + OH^\bullet + H_2O \quad (10)$$

$$\text{Dye} + OH^\bullet \rightarrow CO_2 + H_2O + H^+ \quad (11)$$

Thus, Fe^{2+} is continuously regenerated from the reduction of Fe^{3+}:

$$Fe^{3+} + e^- \rightarrow Fe^{2+} \quad (12)$$

This technique has a major disadvantage that a strong acidic medium is required. As the reactive dyeing process is usually carried out in a basic medium (pH > 10), a high amount of acid has to be added before the treatment. Subsequently, the treated effluent must be neutralised to be discharged. Consequently, the whole process produces a high increase of the wastewater salinity.

Clearly, Method (i) above is more suitable to treat effluents containing large volumes of chloride because there is no requirement of addition of any chemical reagent. However, Fenton reagent is needed in Method (ii). However, in Method (i), the combination of electrochemistry and chloride can produce haloforms such as chloroform, although it is not an inconvenience if the treated water is further treated in a biological plant to remove haloforms.

In fact, the concentration of haloforms in treated water has been verified to be very low, (48 mg L^{-1}) and they do not show any toxic effect on the microorganisms in biological plant [144]. Otherwise it is also possible to remove the generated haloforms by applying UV radiation to the electrochemical cell [145], or by adding H_2O_2 into the wastewater before UV radiation is started. By applying the first approach, López-Grimau and Gutiérrez [146] found improved kinetic rates of electrochemical degradation of some reactive azo dyes at titanium coated by platinum oxide (Ti/PtO) electrodes. The electrochemical method involving chlorine was found to be effective in such dye, as acid dyes [147] or disperse dyes [148]. In conjunction with photoelectrochemistry, Method (ii) yielded better performance for phtalocyanine dye degradation [149], but in this case, the metal ions liberated (as copper) have to be removed.

1.7.4.5 Photoassisted methods

Photoassisted electrochemical methods are based on the exposure of the effluent to a UV light source during the electrochemical treatment. In these procedures, the intensity and the wavelength of the incident light play an important role on the decolouration rate.

The most studied photoassisted method is the photo Fenton [150], which involves the simultaneous use of UV light and H_2O_2 (electrogenerated *in situ* with the presence of Fe^{2+}); and the photocatalysis method [151]. Photocatalysts such as TiO_2, WO_3, SnO_2, ZnO, CdS, act via hydroxyl radical and generate powerful oxidants. However, TiO_2 under UV radiation has been the preferred photocatalyst because of its low cost, nontoxicity, water insolubility and wide band gap, which consequently implies good stability and prevents photocorrosion [152-158].

Xie and Li [159] reported the coupling of electro-Fenton with electrocatalysis for the removal of the azo dye, orange-G. In comparison to other electro-oxidation and photoassisted methods, their results showed 96% of the dye removal in the coupled system. The major disadvantage of these methods is the excessive energy cost of the artificial UV light used. However, the use of sunlight [160] may be an inexpensive energy source although it has less catalytic power.

A brief summary of the advantages and disadvantages discussed in the above dye treatment methods is presented in Table 1.2.

Table 1.2 Advantages and disadvantages of existing dyes removal methods

	Technology	Advantage	Disadvantage	References
Physico-chemical treatment process	Coagulation/ Flocculation	Simple, economically feasible, satisfactory removal of disperse, sulphur and vat dyes	Removal is pH dependent, High sludge production, high cost of ferrous sulphate and ferric chloride, handling and disposal problems	[77]
	Biodegradation	Economically attractive. Direct, disperse and basic dyes have high level of adsorption on to activated sludge. Publicly acceptable treatment.	Slow process due to resistant to biodegradation. Necessary to create an optimal favourable environment. Maintenance and nutrition requirements	[89]
	Adsorption	The most effective adsorbent, great, capacity, produce a high-quality treated effluent	Ineffective against disperse and vat dyes, the regeneration is expensive and results in loos of the adsorbent, non-destructive process	[1, 66]
	Membrane filtration	Removes all dyes types, produce a high-quality treated effluent	High pressures, expensive, incapable of treating large volumes	[1, 72, 73]
	Ion-exchange	No loss of sorbent on regeneration, effective	Economic constraints, regeneration is expensive, not effective for disperse dyes	[1, 76]
Chemical oxidation	O_3	Applied in gaseous state, no alteration of volume. Good removal of almost all types of dyes; specially suitable for reactive dyes,	Removal is pH dependent, poor removal of disperse dyes, high cost of generation coupled with very short half-life time	[1, 83]

		Involves no sludge formation, necessitates short reaction times		
	ClO^-	No sludge production, little or no consumption of chemicals, efficiencnt for azo dye dyes	Unsuitable for disperse dye, formation of aromatic amines by-products	[3, 62]
	Fenton's process	Effective decolourization of both soluble and insoluble dyes; applicable even with high suspended solid concentration. Simple equipment and easy implementation and relatively cheap. Reduction of COD (chemical oxygen demand) possible, except reactive dyes	Effective within narrow pH range of <3.5; and involves sludge generation. Comparatively longer reaction time required	[1, 84]
	UV/H_2O_2	Involves no sludge formation, high COD removal, high colour removal efficiency, necessitates short reaction times	Not applicable for all types of dye, pH dependent, inefficient use of UV light increases the cost of the process	[81]
Biological	White-rot fungi	Economically feasible, natural clean up approach	Not applicable for all dyes, special azo dyes, technical constraints, slow process	[100]
	Microbial cultures	Low operation cost	Produce toxic aromatic amines, slow process, unable to cope with larger volume of wastewater	[2]
	Microbial biomass	Low operating cost, good efficiency and selectivity, no toxic effect on microorganisms	Slow process, performance depends on some external factors(pH, salts, temperature)	[110]

	Electrocoagulation	Effective decolorization of soluble/insoluble dyes; reduction of COD possible. Not affected by presence of salt in wastewater	Sludge production and secondary pollution (from chlorinated organics, heavy metals) are associated with electrocoagulation and indirect oxidation, respectively. Direct anodic oxidation requires further development for industrial acceptance. High cost of electricity is an impediment	[161, 162]
Electrochemical	Electrochemical reduction	Suitable for highly coloured reactive dyes containing wastewater, easy process	Poor efficiency compared to other electrochemical method, generation of toxic amino compounds	[124-126]
	Electrochemical oxidation	High efficiency depending on the anode material, simple process	Produce toxic by-product, high cost of electricity and electrode materials, strong acidic condition is required	[124, 141, 142]
	Photoassisted	No sludge production, considerable reduction of COD, potential of solar light utilization, produce toxic by-products	High cost of artificial UV light, high efficiency, particularly suitable for azo dye degradation	[151, 153, 159]

1.8 Conducting polymers as alternative materials for wastewater treatment

Conducting polymers have encompassed a very wide field of electrochemical research, which has led to numerous new applications in different areas in the last 30 years. Conducting polymer films behave similar to a redox polymer and have potential applications in electrocatalysis, solar energy conversion, corrosion, electronics, and many other areas. The redox polymer reaction is accompanied by a change in the electrical properties of the film from an insulator to an electrical conductor involving both electron and ion transport within the film [163].

Conducting polymers, such as polypyrrole, polythiophene, poly(3,4-ethylenedioxythiophene) and polyaniline are known to possess unusually high electrical conductivity in the doped state. For example, the conductivity of polypyrrole, polythiophene, poly(3,4-ethylenedioxythiophene) and polyaniline was reported to be 2000, 1000, 80 and 200 S cm^{-1} respectively, [164-166]. Therefore, these materials have been of great interests to chemists as well as physicists since their electrical properties were reported [167]. The number of electrochemical papers and patents on conducting polymers is very high. In 2011, Inzelt [168] published an article, in which he reported that the highest number published work was found for polyaniline (46%), followed by polypyrrole (34%), and polythiopene (18%), and small number of work with other polymers, *e.g.*, poly(3,4-ethylenedioxythiophene), polyindole, polycarbazole, polyfurane, poly(o-phenylene diamine), was also observed.

Among those conducting polymers, polypyrrole is especially promising for commercial applications because of its good environmental stability, facile synthesis, and higher conductivity (up to 2000 S cm^{-1}) [164] than many other conducting polymers. In the past decade, many reports about polypyrrole have been published [163, 164, 167-174]. The conductivity, electrochemical property, mechanical and thermal stability of polypyrrole attracted most interests of researchers to use polypyrrole as an electrode material. In 1994, Biswas and Roy [175] studied the thermal stability, morphological, and conductive characteristics of polypyrrole prepared in an aqueous medium. The results showed that the polypyrrole exhibits a spongy texture, the initial decomposition temperature at 180–237 °C, glass-transition temperature at 160–170 °C, and conductivity below 3 S cm^{-1}. Furthermore, all properties depended on the oxidising agent (*e.g.*, $FeCl_3$) and pyrrole feed composition.

Polypyrrole has been used as biosensors [169, 170], gas sensors [172, 173], conducting nano wires [174], microactuators [176], solid electrolytic capacitor [177], electrochromic windows and displays, packaging, polymeric batteries, electronic devices, functional membranes and coatings, *etc*. [178]. Polypyrrole coatings have an excellent thermal stability and are good candidates for use in carbon composites [179]. However, synthetically conductive polypyrrole is insoluble and infusible, which restricts its processing and applications in other fields. The problem has been extensively investigated and new application fields have also been explored in the past several years. For example, polypyrrole-based polymers can be used to load and release drugs and biomolecules [180]. Polypyrrole-based polymer blends can protect the corrosion of metals [181]. Owing to the strong adhesion of polypyrrole to iron or steel treated with nitric acid, polypyrrole-based polymers can be used as good adhesives [182].

Polypyrrole can be easily prepared by either a chemical or electrochemical oxidative polymerisation of pyrrole. In chemical polymerisation, the oxidants used are generally $(NH_4)_2S_2O_8$, H_2O_2 and salts containing transition metal ions, for example, Fe^{3+}, Cu^{2+}, Cr^{6+}, Ce^{4+}, Ru^{3+} and Mn^{7+} [183]. When only $(NH_4)_2S_2O_8$ is used as the oxidant [183], the addition of anionic surfactants causes moderate increases in the yields (1.36 g to 2.65 g) and great decreases in the conductivities (40 S cm^{-1} to 5 S cm^{-1}) [183]. In addition, it takes a very long time to filter the resultant polymers for the formation of fine colloidal particles. These phenomena are caused by interaction between $(NH_4)_2S_2O_8$ and the surfactant polypyrrole doped with sulfonate, as the dissociation of the anionic surfactant is prevented due to the presence of the highly concentrated and strongly electrolytic oxidant, the undissociated molecules of the surfactant appear to be thickly absorbed on the polypyrrole surface in the polymerisation process, so that it may act as the steric stabilizer.

The electropolymerisation reaction of polypyrrole is a complex process and its mechanism is still not fully understood. A number of mechanisms has been proposed [184-187] and are comprehensively reviewed [188, 189]. Among these, Diaz's mechanism [184] is the most accepted one and was supported by Waltman and Bargon [190, 191]. In this mechanism, the pyrrole activation occurs through electron transfer from the monomer forming a radical cation-rich solution near the electrode in several steps. Details of steps involved are given in Scheme 1.14. In this Scheme, step 1 involves the oxidation of the monomer, pyrrole, at the surface of

the electrode to form the cation radical pyrrole$^{+\bullet}$. This step also shows several resonance forms of this cation radical.

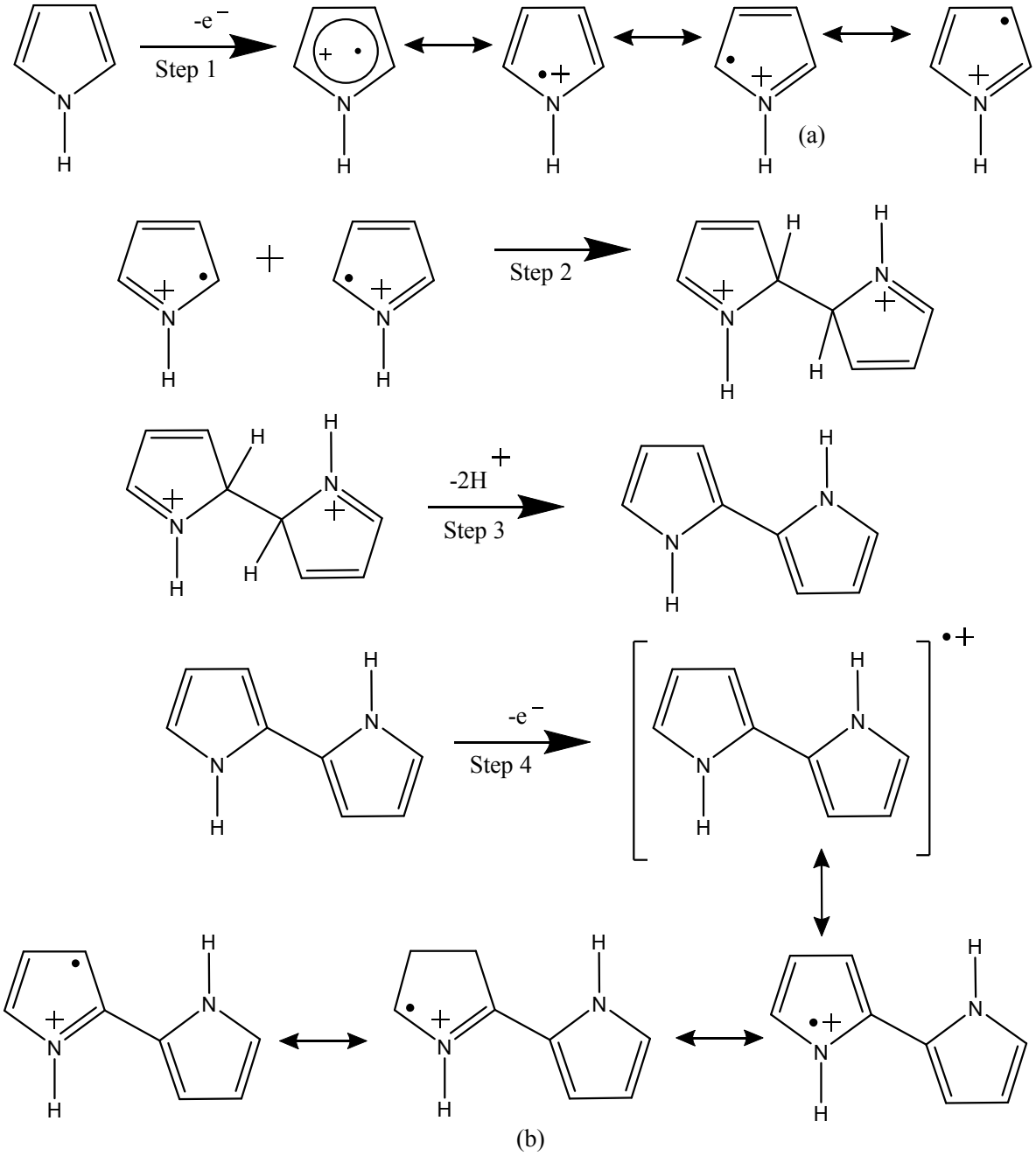

Scheme 1.14 Mechanism of electropolymerisation of pyrrole

The radical cation pyrrole$^{+\bullet}$, having a greater unpaired electron density in the α-position (resonance form (a) in step 1) dimerises *via* the resonance, as shown in step 2. The coupling between two radicals results in the formation of a bond between their α positions and the

formation of the dihydromer dication (product of step 2). In step 3, the loss of two protons stabilises the dihydromer dication to form an aromatic dimer. In step 4, the polymerisation reaction follows the oxidation of the aromatic dimer to the dimer radical cation, in which the unpaired electrons delocalise and form several resonance forms of this dimer cation radical The positions 5-5′ (α-position) are equally the most reactive areas and the resonance form (b) in step 4 is predominant with respect to the other forms.

Then the resonance form (b) reacts by 5 or 5′ with a monomer radical cation (resonance form (a)) to form a trimer dication, which deprotonates to give the neutral trimer and finally oxidation gives the trimer radical cation (steps not shown). The propagation continues via the same sequence of oxidation, coupling and deprotonation until the final polymer product, shown in Figure 1.15(a), is obtained.

The electropolymerisation does not give a neutral nonconducting polymer but its oxidised conducting form (doped). The final polymer chain, in fact, carries a positive charge every 3-4 pyrrole units [188], which is counter balanced by an anion. The structure of the doped polymer is shown in Figure 1.15(b).

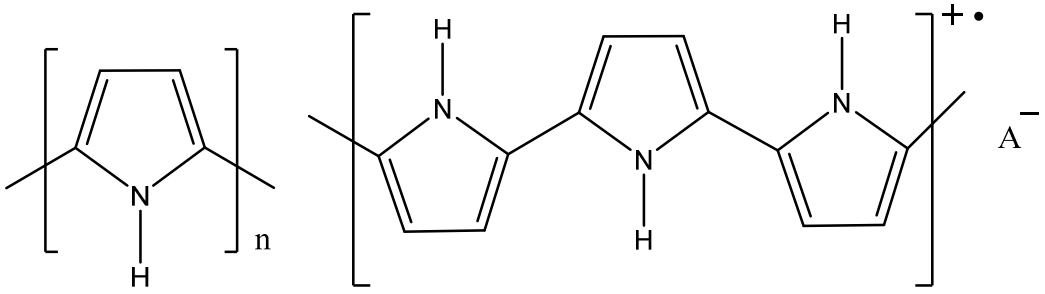

(a) (b)

Figure 1.15 Electropolymerised polypyrrole

Electrochemical film formation is often followed by stoichiometric determination of the number of electrons donated by each molecule. This value is generally found to be in between 2 and 2.7, where 2 electrons serve in the film formation and the excess charge is consumed by the polymer oxidation [192]. This number is generally in agreement with the number of anions found in the polymer by elementary analysis.

There are several reasons why this mechanism is believed to be the best representation of this reaction. Initially, this mechanism is in accord with electron paramagnetic resonance observations that show the existence of a π-type radical [193]. In addition, the elimination of H from the α-position indicated by this mechanism is in agreement with the observed drop in pH of the solution during polymerisation. This mechanism is also in agreement with the number of electrons consumed during the reaction, which has been determined to be 2.25 to 2.33 for pyrrole. In the chronoampromatric studies, Genies *et al*. [184] have shown that the film grows linearly with respect to polymerisation time and not to the polymerisation time half-life. Their observation showed that the rate-determining step during film growth is a coupling process and not the monomer diffusion towards the electrode [184].

Conducting electroactive polymers such as polypyrrole and polyaniline have attracted great attention due to their electrical conductivity and electroactivity [189, 194, 195]. Dye removal technology utilising conducting polymers and their composites are a viable option because of their economic, eco-friendly, abundant, and efficient technique.

The use of conducting polymer in wastewater treatment is a new area. A great interest has been recently directed to conducting polymers for the removal of dyes from wastewater. A limited number of conducting polymers, especially polypyrrole and polyaniline, has been reported to remove dyes from dye containing wastewater. Polypyrrole doped with releasable or exchangeable counter ions has been utilised for the removal of anionic dyes from aqueous solutions based on ion exchange properties of these polymer [196]. Wang *et al*. [197] reported the applicability of chemically synthesised polypyrrole for removal of the Nuclear Fast Red Kernechtrot dye (acts as dopant anion) from its solution. They also suggested that dye removal capacity of NaOH dedoped (NaOH treated) polypyrrole was improved by 40% compared to untreated polypyrrole.

Chowdhury *et al*. [198] studied the dye removal efficiency of organic dyes, methylene blue and procion red from their aqueous solution using chemically synthesised polyaniline. They reported that polyaniline as an adsorbent behaves as a charged surface and thus removes dyes from their aqueous solution.

Ansari and Mosayebzadeh [199, 200] and Ansari *et al*. [196, 201] reported that chemically synthesised polyaniline and polypyrrole can be used for removal of some azo dyes (methylene

blue, methyl orange, eosin y, tartrazine) from their aqueous solutions. Their dye removal method is mainly based on the coating on the surface of an adsorbent materials (*e.g.*, saw dust) with a chemically synthesised polymer (such as polypyrrole or polyaniline) in the presence of an oxidising agent. All the studies suggested that polymer coated adsorbent materials are more efficient in removing dyes than the adsorbent itself. They also suggested that this technique promises an environmental friendly approach for removal of water soluble azo dyes from wastewaters.

Ahmed and Kumar [202] reported the applicability of a chemically synthesised polyaniline / iron oxide composite for the removal of Amido Black 10B from its aqueous solution. They suggested that the composites showed considerable potential for the removal of Amido Black 10B. However, the removal capacity decreased with increasing pH but increased with temperature.

Therefore, the electropolymerised conducting polymer such as polypyrrole can also be used as a dye removal materials for the treatment of dye containing wastewater, due to their conducting property, simple synthesis, and environmentally friendly nature and high dye removal capacity. Moreover, the specially improved properties, for example, conductivity, porosity, surface area, and thermal and mechanical stability, can give a further boost for mass production, which will make products considerably less expensive and can be used in large scale industrial dye effluent treatment.

1.9 Electropolymerised polypyrrole as an ion exchanger membrane for the entrapment-liberation of Acid Red 1

The electrochemically controlled transport of simple anions and cations across conducting polymer membranes has been studied extensively [203-205]. In the case of polypyrrole, the transport mechanism involves an entrapment-liberation mechanism of anions or cations at a polymer membrane during the oxidation and reduction of polypyrrole by applying an oxidation and reduction potential, respectively [206].

The synthesis of polypyrrole usually involves electrochemical oxidation of its monomer, pyrrole, to yield a polymeric chain with a positive backbone, as shown in Scheme 1.14. In order to neutralise this charge, a counter anion (A^-) is entrapped in the backbone structure (Scheme 1.15). Many studies have shown that this entrapment process is electrochemically reversible [207, 208],

enabling polypyrrole to act as an anion exchanger membrane, depending upon the mobility of the entrapped counter anion [209]. Clearly, mobile anions can also be easily liberated from the polymeric film, as shown in Scheme 1.15. In this respect, several researchers have described the transport of small inorganic anions, for example, Cl^-, NO_3^- and SO_4^{2-} [210, 211], and small organic ions such as sodium *p*-toluenesulfonate (Na*p*TS) [210, 212], aza crown ether and tosylate [213-215] across polypyrrole by an anion exchanging mechanism.

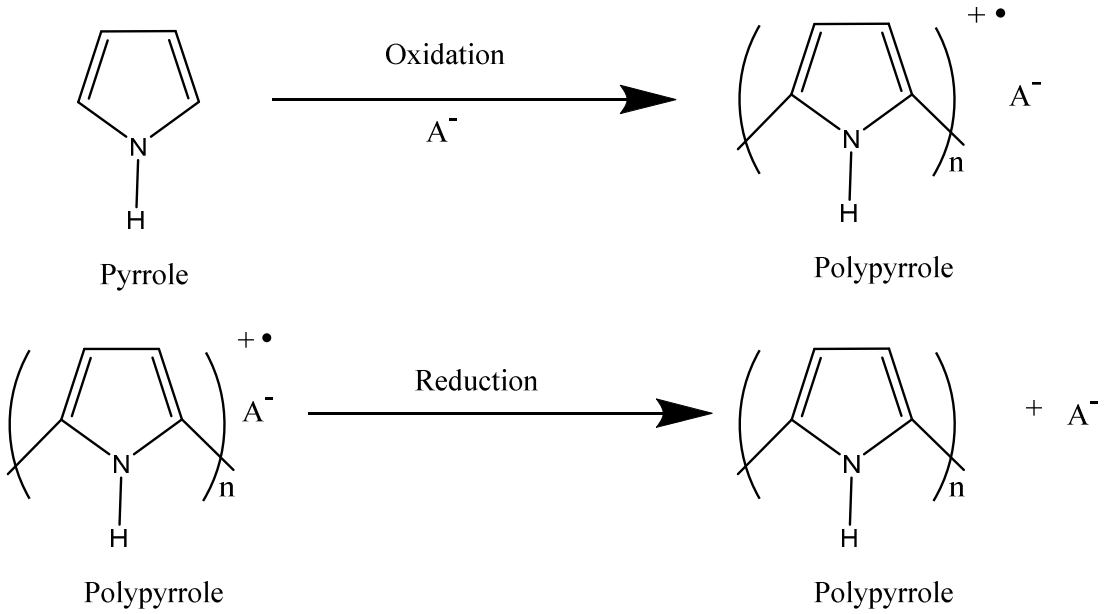

Scheme 1.15 Electrochemical oxidation and reduction of polypyrrole in presence of a counter anion.

The polymerisation of pyrrole in the presence of large counter anions, such as Acid Red 1, has not been studied as extensively as the use of small organic and inorganic ions. Tamm *et al*. [216] reported that the use of dodecylsulfate as a counter anion resulted in the dodecylsulfate ion firmly entrapped in the polymeric film and thus could not escape from the film. Instead, other ions migrate into or out of the film. Mirmohseni *et al*. [206] also noted the immobility of large counter anions such as dodecyl benzene sulfonic acid. Gao *et al*. [217] studied polypyrrole films grown in the presence of indigo carmine. The bulky indigo carmine dopant was found to be less mobile compared to small anions which can move freely in a polymer film, resulting in only slow diffusion over time.

Our interest in this ion exchange system of elecropolymerised conducting polypyrrole has led us to consider the entrapment-liberation of charged organic molecules, such as synthetic azo

dyes, across conducting polymer membrane films for the development of a treatment method for dyes in textile effluents. In the present work, the entrapment-liberation of the sulfonated aromatic compound, Acid Red 1, as an azo dye at elctropolymerised conducting polypyrrole was considered. The entrapment-liberation of Acid Red 1 across the polypyrrole film is expected to expand the scope of potential application in the area of removing and recovering organic pollutants such as dyes from wastewater.

1.10 Scope and aims of the project

Organic dyes are commonly used as colourants in the textile industry. However, their presence in effluent leads to severe environmental problems because of their toxicity, carcinogenicity and undesirable water colouration. Thus it is necessary to treat dye containing wastewater before being discharged in hydrosphere. However, current dye effluent treatment techniques suffer from several limitation such as inefficient treatment, time consuming, high cost and, most importantly, generation of toxic by-products. To minimise these problems, there is a need for development of an alternative treatment technique that is efficient as well as environmentally friendly in removing dyes from industrial wastewater.

Overall main aims of this project are to develop the use of conducting polypyrrole films as a potential green technology for electrochemical treatment of azo dyes in industrial effluents without producing any toxic by-products. More specifically, this work aims to:

(1) Demonstrate the feasibility of electropolymerised polypyrrole film as an efficient tool for the entrapment and liberation of the azo dye, Acid Red 1, from its synthetic solution;
(2) Develop a kinetic model for Acid Red 1 entrapment at electropolymerised polypyrrole films and the associated thermodynamics;
(3) Synthesise and characterise mechanically stable polypyrrole-reduced graphene oxide composite films for Acid Red 1 entrapment and liberation performance.

Each of the following chapters is then devoted to the detailed description and discussion of the results obtained in achieving the respective aim.

Chapter 2 will provide details of experimental techniques used in this research. Here, we will describe the synthesis and characterisation techniques of polypyrrole films, as well as method

for the evaluation of Acid Red 1 entrapment-liberation in polypyrrole films. This chapter will also describe the methods used for experimental data analysis.

In Chapter 3, we report the characterisation of Acid Red 1 entrapped polypyrrole films and optimised Acid Red 1 entrapment parameters in polypyrrole films. We will also evaluate entrapment-liberation efficiency of Acid Red 1 in polypyrrole films.

In Chapter 4, we focus on the kinetics, isotherms and thermodynamics of the electrochemical entrapment of the Acid Red 1, at conducting polypyrrole films.

Chapter 5 is devoted to the synthesis, characterisation and evaluation of Acid Red 1 entrapment and liberation at mechanically stable polypyrrole-reduced graphene oxide composite films.

Finally, in Chapter 6, some concluding remarks on the development and applicability of polypyrrole and polypyrrole-reduced graphene oxide composite films for electrochemical entrapment and liberation of Acid Red 1 will be presented. To this end, limitations of this treatment will also be discussed. Further, several suggestions will be proposed as feasible future work for this project.

1.11 References

1. Robinson, T., McMullan, G., Marchant, R. and Nigam, P. Remediation of dyes in textile effluent: A critical review on current treatment technologies with a proposed alternative. *Bioresource Technology*, 2001. **77**(3): 247-255.
2. Banat, I.M., Nigam, P., Singh, D. and Marchant, R. Microbial decolorization of textile-dyecontaining effluents: A review. *Bioresource Technology*, 1996. **58**(3): 217-227.
3. Hastie, J., Bejan, D., Teutli-León, M. and Bunce, N.J. Electrochemical methods for degradation of Orange II (sodium 4-(2-hydroxy-1-naphthylazo)benzenesulfonate). *Industrial and Engineering Chemistry Research*, 2006. **45**(14): 4898-4904.
4. Van der Zee, F.P. and Villaverde, S. Combined anaerobic-aerobic treatment of azo dyes-a short review of bioreactor studies. *Water Research*, 2005. **39**(8): 1425-1440.
5. Seshadri, S., Bishop, P.L. and Agha, A.M. Anaerobic/aerobic treatment of selected azo dyes in wastewater. *Waste Management*, 1994. **14**(2): 127-137.

6. Pearce, C., Lloyd, J. and Guthrie, J. The removal of colour from textile wastewater using whole bacterial cells: A review. *Dyes and Pigments*, 2003. **58**(3): 179-196.

7. Forgacs, E., Cserháti, T. and Oros, G. Removal of synthetic dyes from wastewaters: A review. *Environment International*, 2004. **30**(7): 953-971.

8. George Z. Kyzas, Margaritis Kostoglou, and, N.K.L. and Bikiaris, D.N. Decolorization of dyeing wastewater using polymeric absorbents - an overview. In *Eco-friendly textile dyeing and finishing*. Gunay, M., ed.2013, InTech: Grece. p. 177-206.

9. Kamilaki, A. The removal of reactive dyes from textile effluents-a bioreactor approach employing whole bacterial cells. 2000, PhD thesis, UK: University of Leeds.

10. Allègre, C., Moulin, P., Maisseu, M. and Charbit, F. Treatment and reuse of reactive dyeing effluents. *Journal of Membrane Science*, 2006. **269**(1–2): 15-34.

11. Kyzas, G.Z., Kostoglou, M., Vassiliou, A.A. and Lazaridis, N.K. Treatment of real effluents from dyeing reactor: Experimental and modeling approach by adsorption onto chitosan. *Chemical Engineering Journal*, 2011. **168**(2): 577-585.

12. Khan, A.A. and Husain, Q. Decolorization and removal of textile and non-textile dyes from polluted wastewater and dyeing effluent by using potato (*solanum tuberosum*) soluble and immobilized polyphenol oxidase. *Bioresource Technology*, 2007. **98**(5): 1012-1019.

13. Aksu, Z. Application of biosorption for the removal of organic pollutants: A review. *Process Biochemistry*, 2005. **40**(3): 997-1026.

14. Vandevivere, P.C., Bianchi, R. and Verstraete, W. Treatment and reuse of wastewater from the textile wet-processing industry: Review of emerging technologies. *Journal of Chemical Technology and Biotechnology*, 1998. **72**(4): 289-302.

15. Sun, Q. and Yang, L. The adsorption of basic dyes from aqueous solution on modified peat-resin particle. *Water Research*, 2003. **37**(7): 1535-1544.

16. Hunger, K. Industrial dyes: Chemistry, properties, applicationsed. 2007: John Wiley and Sons.

17. Rangnekar, D. and Singh, P. An introduction to synthetic dyes. 1980, Himalaya Publishing House: Bombay.

18. Suteu, D., Zaharia, C. and Malutan, T. Removal of Orange 16 reactive dye from aqueous solutions by waste sunflower seed shells. *Journal of the Serbian Chemical Society*, 2011. **76**(4): 607-624.

19. Welham, A. The theory of dyeing (and the secret of life). *Journal of the Society of Dyers and Colourists*, 2000. **116**(5): 140-143.

20. Zollinger, H. Color chemistry : Syntheses, properties, and applications of organic dyes and pigmentsed. 1991, VCH Publishers: New York, USA

21. Nigam, P., Banat, I.M., Singh, D. and Marchant, R. Microbial process for the decolorization of textile effluent containing azo, diazo and reactive dyes. *Process Biochemistry*, 1996. **31**(5): 435-442.

22. Shore, J. Cellulosics dyeing. 1995, Society of Dyers and Colourists: Bradford.

23. Kiernan, J. Classification and naming of dyes, stains and fluorochromes. *Biotechnic and Histochemistry*, 2001. **76**(5-6): 261-278.

24. Venkataraman, K. The chemistry of synthetic dyes. 2012, Elsevier Science: New York.

25. Tiffe, H.W., Matzke, K.H. and Thiessen, G. The acridine dyes: Their purification, physicochemical, and cytochemical properties. *Histochemistry*, 1977. **53**(1): 63-77.

26. Nguyen, T.A. and Juang, R.-S. Treatment of waters and wastewaters containing sulfur dyes: A review. *Chemical Engineering Journal*, 2013. **219**: 109-117.

27. Cariell, C., Barclay, S., Naidoo, N., Buckley, C., Mulholland, D. and Senior, E. Microbial decolourisation of a reactive azo dye under anaerobic conditions. *Water SA*, 1995. **21**(1): 61-69.

28. Bae, J.-S. and Freeman, H.S. Aquatic toxicity evaluation of new direct dyes to the daphnia magna. *Dyes and Pigments*, 2007. **73**(1): 81-85.

29. Kusic, H., Juretic, D., Koprivanac, N., Marin, V. and Božić, A.L. Photooxidation processes for an azo dye in aqueous media: Modeling of degradation kinetic and ecological parameters evaluation. *Journal of Hazardous Materials*, 2011. **185**(2): 1558-1568.

30. Chung, K.T. and Stevens, S.E. Degradation azo dyes by environmental microorganisms and helminths. *Environmental Toxicology and Chemistry*, 1993. **12**(11): 2121-2132.

31. Chang, J.-S., Chou, C., Lin, Y.-C., Lin, P.-J., Ho, J.-Y. and Hu, T.L. Kinetic characteristics of bacterial azo-dye decolorization by *pseudomonas luteola*. *Water Research*, 2001. **35**(12): 2841-2850.

32. Jin, X.-C., Liu, G.-Q., Xu, Z.-H. and Tao, W.-Y. Decolorization of a dye industry effluent by *Aspergillus fumigatus* XC6. *Applied Microbiology and Biotechnology*, 2007. **74**(1): 239-243.

33. Saratale, R., Saratale, G., Chang, J. and Govindwar, S. Bacterial decolorization and degradation of azo dyes: A review. *Journal of the Taiwan Institute of Chemical Engineers*, 2011. **42**(1): 138-157.

34. Zollinger, H. Color chemistry: Synthesis, properties of organic dyes and pigments. 1987, VCH Publishers: New York, USA, p 92–102.

35. Chang, J.-S., Chou, C. and Chen, S.-Y. Decolorization of azo dyes with immobilized *pseudomonas luteola*. *Process Biochemistry*, 2001. **36**(8–9): 757-763.

36. Rajaguru, P., Fairbairn, L.J., Ashby, J., Willington, M., Turner, S., Woolford, L., Chinnasamy, N. and Rafferty, J.A. Genotoxicity studies on the azo dye Direct Red 2 using the *in vivo* mouse bone marrow micronucleus test. *Mutation Research/Genetic Toxicology and Environmental Mutagenesis*, 1999. **444**(1): 175-180.

37. Tsuboy, M.S., Angeli, J.P.F., Mantovani, M.S., Knasmüller, S., Umbuzeiro, G.A. and Ribeiro, L.R. Genotoxic, mutagenic and cytotoxic effects of the commercial dye CI Disperse Blue 291 in the human hepatic cell line HepG2. *Toxicology in Vitro*, 2007. **21**(8): 1650-1655.

38. Esancy, J., Freeman, H. and Claxton, L. The effect of alkoxy substituents on the mutagenicity of some aminoazobenzene dyes and their reductive-cleavage products. *Mutation Research/Reviews in Genetic Toxicology*, 1990. **238**(1): 1-22.

39. Garg, A., Bhat, K.L. and Bock, C.W. Mutagenicity of aminoazobenzene dyes and related structures: A QSAR/QPAR investigation. *Dyes and Pigments*, 2002. **55**(1): 35-52.

40. De Aragão Umbuzeiro, G., Freeman, H., Warren, S.H., Kummrow, F. and Claxton, L.D. Mutagenicity evaluation of the commercial product CI Disperse Blue 291 using

different protocols of the Salmonella assay. *Food and Chemical Toxicology*, 2005. **43**(1): 49-56.

41. Chung, K.-T. and Cerniglia, C.E. Mutagenicity of azo dyes: Structure-activity relationships. *Mutation Research/Reviews in Genetic Toxicology*, 1992. **277**(3): 201-220.

42. Brown, J.P., Roehm, G.W. and Brown, R.J. Mutagenicity testing of certified food colours and related azo, xanthene and triphenylmethane dyes with the Salmonella/microsome system. *Mutation Research/Fundamental and Molecular Mechanisms of Mutagenesis*, 1978. **56**(3): 249-271.

43. Venturini, S. and Tamaro, M. Mutagenicity of anthraquinone and azo dyes in Ames' *Salmonella typhimurium* test. *Mutation Research/Genetic Toxicology*, 1979. **68**(4): 307-312.

44. Nestmann, E.R., Kowbel, D.J. and Wheat, J.A. Mutagenicity in Salmonella of dyes used by defence personnel for the detection of liquid chemical warfare agents. *Carcinogenesis*, 1981. **2**(9): 879-883.

45. Chung, K.-T., Stevens, S.E. and Cerniglia, C.E. The reduction of azo dyes by the intestinal microflora. *Critical Reviews in Microbiology*, 1992. **18**(3): 175-190.

46. Fujita, S. and Peisach, J. Liver microsomal cytochromes P-450 and azoreductase activity. *Journal of Biological Chemistry*, 1978. **253**(13): 4512-4513.

47. Walker, R. The metabolism of azo compounds: A review of the literature. *Food and Cosmetics Toxicology*, 1970. **8**(6): 659-676.

48. Prival, M.J. and Mitchell, V.D. Analysis of a method for testing azo dyes for mutagenic activity in *Salmonella typhimurium* in the presence of flavin mononucleotide and hamster liver S9. *Mutation Research/Environmental Mutagenesis and Related Subjects*, 1982. **97**(2): 103-116.

49. Choudhary, G. Human health perspectives on environmental exposure to benzidine: A review. *Chemosphere*, 1996. **32**(2): 267-291.

50. Chung, K.-T., Hughes, T.J. and Claxton, L.D. Comparison of the mutagenic specificity induced by four nitro-group-containing aromatic amines in *Salmonella typhimurium his*

genes. *Mutation Research/Genetic Toxicology and Environmental Mutagenesis*, 2000. **465**(1): 165-171.

51. Pinheiro, H., Touraud, E. and Thomas, O. Aromatic amines from azo dye reduction: Status review with emphasis on direct UV spectrophotometric detection in textile industry wastewaters. *Dyes and Pigments*, 2004. **61**(2): 121-139.

52. Khalid, A., Arshad, M. and Crowley, D.E. Biodegradation potential of pure and mixed bacterial cultures for removal of 4-nitroaniline from textile dye wastewater. *Water Research*, 2009. **43**(4): 1110-1116.

53. Saupe, A. High-rate biodegradation of 3-and 4-nitroaniline. *Chemosphere*, 1999. **39**(13): 2325-2346.

54. Weisburger, J.H. Comments on the history and importance of aromatic and heterocyclic amines in public health. *Mutation Research/Fundamental and Molecular Mechanisms of Mutagenesis*, 2002. **506**: 9-20.

55. Ekici, P., Leupold, G. and Parlar, H. Degradability of selected azo dye metabolites in activated sludge systems. *Chemosphere*, 2001. **44**(4): 721-728.

56. Pereira, M.F.R., Soares, S.F., Órfão, J.J.M. and Figueiredo, J.L. Adsorption of dyes on activated carbons: Influence of surface chemical groups. *Carbon*, 2003. **41**(4): 811-821.

57. Marco, A., Esplugas, S. and Saum, G. How and why combine chemical and biological processes for wastewater treatment. *Water Science and Technology*, 1997. **35**(4): 321–327.

58. Crini, G. Non-conventional low-cost adsorbents for dye removal: A review. *Bioresource Technology*, 2006. **97**(9): 1061-1085.

59. Ghoreishi, S.M. and Haghighi, R. Chemical catalytic reaction and biological oxidation for treatment of non-biodegradable textile effluent. *Chemical Engineering Journal*, 2003. **95**(1): 163-169.

60. Sirianuntapiboon, S., Chairattanawan, K. and Jungphungsukpanich, S. Some properties of a sequencing batch reactor system for removal of vat dyes. *Bioresource Technology*, 2006. **97**(10): 1243-1252.

61. Choy, K.K.H., McKay, G. and Porter, J.F. Sorption of acid dyes from effluents using activated carbon. *Resources, Conservation and Recycling*, 1999. **27**(1-2): 57-71.

62. Slokar, Y.M. and Le Marechal, A.M. Methods of decoloration of textile wastewaters. *Dyes and Pigments*, 1998. **37**(4): 335-356.

63. Kumar, M.N.V.R., Sridhari, T.R., Bhavani, K.D. and Dutta, P.K. Trends in color removal from textile mill effluents. *Colourage*, 1998. **45**(8): 25-34.

64. Ramakrishna, K.R. and Viraraghavan, T., Dye removal using low cost adsorbents. *Water Science and Technology*, 1997. **36**(2-3): 189-196.

65. Nassar, M.M. and El-Geundi, M.S. Comparative cost of colour removal from textile effluents using natural adsorbents. *Journal of Chemical Technology and Biotechnology*, 1991. **50**(2): 257-264.

66. Raghavacharya, C. Colour removal from industrial effluents. *Chemical Engineering World*, 1997. **32**(7): 53-54.

67. Rao, K.C.L.N., Krishnaiah, K. and Ashutosh. Colour removal from a dyestuff industry effluent using activated carbon. *Indian Journal of Chemical Technology*, 1994. **1**(1): 13-19.

68. Aktaş, Ö. and Çeçen, F. Bioregeneration of activated carbon: A review. *International Biodeterioration and Biodegradation*, 2007. **59**(4): 257-272.

69. Poots, V.J.P., McKay, G. and Healy, J.J. The removal of acid dye from effluent using natural adsorbents - I. Peat. *Water Research*, 1976. **10**(12): 1061-1066.

70. Nigam, P., Armour, G., Banat, I.M., Singh, D. and Marchant, R. Physical removal of textile dyes from effluents and solid-state fermentation of dye-adsorbed agricultural residues. *Bioresource Technology*, 2000. **72**(3): 219-226.

71. Gupta, G.S., Prasad, G. and Singh, V.N. Removal of chrome dye from aqueous solutions by mixed adsorbents: Fly ash and coal. *Water Research*, 1990. **24**(1): 45-50.

72. Mishra, G. and Tripathy, M. A critical review of the treatments for decolourization of textile effluent. *Colourage*, 1993. **40**(10): 35-38.

73. Xu, Y., Lebrun, R.E., Gallo, P.J. and Blond, P. Treatment of textile dye plant effluent by nanofiltration membrane. *Separation Science and Technology*, 1999. **34**(13): 2501-2519.

74. Babu, B.R., Parande, A., Raghu, S. and Kumar, T.P. Cotton textile processing: Waste generation and effluent treatment. *Journal of Cotton Science*, 2007. **11**(3): 141-153.

75. Sójka-Ledakowicz, J., Koprowski, T., Machnowski, W. and Knudsen, H.H. Membrane filtration of textile dyehouse wastewater for technological water reuse. *Desalination*, 1998. **119**(1–3): 1-9.

76. Anjaneyulu, Y., Sreedhara Chary, N. and Samuel Suman Raj, D. Decolourization of industrial effluents-available methods and emerging technologies-a review. *Reviews in Environmental Science and Bio/Technology*, 2005. **4**(4): 245-273.

77. Gahr, F., Hermanutz, F. and Oppermann, W. Ozonation - an important technique to comply with new german laws for textile wastewater treatment. *Water Science and Technology*, 1994. **30**(3): 255-263.

78. Hosono, M., Arai, H., Aizawa, M., Yamamoto, I., Shimizu, K. and Sugiyama, M. Decoloration and degradation of azo dye in aqueous solution supersaturated with oxygen by irradiation of high-energy electron beams. *Applied Radiation and Isotopes*, 1993. **44**(9): 1199-1203.

79. Metcahf, E. Wastewater engineering: Treatment and reuse. 2003, McGraw-Hill Educatin: New York.

80. Lin, S.H. and Lin, C.M. Treatment of textile waste effluents by ozonation and chemical coagulation. *Water Research*, 1993. **27**(12): 1743-1748.

81. Ince, N.H. and Gönenç, D.T. Treatability of a textile azo dye by UV/H_2O_2. *Environmental Technology*, 1997. **18**(2): 179-185.

82. Alaton, I.A., Balcioglu, I.A. and Bahnemann, D.W. Advanced oxidation of a reactive dyebath effluent: Comparison of O_3, H_2O_2/UV-C and TiO_2/UV-a processes. *Water Research*, 2002. **36**(5): 1143-1154.

83. Evans, G.M. and Furlong, J.C. Environmental biotechnology: Theory and application. 2003, Wiley: UK.

84. Kang, S.F., Liao, C.H. and Po, S.T. Decolorization of textile wastewater by photo-fenton oxidation technology. *Chemosphere*, 2000. **41**(8): 1287-1294.

85. Lin, J.j., Zhao, X.s., Liu, D., Yu, Z.g., Zhang, Y. and Xu, H. The decoloration and mineralization of azo dye CI Acid Red 14 by sonochemical process: Rate improvement via Fenton's reactions. *Journal of Hazardous Materials*, 2008. **157**(2-3): 541-546.

86. Safarzadeh-Amiri, A., James R. Bolton and Cater, S.R. Ferrioxalate-mediated photodegradation of organic pollutants in contaminated water. *Water Research*, 1997. **31**(4): 787–798.

87. Yang, Y., Travis, W.D. and Michael, B. Decolorization of dyes using UV/H_2O_2 photochemical oxidation. *Textile Chemist and Colorist*, 1998. **30**(4): 27-35.

88. Peralta-Zamora, P., Kunz, A., de Moraes, S.G., Pelegrini, R., de Campos Moleiro, P., Reyes, J. and Duran, N. Degradation of reactive dyes I. A comparative study of ozonation, enzymatic and photochemical processes. *Chemosphere*, 1999. **38**(4): 835-852.

89. McMullan, G., Meehan, C., Conneely, A., Kirby, N., Robinson, T., Nigam, P., Banat, I.M., Marchant, R. and Smyth, W.F. Microbial decolourisation and degradation of textile dyes. *Applied Microbiology and Biotechnology*, 2001. **56**(1-2): 81-87.

90. Bhattacharyya, K.G. and Sarma, A. Adsorption characteristics of the dye, Brilliant Green, on neem leaf powder. *Dyes and Pigments*, 2003. **57**(3): 211-222.

91. Barr, D.P. and Aust, S.D. Mechanisms white rot fungi use to degrade pollutants. *Environmental Science and Technology*, 1994. **28**(2): 78A-87A.

92. Chao, W.L. and Lee, S.L. Decoloration of azo dyes by three whiterot fungi: Influence of carbon source. *World Journal of Microbiology and Biotechnology*, 1994. **10**(5): 556-559.

93. Reddy, C.A. The potential for white-rot fungi in the treatment of pollutants. *Current Opinion in Biotechnology*, 1995. **6**(3): 320-328.

94. Davis, M.W., Glaser, J.A., Evans, J.W. and Lamar, R.T. Field evaluation of the lignin-degrading fungus *Phanerochaete sordida* to treat creosote-contaminated soil. *Environmental Science and Technology*, 1993. **27**(12): 2572-2576.

95. Kirby, N., McMullan, G. and Marchant, R. Bioremediation of textile industry wastewater by white-rot fungi. *Studies in Environmental Science*, 1997. **66**: 711-718.

96. Shree, S.N. Microbial degradation of synthetic dyes in wastewatersed. 2014, Springer International Publishing.

97. Archibald, F. and Roy, B. Production of manganic chelates by laccase from the lignin-degrading fungus trametes (coriolus) versicolor. *Applied and Environmental Microbiology*, 1992. **58**(5): 1496-1499.

98. Thurston, C.F. The structure and function of fungal laccases. *Microbiology*, 1994. **140**(1): 19-26.

99. Schliephake, K. and Lonergan, G. Laccase variation during dye decolourisation in a 200 L packed-bed bioreactor. *Biotechnology Letters*, 1996. **18**(8): 881-886.

100. Paszczynski, A. and Crawford, R.L. Potential for bioremediation of xenobiotic compounds by the white-rot fungus phanerochaete chrysosporium. *Biotechnology Progress*, 1995. **11**(4): 368-379.

101. Fernando, E., Keshavarz, T. and Kyazze, G. Simultaneous co-metabolic decolourisation of azo dye mixtures and bio-electricity generation under thermophillic (50 °C) and saline conditions by an adapted anaerobic mixed culture in microbial fuel cells. *Bioresource Technology*, 2013. **127**: 1-8.

102. Knapp, J.S. and Newby, P.S. The microbiological decolorization of an industrial effluent containing a diazo-linked chromophore. *Water Research*, 1995. **29**(7): 1807-1809.

103. Nigam, P. and Marchant, R. Selection of a substratum for composing biofilm system of a textile-effluent decolourizing bacteria. *Biotechnology Letters*, 1995. **17**(9): 993-996.

104. Ogawa, T. and Yatome, C. Biodegradation of azo dyes in multistage rotating biological contractor immobilized by assimilating bacteria. *Bulletin of Environmental Contamination and Toxicology*, 1990. **44**(4): 561-566.

105. Keck, A., Klein, J., Kudlich, M., Stolz, A., Knackmuss, H.J. and Mattes, R. Reduction of azo dyes by redox mediators originating in the naphthalenesulfonic acid degradation pathway of Sphingomonas sp. strain BN6. *Applied and Environmental Microbiology*, 1997. **63**(9): 3684-3690.

106. Kudlich, M., Keck, A., Klein, J. and Stolz, A. Localization of the enzyme system involved in anaerobic reduction of azo dyes by Sphingomonas sp. strain BN6 and effect

of artificial redox mediators on the rate of azo dye reduction. *Applied and Environmental Microbiology*, 1997. **63**(9): 3691-3694.

107. Zissi, U., Lyberatos, G. and Pavlou, S. Biodegradation of *p*-aminoazobenzene by *Bacillus subtilis* under aerobic conditions. *Journal of Industrial Microbiology and Biotechnology*, 1997. **19**(1): 49-55.

108. Banat, I.M., Nigam, P., McMullan, G., Marchant, R. and Singh, D. The isolation of thermophilic bacterial cultures capable of textile dyes decolorization. *Environment International*, 1997. **23**(4): 547-551.

109. Hu, T.-L. Removal of reactive dyes from aqueous solution by different bacterial genera. *Water Science and Technology*, 1996. **34**(10): 89-95.

110. Polman, J.K. and Breckenridge, C.R. Biomass-mediated binding and recovery of textile dyes from waste effluents. *Textile Chemist and Colorist*, 1996. **28**(4): 31-35.

111. Bustard, M., McMullan, G. and McHale, A.P. Biosorption of textile dyes by biomass derived from *Kluyveromyces marxianus* IMB3. *Bioprocess Engineering*, 1998. **19**(6): 427-430.

112. Riordan, C. and McHale, A.P. Removal of lead from solution using non-living residual brewery yeast. *Bioprocess Engineering*, 1998. **19**(4): 277-280.

113. Zhou, W. and Zimmermann, W. Decolorization of industrial effluents containing reactive dyes by actinomycetes. *FEMS Microbiology Letters*, 1993. **107**(2-3): 157-161.

114. Modak, J. and Natarajan, K. Biosorption of metals using nonliving biomass-a review. *Minerals and Metallurgical Processing*, 1995. **12**(4): 189-196.

115. Carneiro, P.A., Osugi, M.E., Fugivara, C.l.S., Boralle, N., Furlan, M. and Zanoni, M.V.B. Evaluation of different electrochemical methods on the oxidation and degradation of Reactive Blue 4 in aqueous solution. *Chemosphere*, 2005. **59**(3): 431-439.

116. Lee, Y.H. and Pavlostathis, S.G. Decolorization and toxicity of reactive anthraquinone textile dyes under methanogenic conditions. *Water Research*, 2004. **38**(7): 1838-1852.

117. Oliveira, G., Ferraz, E., Chequer, F., Grando, M., Angeli, J., Tsuboy, M., Marcarini, J., Mantovani, M., Osugi, M. and Lizier, T. Chlorination treatment of aqueous samples reduces, but does not eliminate, the mutagenic effect of the azo dyes Disperse Red 1,

Disperse Red 13 and Disperse Orange 1. *Mutation Research/Genetic Toxicology and Environmental Mutagenesis*, 2010. **703**(2): 200-208.

118. Carneiro, P.A., Umbuzeiro, G.A., Oliveira, D.P. and Zanoni, M.V.B. Assessment of water contamination caused by a mutagenic textile effluent/dyehouse effluent bearing disperse dyes. *Journal of Hazardous Materials*, 2010. **174**(1): 694-699.

119. Guaratini, C.C.I. and Zanoni, M.V.B. Textile dyes. *Quimica Nova*, 2000. **23**(1): 71-78.

120. Guivarch, E., Trevin, S., Lahitte, C. and Oturan, M.A. Degradation of azo dyes in water by electro-Fenton process. *Environmental Chemistry Letters*, 2003. **1**(1): 38-44.

121. Carmen, Z. and Daniela, S. Textile organic dyes–characteristics, polluting effects and separation/elimination procedures from industrial effluents–a critical overview. In *Organic pollutants ten years after the stockholm convention-environmental and analytical update*. Puzyn, D.T., ed. 2012, Intech: Croatia. p. 55-86.

122. Zaharia, C., Suteu, D., Muresan, A., Muresan, R. and Popescu, A. Textile wastewater treatment by homogeneous oxidation with hydrogen peroxide. *Environmental Engineering and Management Journal*, 2009. **8**(6): 1359-1369.

123. Kobya, M., Demirbas, E., Can, O.T. and Bayramoglu, M. Treatment of levafix orange textile dye solution by electrocoagulation. *Journal of Hazardous Materials*, 2006. **132**(2–3): 183-188.

124. Martínez-Huitle, C.A. and Brillas, E. Decontamination of wastewaters containing synthetic organic dyes by electrochemical methods: A general review. *Applied Catalysis B: Environmental*, 2009. **87**(3): 105-145.

125. Bechtold, T., Mader, C. and Mader, J. Cathodic decolourization of textile dyebaths: Tests with full scale plant. *Journal of Applied Electrochemistry*, 2002. **32**(9): 943-950.

126. Gooding, J.J., Compton, R.G., Brennan, C.M. and Atherton, J.H. The mechanism of the electro-reduction of some azo dyes. *Electroanalysis*, 1996. **8**(6): 519-523.

127. Vaněrková, D., Sakalis, A., Holčapek, M., Jandera, P. and Voulgaropoulos, A. Analysis of electrochemical degradation products of sulphonated azo dyes using high-performance liquid chromatography/tandem mass spectrometry. *Rapid Communications in Mass Spectrometry*, 2006. **20**(19): 2807-2815.

128. Stucki, S., Kötz, R., Carcer, B. and Suter, W. Electrochemical waste water treatment using high overvoltage anodes part II: Anode performance and applications. *Journal of Applied Electrochemistry*, 1991. **21**(2): 99-104.

129. Polcaro, A.M., Palmas, S., Renoldi, F. and Mascia, M. On the performance of Ti/SnO_2 and Ti/PbO_2 anodes in electrochemical degradation of 2-chlorophenol for wastewater treatment. *Journal of Applied Electrochemistry*, 1999. **29**(2): 147-151.

130. Feng, J., Houk, L.L., Johnson, D.C., Lowery, S.N. and Carey, J.J. Electrocatalysis of anodic oxygen-transfer reactions: The electrochemical incineration of benzoquinone. *Journal of the Electrochemical Society*, 1995. **142**(11): 3626-3632.

131. Tahar, N.B. and Savall, A. Electrochemical degradation of phenol in aqueous solution on bismuth doped lead dioxide: A comparison of the activities of various electrode formulations. *Journal of Applied Electrochemistry*, 1999. **29**(3): 277-283.

132. Cañizares, P., Díaz, M., Domínguez, J.A., García-Gómez, J. and Rodrigo, M.A. Electrochemical oxidation of aqueous phenol wastes on synthetic diamond thin-film electrodes. *Industrial and Engineering Chemistry Research*, 2002. **41**(17): 4187-4194.

133. Gherardini, L., Michaud, P., Panizza, M., Comninellis, C. and Vatistas, N. Electrochemical oxidation of 4-chlorophenol for wastewater treatment: Definition of normalized current efficiency (ϕ). *Journal of the Electrochemical Society*, 2001. **148**(6): D78-D82.

134. Gandini, D., Mahé, E., Michaud, P.A., Haenni, W., Perret, A. and Comninellis, C. Oxidation of carboxylic acids at boron-doped diamond electrodes for wastewater treatment. *Journal of Applied Electrochemistry*, 2000. **30**(12): 1345-1350.

135. Panizza, M., Michaud, P., Cerisola, G. and Comninellis, C. Electrochemical treatment of wastewaters containing organic pollutants on boron-doped diamond electrodes: Prediction of specific energy consumption and required electrode area. *Electrochemistry Communications*, 2001. **3**(7): 336-339.

136. Polcaro, A.M., Mascia, M., Palmas, S. and Vacca, A. Electrochemical degradation of diuron and dichloroaniline at BDD electrode. *Electrochimica Acta*, 2004. **49**(4): 649-656.

137. Panizza, M. and Cerisola, G. Removal of colour and cod from wastewater containing Acid Blue 22 by electrochemical oxidation. *Journal of Hazardous Materials*, 2008. **153**(1): 83-88.

138. Panizza, M. and Cerisola, G. Application of diamond electrodes to electrochemical processes. *Electrochimica Acta*, 2005. **51**(2): 191-199.

139. Martin, H.B., Argoitia, A., Landau, U., Anderson, A.B. and Angus, J.C. Hydrogen and oxygen evolution on boron-doped diamond electrodes. *Journal of the Electrochemical Society*, 1996. **143**(6): L133-L136.

140. Flox, C., Ammar, S., Arias, C., Brillas, E., Vargas-Zavala, A.V. and Abdelhedi, R. Electro-fenton and photoelectro-Fenton degradation of Indigo Carmine in acidic aqueous medium. *Applied Catalysis B: Environmental*, 2006. **67**(1): 93-104.

141. Panizza, M., Barbucci, A., Ricotti, R. and Cerisola, G. Electrochemical degradation of Methylene Blue. *Separation and Purification Technology*, 2007. **54**(3): 382-387.

142. Daneshvar, N., Aber, S., Vatanpour, V. and Rasoulifard, M.H. Electro-Fenton treatment of dye solution containing Orange II: Influence of operational parameters. *Journal of Electroanalytical Chemistry*, 2008. **615**(2): 165-174.

143. Panizza, M. and Cerisola, G. Electro-Fenton degradation of synthetic dyes. *Water Research*, 2009. **43**(2): 339-344.

144. Vilaseca, M., Gutiérrez, M.-C., López-Grimau, V., López-Mesas, M. and Crespi, M. Biological treatment of a textile effluent after electrochemical oxidation of reactive dyes. *Water Environment Research*, 2010. **82**(2): 176-182.

145. Riera-Torres, M. and Gutiérrez, M.-C. Colour removal of three reactive dyes by UV light exposure after electrochemical treatment. *Chemical Engineering Journal*, 2010. **156**(1): 114-120.

146. López-Grimau, V. and Gutierrez, M. Decolourisation of simulated reactive dyebath effluents by electrochemical oxidation assisted by UV light. *Chemosphere*, 2006. **62**(1): 106-112.

147. Oliveira, F.H., Osugi, M.E., Paschoal, F.M., Profeti, D., Olivi, P. and Zanoni, M.V.B. Electrochemical oxidation of an acid dye by active chlorine generated using $Ti/Sn_{(1-x)}Ir_xO_2$ electrodes. *Journal of Applied Electrochemistry*, 2007. **37**(5): 583-592.

148. Osugi, M.E., Rajeshwar, K., Ferraz, E.R., de Oliveira, D.P., Araújo, Â.R. and Zanoni, M.V.B. Comparison of oxidation efficiency of disperse dyes by chemical and photoelectrocatalytic chlorination and removal of mutagenic activity. *Electrochimica Acta*, 2009. **54**(7): 2086-2093.

149. Osugi, M.E., Umbuzeiro, G.A., De Castro, F.J. and Zanoni, M.V.B. Photoelectrocatalytic oxidation of Remazol Turquoise Blue and toxicological assessment of its oxidation products. *Journal of Hazardous Materials*, 2006. **137**(2): 871-877.

150. Devi, L.G., Kumar, S.G., Reddy, K.M. and Munikrishnappa, C. Photo degradation of Methyl Orange an azo dye by advanced Fenton process using zero valent metallic iron: Influence of various reaction parameters and its degradation mechanism. *Journal of Hazardous Materials*, 2009. **164**(2): 459-467.

151. Zhang, Q. and Zhang, Z. Preparation and characterization of nanocrystalline Fe-doped TiO_2 film on different substrates and its application in degrading dyeing water. *Journal of Dispersion Science and Technology*, 2009. **30**(1): 110-114.

152. Rajeshwar, K., Osugi, M., Chanmanee, W., Chenthamarakshan, C., Zanoni, M.V.B., Kajitvichyanukul, P. and Krishnan-Ayer, R. Heterogeneous photocatalytic treatment of organic dyes in air and aqueous media. *Journal of Photochemistry and Photobiology C: Photochemistry Reviews*, 2008. **9**(4): 171-192.

153. Carneiro, P.A., Osugi, M.E., Sene, J.J., Anderson, M.A. and Zanoni, M.V.B. Evaluation of color removal and degradation of a reactive textile azo dye on nanoporous TiO_2 thin-film electrodes. *Electrochimica Acta*, 2004. **49**(22): 3807-3820.

154. Peralta-Hernández, J., Meas-Vong, Y., Rodríguez, F.J., Chapman, T.W., Maldonado, M.I. and Godínez, L.A. *In situ* electrochemical and photo-electrochemical generation of the Fenton reagent: A potentially important new water treatment technology. *Water Research*, 2006. **40**(9): 1754-1762.

155. Kuo, W. Decolorizing dye wastewater with Fenton's reagent. *Water Research*, 1992. **26**(7): 881-886.

156. Gomes da Silva, C. and Faria, J.L. Photochemical and photocatalytic degradation of an azo dye in aqueous solution by UV irradiation. *Journal of Photochemistry and Photobiology A: Chemistry*, 2003. **155**(1-3): 133-143.

157. Hachem, C., Bocquillon, F., Zahraa, O. and Bouchy, M. Decolourization of textile industry wastewater by the photocatalytic degradation process. *Dyes and Pigments*, 2001. **49**(2): 117-125.

158. Epling, G.A. and Lin, C. Photoassisted bleaching of dyes utilizing TiO_2 and visible light. *Chemosphere*, 2002. **46**(4): 561-570.

159. Xie, Y.B. and Li, X.Z. Interactive oxidation of photoelectrocatalysis and electro-fenton for azo dye degradation using TiO_2–Ti mesh and reticulated vitreous carbon electrodes. *Materials Chemistry and Physics*, 2006. **95**(1): 39-50.

160. Durán, A., Monteagudo, J.M. and Amores, E. Solar photo-Fenton degradation of Reactive Blue 4 in a CPC reactor. *Applied Catalysis B: Environmental*, 2008. **80**(1–2): 42-50.

161. Raghu, S. and Basha, C.A. Chemical or electrochemical techniques, followed by ion exchange, for recycle of textile dye wastewater. *Journal of Hazardous Materials*, 2007. **149**(2): 324-330.

162. Daneshvar, N., Khataee, A., Ghadim, A.A. and Rasoulifard, M. Decolorization of CI Acid Yellow 23 solution by electrocoagulation process: Investigation of operational parameters and evaluation of specific electrical energy consumption (SEEC). *Journal of Hazardous Materials*, 2007. **148**(3): 566-572.

163. Kaplin, D.A. and Qutubuddin, S. Electrochemically synthesized polypyrrole films: Effects of polymerization potential and electrolyte type. *Polymer*, 1995. **36**(6): 1275-1286.

164. Qi, G., Huang, L. and Wang, H. Highly conductive free standing polypyrrole films prepared by freezing interfacial polymerization. *Chemical Communications*, 2012. **48**(66): 8246-8248.

165. Balint, R., Cassidy, N.J. and Cartmell, S.H. Conductive polymers: Towards a smart biomaterial for tissue engineering. *Acta Biomaterialia*, 2014. **10**(6): 2341-2353.

166. Kim, J., Jung, J., Lee, D. and Joo, J. Enhancement of electrical conductivity of poly (3, 4-ethylenedioxythiophene)/poly (4-styrenesulfonate) by a change of solvents. *Synthetic Metals*, 2002. **126**(2): 311-316.

167. Diaz, A., Kanazawa, K.K. and Gardini, G.P. Electrochemical polymerization of pyrrole. *Journal of the Chemical Society, Chemical Communications*, 1979(14): 635-636.

168. Inzelt, G. Rise and rise of conducting polymers. *Journal of Solid State Electrochemistry*, 2011. **15**(7-8): 1711-1718.

169. Vidal, J.C., García, E. and Castillo, J.R. *In situ* preparation of a cholesterol biosensor: Entrapment of cholesterol oxidase in an overoxidized polypyrrole film electrodeposited in a flow system. Determination of total cholesterol in serum. *Analytica Chimica Acta*, 1999. **385**(1-3): 213-222.

170. Campbell, T.E., Hodgson, A.J. and Wallace, G.G. Incorporation of erythrocytes into polypyrrole to form the basis of a biosensor to screen for rhesus (D) blood groups and rhesus (D) antibodies. *Electroanalysis*, 1999. **11**(4): 215-222.

171. Su, W. and Iroh, J.O. Effects of electrochemical process parameters on the synthesis and properties of polypyrrole coatings on steel. *Synthetic Metals*, 1998. **95**(3): 159-167.

172. Kincal, D., Kumar, A., Child, A.D. and Reynolds, J.R. Conductivity switching in polypyrrole-coated textile fabrics as gas sensors. *Synthetic Metals*, 1998. **92**(1): 53-56.

173. Kemp, N.T., Flanagan, G.U., Kaiser, A.B., Trodahl, H.J., Chapman, B., Partridge, A.C. and Buckley, R.G. Temperature-dependent conductivity of conducting polymers exposed to gases. *Synthetic Metals*, 1999. **101**(1): 434-435.

174. Jérôme, C., Labaye, D., Bodart, I. and Jérôme, R. Electrosynthesis of polyacrylic/polypyrrole composites: Formation of polypyrrole wires. *Synthetic Metals*, 1999. **101**(1): 3-4.

175. Biswas, M. and Roy, A. Thermal, stability, morphological, and conductivity characteristics of polypyrrole prepared in aqueous medium. *Journal of Applied Polymer Science*, 1994. **51**(9): 1575-1580.

176. Smela, E. Microfabrication of PPy microactuators and other conjugated polymer devices. *Journal of Micromechanics and Microengineering*, 1999. **9**(1): 1.

177. Kudoh, Y., Fukuyama, M. and Yoshimura, S. Stability study of polypyrrole and application to highly thermostable aluminum solid electrolytic capacitor. *Synthetic Metals*, 1994. **66**(2): 157-164.

178. Wallace, G., Spinks, G. and Teasdale, P. Conductive electroactive polymers technomic: Intelligent material systems. 1997, Technomic Publ. Co.:Lancaster.

179. Iroh, J.O. and Williams, C. Formation of thermally stable polypyrrole-naphthalene/benzene sulfonate-carbon fiber composites by an electrochemical process. *Synthetic Metals*, 1999. **99**(1): 1-8.

180. Reynolds, J.R., Ly, H., Selampinar, F. and Kinlen, P.J. Controlled drug and biomolecule release from electroactive host polymer systems. In *American Chemical Society, Polymer Preprints, Division of Polymer Chemistry*, 1999.

181. Lu, W.-K. and Elsenbaumer, R.L. Corrosion protection of metals by conductive polymers. II. Pitting corrosion. In *Annual Technical Conference - ANTEC, Conference Proceedings*, 1998.

182. Fraoua, K., Aeiyach, S., Aubard, J., Delamar, M., Lacaze, P.C. and Ferreira, C.A. XPS and SERS evidence for iron nitride species responsible for the strong adhesion of polypyrrole to iron or steel treated with nitric acid. *Journal of Adhesion Science and Technology*, 1999. **13**(4): 517-522.

183. Kudoh, Y. Properties of polypyrrole prepared by chemical polymerization using aqueous solution containing $Fe_2(SO_4)_3$ and anionic surfactant. *Synthetic Metals*, 1996. **79**(1): 17-22.

184. Genies, E.M., Bidan, G. and Diaz, A.F. Spectroelectrochemical study of polypyrrole films. *Journal of Electroanalytical Chemistry and Interfacial Electrochemistry*, 1983. **149**(1–2): 101-113.

185. Kim, K.-J., Song, H.-S., Kim, J.-D. and Chon, J.-K. Mechanism of electropolymerization of pyrrole in acidic aqueous solutions. *Bulletin of the Korean Chemical Society*, 1988. **9**(4): 248-251.

186. Asavapiriyanont, S., Chandler, G.K., Gunawardena, G.A. and Pletcher, D. The electrodeposition of polypyrrole films from aqueous solutions. *Journal of*

Electroanalytical Chemistry and Interfacial Electrochemistry, 1984. **177**(1–2): 229-244.

187. Qiu, Y.J. and Reynolds, J.R. Electrochemically initiated chain polymerization of pyrrole in aqueous media. *Journal of Polymer Science Part A: Polymer Chemistry*, 1992. **30**(7): 1315-1325.

188. Sadki, S., Schottland, P., Brodie, N. and Sabouraud, G. The mechanisms of pyrrole electropolymerization. *Chemical Society Reviews*, 2000. **29**(5): 283-293.

189. Khalkhali, R.A. Electrochemical synthesis and characterization of electroactive conducting polypyrrole polymers. *Russian Journal of Electrochemistry*, 2005. **41**(9): 950-955.

190. Waltman, R.J. and Bargon, J. Reactivity/structure correlations for the electropolymerization of pyrrole: An INDO/CNDO study of the reactive sites of oligomeric radical cations. *Tetrahedron*, 1984. **40**(20): 3963-3970.

191. Waltman, R. and Bargon, J. Electrically conducting polymers: A review of the electropolymerization reaction, of the effects of chemical structure on polymer film properties, and of applications towards technology. *Canadian Journal of Chemistry*, 1986. **64**(1): 76-95.

192. Funt, B. and Diaz, A. Organic electrochemistry: An introduction and a guide. 1991, Marcel Dekker: New York.

193. Street, G.B. and Skotheim, T. Handbook of conducting polymers. 1986, Marcel Dekker: New York.

194. Wallace, G.G., Teasdale, P.R., Spinks, G.M. and Kane-Maguire, L.A. Conductive electroactive polymers: Intelligent polymer systems. 2008, CRC Press:

195. Wang, L.-X., Li, X.-G. and Yang, Y.-L. Preparation, properties and applications of polypyrroles. *Reactive and Functional Polymers*, 2001. **47**(2): 125-139.

196. Ansari, R. and Mosayebzadeh, Z. Removal of Eosin Y, an anionic dye from aqueous solution using conducting electroactive polymers. *Iranian Polymer Journal*, 2010. **19**(7): 541-551.

197. Wang, H., Lin, T. and Kaynak, A. Polypyrrole nanoparticles and dye absorption properties. *Synthetic Metals*, 2005. **151**(2): 136-140.

198. Chowdhury, A.N., Jesmeen, S.R. and Hossain, M.M. Removal of dyes from water by conducting polymeric adsorbent. *Polymers for Advanced Technologies*, 2004. **15**(11): 633-638.

199. Ansari, R. and Mosayebzadeh, Z. Application of polyaniline as an efficient and novel adsorbent for azo dyes removal from textile wastewaters. *Chemical Papers*, 2011. **65**(1): 1-8.

200. Ansari, R. and Mosayebzadeh, Z. Removal of basic dye methylene blue from aqueous solutions using sawdust and sawdust coated with polypyrrole. *Journal of the Iranian Chemical Society*, 2010. **7**(2): 339-350.

201. Ansari, R., Keivani, M.B. and Delavar, A.F. Application of polyaniline nanolayer composite for removal of Tartrazine dye from aqueous solutions. *Journal of Polymer Research*, 2011. **18**(6): 1931-1939.

202. Ahmad, R. and Kumar, R. Conducting polyaniline/iron oxide composite: A novel adsorbent for the removal of Amido Black 10B. *Journal of Chemical and Engineering Data*, 2010. **55**(9): 3489-3493.

203. Zhao, H., Price, W.E. and Wallace, G.G. Transport of copper (II) across stand-alone conducting polypyrrole membranes: The effect of applied potential waveforms. *Polymer*, 1993. **34**(1): 16-20.

204. Zhao, H., Price, W.E. and Wallace, G.G. Effect of the counterion employed during synthesis on the properties of polypyrrole membranes. *Journal of Membrane Science*, 1994. **87**(1): 47-56.

205. Zhao, H., Price, W.E. and Wallace, G.G. Electrochemically controlled transport of potassium chloride across a conducting electro-active polymer membrane. *Journal of Electroanalytical Chemistry*, 1992. **334**(1): 111-120.

206. Mirmohseni, A., Price, W.E. and Wallace, G.G. Electrochemically controlled transport of small charged organic molecules across conducting polymer membranes. *Journal of Membrane Science*, 1995. **100**(3): 239-248.

207. Masubuchi, S., Kazama, S., Mizoguchi, K., Shimizu, F., Kume, K., Matsushita, R. and Matsuyama, T. The transport properties of metallic shirakawa polyacetylenes with different dopant species. *Synthetic Metals*, 1995. **69**(1): 71-72.

208. Arrieta Almario, A.A. and Tarazona Caceres, R.L. Study of kinetic formation and the electrochemical behavior of polypyrrole films. *Journal of the Chilean Chemical Society*, 2009. **54**(1): 14-19.

209. Ansari Khalkhali, R., Price, W. and Wallace, G.G. Quartz crystal microbalance studies of the effect of solution temperature on the ion-exchange properties of polypyrrole conducting electroactive polymers. *Reactive and Functional polymers*, 2003. **56**(3): 141-146.

210. Raudsepp, T., Marandi, M., Tamm, T., Sammelselg, V. and Tamm, J. Influence of ion-exchange on the electrochemical properties of polypyrrole films. *Electrochimica Acta*, 2014. **122**(0): 79-86.

211. Curtin, L.S., Komplin, G.C. and Pietro, W.J. Diffusive anion exchange in polypyrrole films. *The Journal of Physical Chemistry*, 1988. **92**(1): 12-13.

212. Jin, C., Yang, F. and Yang, W. Electropolymerization and ion exchange properties of a polypyrrole film doped by para-toluene sulfonate. *Journal of Applied Polymer Science*, 2006. **101**(4): 2518-2522.

213. Fabre, B. and Simonet, J. Electroactive polymers containing crown ether or polyether ligands as cation-responsive materials. *Coordination Chemistry Reviews*, 1998. **178**: 1211-1250.

214. Korri Youssoufi, H., Yassar, A., Baiteche, S., Hmyene, M. and Garnier, F. Designing polypyrrole-based sensors: Selective electrochemical cation in aza crown ethers. *Synthetic Metals*, 1994. **67**(1): 251-254.

215. Schmidt, V.M. and Heitbaum, J. Ion exchange mechanism of polypyrrole and poly-n-methylpyrrole with toslylate as doping anion: An electrochemical quartz crystal microbalance study. *Electrochimica Acta*, 1993. **38**(2): 349-356.

216. Tamm, J., Hallik, A. and Alumaa, A. Electrochemical properties of dodecylsulphate doped polypyrrole films. *Synthetic Metals*, 1993. **55**(2): 1473-1476.

217. Gao, Z., Bobacka, J., Lewenstam, A. and Ivaska, A. Electrochemical behaviour of polypyrrole film polymerized in Indigo Carmine solution. *Electrochimica Acta*, 1994. **39**(5): 755-762.

CHAPTER 2

EXPERIMENTAL

2.1 Introduction

A long-term goal of this work is to develop an electrochemically green tool for treatment of azo dye containing industrial wastewater. More specifically, this work was aimed at investigating the feasibility of applying eletropolymerised conducting polypyrrole films for treating azo dye containing synthetic wastewater. To achieve this aim, electropolymerised polypyrrole and its graphene composite films were synthesised. Polypyrrole and its graphene oxide composite films were then used for entrapment and liberation of the azo dye, Acid Red 1, from its synthetic solution by applying an oxidation and a reduction potential, respectively. In our work, a two-level factorial design approach was used for identification of the significant factors and their interactions in Acid Red 1 entrapment in polypyrrole. Characterisation of the synthesised polypyrrole films were performed by cyclic voltammetry, spectroscopy, microscopy, and physical and mechanical properties evaluation. Acid Red 1 entrapment and liberation experiments were also performed to evaluate the dye entrapment and liberation efficiency of the polypyrrole films. This chapter outlines the detailed descriptions of the instrumentations and experimental procedures adopted to ensure that the most reliable results were obtained. Results obtained are then presented and discussed in the next three chapters.

2.2 Reagents

Graphite power, Acid Red 1, potassium nitrate and pyrrole were purchased from Sigma-Aldrich (Castle Hill, Sydney, Australia). Pyrrole was always doubly vacuum distilled at 130 °C and then stored in a light protected bottle at 4 °C until required for use. All aqueous solutions were prepared using deionised water purified by a Milli Q water system (Millipore). High purity nitrogen gas (BOC) was used to purge all analyte solutions for 10 min at the beginning of an experiment in order to remove dissolved oxygen from solution.

2.3 Apparatus

All voltammetric studies were performed using a MacLab/200 system operated by EChem and Chart software (eDaq Pty Ltd, Sydney, Australia). A 50-mL vial was used as an electrochemical cell accommodating a three-electrode system. Stainless steel electrodes (3 cm × 1.5 cm) or stainless steel mesh electrodes (3 cm × 1.5 cm) both manufactured by Macquarie Engineering and Technical Services, Macquarie University were respectively used as a working electrode and a counter electrode. All potentials were recorded relative to a Ag|AgCl (in 3 mol L^{-1} KCl) reference electrode. UV-visible spectroscopy for measuring absorbance of Acid Red 1 solutions was performed using a Bio Spectrophotometer (Eppendorf, Australia). Conductivity measurements were performed using a locally constructed four-point probe. Fourier transform infrared (FTIR) spectrometry analysis was performed using a Nicolet iS10 FTIR spectrometer (Thermo Scientific, USA). The crystalline phase of the polypyrrole-Acid Red 1 film samples was identified using an X'Pert Pro MPD X-ray diffractometer ((Philips®, Netherlands). X-ray photoelectron spectroscopy (XPS) analysis was performed using a VG scientific ESCALAB250Xi spectrometer (Thermo Scientific, UK). Scanning electron microscopy (SEM) analysis was carried out using a JEOL JSM- 6480 LA scanning electron microscope (JEOL, Japan). Brunauer, Emmett and Teller (BET) surface area analysis was carried out using a Tristar 3000 analyser (Micromeritics, USA) under a nitrogen environment. Thermogravimetric analysis was conducted using a Shimadzu TG 50 thermogravimetric analyser. Mechanical properties of polypyrrole films were measured using an Instron 4302 tensile testing device.

2.4 Preparation of graphite oxide and graphene oxide

Graphite oxide was synthesised from graphite powder (1-2 μm) using a modified Hummers-Offeman method [1]. Briefly, potassium persulfate (8 g) and phosphorus pentoxide (4 g) were initially dissolved in 24 mL of hot sulfuric acid and then 4 g of graphite powder was added. The mixture was then kept at 75 ºC for 1 h, allowed to cool to room temperature, then cooled in ice, and diluted with deionised water until the solution reached pH 6. The solution was filtered and the residue containing modified graphite powder was dried at 80 ºC overnight.

The activated graphite was washed 3 times with deionised water and then treated with concentrated cold sulfuric acid (92 mL) in an ice bath. Potassium permanganate (12 g) and sodium nitrate (2 g) were gradually added over a 1 h period, after which the mixture was

removed from the ice bath and allowed to warm to room temperature for 2 h. The mixture was then returned to the ice bath and diluted with deionised water (200 mL) for a period of 30 min. The ice bath was removed and then the mixture was stirred at room temperature for 2 h. The resultant bright-yellow suspension was diluted by the addition of deionised water (560 mL) to terminate oxidation process and further treated with 30% hydrogen peroxide (10 mL). The yellowish brown mixture was washed once with 1 M hydrochloric acid (100 mL) and five times with deionised water (300 mL each). Finally, to obtain hydrophilic graphite oxide, the brown mixture was dried by vacuum filtration (pore size 0.45 µm).

The exfoliation of graphite oxide to graphene oxide was achieved by ultrasonication of graphite oxide for 30 min at 45% amplitude using an Extech ultrasonic processor. Then the exfoliated material was subjected to centrifugation at 1000 rpm for 2 min and discarded residue to remove settled graphene oxide agglomerate. Finally, the suspension was again centrifuged at 8000 rpm for 15 min and dried 60 °C for 48 h under vacuum.

2.5 Electropolymerisation experiments

2.5.1 Electrochemical synthesis of polypyrrole-Acid Red 1 films

Each polypyrrole–Acid Red 1 film was potentiostatically polymerised on a stainless steel working electrode by applying a potential of +0.88 V (the use of this potential will be justified in Section 3.3.1.1) in the presence of 0.2 mol L^{-1} pyrrole and 60 – 2000 mg L^{-1} Acid Red 1 for a duration from 20 to 480 min. This process is schematically is shown in Figure 2.1. The polypyrrole-Acid Red 1 film was carefully removed from the electrode and oven dried at 80 °C for 24 h before being used in further characterisation experiments. The remaining electrolyte solution in the cell was analysed by UV-visible spectroscopy at 532 nm using a Bio Spectrophotometer (Eppendorf, Australia) for Acid Red 1 entrapment evaluation.

2.5.2 Electrochemical synthesis of polypyrrole-reduced graphene oxide composite films

In preparing mechanically stable polypyrrole-reduced graphene oxide composite films, Acid Red 1 initially entrapped in a polypyrrole-graphene oxide film which was potentiostatically synthesised by *in situ* polymerisation on a stainless steel mesh electrode by applying a potential of +1.0 V in the presence of 0.2 mol L^{-1} pyrrole, 1500 mg L^{-1} Acid Red 1 and a ratio of 20:1 (w/w) between pyrrole and graphene oxide (justification for this mass ratio is given in Section

5.3.1.9) for 480 min. The resulting composite was designated as polypyrrole-graphene oxide film. The polypyrrole-graphene oxide film was then reduced by applying a reduction potential of -1.3 V for 240 min in 0.5 M NaOH solution to prepare polypyrrole-reduced graphene oxide film. The entrapment evaluation of Acid Red 1 in a 1500 mg L^{-1} solution was then performed at the respective polypyrrole, polypyrrole-graphene oxide and polypyrrole-reduced graphene oxide films for duration from 20 to up to 480 min by applying an oxidation potential of +1.0 V. This process is schematically is shown in Figure 2.2.

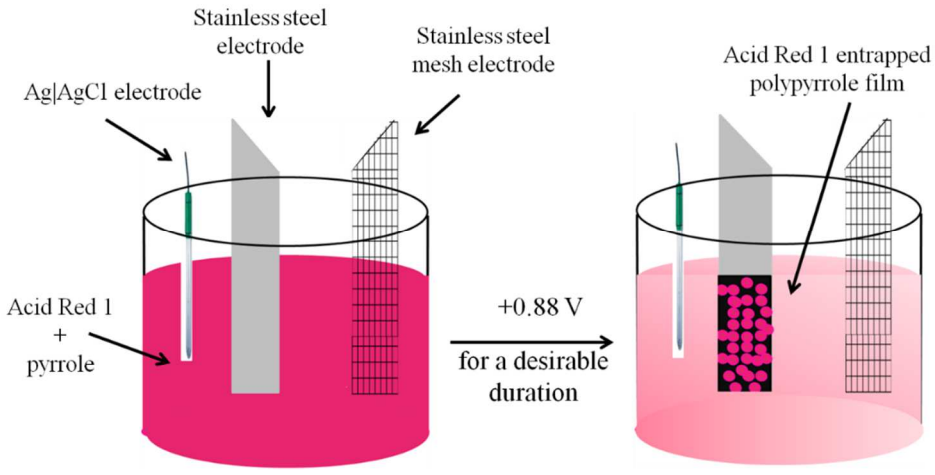

Figure 2.1 A three-electrode voltammetric cell used for the electropolymerisation of pyrrole.

2.6 Optimisation experiments of synthesis of polypyrrole-Acid Red 1films

A two-level full factorial design was used to identify the significant factors in Acid Red 1 entrapment in polypyrrole films. These factors included solution pH, polymerisation time, Acid Red 1 concentration and pyrrole concentration.

2.7 Entrapment and liberation experiments

All experiments were carried out at room temperature. At the end of each polymerisation experiment, the remaining solution in the electrochemical cell was analysed by UV-visible spectrophotometry at 532 nm to estimate the final concentration of Acid Red 1. The percentage of Acid Red 1 entrapped in a polypyrrole, polypyrrole-graphene oxide and polypyrrole-reduced graphene oxide films was then evaluated based on the difference (in mg L^{-1}) between the initial concentration ($C_{initial}$) and the final concentration (C_{final}) of Acid Red 1 in the solution using UV-visible spectrophotometry according to Equation (2.1).

$$\%Entrapment = \frac{\left| C_{final} - C_{initial} \right|}{C_{initial}} \times 100 \qquad \text{Equation (2.1)}$$

To evaluate the liberation efficiency, the resulting three types of Acid Red 1 entrapped films were subjected to a reduction process. In our experiments, Acid Red 1 was cathodically liberated from dye-entrapped polypyrrole, polypyrrole-graphene oxide or polypyrrole-reduced graphene oxide films placed in a 0.5 M NaOH by applying a reduction potential of –0.80 V (versus Ag|AgCl) for a desired time. The resultant solution concentration ($C_{liberation}$) was again spectrophotometrically analysed at 532 nm to determine the liberation efficiency according to Equation (2.2).

$$\%Liberation = \frac{C_{liberation}}{\left| C_{final} - C_{initial} \right|} \times 100 \qquad \text{Equation (2.2)}$$

Schematic representation of Entrapment-liberation of Acid Red 1 in polypyrrole / polypyrrole-reduced graphene oxide composite films shown in Figure 2.2.

2.8 Entrapment kinetics, isotherm and thermodynamics

All entrapment experiments were carried out during the electropolymerisation of pyrrole to form polypyrrole in the presence of Acid Red 1, as described in section 2.7. In addition, to evaluate the effect of temperature, these entrapment experiments were conducted at five temperatures of 298 K, 303 K, 308 K, 313 K and 318 K. The quantity of Acid Red 1 in a polypyrrole film was evaluated based on the difference (in mg L^{-1}) between the final concentration (C_{final}) after entrapment and the initial concentration ($C_{initial}$) of Acid Red 1 in an electrochemical cell using UV-visible spectrophotometry. All Acid Red 1 concentrations were estimated from a plot of absorbance against concentration of standard Acid Red 1 solutions. Taking into consideration the total solution volume (V in L) and the total mass of the polypyrrole film (W in g), at the completion of an entrapment experiment, we then used the same concentration difference to estimate the mass of Acid Red 1 per mass of polypyrrole film (q_t in mg g^{-1}). We shall hereafter refer to q_t as the entrapment capacity after a polymerisation duration t.

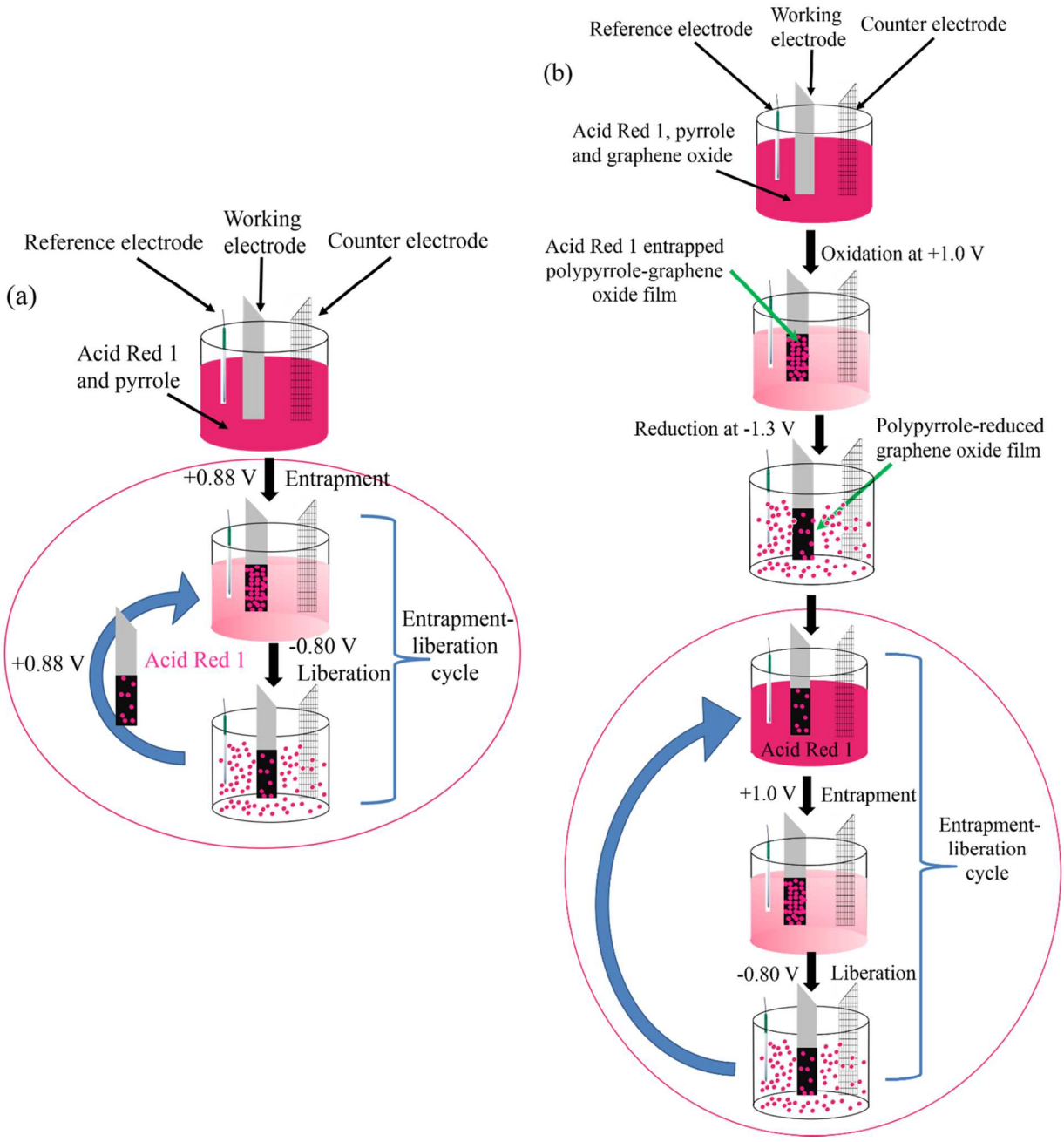

Figure 2.2 Steps followed to entrap and liberate of Acid Red 1 at (a) polypyrrole film and (b) polypyrrole-reduced graphene oxide film.

2.9 Characterisation

2.9.1 XRD analysis

XRD analysis was conducted to identify the crystalline phase of the Acid Red 1 entrapped polypyrrole, polypyrrole-graphene oxide and polypyrrole-reduced graphene oxide film

samples. In these experiments, each sample was placed on a Si wafer (111) before being analysed on an X'Pert Pro MPD X-ray diffractometer (Philips®, Netherlands). A voltage of 40 kV and an anode current of 40 mA were applied. A Cu Kα radiation (λ = 0.15405 nm) was used in a continuous scanning mode with 0.02 step size and 0.5 s set time for collecting the data in a 2θ scan range of 4°–80°.

2.9.2 FTIR analysis

FTIR was used to analyse polypyrrole and composite films. The spectra were obtained over 16 scans covering the 4000-650 cm^{-1} wavenumber range at 4 cm^{-1} resolution and at 25 °C using a Thermo Scientific Nicolet iS10 FTIR spectrometer.

2.9.3 XPS analysis

XPS analysis was carried out on a VG scientific ESCALAB250Xi spectrometer (Thermo Scientific, UK) using a monochromatised Al Kα X-ray source (1486.68 eV photons) with electrical input power of 200 V and take-off angle of 90°.

2.9.4 SEM

SEM studies were performed to investigate the surface morphology of all samples. All SEM measurements were carried out using a JEOL JSM- 6480 LA scanning electron microscope (JEOL, Japan) operated with an accelerating voltage of 10 kV and in a vacuum condition. The film samples were placed on an aluminium holder and then coated with a thin layer of gold.

2.9.5 TGA

TGA of samples was conducted using a Shimadzu TG 50 thermogravimetric analyser in the temperature range of 20-700 °C, at a heating rate of 10 °C min^{-1} under a nitrogen protection atmosphere. TGA gives information about the thermal characteristics of polypyrrole and its composites including degradation temperature, absorbed moisture content and the level of oligomer in polymer.

2.9.6 BET surface area analysis

Specific surface area of materials is often evaluated by Brunauer-Emmett-Teller (BET) model using nitrogen adsorption measured as a function of relative pressure. The technique involves both external area and pore area evaluations to estimate the total specific surface area in

m^2 g^{-1}, yielding important information in studying the effects of surface porosity and particle size in many applications. The surface area of polypyrrole and its composite films was measured by a BET plot of nitrogen adsorption desorption isotherm [2]. In this work, the analysis was performed on a Tristar 3000 surface area analyser (Micromeritics, USA) using the technique of nitrogen physisorption. After placing a sample in a vacuum within the surface area analyser for 3h at 150 °C prior to analysis. The volume of nitrogen gas adsorbed was evaluated and data are treated according to the BET adsorption isotherm equation [2], the adsorption isotherm equation of gas can be expressed as:

$$\frac{1}{Q\left(\frac{p}{P_0}-1\right)} = \frac{C-1}{Q_m C} \times \frac{P}{P_0} + \frac{1}{Q_m C} \qquad \text{Equation (2.4)}$$

where Q and Q_m are the volume of nitrogen gas adsorbed at the relative equilibrium pressure P/P_0 (ratio between the vapour pressure above the sample (P) and saturation pressure (P_0)), and the monolayer capacity of adsorbent materials respectively, C is a dimensionless constant related to the interaction between the gas and the adsorbent.

According to Equation (2.4), a plot of $1/[Q(P/P_0 - 1)]$ versus P/P_0 will yield a straight line with a slope of $(C-1)/Q_m C$, and intercept, $1/Q_m C$. The value of Q_m can be estimated from the reciprocal of the sum of the slope and intercept. From the value of Q_m, the specific surface area, S_{BET} , can be evaluated using Equation (2.5) [2].

$$S_{BET} = \frac{Q_m N_A A_m}{V_{mol}} \qquad \text{Equation (2.5)}$$

where, N_A , is the Avogadro's constant, A_m the molecular cross-sectional area of gas, and V_{mol} , is the molar volume of gas. The values of A_m and V_{mol} for nitrogen gas are 0.61620 nm^2 and 22400 mL (at standard temperature and pressure), respectively [2].

2.9.7 Mechanical properties

Tensile test was conducted to determine the tensile strength and Young's modulus of polypyrrole and its composite films according to ASTM D882-91 at a crosshead speed of 10 mm min^{-1} using an Instron 4302 tensile testing device at room temperature. In all experiments,

polypyrrole and its composite films of dimension 15 mm × 5mm × 0.30 mm were used. The average of five films and standard deviation values were reported for each type of films or composites.

Tensile strength (S_T) was evaluated by dividing the maximum load at break, $P_{\max}$, in Newtons (N) by the original minimum cross-sectional area A_0 (in m^2) of a film used [3]. The result is expressed in megapascals (MPa).

$$S_T = P_{\max} / A_0 \qquad \text{Equation (2.6)}$$

Young's modulus is the modulus of elasticity, which denotes the ease of deformation by stretching a material. Young's modulus, E can be evaluated from a stress-strain curve of a material. It is unique for each material and is found by recording the amount of deformation (strain) at distinct intervals of tensile or compressive loading (stress). Figure 2.3 shows a typical stress-strain curve. By drawing a tangent to the linear portion (A and B) of the stress-strain curve, the slope of this tangent yields an estimate of E [3], as indicated by Equation (2.7).

$$E = \frac{F/A}{\Delta L/L} \qquad \text{Equation (2.7)}$$

where, F is the load at the point of tangent in N, A is the average original cross section of the test specimen in m^2, ΔL is elongation at point on tangent in metres (m) and L is original length in metres (m). The result is expressed in gigapascals (GPa).

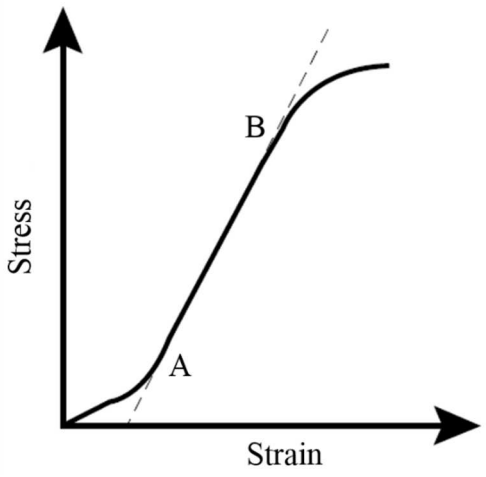

Figure 2.3 A typical stress-strain curve

2.9.8 Electrical property

Conductivity measurements were performed using an in-house built four-probe conductivity device schematically shown in Figure 2.4. The design of this device was derived from the literature [4]. Thin strips of polypyrrole and its composite films, typically ~3 mm wide and 10~20 mm long, were cut using a scalpel and steel ruler and width and thickness measurements at three approximately evenly spaced site along the strips measured using vernier calipers and a micrometer, respectively.

A conductivity measurement was typically carried out at room temperature using the following procedure. With the electrode-facing surface of the film containing the four copper probes (contacts) and the thumb screws firmly tightened, 0.1 mA was passed through the outer pair of probes and the voltage drop across the inner pair of probes measured using E-chem software.

Ten sets of current and voltage data were thus collected from which a single average conductivity value was derived for that test surface. After this set of measurements, the same film strip was turned over so that the solution-facing surface now contacted the copper probes and the measurement procedure repeated. Unless stated otherwise, the conductivity value for a strip was taken as the average of the conductivity of two surfaces. Film conductivity (σ_f in S cm^{-1}) was evaluated according to Equation (2.8) [4]:

$$\sigma_f = \frac{I}{V} \times \frac{s}{Dh} \qquad \text{Equation (2.8)}$$

where I is the applied current (in mA), V the measured voltage (in mV), s the spacing of the inner probe pair (in cm), D the width of the polypyrrole film strip (in cm), and h the thickness of the polypyrrole film strip (in cm).

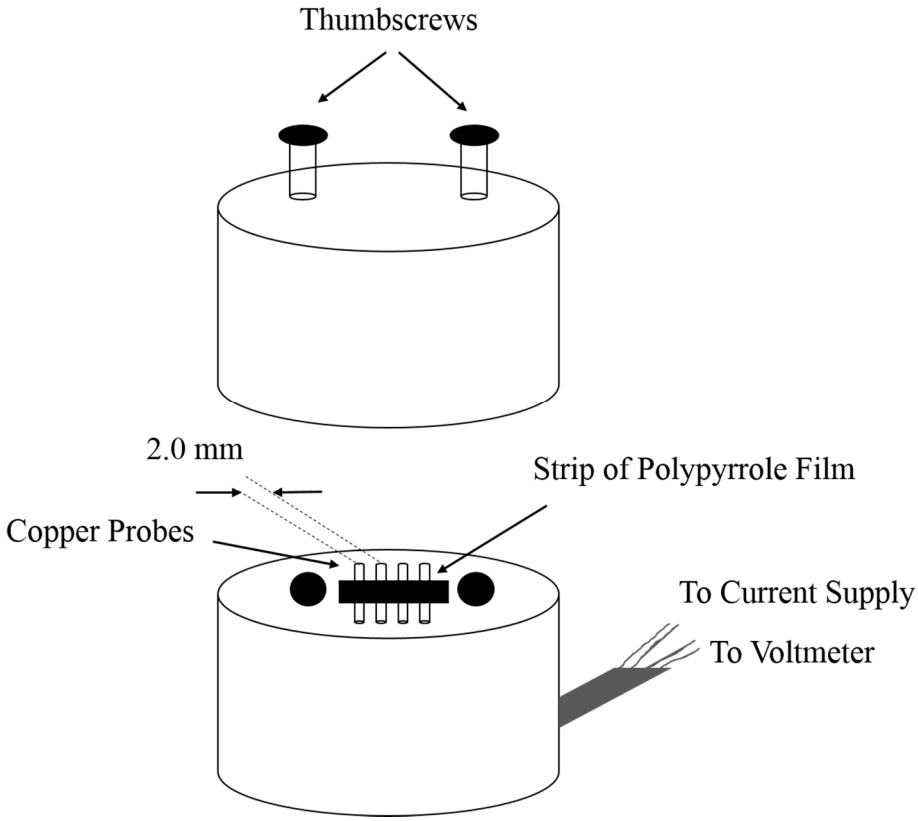

Figure 2.5 Four-point probe conductivity measuring device.

2.10 Data analysis

In the entrapment experiment, each entrapment data point represents the mean value of three measurements and the standard deviation value was calculated. Linearity of a relation was assessed based on both the random pattern in the corresponding residual plot and the statistical significance of the correlation coefficient at the 95% confidence level using Student's *t*-test. Uncertainties associated with the slopes and ordinate intercepts of all linear relations are denoted by the 95% confidence intervals.

2.11 References

1. Hummers Jr, W.S. and Offeman, R.E. Preparation of graphitic oxide. *Journal of the American Chemical Society*, 1958. **80**(6): 1339-1339.
2. Brunauer, S., Emmett, P.H. and Teller, E. Adsorption of gases in multimolecular layers. *Journal of the American Chemical Society*, 1938. **60**(2): 309-319.

3. Gandhi, M., Spinks, G.M., Burford, R.P. and Wallace, G.G. Film substructure and mechanical properties of electrochemically prepared polypyrrole. *Polymer*, 1995. **36**(25): 4761-4765.
4. Runyan, W.R. Semiconductor measurements and instrumentation. 1975, McGraw-Hill Publishers: New York.

CHAPTER 3

DEVELOPMENT AND CHARACTERISATION OF CONDUCTING POLYPRROLE FILMS AS A POTENTIAL TOOL FOR ELECTROCHEMICAL TREATMENT OF AZO DYES IN TEXTILE WASTEWATERS

3.1 Introduction

Azo dyes are among the most widely used groups of dyes in textile applications [1]. This is mainly due to their cost effectiveness, ease of synthesis and intense colouring properties. Owing to their high solubility in water [2], potential carcinogenicity [3], intense colours [4] and non-reactive nature [5], azo dyes are known to exhibit various adverse effects upon aquatic flora and fauna [2]. This becomes an even more severe issue in environments where existence of dyes persists for a long period of time. Their intense colours in an aqueous system also inevitably decrease the amount of sunlight penetration, causing a reduction in the rate of photosynthesis, which in turn affects various life forms in the water body [6].

Several treatment methods for azo dyes have hitherto been reported. These include microbial degradation [7], adsorbents (*e.g.* active carbon) [8, 9], sacrificial iron electrodes [10], electrolysis [11, 12], electrocoagulation [13, 14], ion-pair extraction [15], Fenton's process and other advanced electrochemical oxidation processes [16, 17]. However, there are severe limitations associated with these methods. For example, there are disposal problems associated with spent carbon where active carbon is used as an adsorbent [18, 19]. Fenton's process also generates appreciable quantity of ferric hydroxide sludge that requires further treatment before proper disposal [20]. On the other hand, microbial degradation-based biological treatments are very slow processes due to their limitation in decomposing macromolecular dyes. In addition, the majority of these dyes are chemically stable and resistant to microbiological attack as a result of low degradation efficiency [21]. Notably, chemical and electrochemical oxidation

treatments often produce toxic by-products during operation. As an example, the electrochemical oxidation of the azo dyes, azobenzene, *p*-methyl red, methyl orange, Orange G and Sunset Yellow FCF produced 1,4–benzoquinone, pyrocatechol, 4-nitrocatechol, 1,3,5-trihydroxynitrobenzene, *p*-nitrophenol, hydrazine, aromatic amines, respectively, which are carcinogenic and more toxic than the original dye molecules [15, 22, 23]. Therefore, there is a need for developing alternative treatments that are effective and environmentally friendly in removing dyes from textile effluents.

Among the azo dyes, Acid Red 1 (5-(acetylamino)-4-hydroxy-3-[[4-(phenylamino) phenyl]azo]-2,7-naphthalenedisulfonic acid disodium salt), the structure of which is shown in Figure 3.1, has been classified as a non-biodegradable dye by the Environment Protection Agency [24]. This is a potential environmental concern, not only that it generates aesthetical problems associated with decolourisation of the water body, but there are also evidences for the carcinogenic effect of its degradation products in anaerobic conditions [25-27].

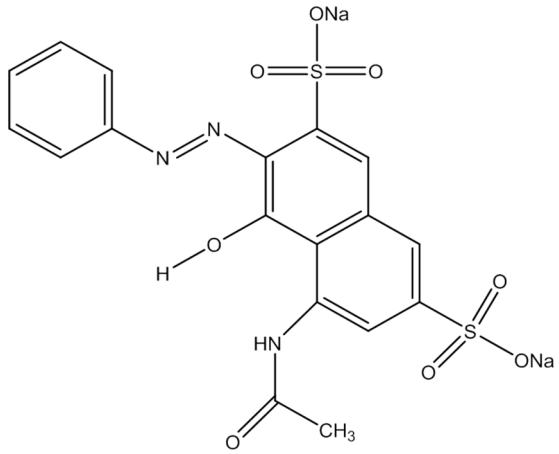

Figure 3.1 Structure of the Azo dye, Acid Red 1.

Among conducting polymers, polypyrrole has received a lot of recognition due to its high conductivity (up to 2000 S cm^{-1}) [28] and thermal stability [29, 30]. As shown in Figure 3.2 below, the synthesis of polypyrrole usually involves electrochemical oxidation of its monomer, pyrrole, to yield a polymeric chain with a positive backbone. In order to neutralise this charge, a counter anion, for example, that of *p*-toluene sulfonate ($p$$TS^-$), is entrapped in the backbone structure. The polypyrrole–$p$$TS^-$ film has long been known to exhibit conductivity as high as 160 S cm^{-1} [31]. Many studies have shown that this entrapment process is electrochemically

reversible [30, 32], enabling polypyrrole to act as an anion exchanger, depending upon the mobility of the entrapped counter anion [33]. Clearly, mobile anions can also be easily liberated from the polymeric film, as shown in Figure 3.2. In this respect, several researchers have described the transport of small organic molecules, for example, aza crown ether and tosylate, across polypyrrole by an anion exchanging mechanism [34-36]. These reports also found that the polypyrrole films are selective towards the original counter anion used, and the size of the counter anion controls the microstructure and porosity of the films. The relation between the porosity of the membrane and affinity for certain anions suggests a memory effect in terms of selectivity of the polypyrrole films [37]. In other words, after entrapping a particular anion in the polypyrrole film, specific channels for the anion are formed. This behaviour was used to explain the polypyrrole–anion films selectivity towards the targeted anion.

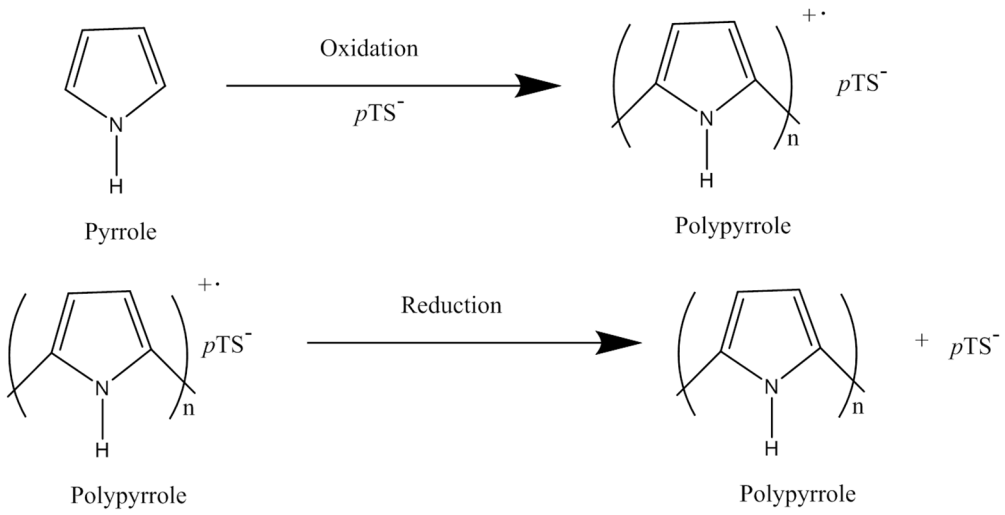

Figure 3.2 Schematic diagram for pyrrole oxidation and polypyrrole reduction in the presence of the counter ion, *p*TS$^-$.

In this chapter, we will demonstrate the application of polypyrrole as a potential tool for treatment of azo dyes in textile effluents, using Acid Red 1 as a model dye. Initially, pyrrole was electrochemically oxidise in the presence of Acid Red 1 as a counter ion to synthesise an Acid Red 1-entrapped polypyrrole film (denoted as polypyrrole-Acid Red 1 film). The films obtained were then characterised by electrochemistry, scanning electron microscopy and spectrophotometry. Unlike many other optimisation experiments conducted by changing- one-parameter-at-a time procedure, experimental parameters for Acid Red 1 entrapment in polypyrrole film were optimised using a two level-factorial design to identify the significant

parameters and possible interactions among the parameters. Finally, we will evaluate the liberation efficiency of Acid Red 1 after electrochemically reducing polypyrrole-Acid Red 1 films.

3.2 Experimental

The details of the experimental procedure adopted for experiment in this chapter have been presented in Chapter 2. Briefly, each polypyrrole-Acid Red 1 film was potentiostatically polymerised on a stainless steel working electrode in an electrochemical cell accommodating a three-electrode system in the presence of 0.2 mol L^{-1} pyrrole and Acid Red 1 of concentration 60 – 2000 mg L^{-1} for a duration from 20 to 420 min. The polypyrrole-Acid Red 1 film was carefully peeled off using a scalpel from the electrode before being used in further characterisation experiments such as X-ray diffraction (XRD), Fourier transform infrared spectroscopy (FTIR), scanning electron microscopy (SEM). Film conductivity measurements were performed using a locally constructed four-point probe. The remaining electrolyte solution in the cell was used to evaluate the percentage of Acid Red 1 entrapped in a polypyrrole film by UV-visible spectrophotometry. The liberation experiment of the same film was also performed and the resultant solution was again spectrophotometrically analysed to determine the liberation efficiency of Acid Red 1 entrapped polypyrrole film. A two-factorial design was also used to identify the significant factors in Acid Red 1 entrapment in polypyrrole films. These factors included solution pH, adsorption time, Acid Red 1 concentration and pyrrole concentration.

3.3 Results and discussion

3.3.1 Characterisation of electropolymerised polypyrrole films

3.3.1.1 Electrochemical characterisation of polypyrrole-Acid Red 1 films

In this work, we are exploiting the anion entrapping-liberating mechanism in a polypyrrole film to develop a feasible treatment method for dye molecules in textile effluents. We have chosen the azo dye, Acid Red 1, as a model analyte in this pilot study. Initially, cyclic voltammetry of 0.2 mol L^{-1} pyrrole was conducted at a stainless steel electrode in the presence of 1500 mg L^{-1} Acid Red 1 as a supporting electrolyte. We have used a stainless steel electrode in this work solely because it is an economical material for construction of bigger-size electrodes when necessary. Trace (a) in Figure 3.3 shows the cyclic voltammogram obtained, in which the

potential was initially scanned positively from 0.0 V to 1.0 V. This was then scanned negatively to -1.0 V, followed by a positive scan to 0.0 V to terminate the experiment. Note the difference in current at the beginning and at the end of the scan at 0.0 V. This has most likely arisen from the use of a stainless steel electrode at the beginning of the scan, and a polypyrrole coated stainless steel electrode towards the end of the scan, which has given rise to different residual current in the cyclic voltammogram. Here, an oxidation peak at 0.76 V was observed as the potential was scanned from -1.0 V to 1.0 V, and a reduction peak at -0.64 V as the potential was scanned backward. The former peak was attributed to the oxidation of pyrrole to form polypyrrole with a positively charged backbone with entrapped Acid Red 1 anion, while the latter peak arose from the reduction of polypyrrole to form an uncharged, Acid Red 1 liberated film. The voltammogram shown in trace (a) is comparable to that of a very broad oxidation peak between 0.1-0.6 V and a sharper reduction peak at -0.7 V (versus Ag|AgCl) for the formation of polypyrrole films in the presence of 1.0 M KNO_3 [38]. A peak separation of ~1.4 V between the oxidation peak and the reduction peak was observed in Figure 3.3. This is comparable to ~1.4 V in the cyclic voltammogram obtained after electropolymerising pyrrole in KNO_3 on stainless steel electrode [39], and ~1.2 V in the cyclic voltammogram obtained after electropolymerising pyrrole in KCl on a platinum electrode [40]. Notably, the peak separation is affected by the overpotential needed to facilitate the electron transfer kinetics at an electrode, which will vary at different electrode materials. In contrast, trace (b) shows a featureless cyclic voltammogram obtained in the Acid Red 1 supporting electrolyte without any pyrrole. Notably, Wang *et al.* also observed no Acid Red 1 oxidation / reduction peaks at a glassy carbon electrode in 0.1 mol L^{-1} Na_2SO_4 solution between -1.0 V and 1.0 V [41]. There are two additional small oxidation peaks at +0.1 V and +0.3 V, and two additional reduction peaks at -0.1 V and -0.4 V. We attribute these to the presence of unknown impurities in the Acid Red 1 solution. As these peaks were not observed in identical experiments using the same electrochemical cell, after replacing the Acid Red 1 solution. Note that these peaks are not of major concern in this work. Based on trace (a), an oxidation potential of +0.88 V, which is more positive than the oxidation peak potential, but not more than +0.9 V to avoid overoxidation of pyrrole and a reduction potential of -0.80 V, which is more negative than the reduction peak potential, were selected to be the respective potential for entrapment and liberation of Acid Red 1 in polypyrrole films in our studies below.

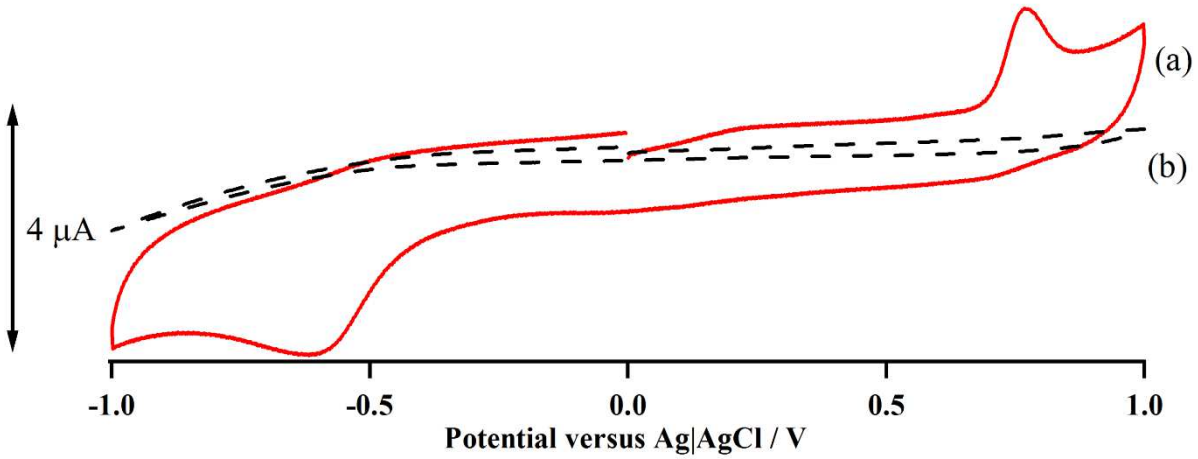

Figure 3.3 Cyclic voltammetry of (a) 0.2 M pyrrole at a stainless steel electrode in 1500 mg L^{-1} Acid Red 1 as supporting electrolyte and (b) 1500 mg L^{-1} Acid Red 1 supporting electrolyte without any pyrrole; scan rate 100 mV s^{-1}.

3.3.1.2 Conductivity of polypyrrole-Acid Red 1 films

It was necessary to synthesise conductive films for electrochemical dye entrapment and liberation. In our work, we have measured the conductivity of polypyrrole-Acid Red 1 formed in 0.2 M pyrrole and 1500 mg L^{-1} of Acid Red 1 solution to be 18 S cm^{-1} (with a standard deviation of 1.2 S cm^{-1}; N = 7). Our results are comparable to 2-18 S cm^{-1} obtained by Wang *et al.* using polypyrrole films doped with different sulfonic acids [42]. Clearly Acid Red 1 is bulkier and less mobile than smaller aromatic sulfonates such as *p*TS^-, and this leads to less well ordered polypyrrole films of lower conductivity.

3.3.1.3 Scanning electron microscopic study of polypyrrole-Acid Red 1 films

Scanning electron microscopy was employed to study the surface morphology of the polypyrrole-Acid Red 1 films. Figure 3.4 shows the scanning electron micrograph of the surface of a polypyrrole film directly exposed to the electrolyte in the cell. In this micrograph, we observe typical 'cauliflower' like structures on such films, similar to those previously observed at polypyrrole films polymerised in the presence of *p*TS [43]. Notably, the film surface is not flat, but consists of a series of peaks and valleys with considerable surface roughness associated with a high degree of film porosity.

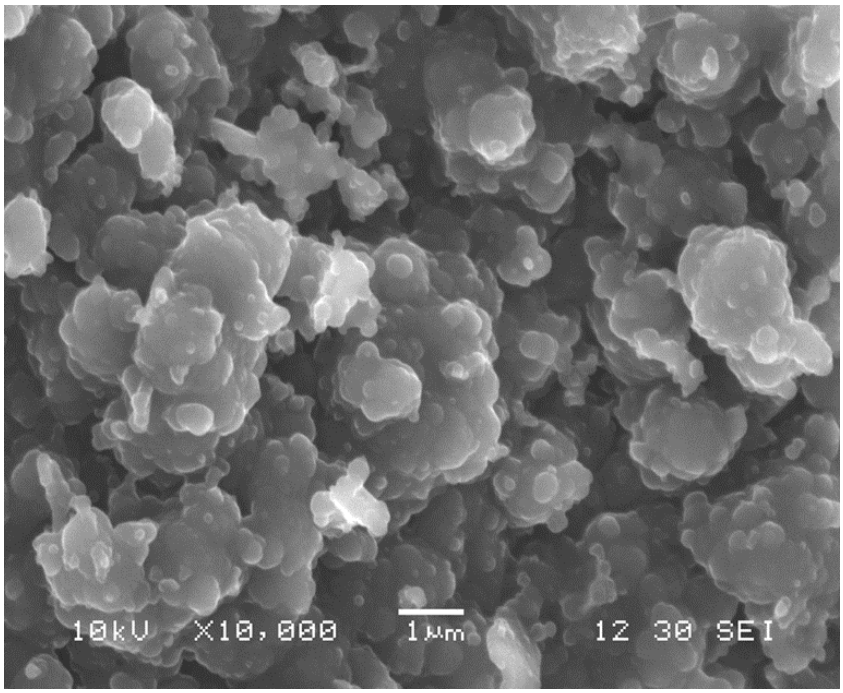

Figure 3.4 Scanning electron micrograph of the electrolyte-facing surface of a polypyrrole-Acid Red 1 film.

3.3.1.4 FTIR of polypyrrole-Acid Red 1 films

The polypyrrole-Acid Red 1 films was also analysed by FTIR. The spectrum of a polypyrrole-Acid Red 1 film is shown in Figure 3.5. For comparison, the spectra of Acid Red 1 alone and a polypyrrole-NO_3^- film are also included in Figure 3.5. The spectra of both polypyrrole-Acid Red 1 (trace a) and polypyrrole-NO_3^- (trace b) show three groups of weak bands at (1) ~1660, 1490-1530 and 1410 cm^{-1}, (2) ~1050-1150 cm^{-1}, (3) ~980 and 880 cm^{-1}. Similar results were observed by Zhang *et al*. [44] and they have assigned these three groups of bands to ring stretching, N-H bending of polypyrrole, in-plane and out-of-plane C-H bending, respectively. In addition, according to Zhang *et al*. [44] and Li *et al*. [45] the absorption peaks at 898, 1256 cm^{-1} indicate the coupling of S=O with the stretching vibration of the pyrrole ring. In comparison, the FTIR spectrum of Acid Red 1 alone in Figure 3.5(c) shows characteristic absorption bands at 750, 1256 cm^{-1} corresponding to the strong stretching vibration of S=O group and the peak at 1750 cm^{-1} corresponding to C=O stretching of Acid Red 1. Therefore, the presence of these peaks in Figure 3.5(a) provides further evidence of Acid Red 1 entrapment in polypyrrole.

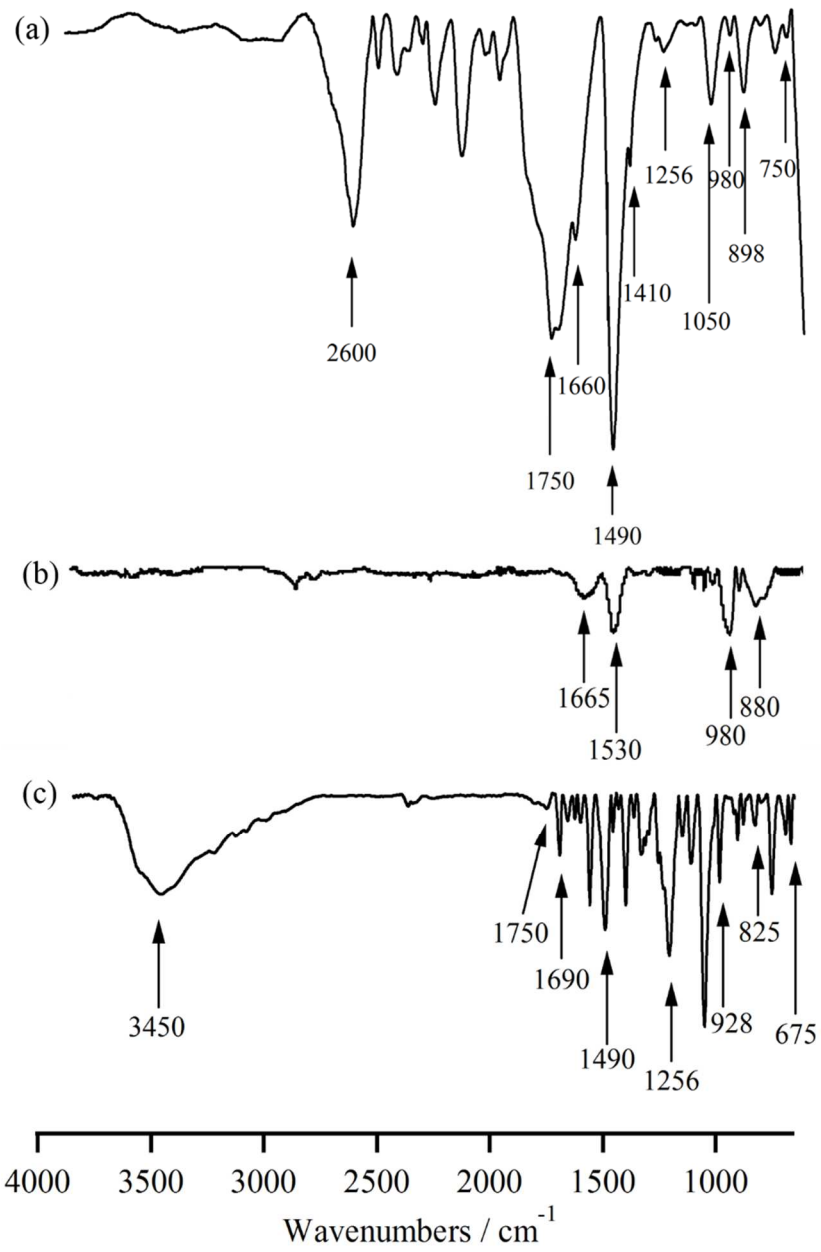

Figure 3.5 FTIR spectra of (a) a polypyrrole-Acid Red 1 film, (b) polypyrrole-NO_3^- film and (b) Acid Red 1 alone.

3.3.1.5 XRD analysis of polypyrrole-Acid Red 1 films

In this experiment, XRD analysis was carried out as a complementary technique for examining the entrapment of Acid Red 1 in polypyrrole films. Previously, Ferreira *et al.* [46] analysed XRD patterns of polypyrrole synthesised with the dyes Remazol Black B and Dianix Red. In their work, they proposed a structure consisting of a dye sandwiched between two polypyrrole

chains separated by a perpendicular distance termed "*d*-spacing", which can be evaluated based on Bragg's law [46] in Equation (3.1).

$$\lambda = 2\, d \sin\theta \qquad \text{Equation (3.1)}$$

where λ denotes the Cu Kα radiation wavelength (λ = 0.15405 nm in our work) and sin θ is derived from the lowest 2θ signal in a diffraction pattern. The diffraction patterns of a polypyrrole-Acid Red 1 film, depicted in Figure 3.6(a), shows a sharp peak at the lowest 2θ diffraction angle of 8.62. For comparison, the XRD patterns of a polypyrrole-NO_3^- film alone, shown in Figure 3.6(b), do not reveal any distinct peaks. The result of Acid Red 1 alone is displayed in Figure 3.6(c), which also shows a 2θ peak at 8.62, supporting the origin of this peak in Figure 3.6(a). Accordingly, a *d*-spacing of 10.3 Å was estimated from Equation (3). This distance suggests that, Acid Red 1 is sandwiched between two polymer chains, and it may act as a bridge between the chains.

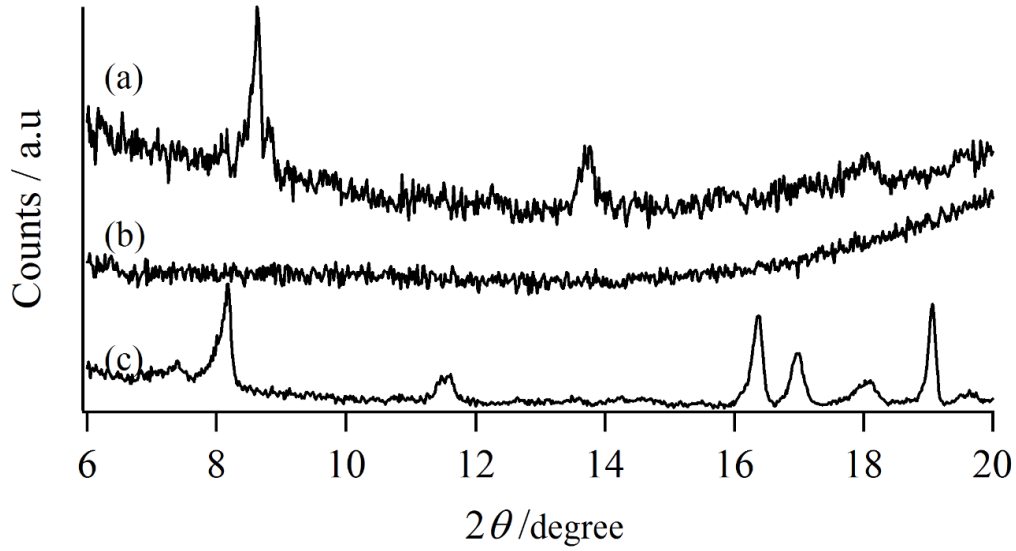

Figure 3.6 XRD patterns of (a) polypyrrole-Acid Red 1, (b) polypyrrole-NO_3^- and (c) Acid Red 1.

3.3.2 Polypyrrole yield

Evidently, the yield of polypyrrole obtained by electropolymerisation of pyrrole is affected by several factors including the counter ion, solvent, electropolymerisation conditions (*e.g.* electrode size, applied potential), temperature and pH. This particular aspect of polymerisation of pyrrole to form polypyrrole has been studied by quite a few research groups [47-49]. In

particular, Maiti *et al.* [49] obtained a yield of ~6% by electropolymerising pyrrole (0.2 M) in the presence of *p*TS (0.05 M) at an applied voltage 2.0 V for 1 h at a temperature of 298 K. The percent yield of polymer from its monomer was estimated from the ratio of the amount of monomer used to the amount of polymer formed. By adopting similar approach reported by Maiti *et al*., we estimated a 2-15% yield after electropolymerising 0.2 M pyrrole,at +0.88 V in the presence of 60-1500 mg L^{-1} Acid Red 1 for 420 min, at 298 K. In these experiments, a solution pH of 4 was used throughout.

3.3.3 Optimisation of Acid Red 1 entrapment parameters

Initially, it is necessary to determine the optimum experimental conditions for Acid Red 1 entrapment in polypyrrole films. In our work, we have used a two-level factorial design not only to identify the significant factors and determine their optimal values, but also to study possible interactions among these factors [50]. We have considered factors including solution pH (denoted as X_1), pyrrole concentration ($C_{pyrrole}$; X_2), Acid Red 1 concentration ($C_{Acid\ Red\ 1}$; X_3) and polymerisation time (X_4). Accordingly, a 2^4 factorial design for four factors (16 experiments in total) was adopted. Table 3.1 shows the experimental factors and their levels employed in the 2^4 factorial design. Based on earlier experimental results and practical operation conditions, a low (–) and a high (+) level were assigned to each factor. Following electropolymerisation under the conditions specified for each run, the percentage weight of Acid Red 1 adsorbed per weight of polypyrrole film was evaluated using Equation (1). Two replicate measurements were conducted at each condition and the average results obtained at different computation of effects and interactions (X_1X_2, X_1X_3, X_1X_4, X_2X_3, X_2X_4, X_3X_4, $X_1X_2X_3$, $X_1X_3X_4$, $X_2X_3X_4$, $X_1X_2X_3X_4$) for a 2^4 factorial design are shown in Table 3.2. Also, in Table 3.2, the Effect row represents the average of the high (+) and the low (–) values of each experimental factor, while t_E represents a signal-to-noise ratio calculated by the expression

$$t_E = \frac{\text{Effect}}{2s_p / \sqrt{n_F}}$$

$$s_p = \sqrt{\frac{\sum_{i=1}^{m}(\text{degrees of freedom} \times \text{variance})}{\sum_{i=1}^{m}\text{degrees of freedom}}}$$

where s_p is a pooled standard deviation, and m is the number of experimental conditions (m=16 in this work), n_F is the number of experimental replications (n_F=32). When the absolute value of t_E is larger than the tabulated *t*-value (denoted by *t** of 2.12) at the 95% confidence level, the effect of a particular factor or interaction between factors is considered significant. Accordingly, the results in Table 3.2 reveal that X_1, X_3 and X_4 are statistically significant and X_2 is not significant. None of the interaction was found to be significant. These results are also graphically shown in a Pareto chart and interaction plots in Figure 3.7 and 3.8, respectively. The vertical line in the Pareto chart in Figure 3.7 shows the minimum value of 2.12 for 16 degree of freedom at 95% confidence interval statistically significant effect. Those factors and interactions with absolute effects greater than the vertical line were found to be statistically significant. Figure 3.8, further support that interactions between factors are not significant. In this way, a prediction equation for our system can be written as:

$$Y = 291.46 - \left(\frac{41.62}{2}\right)X_1 + \left(\frac{468.46}{2}\right)X_3 + \left(\frac{85.87}{2}\right)X_4$$
$$= 291.46 - 20.81X_1 + 234.23X_3 + 42.94X_4$$

Table 3.1 Experimental factors and their levels employed in a 2^4 factorial design.

Factor	Definition	Label	Low level (-)	High level (+)
1	Solution pH	X_1	2	12
2	$C_{pyrrole}$ /mol L^{-1}	X_2	0.1	0.6
3	$C_{Acid\ Red\ 1}$ / mg L^{-1}	X_3	60	2000
4	Time / min	X_4	20	480

Table 3.2 Model matrix and the results of the 2^4 factorial design.

	Code X values																	
Run	Mean	X_1	X_2	X_3	X_4	X_1X_2	X_1X_3	X_1X_4	X_2X_3	X_2X_4	X_3X_4	$X_1X_2X_3$	$X_1X_3X_4$	$X_2X_3X_4$	$X_1X_2X_3X_4$	Average Dye Entrapped / mg g^{-1}	Variance	DF
1	+	−	−	−	−	+	+	+	+	+	+	−	−	−	+	32.22	31.13	1
2	+	+	−	−	−	−	−	−	+	+	+	+	+	−	−	6.27	6.16	1
3	+	−	+	−	−	−	+	+	−	−	+	+	−	+	−	38.96	9.72	1
4	+	+	+	−	−	+	−	−	−	−	+	−	+	+	+	8.00	24.50	1
5	+	−	−	+	−	+	−	+	−	+	−	+	+	+	−	480.60	873.62	1
6	+	+	−	+	−	−	+	−	−	+	−	−	−	+	+	450.46	2670.34	1
7	+	−	+	+	−	−	−	+	+	−	−	−	+	−	+	490.75	1225.13	1
8	+	+	+	+	−	+	+	−	+	−	−	+	−	−	−	460.94	2538.28	1
9	+	−	−	−	+	+	+	−	+	−	−	−	+	+	−	95.87	123.56	1
10	+	+	−	−	+	−	−	+	+	−	−	+	−	+	+	65.58	59.08	1
11	+	−	+	−	+	−	+	−	−	+	−	+	+	−	+	98.44	65.90	1
12	+	+	+	−	+	+	−	+	−	+	−	−	−	−	−	92.52	107.90	1
13	+	−	−	+	+	+	−	−	−	−	+	+	−	−	+	600.56	2051.20	1
14	+	+	−	+	+	−	+	+	−	−	+	−	+	−	−	520.93	3862.33	1
15	+	−	+	+	+	−	−	−	+	+	+	−	−	+	−	660.75	2346.13	1
16	+	+	+	+	+	+	+	+	+	+	+	+	+	+	+	540.53	3532.20	1
Σ(+)	4663.34	2165.2	2400.87	4205.5	2675.16	2321.22	2238.33	2262.06	2362.89	2371.77	2428.19	2301.85	2261.38	2350.74	2296.52			
Σ(-)	0	2498.14	2262.47	457.84	1988.18	2342.12	2425.01	2401.28	2300.45	2291.57	2235.15	2361.49	2401.96	2312.6	2366.82			
Σ(+)+Σ(-)	4663.34	4663.34	4663.34	4663.34	4663.34	4663.34	4663.34	4663.34	4663.34	4663.34	4663.34	4663.34	4663.34	4663.34	4663.34			
Σ(+)-Σ(-)	4663.34	-332.94	138.41	3747.67	686.98	-20.9	-186.69	-139.22	62.43	80.2	193.05	-59.63	-140.59	38.13	-70.3			
Effect	291.46	-41.62	17.3	468.46	85.87	-2.61	-23.34	-17.4	7.8	10.03	24.13	-7.45	-17.57	4.77	-8.79			
t_E		**-3.37**	1.4	**37.93**	**6.95**	-0.21	-1.89	-1.41	0.63	0.81	1.95	-0.6	-1.42	0.39	-0.71	t*(16)=2.12		

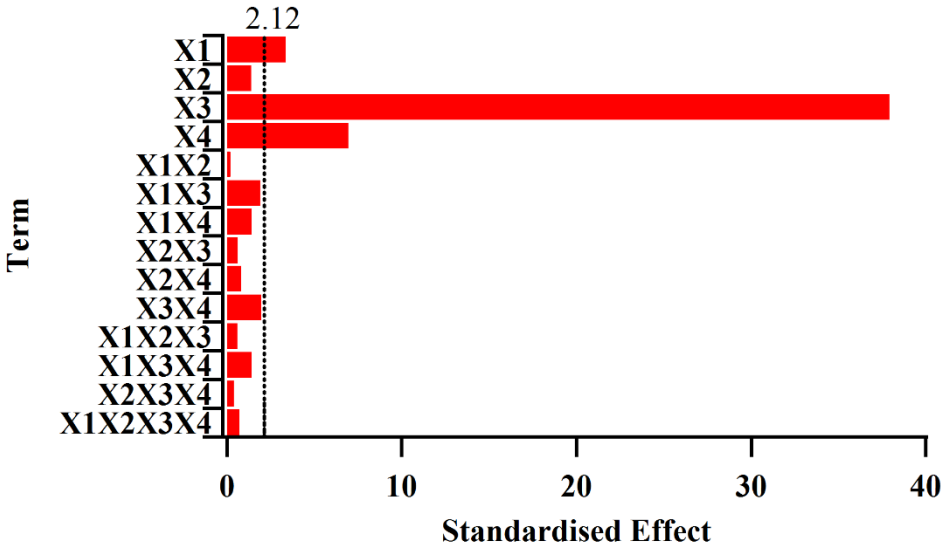

Figure 3.7 Pareto chart of the standardised effects on the entrapment of Acid Red 1 in polypyrrole film using 2^4 factorial design (presented in Table 3.2) at the 95% confidence level.

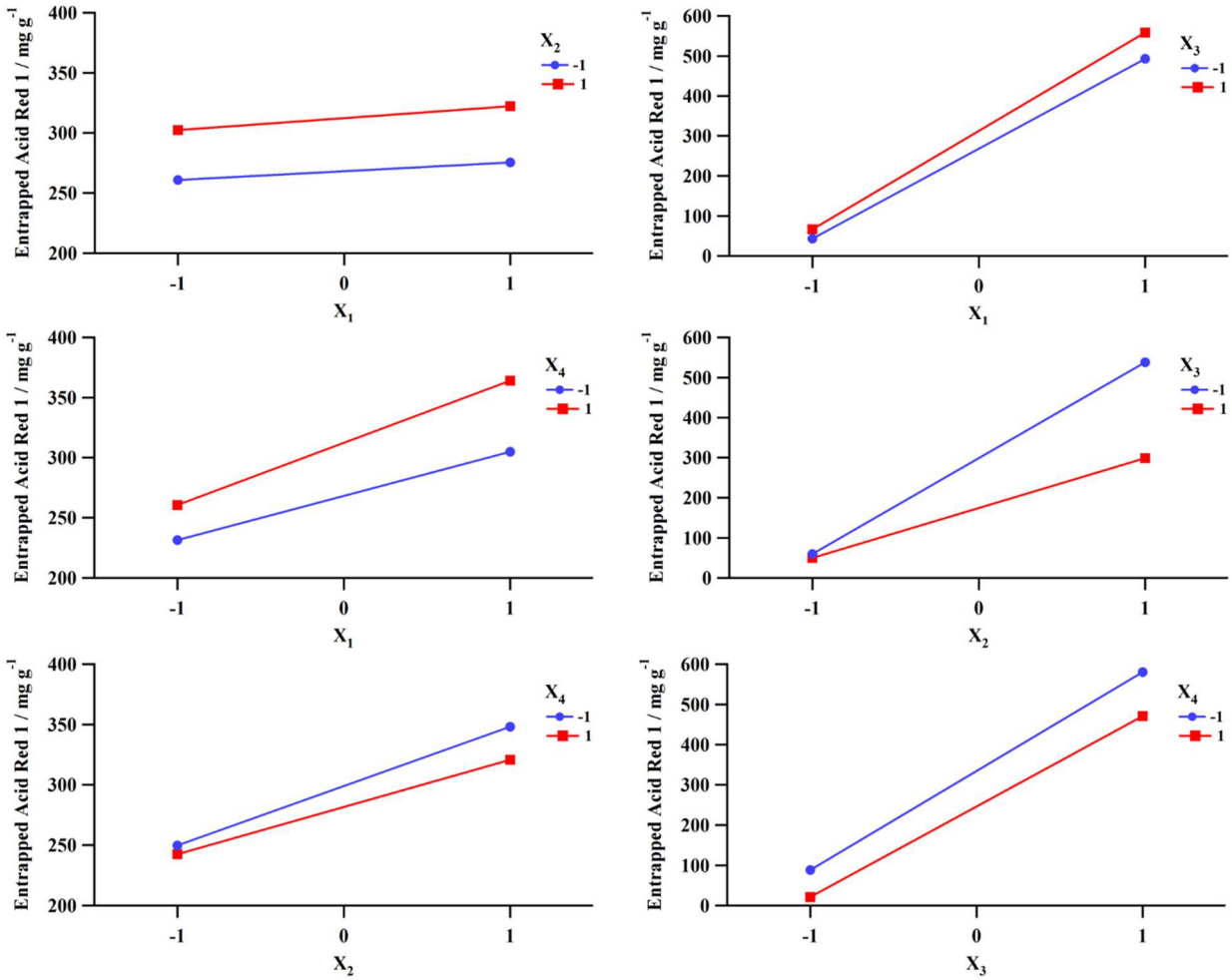

Figure 3.8 Interaction plots, for entrapment of Acid Red 1 using the full 2^4 factorial design (Table 3.2) at the 95% confidence level.

3.3.4 Entrapment of Acid Red 1 in polypyrrole films

3.3.4.1 Effect of solution pH on Acid Red 1 entrapment in polypyrrole films

The pH of the Acid Red 1 solutions is one of the important factors influencing the entrapment process. The effect of the initial dye solution pH on Acid Red 1 entrapment efficiency in polypyrrole was studied between pH 2 and 12 and the results are shown in Figure 3.9(a). A 480 min duration was allowed to entrap Acid Red 1 at different solution pH. In general, more Acid Red 1 was entrapped in polypyrrole films in the pH 2-4 range and a maximum was observed at approximately pH 4. However, this entrapment efficiency of Acid Red 1 then decreased with higher solution pH. Previously, pyrrole was reported to be readily oxidised forming thick, smooth and conducting polypyrrole films in acidic media ~~a~~nd almost insulating films under neutral conditions [45]. However, no film formation was observed in alkaline media owing to an inhibited oxidation of pyrrole [51]. In this work, we observed that thin, fragile polypyrrole films were formed in neutral and alkaline media, which did not favour efficient entrapment of Acid Red 1.

3.3.4.2 Effect of initial Acid Red 1 concentration and polymerisation time on entrapment

Entrapment of Acid Red 1 is also affected by the initial Acid Red 1 concentration and polymerisation time of polypyrrole. Figure 3.9(b) shows the extent of Acid Red 1 entrapped in polypyrrole films with increasing polymerisation time at various initial dye concentrations. Notably, when the initial Acid Red 1 concentration was increased from 60 to 2000 mg L^{-1}, the extent of Acid Red 1 entrapped after 480 min increased from ~51 to 690 mg g^{-1}. This is clearly attributed to an increased driving force arising from the concentration gradient with the higher initial dye concentration. However, over the same Acid Red 1 concentration range, the relative percentage of entrapped Acid Red 1 in polypyrrole films decreased from 68 to 44% (depicted in Figure 3.9(c)). This is most likely due to a limited number of active entrapment sites on polypyrrole films, which were saturated at a particular concentration [52]. Figure 3.9 also shows that equilibrium was attained at an initial dye concentration of 1500 mg L^{-1} with little change at 2000 mg L^{-1}.

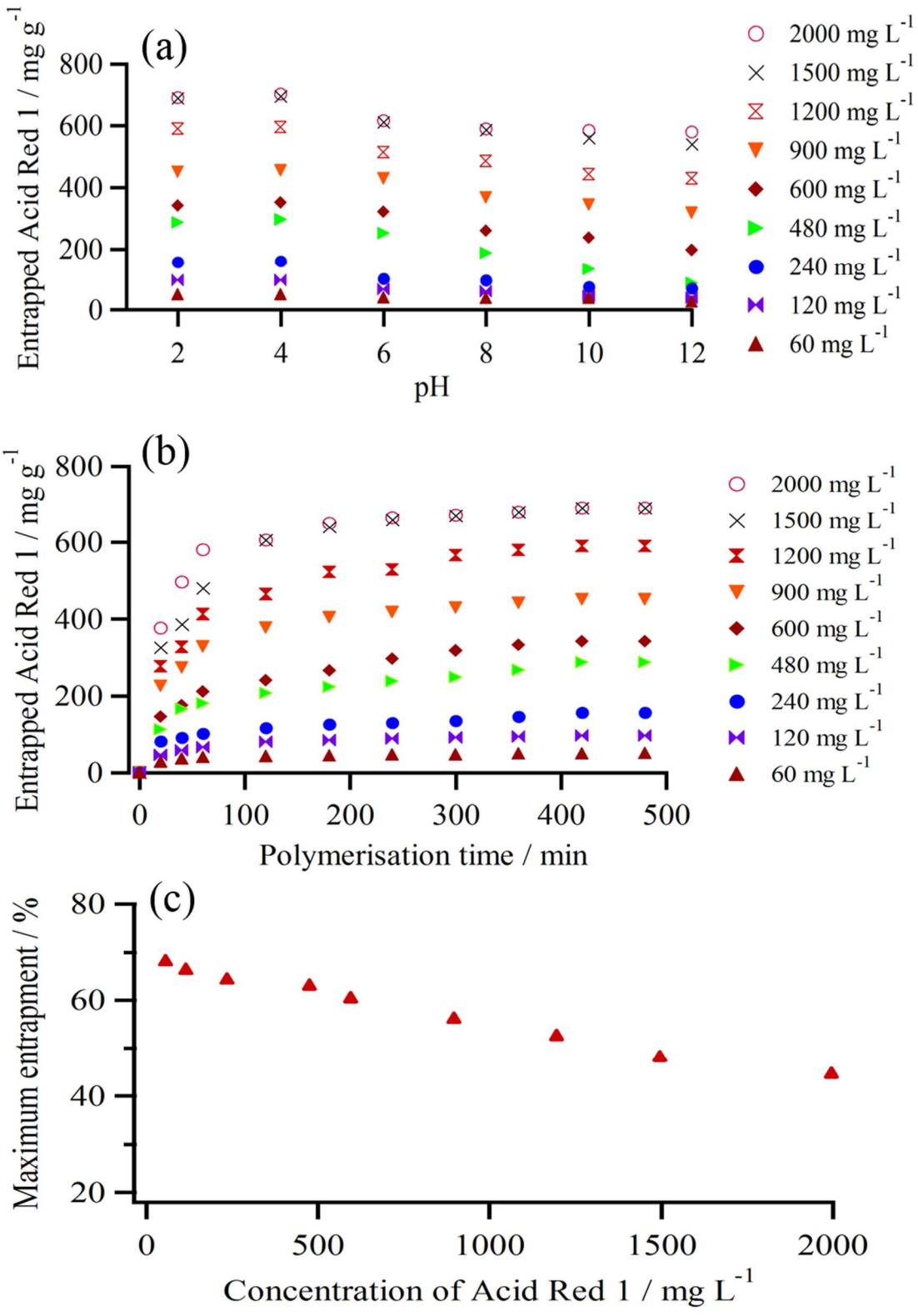

Figure 3.9 Effect of (a) pH, (b) polymerisation time and (c) Acid Red 1 concentration on Acid Red 1 entrapment in polypyrrole films.

3.3.5 Liberation of Acid Red 1 from polypyrrole films

A polypyrrole film-electrolyte system involves the redox couple, polypyrrole$^{+\bullet}$ / polypyrrole [53], where polypyrrole$^{+\bullet}$ is the radical cationic species and polypyrrole is the neutral species. During oxidation, polypyrrole$^{+\bullet}$ will electrostatically attract the anionic Acid Red 1 in the polypyrrole matrix so as to maintain electroneutrality. Similarly, during reduction, electrons are supplied and polypyrrole becomes neutral, leading to the liberation of Acid Red 1 from the polypyrrole film to the solution. Indeed, this particular feature distinguishes the potential treatment method of textile effluents using polypyrrole films from many others reported in literature. In this way, Acid Red 1 itself can be recovered in the process.

In this study, using UV-visible spectrophotometry, we have evaluated the liberation percentage of Acid Red 1 from polypyrrole film by measuring the concentration of the liberated Acid Red 1 in 0.1 mol L^{-1} KNO_3 after applying a reduction potential of -0.80 V for a defined period. This study was conducted with polypyrrole films prepared with 1500 mg L^{-1} Acid Red 1. The results obtained are shown in Figure 3.10. In general, the liberation percentage of Acid Red 1 increased as the initial Acid Red 1 concentration was increased. However, no significant increase in liberation of Acid Red 1 was observed after prolonging the reduction process beyond 180 min. This is most likely because Acid Red 1 entrapped deep in the multilayered film matrix on the stainless steel electrode would be unable to diffuse out from the film interface. Consequently, a low recovery rate was observed. In this experiment, in the presence of an initial Acid Red 1 concentration of 1500 mg L^{-1}, a maximum liberation rate of 21% was estimated following a reduction period of 300 min.

Previously, the base treatment (NaOH treatment) was reported to deprotonate the film, resulting in the removal of the Acid Red 1 counter ions from the film. However, the acid treatment was reported to result in reprotonation of the film and its return with an oxidise state [54]. To improve the liberation performance of the polypyrole film, we have then attempted to measure liberation efficiency of Acid Red 1 in 0.5 mol L^{-1} NaOH solution after applying a reduction potential of -0.80 V for a desired period. Figure 3.13 shows that the liberation efficiency was increased when the reduction process performed in NaOH solution than in KNO_3. This is because hydroxyl ions can react with polypryyole backbone resulting in some formation of quinoid units through deprotonation [55] that replace the Acid Red 1 counter anion in the subsequent treatment.

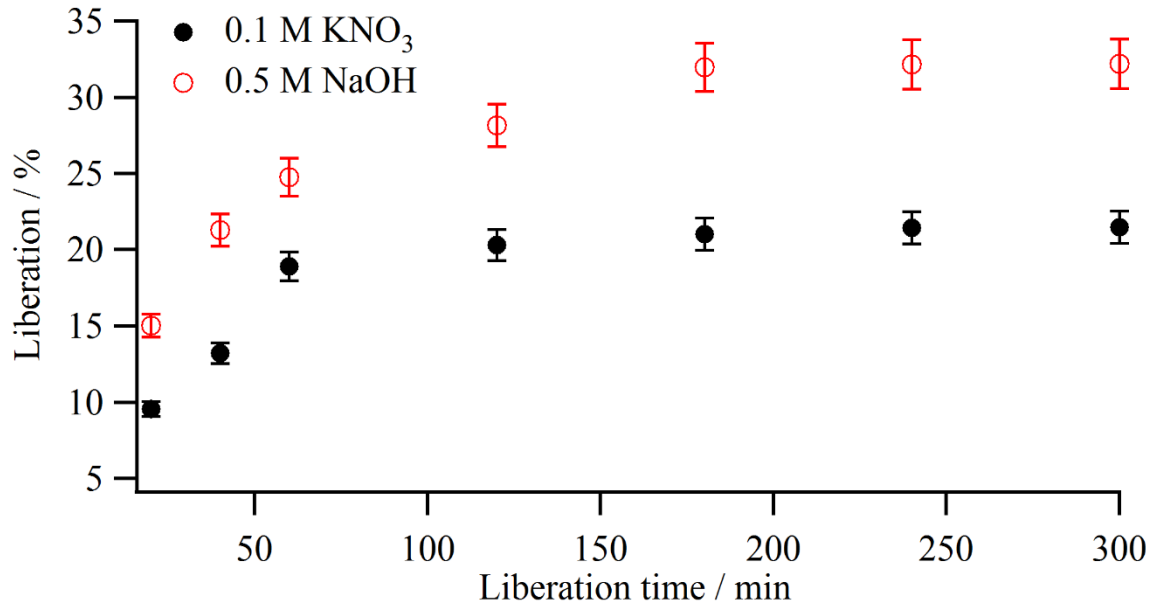

Figure 3.10 Acid Red 1 liberation percentage from polypyrrole in solution containing in 0.1 M KNO_3 and 0.5 M NaOH.

3.3.6 Evaluation of Acid Red 1 entrapment-liberation efficiency in polypyrrole film at different entrapment-liberation cycles

To reduce the treatment cost of dye containing wastewater it is necessary to reuse the polypyrrole film. In order to study the feasibility of reuse of polypyrrole film for Acid Red 1 entrapment liberation, three consecutive entrapment-liberation cycles were performed with the same films. Notably, this entrapment study was conducted using polypyrrole films synthesised in presence of 1500 mg L^{-1} Acid Red 1, 0.2 M pyrrole and the initial solution pH of 4 by applying an oxidation potential of 0.88 V for a duration of 480 min.

Figure 3.11 shows the Acid Red 1 entrapment percentage in polypyrrole films with three consecutive entrapment cycles of the same film. The entrapment percentage of Acid Red 1 for second and third cycles were approximately 24% and 50% less than the first entrapment cycle, respectively. Because, some dye molecules are firmly trapped to the polymer network chain, which was also confirmed by XRD analysis reported in section 3.3.1.8 in this chapter, resulting in low liberation efficiency as well as the breakdown of polypyrrole film because of swelling and shrinkage of the film that happened during oxidation reduction cycle, which reduces the Acid Red 1 re-entrapment in polypyrrole film with consecutive entrapment cycle [56-58]. The

maximum entrapment for first, second and third entrapment cycles was estimated to be 58%, 34% and 10%, respectively, after a polymerisation period of 480 min.

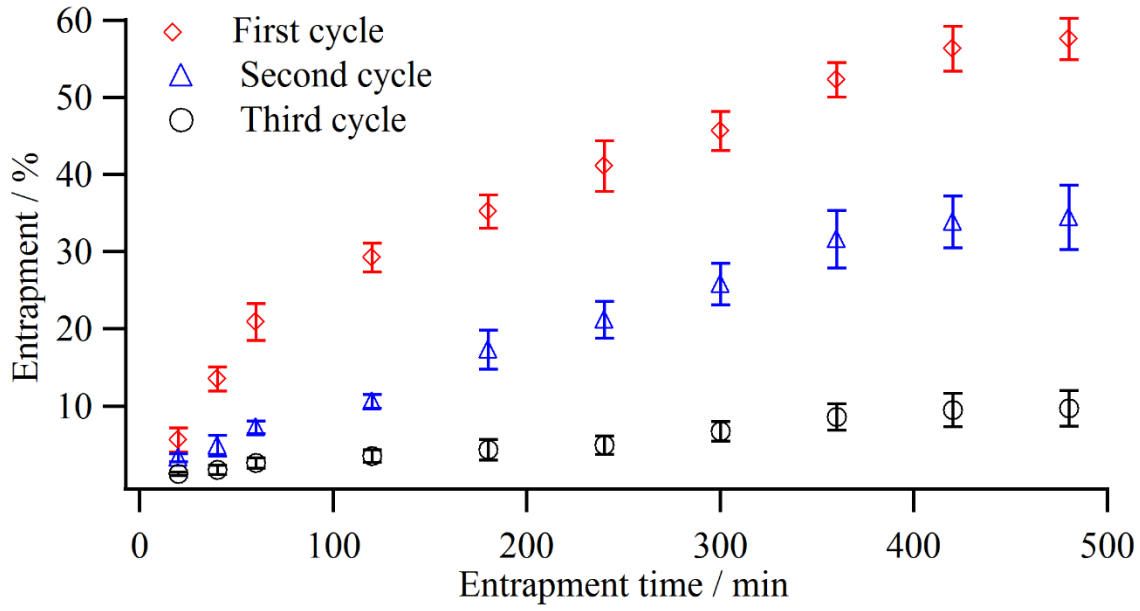

Figure 3.11 Acid Red 1 entrapment percentage in polypyrrole at different cycle

To study the Acid Red 1 liberation efficiency of polypyrrole film at different liberation cycle, we have evaluated the liberation percentage of Acid Red 1 from polypyrrole film, by applying a reduction potential of -0.80 V (*vs* Ag | AgCl) in 0.5 mol L^{-1} NaOH for a duration of 300 min. The results obtained are shown in Figure 3.12. In general, liberation percentage of Acid Red 1 increases with increasing liberation time. However, no significant increase in the liberation of Acid Red 1 was observed after prolonging the reduction process beyond 180 min. This is most likely because Acid Red 1 was entrapped deep in the sandwiched / multilayered film matrix on the stainless steel electrode and it was difficult to diffuse out from the film interface. Consequently, a low recovery rate was observed. Moreover, the liberation percentage of Acid Red 1 decrease in the second and third liberation cycle than the first liberation cycle, due to both compacted sandwiched film matrix and mechanical degradation of the film during reuse. In this experiment, in the presence of an initial Acid Red 1 concentration of 1500 mg L^{-1}, a maximum liberation rate of 32%, 20% and 8% were estimated for first, second and third liberation cycle of Acid Red 1 entrapped polypyrrole films, respectively after a liberation time of 300 min.

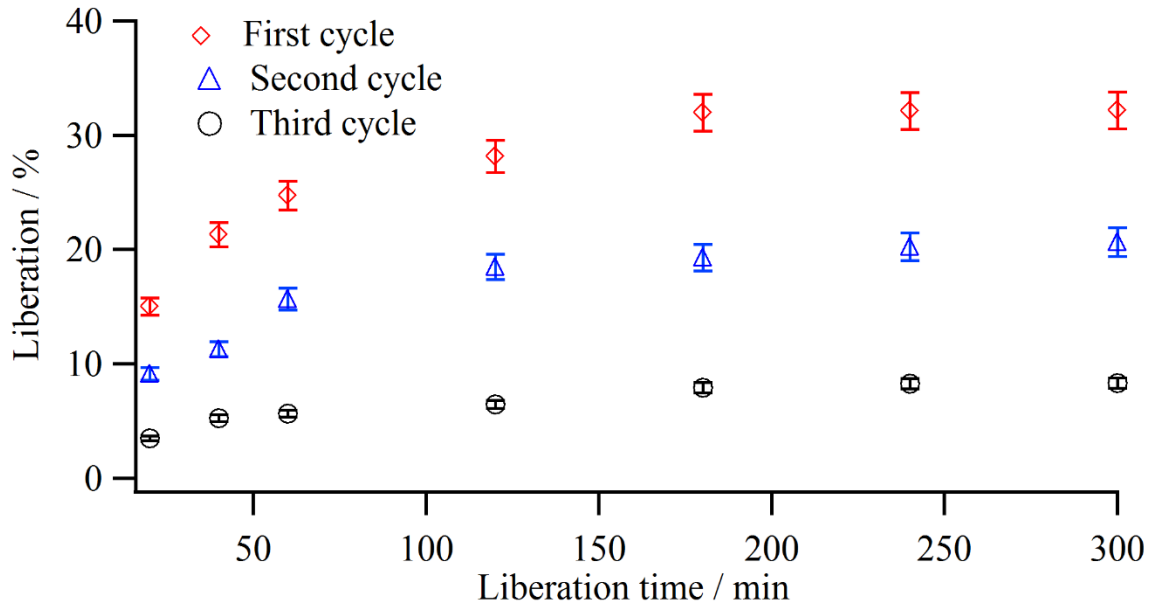

Figure 3.12 Acid Red 1 liberation percentage at polypyrrole in different cycle

3.4 Conclusion

In this study, we have exploited the anion entrapping-liberating property of conducting polypyrrole films to develop a green treatment method for the model azo dye, Acid Red 1. By oxidising pyrrole at 0.88 V in the presence of Acid Red 1, the dye was readily entrapped in the polypyrrole film. We then employed cyclic voltammetry, conductivity measurements, FTIR and X-ray diffraction to characterise these polypyrrole-Acid Red 1 films and all results supported the presence of Acid Red 1 in polypyrrole films synthesised in this way. In addition, based on a two level-factorial design, the entrapment process was found to be dependent on pH, concentration of Acid Red 1 in solution and polymerisation time. The entrapped Acid Red 1 was then liberated from a polypyrrole film by applying a reduction potential of -0.80 V. Our results suggest that electropolymerised conducting polypyrrole films can be further developed as an effective and alternative material for treatment of dye effluents.

3.5 References

1. Ruiz, E.J., Arias, C., Brillas, E., Hernández-Ramírez, A. and Peralta-Hernández, J. Mineralization of Acid Yellow 36 azo dye by electro-fenton and solar photoelectro-fenton processes with a boron-doped diamond anode. *Chemosphere*, 2011. **82**(4): 495-501.

2. Riu, J., Schönsee, I., Barcelo, D. and Rafols, C. Determination of sulphonated azo dyes in water and wastewater. *TrAC Trends in Analytical Chemistry*, 1997. **16**(7): 405-419.

3. Li, P., Zhao, G., Zhao, K., Gao, J. and Wu, T. An efficient and energy saving approach to photocatalytic degradation of opaque high-chroma Methylene Blue wastewater by electrocatalytic pre-oxidation. *Dyes and Pigments*, 2012. **92**(3): 923-928.

4. Sarala, P. and Venkatesha, T. Electrochemical degradation of p-aminobenzoic acid β-naphthol azo dye in alkaline solution. *Journal of Environmental Chemistry and Ecotoxicology*, 2012. **4**(6): 116-123.

5. McClung, S.M. and Lemley, A.T. Electrochemical treatment and HPLC analysis of wastewater containing acid dyes. *Textile Chemist and Colorist*, 1994. **26**(8): 17-22.

6. Banat, I.M., Nigam, P., Singh, D. and Marchant, R. Microbial decolorization of textile-dyecontaining effluents: A review. *Bioresource Technology*, 1996. **58**(3): 217-227.

7. Ma, L., Zhuo, R., Liu, H., Yu, D., Jiang, M., Zhang, X. and Yang, Y. Efficient decolorization and detoxification of the sulfonated azo dye Reactive Orange 16 and simulated textile wastewater containing Reactive Orange 16 by the white-rot fungus *Ganoderma* sp. En3 isolated from the forest of Tzu-chin mountain in china. *Biochemical Engineering Journal*, 2014. **82**: 1-9.

8. Foo, K.Y. and Hameed, B.H. An overview of dye removal via activated carbon adsorption process. *Desalination and Water Treatment*, 2010. **19**(1-3): 255-274.

9. Dermentzis, K. Removal of nickel from electroplating rinse waters using electrostatic shielding electrodialysis/electrodeionization. *Journal of Hazardous Materials*, 2010. **173**(1): 647-652.

10. Mollah, M.Y., Pathak, S.R., Patil, P.K., Vayuvegula, M., Agrawal, T.S., Gomes, J.A., Kesmez, M. and Cocke, D.L. Treatment of Orange II azo-dye by electrocoagulation (EC) technique in a continuous flow cell using sacrificial iron electrodes. *Journal of Hazardous Materials*, 2004. **109**(1): 165-171.

11. Kupferle, M.J., Galal, A. and Bishop, P.L. Electrolytic treatment of azo dye wastewaters: Impact of matrix chloride content. *Journal of Environmental Engineering*, 2006. **132**(5): 514-518.

12. Xu, L., Zhao, H., Shi, S., Zhang, G. and Ni, J. Electrolytic treatment of CI Acid Orange 7 in aqueous solution using a three-dimensional electrode reactor. *Dyes and Pigments*, 2008. **77**(1): 158-164.

13. Aleboyeh, A., Daneshvar, N. and Kasiri, M. Optimization of CI Acid Red 14 azo dye removal by electrocoagulation batch process with response surface methodology. *Chemical Engineering and Processing: Process Intensification*, 2008. **47**(5): 827-832.

14. Can, O., Kobya, M., Demirbas, E. and Bayramoglu, M. Treatment of the textile wastewater by combined electrocoagulation. *Chemosphere*, 2006. **62**(2): 181-187.

15. Gooding, J.J., Compton, R.G., Brennan, C.M. and Atherton, J.H. The mechanism of the electro-reduction of some azo dyes. *Electroanalysis*, 1996. **8**(6): 519-523.

16. Chu, Y.-Y., Wang, W.-J. and Wang, M. Anodic oxidation process for the degradation of 2, 4-dichlorophenol in aqueous solution and the enhancement of biodegradability. *Journal of Hazardous Materials*, 2010. **180**(1): 247-252.

17. El-Desoky, H.S., Ghoneim, M.M. and Zidan, N.M. Decolorization and degradation of Ponceau S azo-dye in aqueous solutions by the electrochemical advanced Fenton oxidation. *Desalination*, 2010. **264**(1): 143-150.

18. Hubbe, M.A., Beck, K.R., O'Neal, W.G. and Sharma, Y.C. Cellulosic substrates for removal of pollutants from aqueous systems: A review. 2. Dyes. *BioResources*, 2012. **7**(2): 2592-2687.

19. Qu, J. Research progress of novel adsorption processes in water purification: A review. *Journal of Environmental Sciences*, 2008. **20**(1): 1-13.

20. Chang, P., Huang, Y., Hsueh, C., Lu, M. and Huang, G. Treatment of non-biodegradable wastewater by electro-Fenton method. *Water Science and Technology*, 2004. **49**(4): 213-218.

21. Pearce, C., Lloyd, J. and Guthrie, J. The removal of colour from textile wastewater using whole bacterial cells: A review. *Dyes and Pigments*, 2003. **58**(3): 179-196.

22. Guivarch, E., Trevin, S., Lahitte, C. and Oturan, M.A. Degradation of azo dyes in water by electro-fenton process. *Environmental Chemistry Letters*, 2003. **1**(1): 38-44.

23. Tauber, M.M., Guebitz, G.M. and Rehorek, A. Degradation of azo dyes by laccase and ultrasound treatment. *Applied and Environmental Microbiology*, 2005. **71**(5): 2600-2607.

24. Shu, H.-Y., Huang, C.-R. and Chang, M.-C. Decolorization of mono-azo dyes in wastewater by advanced oxidation process: A case study of Acid Red 1 and Acid Yellow 23. *Chemosphere*, 1994. **29**(12): 2597-2607.

25. Golka, K., Kopps, S. and Myslak, Z.W. Carcinogenicity of azo colorants: Influence of solubility and bioavailability. *Toxicology Letters*, 2004. **151**(1): 203-210.

26. Van der Zee, F.P. and Villaverde, S. Combined anaerobic–aerobic treatment of azo dyes - a short review of bioreactor studies. *Water Research*, 2005. **39**(8): 1425-1440.

27. Pinheiro, H., Touraud, E. and Thomas, O. Aromatic amines from azo dye reduction: Status review with emphasis on direct UV spectrophotometric detection in textile industry wastewaters. *Dyes and Pigments*, 2004. **61**(2): 121-139.

28. Qi, G., Huang, L. and Wang, H. Highly conductive free standing polypyrrole films prepared by freezing interfacial polymerization. *Chemical Communications*, 2012. **48**(66): 8246-8248.

29. Chronakis, I.S., Grapenson, S. and Jakob, A. Conductive polypyrrole nanofibers via electrospinning: Electrical and morphological properties. *Polymer*, 2006. **47**(5): 1597-1603.

30. Masubuchi, S., Kazama, S., Mizoguchi, K., Shimizu, F., Kume, K., Matsushita, R. and Matsuyama, T. The transport properties of metallic shirakawa polyacetylenes with different dopant species. *Synthetic Metals*, 1995. **69**(1): 71-72.

31. Masuda, H. and Asano, D. Preparation and properties of polypyrrole. *Synthetic metals*, 2003. **135**(136): 43-44.

32. Arrieta Almario, A.A. and Tarazona Caceres, R.L. Study of kinetic formation and the electrochemical behavior of polypyrrole films. *Journal of the Chilean Chemical Society*, 2009. **54**(1): 14-19.

33. Ansari Khalkhali, R., Price, W. and Wallace, G.G. Quartz crystal microbalance studies of the effect of solution temperature on the ion-exchange properties of polypyrrole conducting electroactive polymers. *Reactive and Functional polymers*, 2003. **56**(3): 141-146.

34. Fabre, B. and Simonet, J. Electroactive polymers containing crown ether or polyether ligands as cation-responsive materials. *Coordination Chemistry Reviews*, 1998. **178**: 1211-1250.

35. Korri Youssoufi, H., Yassar, A., Baiteche, S., Hmyene, M. and Garnier, F. Designing polypyrrole-based sensors: Selective electrochemical cation in aza crown ethers. *Synthetic Metals*, 1994. **67**(1): 251-254.

36. Schmidt, V.M. and Heitbaum, J. Ion exchange mechanism of polypyrrole and poly-n-methylpyrrole with toslylate as doping anion: An electrochemical quartz crystal microbalance study. *Electrochimica Acta*, 1993. **38**(2): 349-356.

37. Beck, F., Braun, P. and Oberst, M. Organic electrochemistry in the solid state-overoxidation of polypyrrole. *Berichte Der Bunsen-Gesellschaft-Physical Chemistry Chemical Physics*, 1987. **91**(9): 967-974.

38. Rangamani, A.G., McTigue, P.T. and Verity, B. Slow deactivation of polypyrrole during oxidation-reduction cycles. *Synthetic metals*, 1995. **68**(2): 183-190.

39. Fernandez, I., Trueba, M., Nunez, C.A. and Rieumont, J. Some features of the overoxidation of polypyrrole synthesized on austenitic stainless steel electrodes in aqueous nitrate solutions. *Surface and Coatings Technology*, 2005. **191**(1): 134-139

40. Liu, A., Li, C., Bai, H. and Shi, G. Electrochemical deposition of polypyrrole/sulfonated graphene composite films. *The Journal of Physical Chemistry C*, 2010. **114**(51): 22783-22789.

41. Wang, X., Cheng, X. and Sun, D. Interaction in anaerobic biodecolorization of mixed azo dyes of Acid Red 1 and Reactive Black 5 under batch and continuous conditions. *Colloids and Surfaces A: Physicochemical and Engineering Aspects*, 2011. **379**(1–3): 127-135.

42. Wang, L.-X., Li, X.-G. and Yang, Y.-L. Preparation, properties and applications of polypyrroles. *Reactive and Functional Polymers*, 2001. **47**(2): 125-139.

43. Liu, A.S., Bezerra, M.C. and Cho, L.Y. Electrodeposition of polypyrrole films on aluminum surfaces from a *p*-toluene sulfonic acid medium. *Materials Research*, 2009. **12**(4): 503-507.

44. Zhang, G., Yang, F., Gao, M., Fang, X. and Liu, L. Electro-Fenton degradation of azo dye using polypyrrole/anthraquinonedisulphonate composite film modified graphite cathode in acidic aqueous solutions. *Electrochimica Acta*, 2008. **53**(16): 5155-5161.

45. Li, M., Li, W., Liu, J. and Yao, J. Preparation and characterization of PPy with Methyl Orange as soft template. *Journal of Materials Science: Materials in Electronics*, 2013. **24**(3): 906-910.

46. Ferreira, J., Santos, M.J.L., Matos, R., Ferreira, O.P., Rubira, A.F. and Girotto, E.M. Structural and electrochromic study of polypyrrole synthesized with azo and anthraquinone dyes. *Journal of Electroanalytical Chemistry*, 2006. **591**(1): 27-32.

47. Sadki, S., Schottland, P., Brodie, N. and Sabouraud, G. The mechanisms of pyrrole electropolymerization. *Chemical Society Reviews*, 2000. **29**(5): 283-293.

48. Della Pina, C., Falletta, E. and Rossi, M. Conductive materials by metal catalyzed polymerization. *Catalysis Today*, 2011. **160**(1): 11-27.

49. Maiti, S., Das, D. and Sen, K. Electrochemical polymerization of pyrrole: Key process control parameters. *Journal of the Electrochemical Society*, 2012. **159**(9): E154-E158.

50. Lawson, J. and Erjavec, J. Basic two-level factorial experiments. In *Modern statistics for engineering and quality improvement*.2000, Cengage Learning: Duxbury. p. 199-241.

51. Asavapiriyanont, S., Chandler, G.K., Gunawardena, G.A. and Pletcher, D. The electrodeposition of polypyrrole films from aqueous solutions. *Journal of Electroanalytical Chemistry and Interfacial Electrochemistry*, 1984. **177**(1–2): 229-244.

52. Palanisamy, P., Agalya, A. and Sivakumar, P. Polymer composite-a potential biomaterial for the removal of reactive dye. *Journal of Chemistry*, 2012. **9**(4): 1823-1834.

53. Kaplin, D.A. and Qutubuddin, S. Electrochemically synthesized polypyrrole films: Effects of polymerization potential and electrolyte type. *Polymer*, 1995. **36**(6): 1275-1286.

54. Pickup, N.L., Shapiro, J.S. and Wong, D.K. Extraction of mercury and silver into base-acid treated polypyrrole films: A possible pollution control technology. *Journal of Polymer Research*, 2001. **8**(3): 151-157.

55. Forsyth, M. and Truong, V.-T. A study of acid/base treatments of polypyrrole films using 13 C NMR spectroscopy. *Polymer*, 1995. **36**(4): 725-730.

56. Fan, L.Z., Hu, Y.S., Maier, J., Adelhelm, P., Smarsly, B. and Antonietti, M. High electroactivity of polyaniline in supercapacitors by using a hierarchically porous carbon monolith as a support. *Advanced Functional Materials*, 2007. **17**(16): 3083-3087.

57. Li, L., Song, H., Zhang, Q., Yao, J. and Chen, X. Effect of compounding process on the structure and electrochemical properties of ordered mesoporous carbon/polyaniline composites as electrodes for supercapacitors. *Journal of Power Sources*, 2009. **187**(1): 268-274.

58. Konwer, S., Boruah, R. and Dolui, S. Studies on conducting polypyrrole/graphene oxide composites as supercapacitor electrode. *Journal of Electronic Materials*, 2011. **40**(11): 2248-2255.

CHAPTER 4

KINETIC MODEL AND THERMODYNAMIC STUDIES OF ACID RED 1 ENTRAPMENT IN ELECTROPOLYMERISED POLYPYRROLE FILMS

4.1 Introduction

Azo dyes are commonly used as colouring materials in the printing, textile, paper and leather industries. Without proper treatment, dye-containing effluents discharged into the hydrosphere will contribute a significant source of pollution due to both their visibility even at low concentrations (<1 mg L^{-1}) and the resultant undesirable colour to a water body [1]. Notably, this will not only directly reduce sunlight penetration in a water system, which will resist photosynthetic activity [2], but their toxic and even mutagenic degradation products are also of great concern [3]. In addition, azo dyes from industrial effluents are major sources of environmental pollution because they are non-biodegradable, non-reactive and highly soluble in water [4]. Therefore, stringent rules are imposed in many countries for controlling the discharge of industrial effluents.

A range of conventional biological, physico-chemical and chemical treatment technologies for dye removal including microbial degradation [5-8], adsorbent (*e.g.* active carbon, natural cellulose-based fibre) [9, 10], sacrificial iron electrodes [11], electrolysis [12-14], electrocoagulation [15, 16], and ion-pair extraction [17]. Fenton's process and advanced electrochemical oxidation process [18-20] has hitherto been reported. However, there are some severe limitations associated with these methods. For example, the current physico-chemical and adsorbent methods produce a significant quantity of residue that requires additional treatments. Chemical / electrochemical oxidation and Fenton's process generate appreciable quantity of toxic by-products such as aniline derivatives and ferric hydroxide sludge with toxic hydroxylated aromatic derivatives [18] that demand further treatment before proper disposal

[21]. Also, microbial degradation-based treatments are very slow processes due to their limitation in decomposing macromolecular dyes [22, 23]. Therefore, there is a need for developing alternative treatments that are effective and environmentally friendly in removing dyes from textile effluents.

In Chapter 3, we reported the application of a conducting polymer, polypyrrole, as a potentially green technology for electrochemical treatment of azo dyes using Acid Red 1 (5-(acetylamino)-4-hydroxy-3-(phenylazo)-2,7-naphthalenedisulfonic acid) as a model dye [24]. The structural formula of Acid Red 1 is depicted in Figure 3.1 of the previous section. Polypyrrole is well known for its high conductivity (up to 2000 S cm^{-1}) [25] and mechanical and thermal stability [26-32]. In our proposed dye treatment, the monomer, pyrrole, is electrochemically oxidised at +0.88 V (relative to a Ag|AgCl electrode) to yield a polymeric chain in the presence of the anionic Acid Red 1. This polymeric chain is positively charged and will therefore easily attract the Acid Red 1 as a counter anion to neutralise the charge. In this way, an Acid Red 1 entrapped polypyrrole film is synthesised. Similarly, by applying a reduction potential of -0.80 V, the polypyrrole film gains electrons and becomes neutral, resulting in the liberation of Acid Red 1 from the film [24]. In the presence of an Acid Red 1 solution, the dye is then easily re-entrapped in the film at +0.88 V for a desired period and again liberated at -0.80 V. In our pilot study [24], we have successfully synthesised polypyrrole-Acid Red 1 films and characterised them by microscopy and spectroscopy, the results of which supported Acid Red 1 entrapment by polypyrrole during oxidation of pyrrole. In the same study, we have used a two-level full factorial design to determine that the solution pH, initial concentration of Acid Red 1 and polymerisation time were all significant factors affecting the Acid Red 1 entrapment process in polypyrrole films. Unlike many other reported methods, the feasibility of entrapping Acid Red 1 without producing any toxic by-products and recycling the dye in the treatment makes it a potentially green technology.

In this chapter, we will further study the mechanism of Acid Red 1 entrapment in electropolymerised polypyrrole films based on kinetics, isotherms and thermodynamic approaches. Different dye adsorption kinetics, isotherms and thermodynamics at different materials have already been reported in literature, for example, reactive dye at chemically prepared polypyrrole-saw dust [33], tartrazine at chemically oxidised polypyrrole and polyaniline [34, 35], Amido Black 10B at chemically oxidised polyaniline/iron oxide composite [36], Acid blue 193 at benzyltrimethylammonium bentonite [37] and natural sepiolite [38]. In

contrast, a significant aspect of this work was to focus on dye entrapment mechanism at electropolymerised polypyrrole films. The main purpose of this work is thus to understand the appropriate kinetics and to determine the applicability of different isotherm models. Three different kinetic models including pseudofirst-order, pseudosecond-order and intra-particle diffusion model were initially examined for the entrapment of Acid Red 1. Data obtained during entrapment were then also tested based on the Langmuir and Freundlich isotherm models. Finally, thermodynamic parameters such as standard Gibb's free energy (ΔG°), standard enthalpy change (ΔH°) and standard entropy change (ΔS°) were evaluated at equilibrium conditions to gain an understanding of the nature of entrapment. Results obtained in such a fundamental study will be useful in designing a batch entrapment for the treatment of Acid Red 1 containing effluents generated in dying industries.

4.2 Experimental

Details of the procedure adopted for experiments described in this chapter have been presented in Chapter 2. Entrapment experiments were carried out during the electropolymerisation of pyrrole to form polypyrrole–Acid Red 1 film in the presence of 0.2 mol L^{-1} pyrrole and 60 – 2000 mg L^{-1} Acid Red 1 for a duration from 20 to 480 min. These entrapment experiments were conducted at five temperatures of 298 K, 303 K, 308 K, 313 K and 318 K. The quantity of Acid Red 1 entrapped in polypyrrole film was evaluated based on the difference (in mg L^{-1}) between the final concentration (C_{final}) after entrapment and the initial concentration ($C_{initial}$) of Acid Red 1 in an electrochemical cell. All Acid Red 1 concentrations were estimated from a plot of absorbance against concentration of standard Acid Red 1 solutions. Taking into consideration the total solution volume (V in L) and the total mass of the polypyrrole film (W in g) at the completion of an entrapment experiment, we then used the same concentration difference to estimate the mass of Acid Red 1 per mass of polypyrrole film (q_t in mg g^{-1}), as shown in Equation (4.1). We shall hereafter refer to q_t as the entrapment capacity after a polymerisation duration t

$$q_t = \frac{C_{final} - C_{initial}}{W} \times V \qquad \text{Equation (4.1)}$$

4.3 Results and discussion

4.3.1 Entrapment of Acid Red 1 in polypyrrole films as a function of Acid Red 1 concentration and polymerisation time

In this work, we begin by examining q_t of Acid Red 1 in polypyrrole films from its aqueous solution. In these experiments, 0.2 mol L^{-1} pyrrole was electropolymerised at +0.88 V in the presence of Acid Red 1 as a supporting electrolyte (the solution was acidified to pH 4), where the Acid Red 1 concentration was arbitrarily increased from 60 mg L^{-1} to 2000 mg L^{-1}. A t between 20 min and 480 min was used at the corresponding temperature of 298 K, 303 K, 308 K, 313 K and 318 K. Notably, the solution pH was found to increase to pH 5-5.5 at the end of the polymerisation process. However, this is still within an acidic pH range and is thus not expected to have negatively affected the electropolymerisation of pyrrole [39]. Results obtained are shown in Figure 4.1 and each data point in the figure represents the mean value of three measurements. In Figure 4.1, we have also included an expanded q_t versus t plot for 313 K to illustrate the variability of the results. Notably, q_t increases with Acid Red 1 concentration from 60 to 2000 mg L^{-1} at a constant temperature, which is attributable to an increased driving force arising from the concentration gradient with the higher initial dye concentration. Figure 4.1 also shows that the entrapment reached equilibrium at 1500 mg L^{-1}, beyond which no significant increase of q_t was observed. This is because polypyrrole has limited active sites for Acid Red 1 entrapment and presumably complete coverage of the active sites of polypyrrole at dye concentrations higher than 1500 mg L^{-1} restricts further Acid Red 1 entrapment into a polypyrrole film. Moreover, q_t of Acid Red 1 increases with polymerisation time and finally attained saturation at approximately 420 min. Accordingly, we have hereafter assigned an equilibrium time of 420 min in this work. The results in Figure 4.1 also show q_t of Acid Red 1 increases with temperature, most likely due to enhanced mobility of Acid Red 1 with increased kinetic energy, which aided in Acid Red 1 diffusion towards the polypyrrole film.

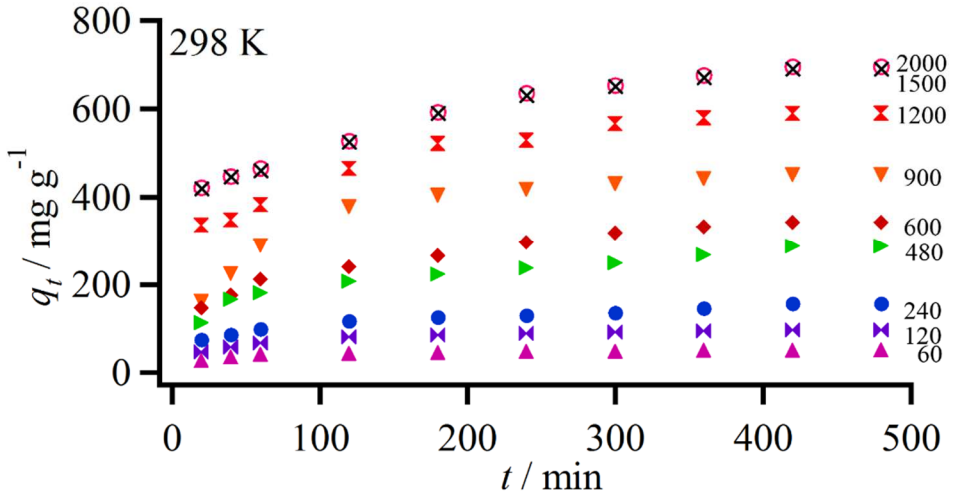
298 K
800
600
400
200
0
q_t / mg g^{-1}
0
100
200
300
400
500
t / min
2000
1500
1200
900
600
480
240
120
60

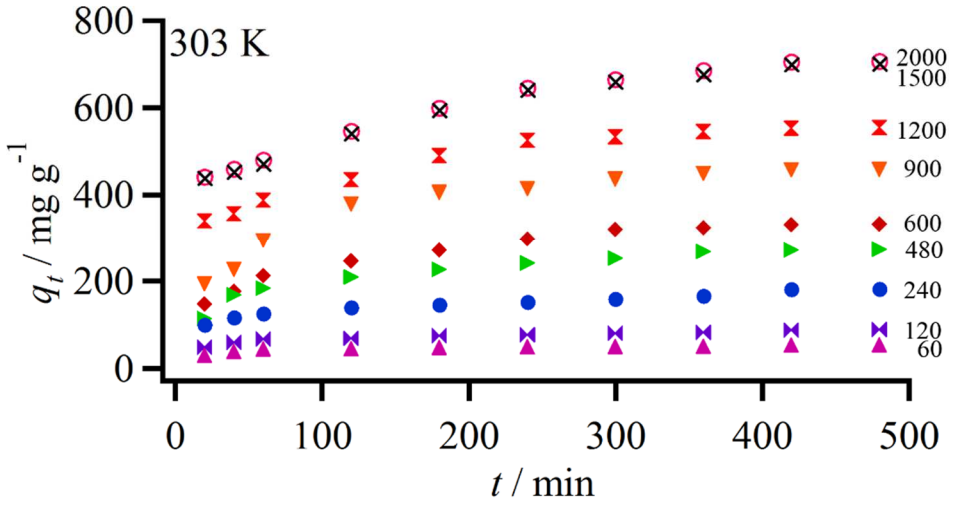
303 K
800
600
400
200
0
q_t / mg g^{-1}
0
100
200
300
400
500
t / min
2000
1500
1200
900
600
480
240
120
60

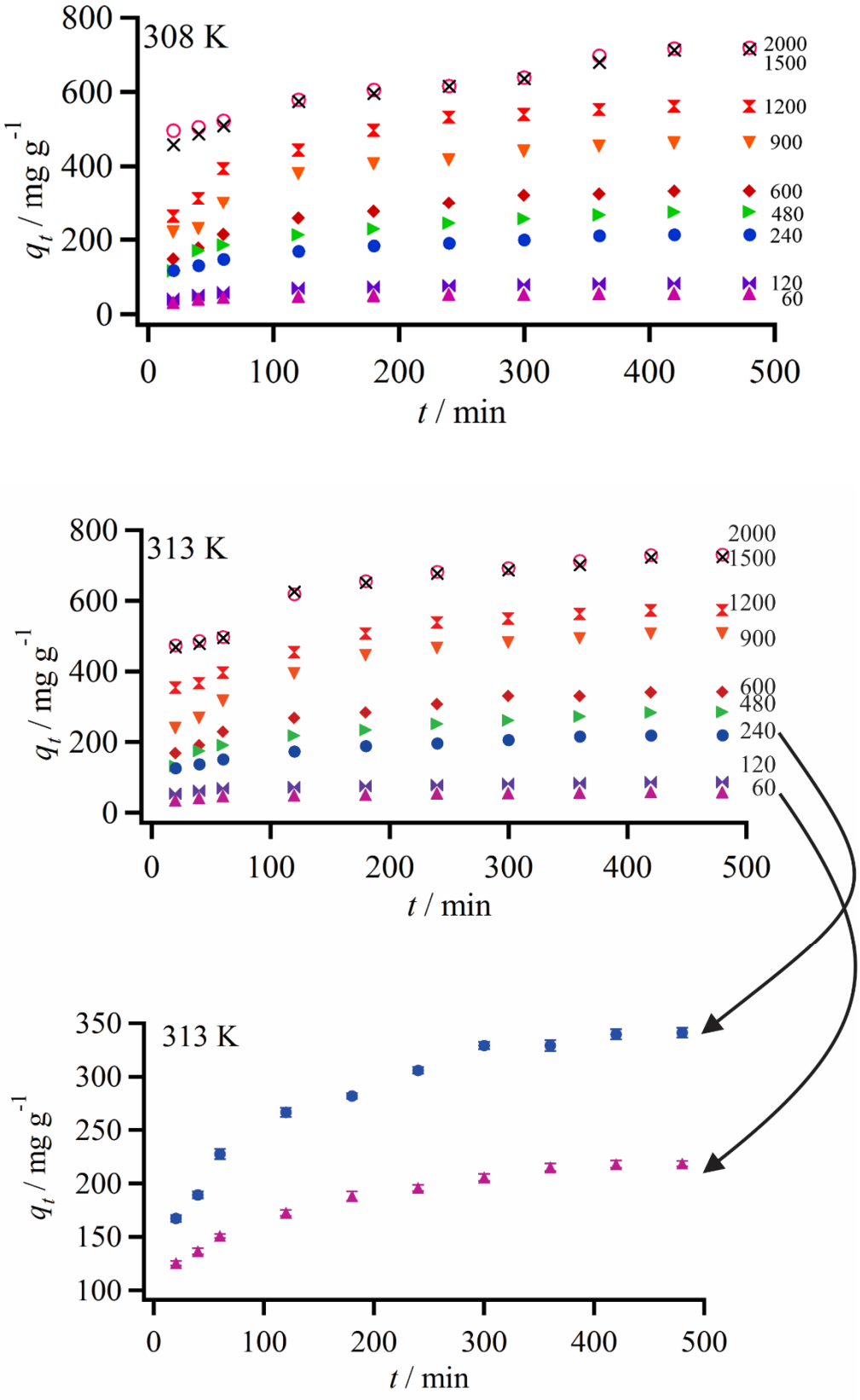
308 K
313 K
313 K
q_t / mg g^{-1}
t / min
2000
1500
1200
900
600
480
240
120
60

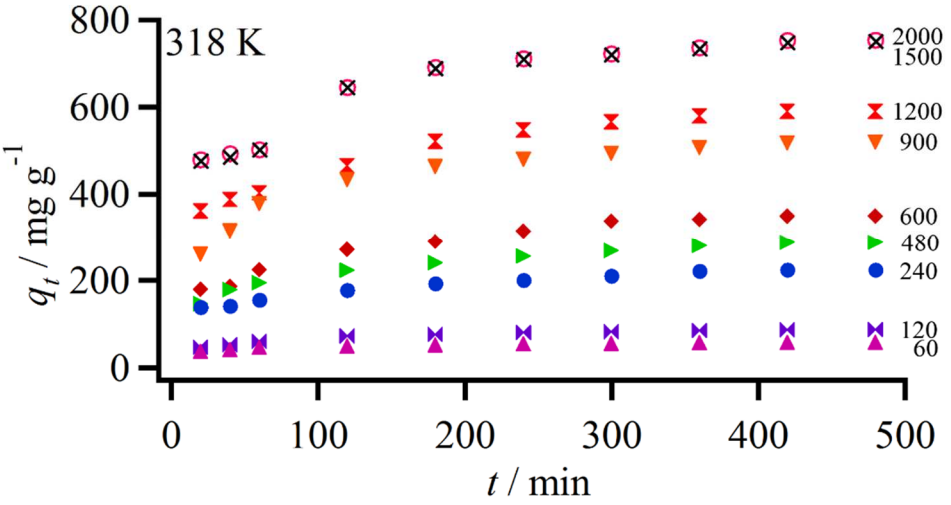

Figure 4.1 Entrapment capacity (q_t) of Acid Red 1 in polypyrrole film as a function of initial Acid Red 1 concentration and polymerisation time (t) at five different temperature of 298 K, 303 K, 308 K, 313 K and 318 K. All specified Acid Red 1 concentrations are given in mg L^{-1}.

4.3.2 Entrapment kinetics

Entrapment kinetics of Acid Red 1 into polypyrrole films in an aqueous medium were studied at increasing Acid Red 1 concentrations in order to investigate the entrapment mechanism involved in this process. Initially, we have considered a pseudofirst-order model in which the entrapment rate is assumed to be solely dependent on Acid Red 1 concentration. This is represented by Equation (4.2) [36].

$$\log\left(q_e - q_t\right) = \log q_e - \frac{k_1 t}{2.303} \qquad \text{Equation (4.2)}$$

where k_1 is the pseudofirst-order rate constant for the entrapment process (in min^{-1}), q_e (mg g^{-1}) denote the entrapment capacity of Acid Red 1 in a polypyrrole film at equilibrium (approximated by the Acid Red 1 concentration at 420 min). Accordingly, for a pseudofirst-order model, we expect a linear relation between $\log(q_e - q_t)$ and t, from which k_1 is estimated from the slope. From q_t at a specified temperature in Figure 4.1, plots of $\log(q_e - q_t)$ *versus* t were obtained (shown in Figure 4.2) for different Acid Red 1 concentration. Unfortunately, the plots obtained at 298 K, 303 K, 308 K, 313 K and 318 K are not linear and they follow an irregular trend with increasing Acid Red 1 concentration, which may be due to a poor fit of the

data with pseudofirst-order kinetic model. The correlation coefficient, R_1, for this model was found to range between 0.7709 and 0.9725 (N=10). The corresponding residual plots all showed non-randomly distributed data points, further supporting that this entrapment system is unlikely to follow a pseudofirst-order kinetic model. Accordingly, we did not proceed further in estimating any kinetic parameters based on a pseudofirst-order model.

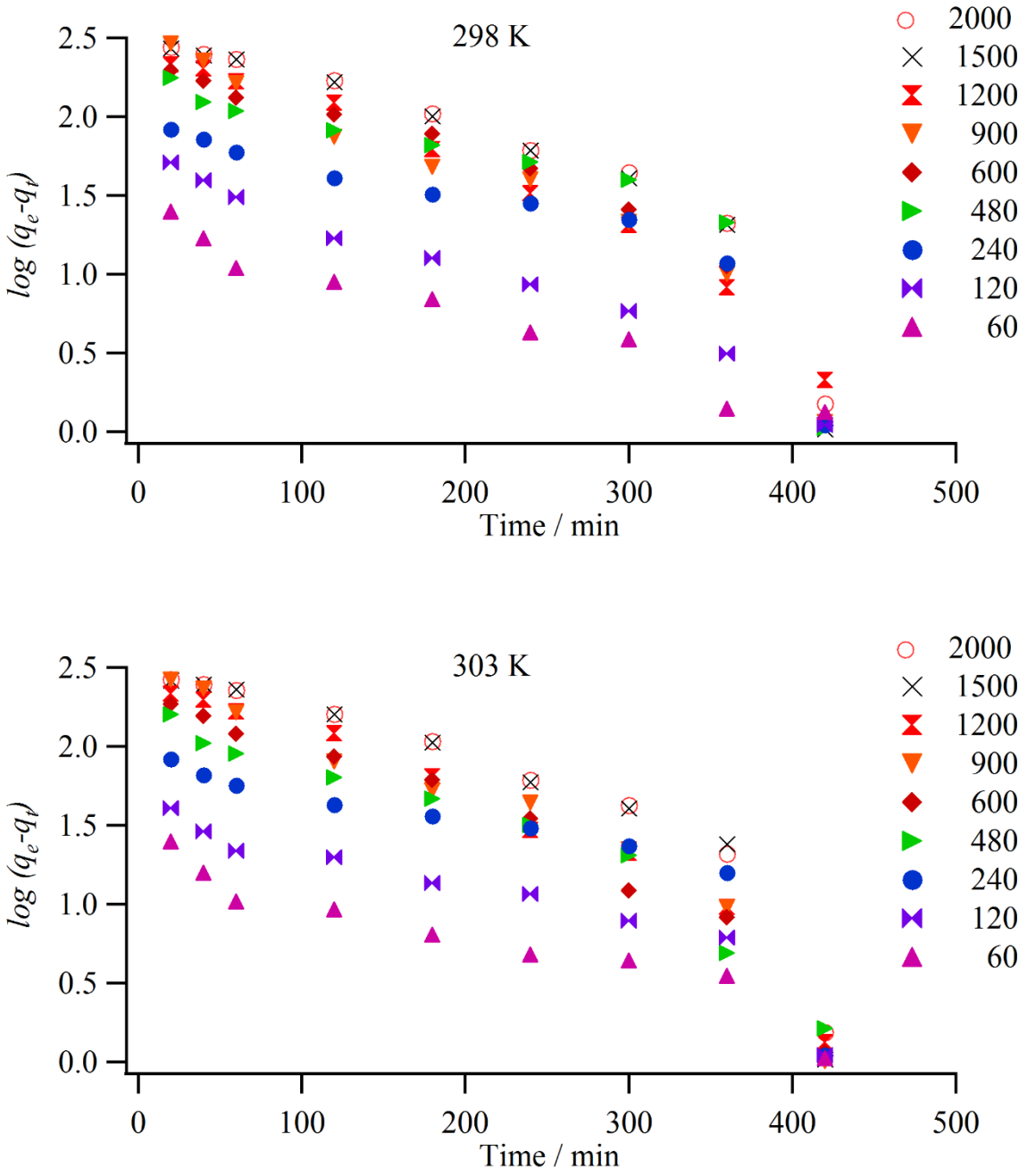

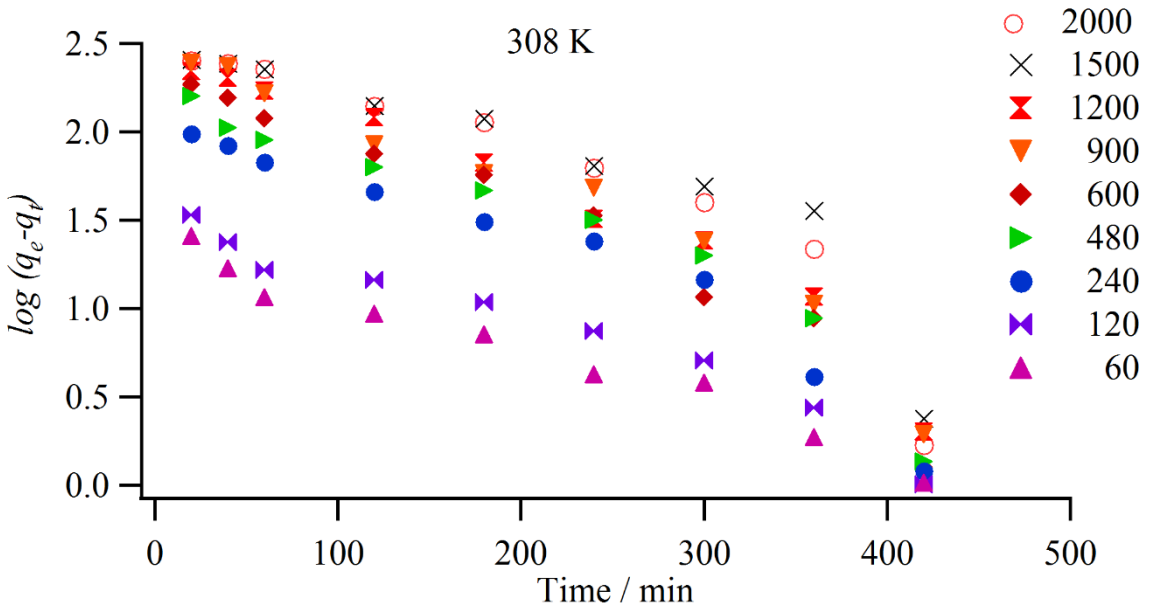
308 K
2000
1500
1200
900
600
480
240
120
60
log (qe-qt)
2.5
2.0
1.5
1.0
0.5
0.0
0
100
200
300
400
500
Time / min

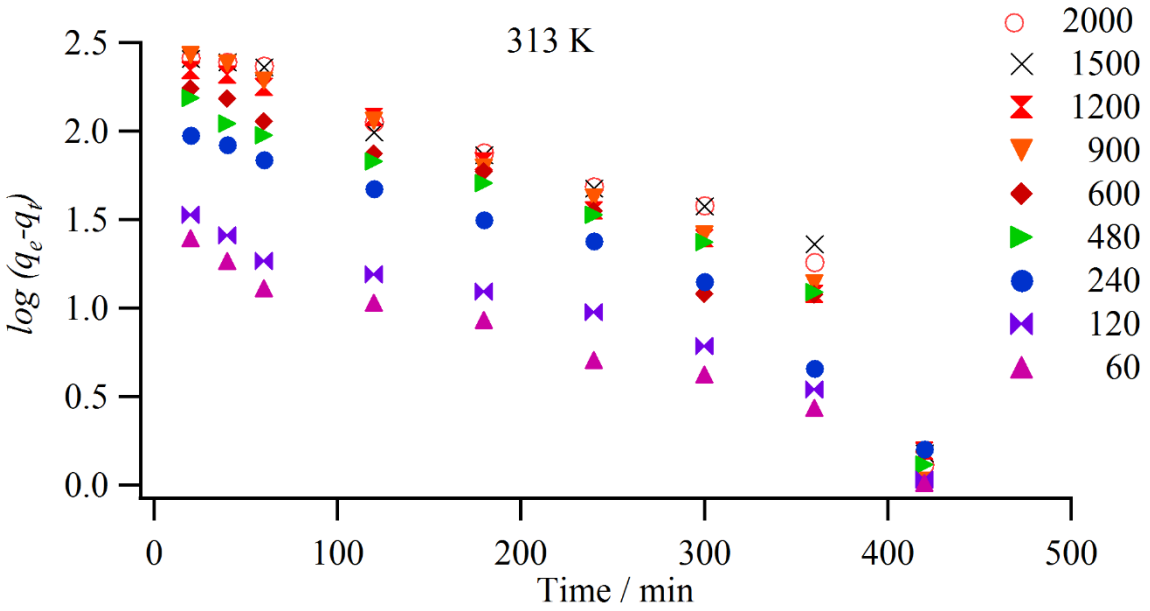
313 K
2000
1500
1200
900
600
480
240
120
60
log (qe-qt)
2.5
2.0
1.5
1.0
0.5
0.0
0
100
200
300
400
500
Time / min

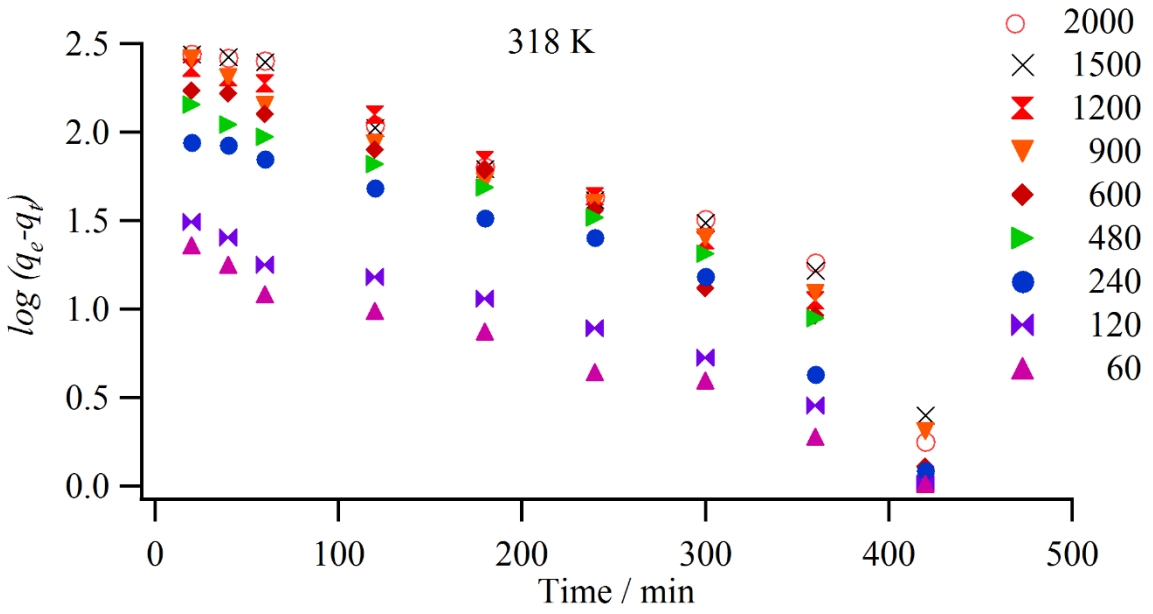

Figure 4.2 Pseudofirst-order kinetic plots for the entrapment of Acid Red 1 in polypyrrole films at various temperatures of 298 K, 303 K, 308 K, 313 K and 318 K. All specified Acid Red 1 concentrations are given in mg L^{-1}.

We have next considered a pseudosecond-order model in which the entrapment rate is dependent on the square of the Acid Red 1 concentration. This is represented by Equation (4.3) [40].

$$\frac{t}{q_t} = \frac{1}{k_2 (q_e)^2} + \frac{t}{q_e} \qquad \text{Equation (4.3)}$$

where k_2 denotes the rate constant of a pseudosecond-order model (g mg^{-1} min^{-1}). In Equation 3, a t/q_t *versus* t plot is expected to yield a linear relation with k_2 estimated from the ordinate intercept of the plot, after evaluating q_e from the slope. When the experimental results at 298 K, 303 K, 308 K, 313 K and 318 K were plotted according to Equation 4.3, linear plots, as shown in Figure 4.3, were obtained and the corresponding kinetic parameters were evaluated and these are tabulated in Table 4.1. The correlation coefficient, R_2, for the pseudosecond-order kinetic model at different concentrations and temperatures, ranges between 0.9948 and 0.9998 (N=10), and were found to be statistically significant at the 95% confidence level. Similarly, residual plots with randomly distributed data points were obtained. The values of k_2 decreased from 7.7 × 10^{-4} to 0.44 × 10^{-4} g mg^{-1} min^{-1} at 298 K, when the initial dye

concentration was increased from 60 to 2000 mg L^{-1}, most likely due to a decrease in availability of vacant positive sites in polypyrrole for attraction of negatively charged Acid Red 1. However, at an initial Acid Red 1 concentration of 60 mg L^{-1}, the pseudo-second order rate constants were estimated to be 7.7×10^{-4}, 7.8×10^{-4}, 7.9×10^{-4}, 8.0×10^{-4} and 8.2×10^{-4} g mg^{-1} min^{-1} at the corresponding solution temperature of 298 K, 303 K, 308 K, 313 K and 318 K, respectively. This increase in k_2 value is most likely due to increased mobility of Acid Red 1 with temperature, which confirms that the entrapment process is endothermic in nature [41, 42]. Good agreement between $(q_e)_{expt}$ and $(q_e)_{pred}$ (summarised in Table 4.1) was also achieved. Therefore, the pseudo second-order kinetic model provided a better fit than the pseudofirst-order model for the Acid Red 1 entrapment in polypyrrole films, which agree with the entrapment kinetics of many dye species at various materials [37, 43-46].

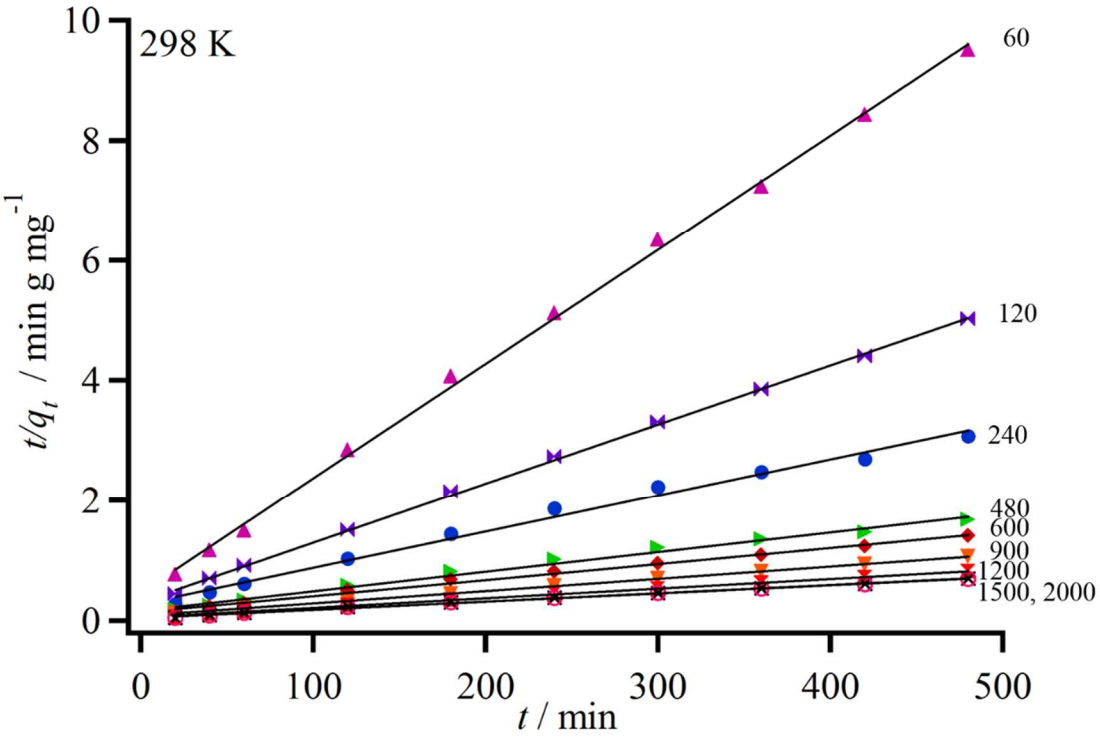

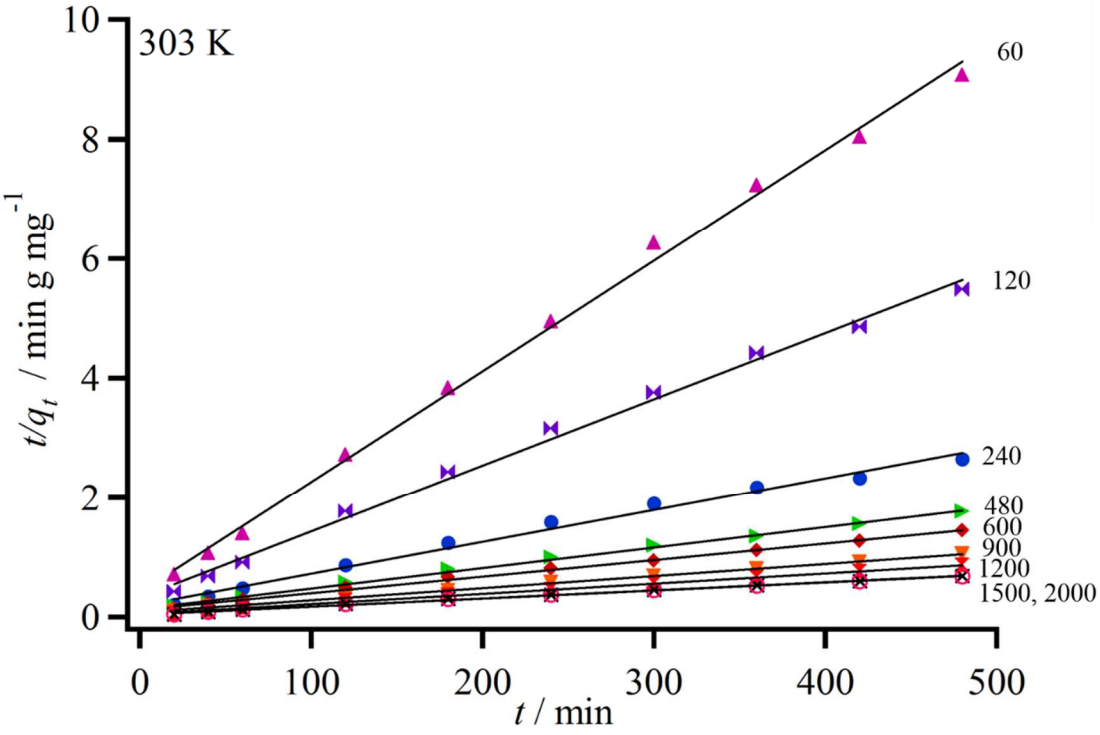
303 K
60
120
240
480
600
900
1200
1500, 2000
t/q_t / min g mg^{-1}
t / min
0
2
4
6
8
10
0
100
200
300
400
500

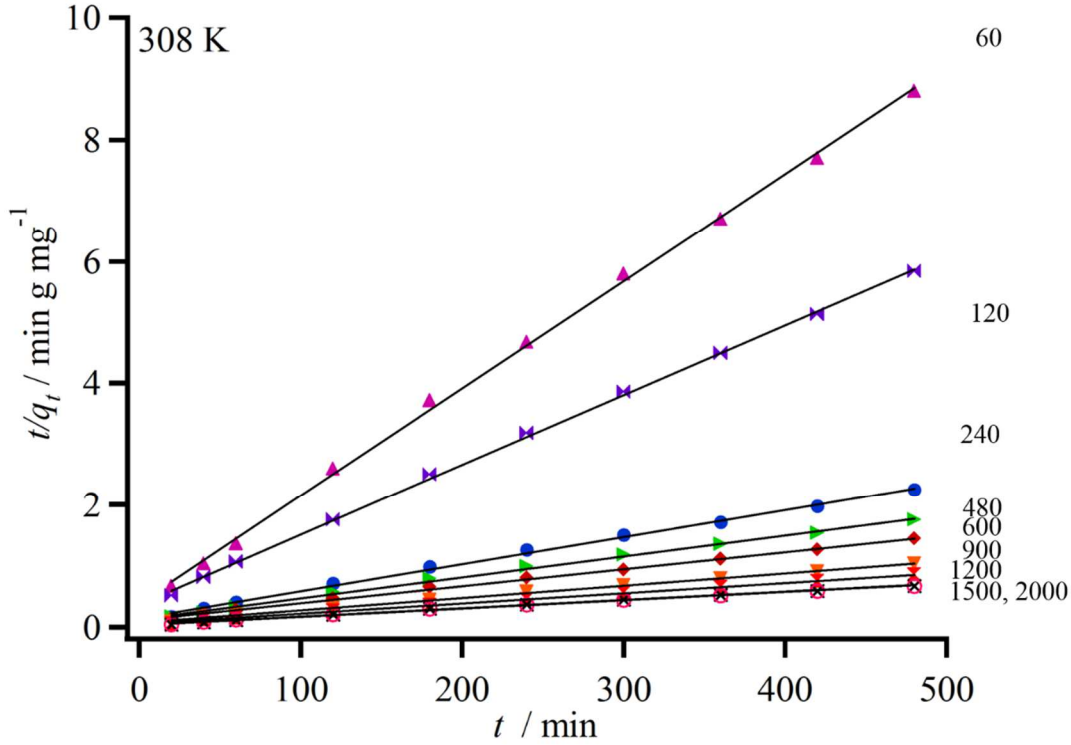
308 K
60
120
240
480
600
900
1200
1500, 2000
t/q_t / min g mg^{-1}
t / min
0
2
4
6
8
10
0
100
200
300
400
500

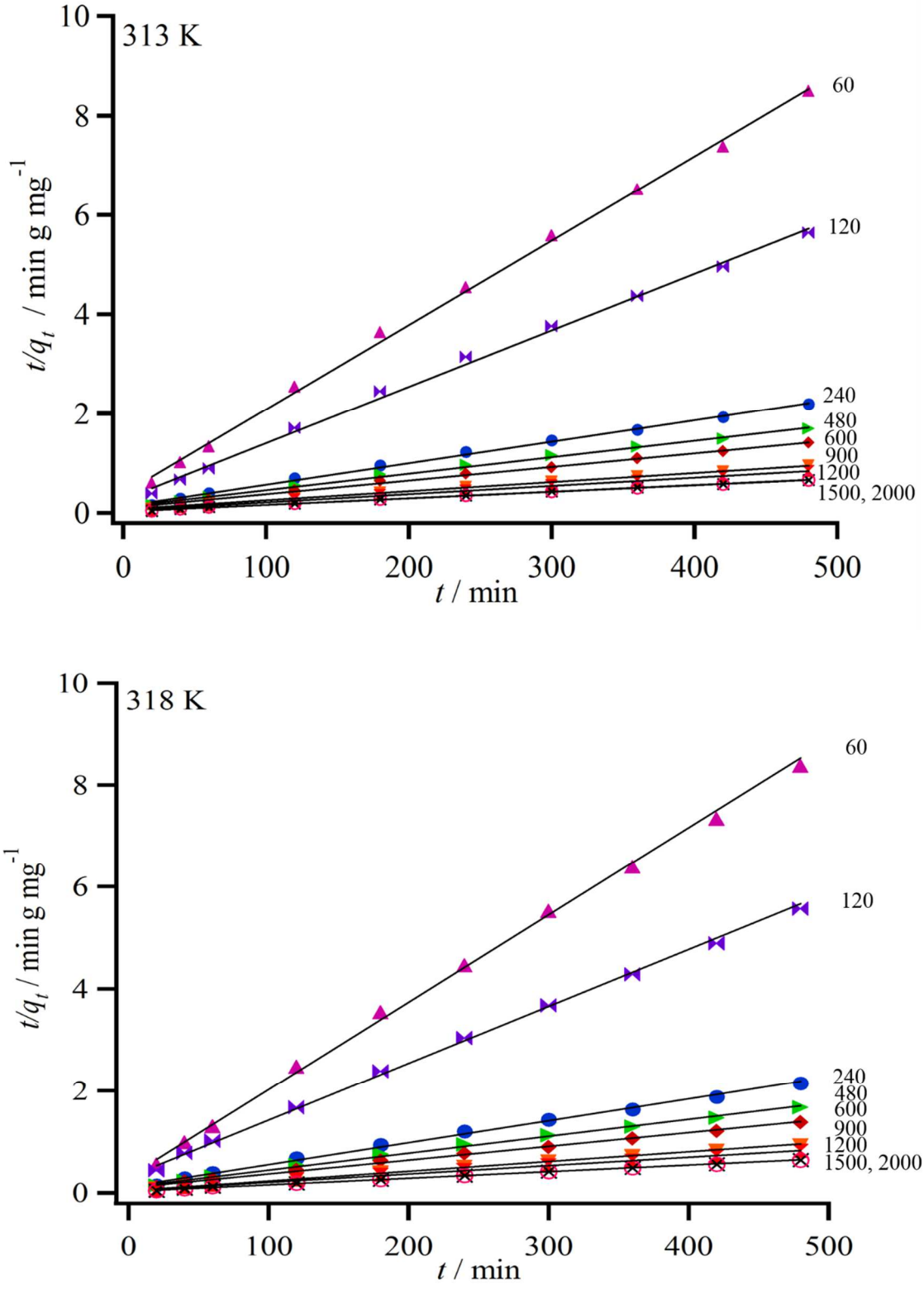

Figure 4.3 Pseudosecond-order kinetic plots for the entrapment of Acid Red 1 in polypyrrole films at various temperatures of 298 K, 303 K, 308 K, 313 K and 318 K. All specified Acid Red 1 concentrations are given in mg L^{-1}.

In order to further investigate the entrapment mechanism of Acid Red 1 in polypyrrole films, an intra-particle diffusion based mechanism was also considered. According to Cheung *et al*. [47], intra-particle diffusion is a transport process involving movement of particles from the bulk of the solution to the solid phase either by a pore diffusion process through the liquid filled pores or by a solid surface diffusion mechanism. They proposed that a dye entrapment system can be considered to involve either (i) diffusion across the liquid layer surrounding the external boundary film (external diffusion or film diffusion), (ii) diffusion in the liquid contained in the pores or along the pore walls (the intra-particle diffusion rate), or (iii) mass transfer (entrapment) at active sites on the surface, which is an extremely rapid process for physical and chemical systems and is often neglected for kinetic study. In this work, we will therefore investigate whether liquid film diffusion or intra-particle diffusion or both mechanisms were involved in the Acid Red 1 entrapment in polypyrrole films. In proposing an intra-particle diffusion model, Weber-Morris derived the following equation (4.4) [48].

$$q_t = k_p \sqrt{t} \qquad \text{Equation (4.4)}$$

where k_p refers to the intra-particle diffusion rate constant (mg g^{-1} $min^{-½}$). Accordingly, a linear q_t *versus* $\sqrt{t}$ plot passing through the origin is expected if the intra-particle diffusion is the only rate-controlling step for the entrapment process [45, 46, 49-51]. However, plots obtained at 298 K, 303 K, 308 K, 313 K and 318 K, as shown in Figure 4.4, displayed an initial non-linearity (~20-60 min), followed by a more linear dependence (~120-240 min) and a plateau (~300-480 min) over the duration used in this study, indicating that two or more steps may have been involved in the entrapment process. In a study of acid dye adsorption at chitosan, Cheung *et al*. [47] attributed the non-linear feature to a boundary layer diffusion, the linear dependence to intra-particle diffusion, and the plateau to equilibrium. As the plots in Figure 3.4 did not pass through the origin, the intra-particle diffusion would not be the sole rate-controlling step, but other processes might control the rate of entrapment, all of which may be in operation simultaneously. The correlation coefficients R_3 obtained from the linear portion of the plot (~120-240 min) were estimated between 0.9802 and 0.9999 (N=10), the statistical significance of which confirmed the linearity of that portion of the plot. This was also supported by randomly distributed data points in the residual plots. Based on the slopes of the linear portion of the plot in Figure 4.4, the intra-particle diffusion constant, k_p, was estimated and data are tabulated in Table 4.1. The data show that the rate of diffusion increased with an

increase in initial Acid Red 1 concentration and solution temperature. This is due to a greater driving force with increasing Acid Red 1 concentration, resulting in enhancing the diffusion of dye from the solution towards the polymer, while reducing the diffusion of dye anions from the polymer interface to the solution [52]. As shown in Table 4.1, the increase in k_p with the temperature is due to the rise of particle movement, as a result of enhanced pore diffusion and intra-particle diffusion rate.

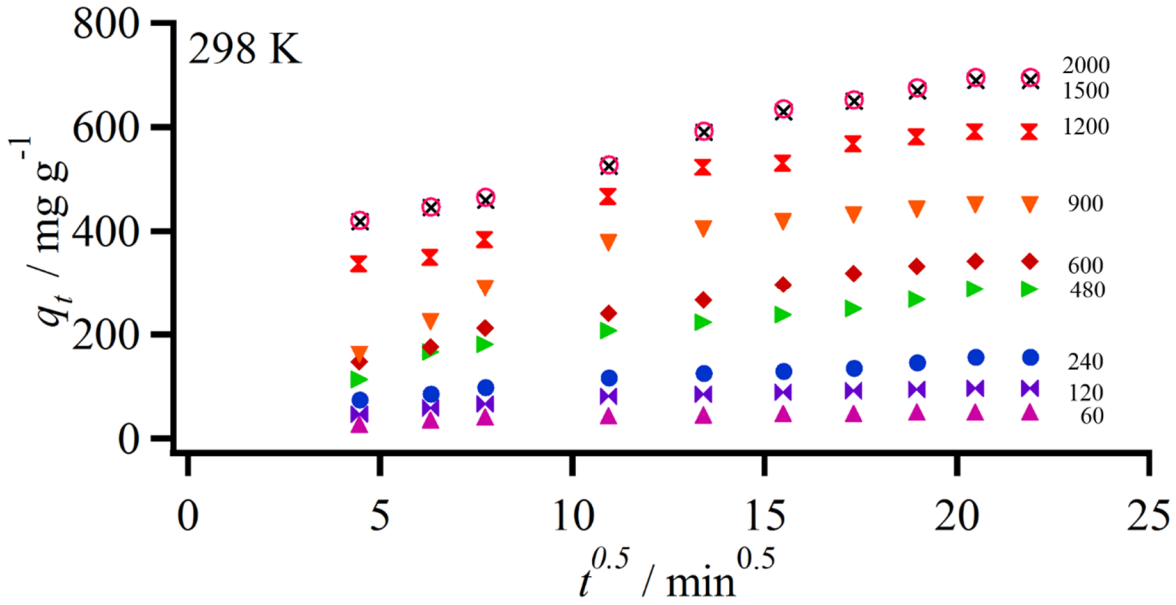

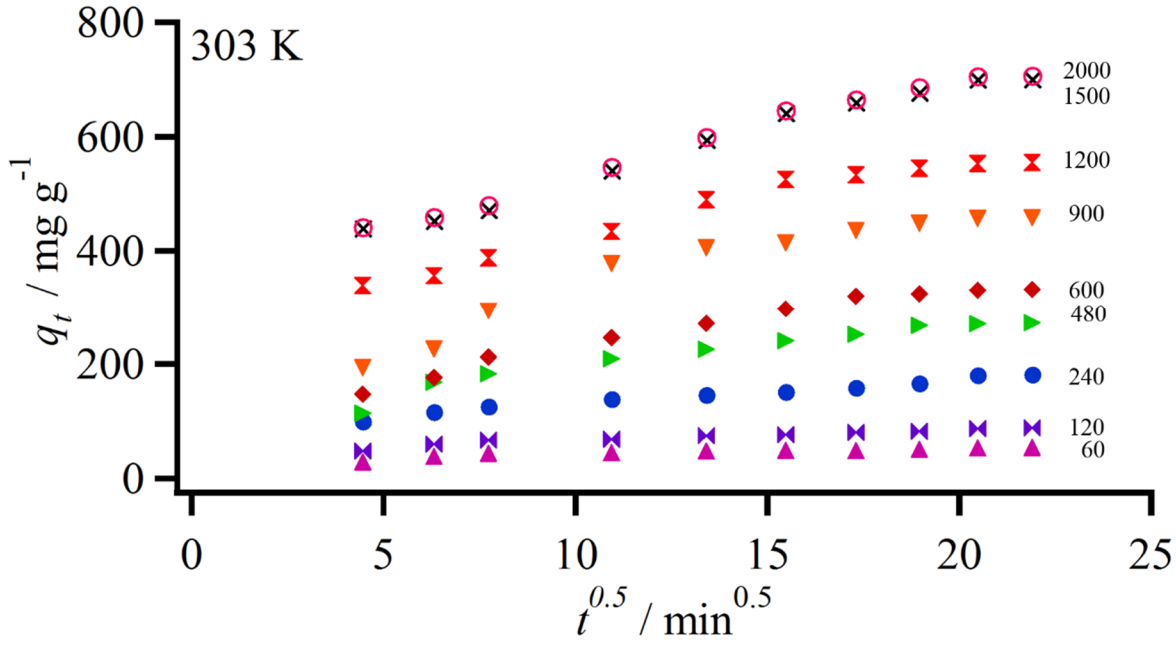

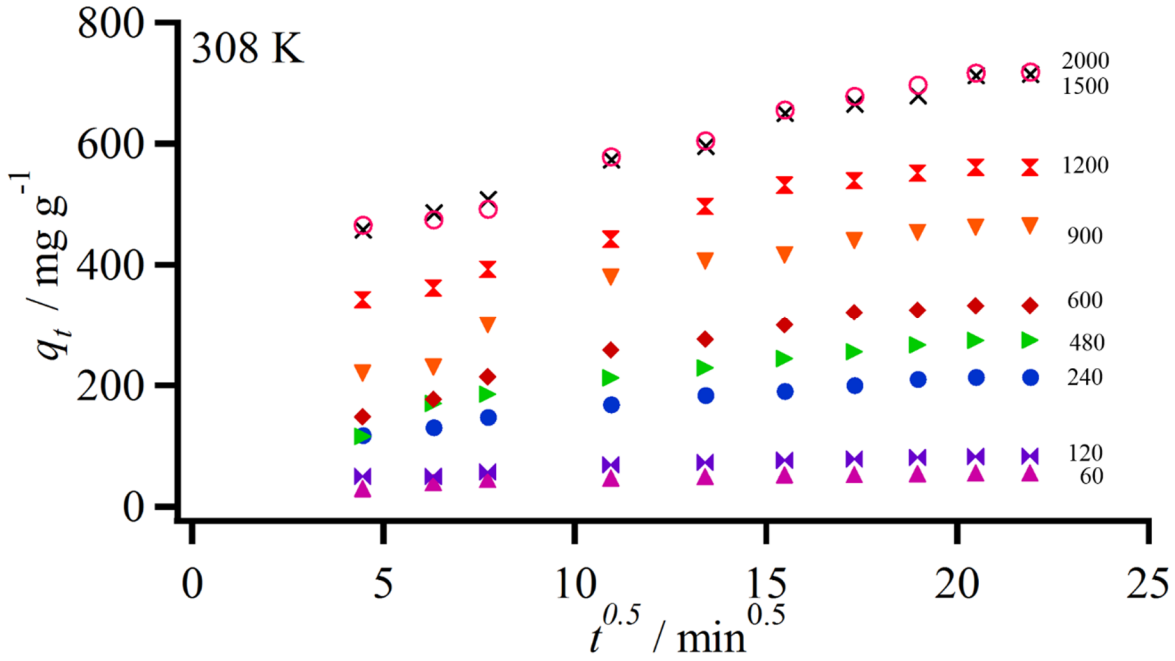
308 K
800
600
400
200
0
q_t / mg g^{-1}
0
5
10
15
20
25
$t^{0.5}$ / min$^{0.5}$
2000
1500
1200
900
600
480
240
120
60

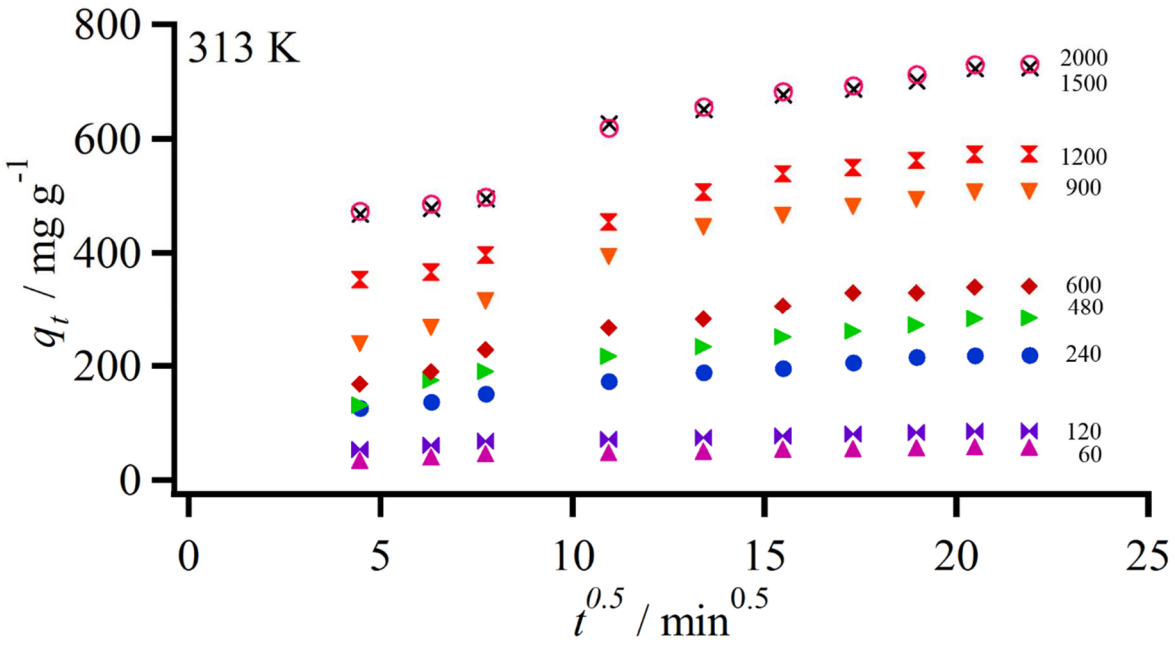
313 K
800
600
400
200
0
q_t / mg g^{-1}
0
5
10
15
20
25
$t^{0.5}$ / min$^{0.5}$
2000
1500
1200
900
600
480
240
120
60

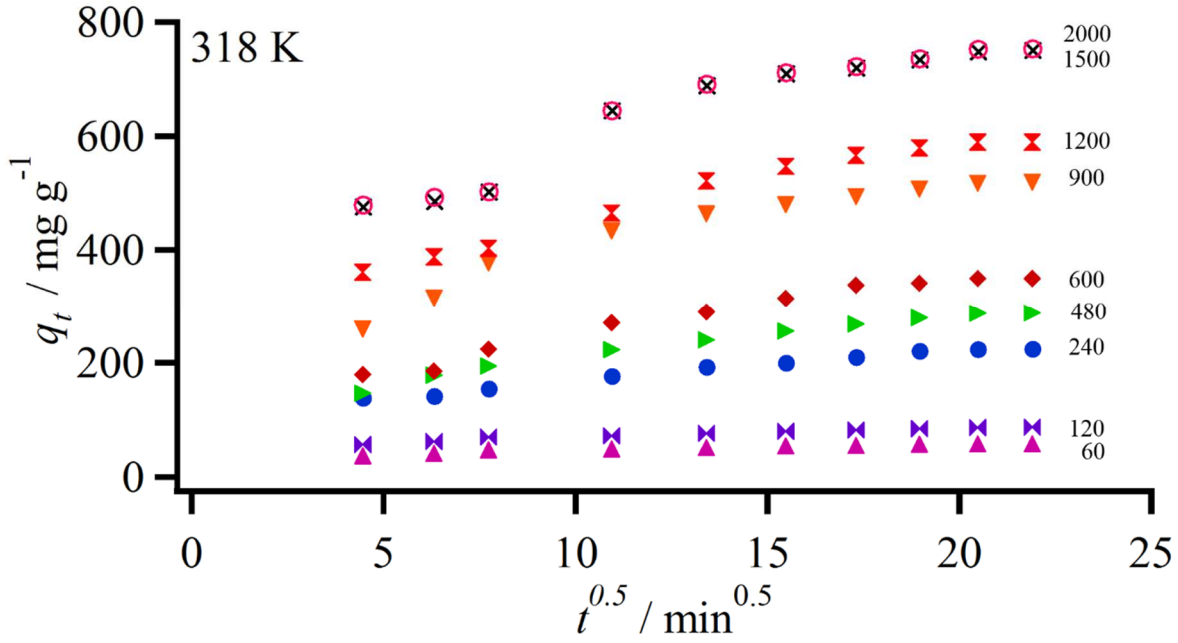

Figure 4.4 Intra-particle diffusion model for entrapment of Acid Red 1 in polypyrrole films with different initial Acid Red 1 concentrations at temperatures 298 K, 303 K, 308 K, 313 K and 318 K. All specified Acid Red 1 concentrations are given in mg L^{-1}.

4.3.3 Isotherm studies

Many research groups [38, 41-44, 49, 53] have developed dye removal methods in which dyes were allowed to adsorb on a substrate surface for a desired period. This has led to their consideration of several equilibrium adsorption isotherms including the Langmuir, Freundlich, Temkin and Dubinin-Radushkevich models to explain the interactive characteristics between a dye and the corresponding surface. In contrast to such work, Acid Red 1 was electrostatically attracted to a positively charged polypyrrole backbone in the present study over a desired duration, resulting in Acid Red 1 being entrapped in the polymer chains. Indeed, X-ray diffraction results in our earlier study provided evidence that Acid Red 1 was entrapped between polypyrrole chains [24], indicating that the incorporation of Acid Red 1 was not limited to surface adsorption. In this context, by considering entrapment of Acid Red 1 during an initial polymerisation period no longer than 60 min, we assumed surface adsorption of Acid Red 1 to be the primary process in a polypyrrole film during this relatively short duration. However, the

poor fit of the equilibrium data (not shown here, see appendix) obtained for entrapment of Acid Red 1 in polypyrrole films, even within a 60 min polymerisation period, demonstrating that the data did not obey any of the adsorption model, but Acid Red 1 was entrapped in a polypyrrole film. In this way, we expect a higher entrapment of Acid Red 1 possible in a polypyrrole film compared to adsorption methods that required diffusion of a dye towards an adsorbate. This will in turn make the entrapment method in polypyrrole films a more effective and efficient treatment method compared to those relying on adsorption. Similarly, the entrapment method may also aid in preventing dye leakage from polypyrrole films back to a sample matrix.

Table 4.1 Kinetic data obtained for Acid Red 1 entrapment in polypyrrole films.

Temperature / K	[Acid Red 1] / mg L^{-1}	Pseudosecond order				Intra-particle diffusion	
		$k_2 \times 10^4$ / g mg^{-1} min^{-1}	$(q_e)_{pred}$ / mg g^{-1}	$(q_e)_{exp\,t}$ / mg g^{-1}	R_2	k_p / mg g^{-1} $min^{-½}$	R_3
298	60	7.733	52.63	50.50	0.9993	1.02	0.9813
	120	3.057	102.0	95.60	0.9997	1.75	0.9984
	240	1.311	166.6	156.2	0.9951	2.80	0.9867
	480	0.6690	303.0	287.2	0.9948	6.63	0.9997
	600	0.5420	370.4	341.6	0.9968	8.78	0.9931
	900	0.4690	500.0	450.3	0.9998	9.19	0.9852
	1200	0.4750	625.0	589.1	0.9989	18.0	0.9995
	1500	0.4420	714.3	690.2	0.9983	22.3	0.9984
	2000	0.4410	714.3	695.2	0.9983	22.8	0.9981
303	60	7.822	54.05	52.90	0.9972	1.08	0.9942
	120	3.113	90.09	87.60	0.9950	1.83	0.9821
	240	1.455	188.7	181.3	0.9996	2.74	0.9999
	480	0.8480	294.1	271.9	0.9971	6.97	0.9999
	600	0.6320	357.1	331.7	0.9969	11.3	0.9977
	900	0.4880	500.0	457.3	0.9991	8.00	0.9722
	1200	0.5960	588.2	553.5	0.9981	20.1	0.9968
	1500	0.4610	714.3	700.1	0.9967	22.1	0.9999
	2000	0.4030	769.2	706.1	0.9967	21.8	0.9999
308	60	7.888	56.82	54.56	0.9995	1.11	0.9831
	120	3.388	86.96	82.16	0.9997	1.88	0.9987
	240	1.325	227.3	213.2	0.9986	4.78	0.9889
	480	0.8750	294.1	273.6	0.9987	6.87	0.9997
	600	0.6680	357.1	332.2	0.9990	9.03	0.9842

	900	0.5070	500.0	463.5	0.9992	9.05	0.9861
	1200	0.5040	588.2	560.5	0.9996	18.0	0.9954
	1500	0.4900	714.3	714.9	0.9963	18.2	0.9999
	2000	0.4490	769.2	718.2	0.9963	22.6	0.9802
	60	8.033	58.82	56.51	0.9984	1.23	0.9843
	120	3.554	90.09	85.17	0.9973	1.33	0.9997
	240	1.340	232.6	218.7	0.9973	5.14	0.9894
	480	0.8510	303.0	283.7	0.9964	7.40	0.9980
313	600	0.6780	370.4	341.0	0.9974	8.54	0.9844
	900	0.4430	555.6	506.5	0.9987	16.0	0.9807
	1200	0.6100	588.2	572.4	0.9983	18.7	0.9957
	1500	0.5210	769.2	724.1	0.9987	21.2	0.9983
	2000	0.5120	769.2	730.2	0.9986	24.0	0.9992
	60	8.180	59.17	57.29	0.9994	1.16	0.9831
	120	3.600	90.91	86.27	0.9994	1.18	0.9981
	240	1.340	238.1	223.9	0.9983	6.64	0.9994
	480	0.9240	303.0	287.3	0.9983	7.14	0.9997
318	600	0.6820	370.4	348.8	0.9997	9.49	0.9842
	900	0.6100	555.6	518.2	0.9991	10.2	0.9843
	1200	0.5530	625.0	588.5	0.9983	19.1	0.9916
	1500	0.5350	769.2	750.6	0.9995	26.7	0.9807
	2000	0.5350	769.2	753.1	0.9994	27.0	0.9818

4.3.4 Thermodynamic parameters

In order to study the effect of temperature on Acid Red 1 entrapment in polypyrrole films, thermodynamic parameters including the standard Gibbs free energy change (ΔG°), standard enthalpy change (ΔH°) and standard entropy change (ΔS°) were also determined in the present work. The free energy, ΔG, for entrapment of Acid Red 1 in a polypyrrole film is defined by Equation (4.5).

$$\Delta G = \Delta G^{\circ} + RT \ln K_C \qquad \text{Equation (4.5)}$$

where R is the universal gas constant (8.314 J mol^{-1} K^{-1}), T is the absolute temperature in K and K_C is the equilibrium constant ((q_e / C_e), where C_e is the Acid Red 1 concentration at equilibrium). At equilibrium, $\Delta G = 0$, we thus obtain

$$\Delta G^{\circ} = -RT \ln K_C \qquad \text{Equation (4.6)}$$

The ΔG^0 was found to be -1.46±0.78, -1.86±0.22, -2.14±0.89, -2.58±0.29 and -2.94±0.24 kJ mol^{-1} at the corresponding temperature of 298 K, 303 K, 308 K, 313 K and 318 K. The negative free energy change indicates a spontaneous entrapment of Acid Red 1 in polypyrrole film during electropolymerisation of pyrrole at all temperatures. Generally, the change of free energy for a physical process is in a range of -20 to 0 kJ mol^{-1}, while the corresponding change for a chemical process is between -80 and -400 kJ mol^{-1} [38]. Accordingly, the ΔG^0 values in this work indicate the Acid Red 1 entrapment in polypyrrole films is physical in nature.

Standard enthalpy and entropy change values for Acid Red 1 entrapment in a polypyrrole film were evaluated from the Van't Hoff equation:

$$\ln K_C = \frac{\Delta S^{\circ}}{R} - \frac{\Delta H^{\circ}}{RT} \qquad \text{Equation (4.7)}$$

Both ΔH° and ΔS^0 were estimated from the slope and ordinate intercept of the $\ln K_C$ *versus* $1/T$ plot shown in Figure 4.5(a). The positive value of ΔH° (20.5±2.5 kJ mol^{-1}; N=5) suggests that the Acid Red 1 entrapment in polypyrrole is endothermic.[53, 54] Also, a positive ΔS^0, estimated to be 73.6±8.2 J mol^{-1} K^{-1} (N=5), indicates an increased randomness in the polypyrrole solid/Acid Red 1 solution interface and an affinity of Acid Red 1 towards

polypyrrole film. Thus, from the thermodynamic viewpoint, entropy seems to be a driving force of Acid Red 1 entrapment in polypyrrole film [34]

In addition, activation energy gives information about the entrapment mechanism. The activation energy is obtained based on the Arrhenius equation:

$$\ln k_2 = \ln A - \frac{E_a}{RT} \qquad \text{Equation (4.8)}$$

where k_2 is the pseudosecond-order rate constant, E_a is the Arrhenius activation energy, A, the Arrhenius factor. From the $\ln k_2$ *versus* $1/T$ plot shown in Figure 4.5(b), a straight line with slope $-E_a/R$ is obtained. In general, equilibrium is usually attained rapidly and is easily reversible in a physical process because the forces involved in the process are weak, leading to low energy requirements. In contrast, a chemical process is specific and the forces involved are much stronger than in physical process. Accordingly, low activation energy (<40 kJ mol^{-1}) is often characteristic of a physical process, while high activation energy (40 – 400 kJ mol^{-1}) is associated with a chemical process [38]. In this work, the activation energy for the entrapment of Acid Red 1 in polypyrrole films was estimated to be 7.67±0.8 kJ mol^{-1} (N=5), indicating the Acid Red 1 entrapment in polypyrrole film is primarily governed by a physical process.

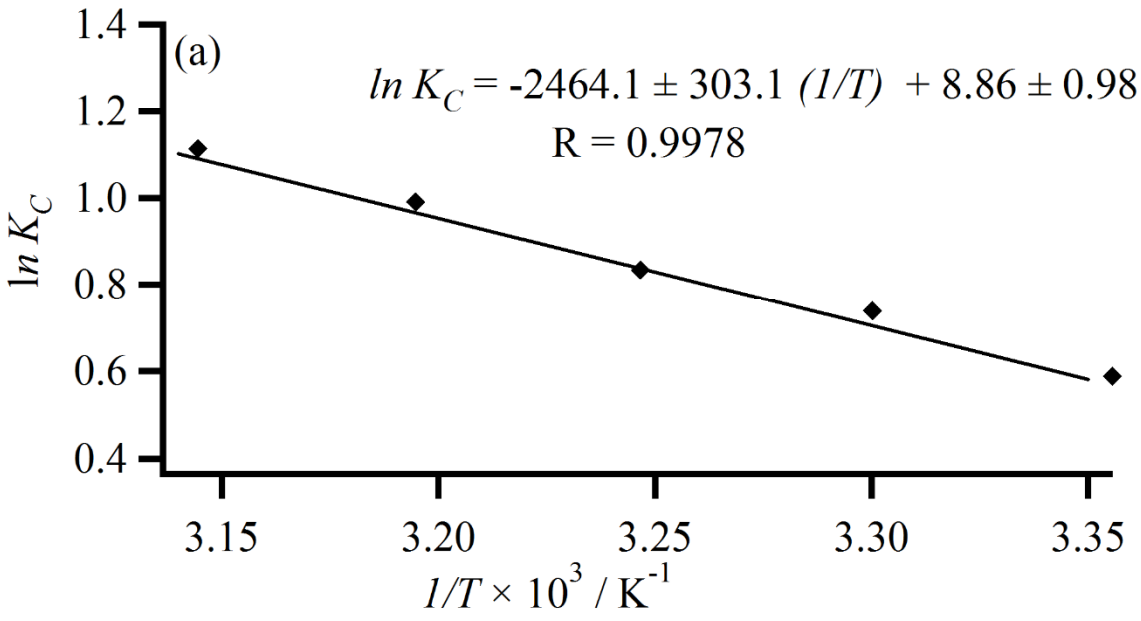

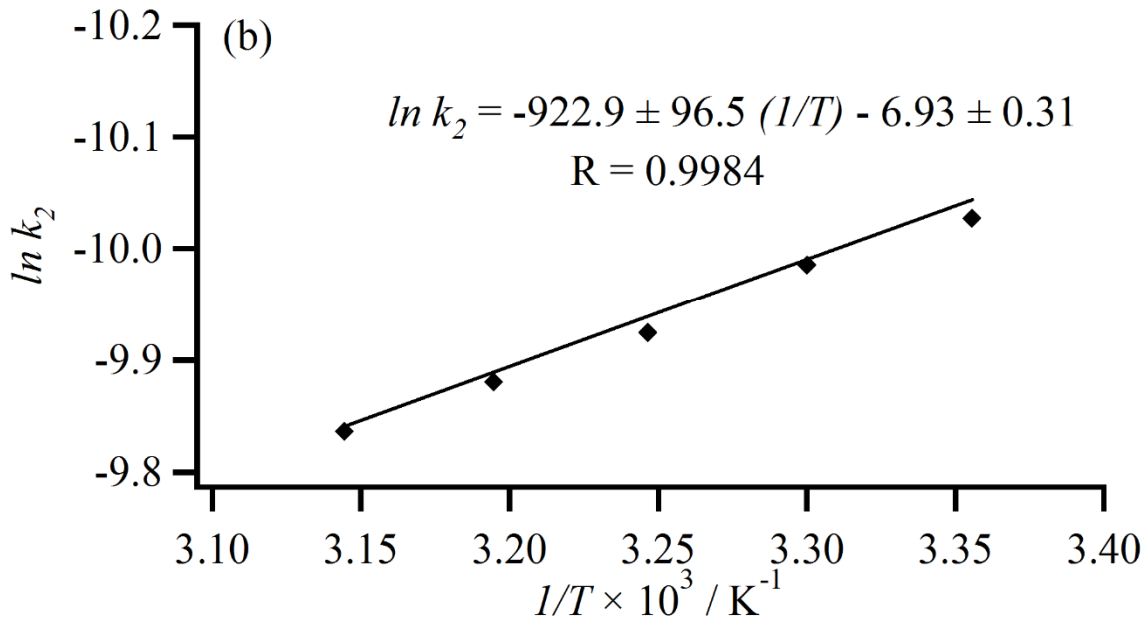

Figure 4.5 (a) Plot of $\ln K_C$ *versus* $1/T$ for estimation of thermodynamic parameters for entrapment of Acid Red 1 in polypyrrole films. (b) An Arrhenius plot for the entrapment of Acid Red 1 in polypyrrole films.

4.4 Conclusion

In this chapter, we have investigated the kinetics, isotherms and thermodynamics of Acid Red 1 entrapment in polypyrrole films. The kinetics data strongly supported that Acid Red 1 entrapment in polypyrrole films follows a pseudosecond order model. Moreover, kinetic study revealed that intra-particle diffusion is also involved in this entrapment system but this is not a rate-controlling step. The isotherm study showed that the equilibrium data of Acid Red 1 entrapment in polypyrrole films did not obey any of the common isotherm models, confirming that the process is not an adsorption but an entrapment process. From the thermodynamic study, a positive $\Delta H°$ (20.5±2.5 kJ mol^{-1}) suggests that the Acid Red 1 entrapment process is endothermic in nature. Also, a positive $\Delta S°$ (73.6±8.2 J mol^{-1} K^{-1}) is indicative of increased randomness of the interface and an affinity of Acid Red 1 towards polypyrrole films. The negative value (-1.46±0.78, -1.86±0.22, -2.14±0.89, -2.58±0.29 and -2.94±0.24 kJ mol^{-1} at the corresponding temperature of 298 K, 303K, 308 K, 313K and 318 K) evaluated for changes in $\Delta G°$ is indicative of a spontaneous entrapment process. Additionally, the low value of

E_a=7.67±0.8 kJ mol^{-1} confirms the Acid Red 1 entrapment in polypyrrole film is a physical process. All the above findings demonstrated that the Acid Red 1 entrapment process in polypyrrole films is an efficient and effective treatment method, which will aid in further development of the electrochemical treatment of effluents containing azo dyes.

4.5 References

1. Robinson, T., McMullan, G., Marchant, R. and Nigam, P. Remediation of dyes in textile effluent: A critical review on current treatment technologies with a proposed alternative. *Bioresource Technology*, 2001. **77**(3): 247-255.

2. Namasivayam, C., Radhika, R. and Suba, S. Uptake of dyes by a promising locally available agricultural solid waste: Coir pith. *Waste Management*, 2001. **21**(4): 381-387.

3. Hastie, J., Bejan, D., Teutli-León, M. and Bunce, N.J. Electrochemical methods for degradation of Orange II (sodium 4-(2-hydroxy-1-naphthylazo)benzenesulfonate). *Industrial and Engineering Chemistry Research*, 2006. **45**(14): 4898-4904.

4. Mahanta, D., Madras, G., Radhakrishnan, S. and Patil, S. Adsorption of sulfonated dyes by polyaniline emeraldine salt and its kinetics. *The Journal of Physical Chemistry B*, 2008. **112**(33): 10153-10157.

5. Ma, L., Zhuo, R., Liu, H., Yu, D., Jiang, M., Zhang, X. and Yang, Y. Efficient decolorization and detoxification of the sulfonated azo dye Reactive Orange 16 and simulated textile wastewater containing Reactive Orange 16 by the white-rot fungus *Ganoderma* sp. En3 isolated from the forest of Tzu-chin mountain in china. *Biochemical Engineering Journal*, 2014. **82**: 1-9.

6. Shah, M.P., Patel, K.A., Nair, S.S., Darji, A. and Maharaul, S. Microbial degradation of azo dye by *Pseudomonas spp*. MPS-2 by an application of sequential microaerophilic and aerobic process. *American Journal of Microbiological Research*, 2013. **1**(4): 105-112.

7. Shah, M.P., Patel, K.A., Nair, S.S. and Darji, A. Microbial decolorization of Methyl Orange dye by *Pseudomonas spp*. *International Journal of Environmental Bioremediation and Biodegradation*, 2013. **1**(2): 54-59.

8. Pandey, A., Singh, P. and Iyengar, L. Bacterial decolorization and degradation of azo dyes. *International Biodeterioration and Biodegradation*, 2007. **59**(2): 73-84.

9. Foo, K.Y. and Hameed, B.H. An overview of dye removal via activated carbon adsorption process. *Desalination and Water Treatment*, 2010. **19**(1-3): 255-274.

10. Dermentzis, K. Removal of nickel from electroplating rinse waters using electrostatic shielding electrodialysis/electrodeionization. *Journal of Hazardous Materials*, 2010. **173**(1): 647-652.

11. Mollah, M.Y., Pathak, S.R., Patil, P.K., Vayuvegula, M., Agrawal, T.S., Gomes, J.A., Kesmez, M. and Cocke, D.L. Treatment of Orange II azo-dye by electrocoagulation (ec) technique in a continuous flow cell using sacrificial iron electrodes. *Journal of Hazardous Materials*, 2004. **109**(1): 165-171.

12. Kupferle, M.J., Galal, A. and Bishop, P.L. Electrolytic treatment of azo dyes containing o, o'-dihydroxyazo complexation sites. *Journal of Environmental Engineering and Science*, 2004. **3**(4): 223-229.

13. Kupferle, M.J., Galal, A. and Bishop, P.L. Electrolytic treatment of azo dye wastewaters: Impact of matrix chloride content. *Journal of Environmental Engineering*, 2006. **132**(5): 514-518.

14. Xu, L., Zhao, H., Shi, S., Zhang, G. and Ni, J. Electrolytic treatment of CI Acid Orange 7 in aqueous solution using a three-dimensional electrode reactor. *Dyes and Pigments*, 2008. **77**(1): 158-164.

15. Aleboyeh, A., Daneshvar, N. and Kasiri, M. Optimization of CI Acid Red 14 azo dye removal by electrocoagulation batch process with response surface methodology. *Chemical Engineering and Processing: Process Intensification*, 2008. **47**(5): 827-832.

16. Can, O., Kobya, M., Demirbas, E. and Bayramoglu, M. Treatment of the textile wastewater by combined electrocoagulation. *Chemosphere*, 2006. **62**(2): 181-187.

17. Gooding, J.J., Compton, R.G., Brennan, C.M. and Atherton, J.H. The mechanism of the electro-reduction of some azo dyes. *Electroanalysis*, 1996. **8**(6): 519-523.

18. Guivarch, E., Trevin, S., Lahitte, C. and Oturan, M.A. Degradation of azo dyes in water by electro-fenton process. *Environmental Chemistry Letters*, 2003. **1**(1): 38-44.

19. Chu, Y.-Y., Wang, W.-J. and Wang, M. Anodic oxidation process for the degradation of 2, 4-dichlorophenol in aqueous solution and the enhancement of biodegradability. *Journal of Hazardous Materials*, 2010. **180**(1): 247-252.

20. El-Desoky, H.S., Ghoneim, M.M. and Zidan, N.M. Decolorization and degradation of Ponceau S azo-dye in aqueous solutions by the electrochemical advanced fenton oxidation. *Desalination*, 2010. **264**(1): 143-150.

21. Chang, P., Huang, Y., Hsueh, C., Lu, M. and Huang, G. Treatment of non-biodegradable wastewater by electro-Fenton method. *Water Science and Technology*, 2004. **49**(4): 213-218.

22. Banat, I.M., Nigam, P., Singh, D. and Marchant, R. Microbial decolorization of textile-dyecontaining effluents: A review. *Bioresource Technology*, 1996. **58**(3): 217-227.

23. McMullan, G., Meehan, C., Conneely, A., Kirby, N., Robinson, T., Nigam, P., Banat, I.M., Marchant, R. and Smyth, W.F. Microbial decolourisation and degradation of textile dyes. *Applied Microbiology and Biotechnology*, 2001. **56**(1-2): 81-87.

24. Haque, M.M., Smith, W.T. and Wong, D.K.Y. Conducting polypyrrole films as a potential tool for electrochemical treatment of azo dyes in textile wastewaters. *Journal of Hazardous Materials*, 2015. **283**(0): 164-170.

25. Qi, G., Huang, L. and Wang, H. Highly conductive free standing polypyrrole films prepared by freezing interfacial polymerization. *Chemical Communications*, 2012. **48**(66): 8246-8248.

26. Jeeju, P.P., Varma, S.J., Francis Xavier, P.A., Sajimol, A.M. and Jayalekshmi, S. Novel polypyrrole films with excellent crystallinity and good thermal stability. *Materials Chemistry and Physics*, 2012. **134**(2): 803-808.

27. Chronakis, I.S., Grapenson, S. and Jakob, A. Conductive polypyrrole nanofibers via electrospinning: Electrical and morphological properties. *Polymer*, 2006. **47**(5): 1597-1603.

28. Omastová, M., Kosina, S., Pionteck, J., Janke, A. and Pavlinec, J. Electrical properties and stability of polypyrrole containing conducting polymer composites. *Synthetic Metals*, 1996. **81**(1): 49-57.

29. Čabala, R., Škarda, J. and Potje-Kamloth, K. Spectroscopic investigation of thermal treatment of doped polypyrrole. *Physical Chemistry Chemical Physics*, 2000. **2**(14): 3283-3291.

30. Maddison, D.S. and Jenden, C.M. Dopant exchange in conducting polypyrrole films. *Polymer International*, 1992. **27**(3): 231-235.

31. Mansouri, J. and Burford, R.P. Novel membranes from conducting polymers. *Journal of Membrane Science*, 1994. **87**(1–2): 23-34.

32. Masubuchi, S., Kazama, S., Mizoguchi, K., Shimizu, F., Kume, K., Matsushita, R. and Matsuyama, T. The transport properties of metallic shirakawa polyacetylenes with different dopant species. *Synthetic Metals*, 1995. **69**(1): 71-72.

33. Palanisamy, P., Agalya, A. and Sivakumar, P. Polymer composite-a potential biomaterial for the removal of reactive dye. *Journal of Chemistry*, 2012. **9**(4): 1823-1834.

34. Ansari, R., Keivani, M.B. and Delavar, A.F. Application of polyaniline nanolayer composite for removal of Tartrazine dye from aqueous solutions. *Journal of Polymer Research*, 2011. **18**(6): 1931-1939.

35. Ansari, R. and Mosayebzadeh, Z. Removal of Eosin Y, an anionic dye from aqueous solution using conducting electroactive polymers. *Iranian Polymer Journal*, 2010. **19**(7): 541-551.

36. Ahmad, R. and Kumar, R. Conducting polyaniline/iron oxide composite: A novel adsorbent for the removal of Amido Black 10B. *Journal of Chemical and Engineering Data*, 2010. **55**(9): 3489-3493.

37. Ozcan, A.S., Erdem, B. and Ozcan, A. Adsorption of acid blue 193 from aqueous solutions onto BTMA-bentonite. *Colloids and Surfaces-A-Physiochemical and Engineering Aspects*, 2005. **266**(1-3): 73-81.

38. Özcan, A., Öncü, E.M. and Özcan, A.S. Kinetics, isotherm and thermodynamic studies of adsorption of Acid Blue 193 from aqueous solutions onto natural sepiolite. *Colloids and Surfaces A: Physicochemical and Engineering Aspects*, 2006. **277**(1–3): 90-97.

39. Shimoda, S. and Smela, E. The effect of pH on polymerization and volume change in PPy (DBS). *Electrochimica Acta*, 1998. **44**(2): 219-238.

40. Ho, Y.-S. and McKay, G. Kinetic models for the sorption of dye from aqueous solution by wood. *Process Safety and Environmental Protection*, 1998. **76**(2): 183-191.

41. Tunali, S., Özcan, A.S., Özcan, A. and Gedikbey, T. Kinetics and equilibrium studies for the adsorption of Acid Red 57 from aqueous solutions onto calcined-alunite. *Journal of Hazardous Materials*, 2006. **135**(1–3): 141-148.

42. Gök, Ö., Özcan, A.S. and Özcan, A. Adsorption kinetics of naphthalene onto Organo-sepiolite from aqueous solutions. *Desalination*, 2008. **220**(1–3): 96-107.

43. Özcan, A.S. and Özcan, A. Adsorption of acid dyes from aqueous solutions onto acid-activated bentonite. *Journal of Colloid and Interface Science*, 2004. **276**(1): 39-46.

44. Özcan, A.S., Erdem, B. and Özcan, A. Adsorption of Acid Blue 193 from aqueous solutions onto Na-bentonite and DTMA-bentonite. *Journal of Colloid and Interface Science*, 2004. **280**(1): 44-54.

45. Özcan, A.S., Tetik, Ş. and Özcan, A. Adsorption of acid dyes from aqueous solutions onto sepiolite. *Separation Science and Technology*, 2005. **39**(2): 301-320.

46. Özcan, A. and Özcan, A.S. Adsorption of Acid Red 57 from aqueous solutions onto surfactant-modified sepiolite. *Journal of Hazardous Materials*, 2005. **125**(1): 252-259.

47. Cheung, W.H., Szeto, Y.S. and McKay, G. Intraparticle diffusion processes during acid dye adsorption onto chitosan. *Bioresource Technology*, 2007. **98**(15): 2897-2904.

48. Weber, W. and Morris, J. Kinetics of adsorption on carbon from solution. *Journal of the Sanitary Engineering Division*, 1963. **89**(17): 31-60.

49. Kannan, N. and Sundaram, M.M. Kinetics and mechanism of removal of Methylene Blue by adsorption on various carbons-a comparative study. *Dyes and Pigments*, 2001. **51**(1): 25-40.

50. Bhattacharyya, K.G. and Sharma, A. Azadirachta indica leaf powder as an effective biosorbent for dyes: A case study with aqueous Congo Red solutions. *Journal of Environmental Management*, 2004. **71**(3): 217-229.

51. Chen, J.P., Wu, S. and Chong, K.-H. Surface modification of a granular activated carbon by citric acid for enhancement of copper adsorption. *Carbon*, 2003. **41**(10): 1979-1986.

52. Aksu, Z., Tatlı, A.İ. and Tunç, Ö. A comparative adsorption/biosorption study of Acid Blue 161: Effect of temperature on equilibrium and kinetic parameters. *Chemical Engineering Journal*, 2008. **142**(1): 23-39.

53. Sharma, P. and Das, M.R. Removal of a cationic dye from aqueous solution using graphene oxide nanosheets: Investigation of adsorption parameters. *Journal of Chemical and Engineering Data*, 2012. **58**(1): 151-158.

54. Bayramoglu, G., Altintas, B. and Arica, M.Y. Adsorption kinetics and thermodynamic parameters of cationic dyes from aqueous solutions by using a new strong cation-exchange resin. *Chemical Engineering Journal*, 2009. **152**(2–3): 339-346.

CHAPTER 5

EVALUATION OF ACID RED 1 ENTRAPMENT-LIBERATION PERFORMANCE BY ELECTROCHEMICALLY SYNTHESISED POLYPYRROLE-GRAPHENE OXIDE AND POLYPYRROLE-REDUCED GRAPHENE OXIDE COMPOSITE FILMS

5.1 Introduction

Globally, water contamination by various pollutants including dyes is a concerning environmental issue. Dyes that are extensively used in many industries, for example, textile, leather, paint, food, pharmaceuticals and cosmetic represent a major polluting group among the different types of water pollutants [1, 2]. Approximately 10-25% of textile dyes are lost during the dyeing process and 2-20% are directly discharged as aqueous effluents [3]. Moreover, these dyes usually have a complex molecular structure that makes them stable and more difficult to biodegrade [4, 5]. As a result, the discharged dye containing wastewater can cause serious hazards to water bodies and plant life, introduce the potential risk of bioaccumulation and thus destroy the entire ecosystem [6]. Furthermore, most of the dye molecules or their metabolites (*e.g.*, aromatic amines) are highly toxic, potentially carcinogenic, mutagenic and allergenic to exposed organisms, thus can contaminate not only the surrounding environment, but also traverse through the entire food chain, leading to biomagnification [7, 8].

Evidently, removal of dyes from effluent before discharging into the water system becomes environmentally important. A range of conventional physico-chemical and biological treatment methods for removal of dye from the effluents, including chemical precipitation, adsorption, activated carbon adsorption [9], reverse osmosis [10], ion exchange, biodegradation, membrane filtration, coagulation and flocculation [11] have been investigated extensively. However, the

above mentioned techniques can produce appreciable toxic by-products during operation. In addition, there is a very limited scope for recovering precious dyes from effluents in applying these techniques.

In Chapter 3, we have reported the application of the conducting polymer, polypyrrole, as a potential green tool for treatment of azo dye using Acid Red as a model dye [12]. Briefly, in our pilot study, we have successfully synthesised polypyrrole-Acid Red 1 films by electropolymerisation of pyrrole in the presence of Acid Red 1 to entrap the dye from its synthetic solution. Similarly, Acid Red 1 liberated from dye entrapped polypyrrole film. In Chapter 4, we have also reported the kinetic models and thermodynamics of the entrapment of Acid Red 1 in polypyrrole films and found significant entrapment capacity of electropolymerised polypyrrole for Acid Red 1.

However, poor stability of polypyrrole films has limited their repeated entrapment-liberation process of Acid Red 1. This poor stability was likely to have caused by swelling and shrinkage during the entrapment-liberation process (or oxidation-reduction cycle of polypyrrole) of Acid Red 1. This has directly led to mechanical degradation of the polypyrrole films and weakening of their electrochemical performance [13-15]. Therefore it is essential to improve the mechanical strength of polypyrrole films before they can be further considered for use in electrochemical treatment of Acid Red 1. Moreover, surface area or porosity of the film is also an important influencing factors for efficient entrapment. Therefore, it is very necessary to prepare nanostructured polypyrrole film with a large surface area to improve its entrapment efficiency.

The introduction of carbon-based materials into conducting polymers provides mechanical reinforcement and increased porosity that accommodates the volumetric changes associated with the charge/discharge process. In addition, the enhanced conductivity provided by the carbon network enables a more rapid charge/discharge [16]. Among the carbon-based materials, graphene, a two-dimensional monolayer of sp^2-bonded carbon atoms has attracted a great deal of attention in recent years, due to its high electrical and thermal conductivities [17], great mechanical strength [18] and large surface area [19, 20]. Graphene or graphene oxide can be easily prepared in large scales from natural graphite. Graphene oxide sheets are heavily oxygenated and this will aid in improving the interaction between graphene oxide and polypyrrole [21]. In addition, graphene oxide is an easily available low cost material. Therefore, graphene oxide is often preferred over other expensive carbon-based materials such

as carbon nanotubes [21, 22]. Moreover, owing to its high water solubility and the presence of oxygen containing functional groups (*e.g.*, epoxy, hydroxyl, and carboxyl groups), graphene oxide will interact strongly with polymers. This makes graphene oxide possible to function as a dopant when it is incorporated in conducting polymers such as polypyrrole [21].

Graphene oxide based composites have attracted a great deal of attention from researchers in preparing conductive polymer composites due to their advantages, which include high conductivity, large surface area, excellent thermal and mechanical properties and low cost synthesis [23]. Recently, some work has been conducted on the preparation of polypyrrole-graphene oxide and polypyrrole-graphene nanocomposites for their applications in supercapacitors, transparent electrodes, artificial actuators, and removal of inorganic anion from its aqueous solution [15, 24-29]. The thermal, mechanical and electrical properties of these composites were found to have improved compared to polypyrrole [30-33]. Composites based on polypyrrole and graphene oxide have shown synergistic properties such as enhancement in electrical conductivity and electrochemical cyclability [34, 35]. Bora and Dolui [21] synthesised polypyrrole-graphene oxide nanocomposites by liquid-liquid interfacial polymerization and their optical, electrical and electrochemical properties were evaluated. They reported that the composites exhibited significant improvement in thermal stability and 2.5 folds increase in electrical conductivity in comparison to pure polypyrrole and showed excellent electrochemical reversibility and good cyclic stability even up to the one hundredth cycle. Therefore, they suggested that the polypyrrole-graphene oxide composite could be applied to electrochemical energy storage devices, rechargeable batteries, biosensor and other fields [21]. Li *et al*. [36] studied the removal of Cr(VI) from an aqueous solution by chemically synthesised polypyrrole-graphene oxide composite nanosheets. They reported that the removal capacity of the polypyrrole-graphene oxide composite nanosheets was about two times larger than that of polypyrrole. Chandra and Kim [37] synthesised polypyrrole-reduced graphene oxide composites via a chemical route and a highly selective Hg^{2+} removal capacity of polypyrrole-reduced graphene oxide (85%) composite compared to polypyrrole (13%) was reported. They also suggested that the highly removal capacity and recycling make this material practically useful for wastewater treatment [37].

In order to improve the thermal and mechanical stability, conductivity, effective surface area, and the dye entrapment efficiency of polypyrrole films, a composite of polypyrrole and graphene oxide was used in the present study. In this chapter, we will evaluate Acid Red 1

removal performance by electrochemically synthesised mechanically and thermally stable polypyrrole-graphene oxide and polypyrrole-reduced graphene oxide films.

Initially, an Acid Red 1 entrapped polypyrrole-graphene oxide film was synthesised via electropolymerisation of pyrrole in presence of Acid Red 1 and graphene oxide. Next, the polypyrrole-reduced graphene oxide film was electrochemically reduced to form a polypyrrole-graphene oxide film. The films obtained were then characterised by electrochemistry, scanning electron microscopy and spectrophotometry, Brunauer, Emmett and Teller (BET) surface area analysis, mechanical and thermogravimetric analysis. Finally, we evaluated the entrapment-liberation efficiency of Acid Red 1 entrapped polypyrrole-graphene oxide and polypyrrole reduced graphene oxide films over different entrapment-liberation cycles. At the end of this Chapter, a preliminary study of Acid Red 1 entrapment in polypyrrole-reduced graphene oxide films in the presence of Indigo Carmine was also performed to investigate the selectivity of polypyrrole reduced graphene oxide towards Acid Red 1.

5.2 Experimental

Details of the procedure adopted for experiments described in this chapter have been presented in Chapter 2. Initially, graphite oxide was synthesised from graphite powder using a modified Hummers-Offeman method [38] (described in Chapter 2) and exfoliation of graphite oxide was performed to prepare graphene oxide using an Extech ultrasonic processor. An Acid Red 1 entrapped polypyrrole-graphene oxide film was potentiostatically–synthesised by *in situ* polymerisation on a stainless steel mesh electrode by applying an oxidation potential of +1.0 V (determined from the cyclic voltammogram of polypyrrole in the presence of Acid Red 1 and graphene oxide as discussed in section 5.3.1) in the presence of 0.2 mol L^{-1} pyrrole and 1500 mg L^{-1} Acid Red 1 for 480 min. The polypyrrole-graphene oxide film was then reduced by applying a reduction potential of -1.3 V for 240 min in 0.5 M NaOH solution to prepare a polypyrrole-reduced graphene oxide film. The entrapment evaluation of Acid Red 1 in a 1500 mg L^{-1} solution was then performed in the respective polypyrrole, polypyrrole-graphene oxide and polypyrrole-reduced graphene oxide films for a duration from 20 to 480 min by applying an oxidation potential of +1.0 V. The synthesised films were then characterised by BET surface area analysis, FTIR, XPS tensile testing, conductivity measurements, TGA and SEM. The remaining electrolyte solutions in the cell were used to evaluate the percentage of Acid Red 1 entrapped in the films by UV-visible spectrophotometry. Liberation experiment at the same films was also performed in the presence of 0.5 M NaOH solution by applying a

reduction potential of -0.80 V for 300 min and the resultant solution was again spectrophotometrically analysed to determine the liberation efficiency of Acid Red 1 entrapped polypyrrole film.

5.3 Results and discussion

5.3.1 Characterisation

5.3.1.1 Cyclic voltammetry

In order to determine the appropriate oxidation-reduction potential for entrapment and liberation of Acid Red 1, cyclic voltammetry of 0.2 mol L^{-1} pyrrole was conducted at a stainless steel mesh electrode in the presence of 1500 mg L^{-1} Acid Red 1 or 1500 mg L^{-1} Acid Red 1 and graphene oxide (20:1 between pyrrole and graphene oxide) as a supporting electrolyte and Acid Red 1 alone. The amount of graphene oxide was chosen based on the conductivity of films as discussed in Section 5.3.1.9. The results obtained are shown in Figure 5.1(a). In all voltammograms, as the potential was scanned from -1.2 V to +1.5 V, a current increase observed between +1.0 V and +1.5 V in the voltammograms obtained at both polypyrrole-Acid Red 1 and polypyrrole-graphene oxide, while a broad reduction peak between -0.80 and -1.0 V was observed as the potential was scanned backward. The former peaks were attributed to the oxidation of pyrrole to form polypyrrole with a positive charged backbone with entrapped anion, whereas the latter peaks arose from the reduction of polypyrrole with uncharged, anion liberated film. Notably, no oxidation / reduction peaks were observed at the stainless steel electrode in Acid Red 1 alone. Witkowski *et al.* [39] reported that overoxidation of pyrrole would occur at potential higher than +1.0 V, while Schlenoff and Xu [40] reported an irreversible oxidation after applying potential greater than +1.4 V. Under overoxidation or irreversible oxidation, electroactivity of the film was negatively affected and the counter anion would not be reincorporated into the film [41]. Based on cyclic voltammetry of pyrrole in the presence of Acid Red 1 or graphene oxide, an oxidation potential of +1.0 V was used in this study to avoid overoxidation of pyrrole and a reduction potential of -0.80 V was adopted. These two potentials were then used in the entrapment and liberation of Acid Red 1, respectively, in polypyrrole and polypyrrole-graphene oxide films in our investigations.

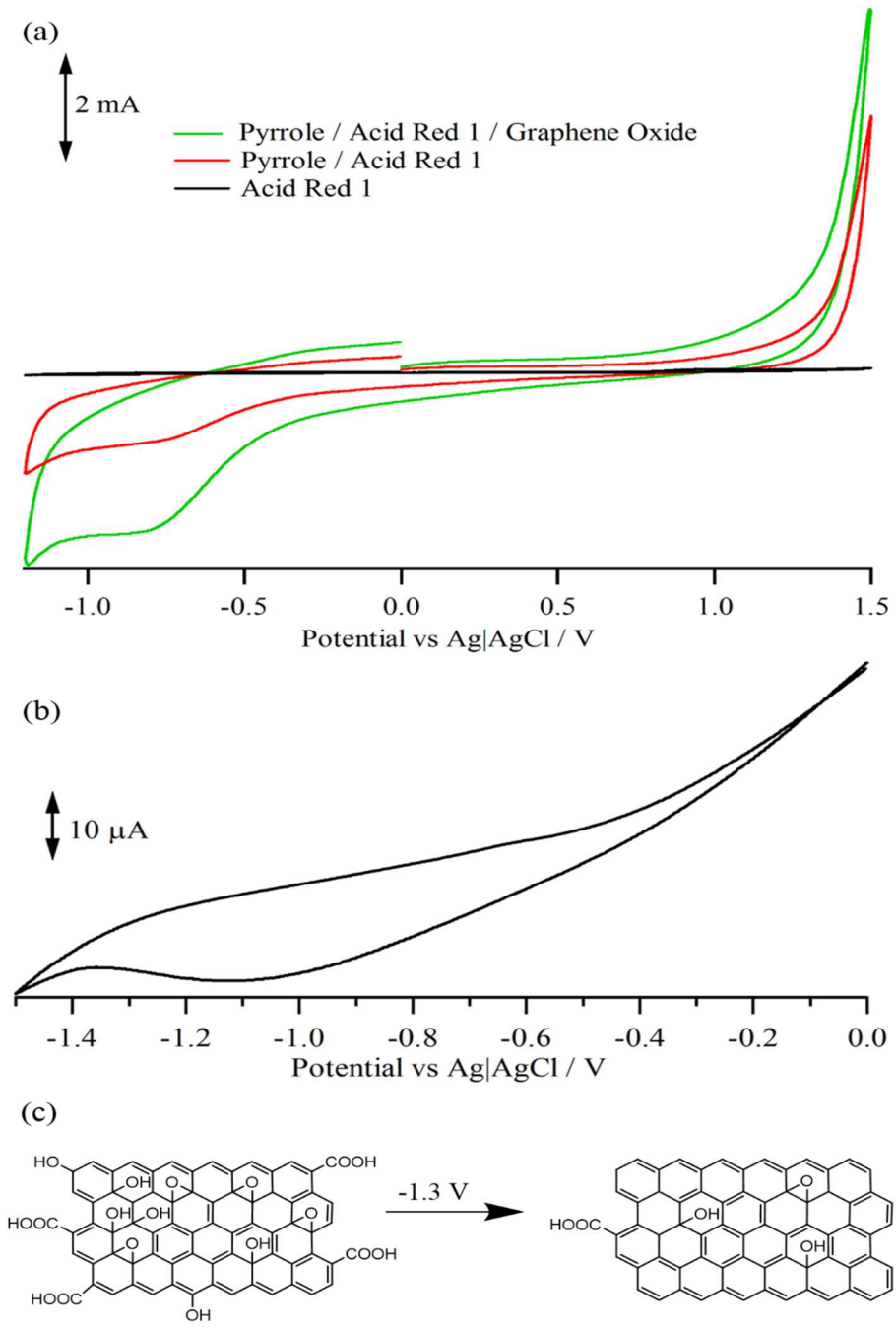

Figure 5.1 Cyclic voltammograms of (a) polypyrrole in the presence of Acid Red 1 or graphene oxide and Acid Red 1 alone; (b) reduction of graphene oxide in a polypyrrole film, and (c) Schematic conversion of graphene oxide to reduced graphene oxide.

The potential for reducing graphene oxide to reduced graphene oxide was then determined. In this experiment, a potential range from 0.0 to -1.5 V was applied to a polypyrrole-graphene oxide film electrode in 0.5 M NaOH aqueous solution. The cyclic voltammogram in Figure 5.1(b) shows a cathodic current peak between -0.80 V and -1.3 V. This large reduction current

arose from the reduction of the surface oxygen groups of graphene oxide. Based on this cyclic voltammogram, -1.3 V was selected as a sufficiently negative potential to reduce graphene oxide in the polypyrrole-graphene oxide film to a polypyrrole-reduced graphene oxide film as the reduction occurs at more negative potentials [42]. As illustrated in Figure 5.1(c), during the reduction process, the number of oxygen containing functional groups decreased, but the π conjugation was enhanced, leading to an increase in conductivity of the film.

5.3.1.2 FTIR analysis

Figure 5.2 shows the FTIR spectra of graphene oxide (trace a), Acid Red 1 entrapped polypyrrole (trace b), polypyrrole-graphene oxide (trace c) and polypyrrole-reduced graphene oxide (trace d) composite films. In trace a, the peaks at 3400, 1750, 1400 and 1045 cm^{-1} are assigned to the stretching vibration of OH, C=O in COOH, and C-O in C-OH / C-O-C (epoxy) functional groups, respectively. These observations are consistent with 3415, 1730 and 1407-1057 cm^{-1} for the vibration of OH, C=O and C-O, respectively in the FTIR spectra of graphene oxide reported by Feng *et al.* [29]. In trace b, the characteristic peaks located at 1490, 1050 and 898 cm^{-1}, due to the pyrrole ring stretching, N-H bending of polypyrrole, and in-plane / out-of-plane C-H bending, respectively. Similar results were observed by Feng *et al.* [29] and Zhang *et al*. [43] for the spectra of polypyrrole. In the FTIR spectra of both Acid Red 1 entrapped polypyrrole-graphene oxide film (trace c) and polypyrrole-reduced graphene oxide film (trace d), all these characteristics peaks of polypyrrole film appeared but either positively or negatively shifted due to the interaction of graphene oxide with polypyrrole. This serves as an indication of the presence of polypyrrole in the composite films [29, 44]. In addition, FTIR spectra of Acid Red 1 entrapped polypyrrole (trace b) and polypyrrole-graphene oxide (trace c) show characteristic peaks at 775 and 1256 cm^{-1} that correspond to the strong stretching vibration of S=O group of Acid Red 1 and the peak at 1750 cm^{-1} corresponds to C=O stretching of Acid Red and / or graphene oxide [12, 43]. Moreover, in the FTIR spectra of polypyrrole-graphene oxide (trace c), a small peak at 1400 cm^{-1} for stretching of C-O in C-OH and a broad peak at 3400 cm^{-1} assigned for stretching of OH confirm the presence of graphene oxide in the film. However, disappearance of peaks at 3400, 1750, and 775 and 1256 cm^{-1} in the FTIR spectra of polypyrrole-reduced graphene oxide film (trace d) may be due to the reduction of OH and C=O groups of graphene oxide and the liberation of Acid Red 1 from the film, respectively, after electrochemical reduction of polypyrrole-graphene oxide film to polypyrrole-reduced graphene oxide film.

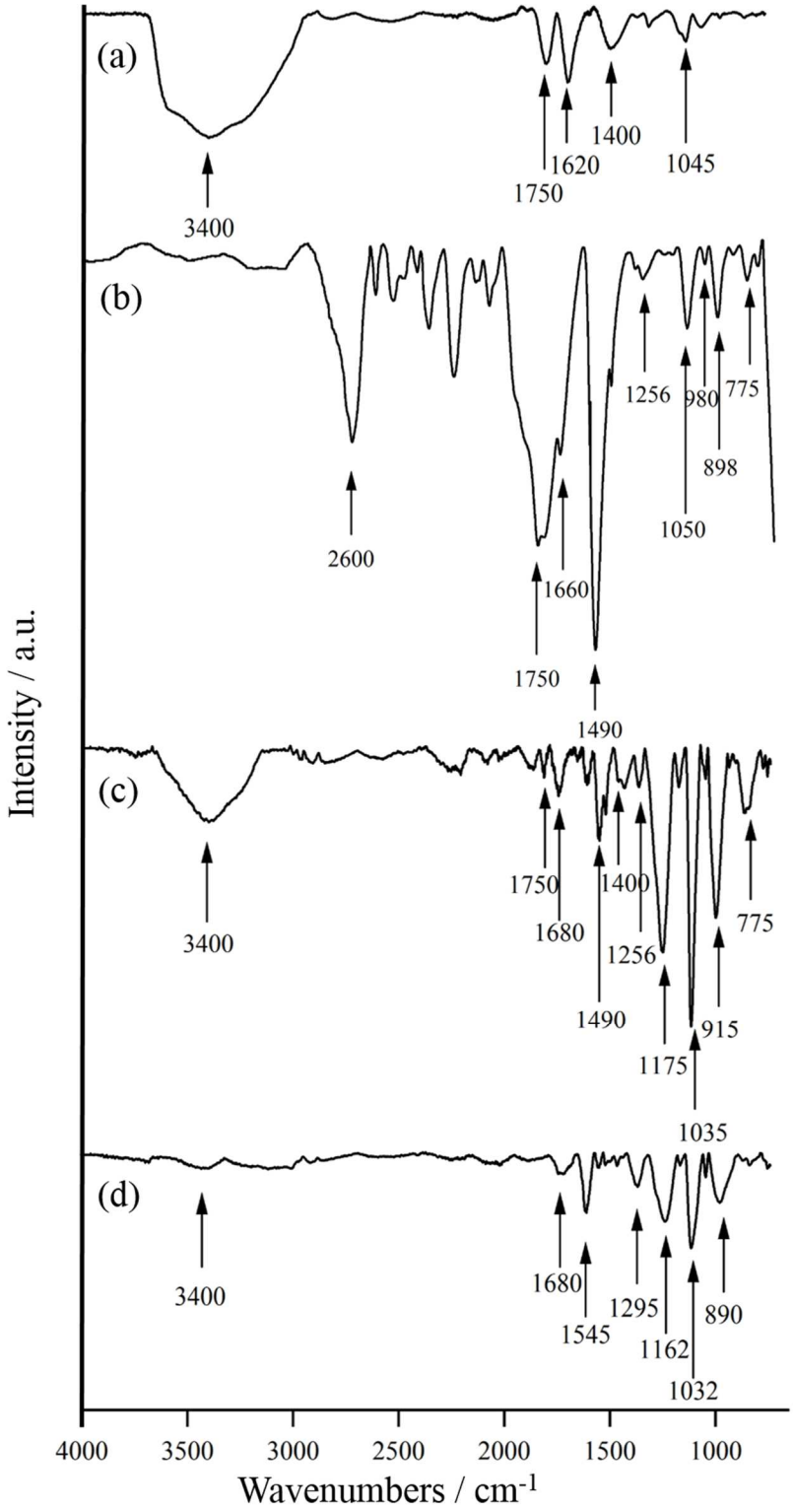

Figure 5.2 FTIR spectra of (a) graphene oxide, and Acid Red 1 entrapped (b) polypyrrole, (c) polypyrrole-graphene oxide and (d) polypyrrole-reduced graphene oxide composite films.

5.3.1.3 XRD analysis

The structure of the polypyrrole, polypyrrole-graphene oxide and polypyrrole-reduced graphene oxide composite films was investigated by XRD measurements. Figure 5.3 shows the XRD patterns of graphene oxide (trace a), polypyrrole in the presence of KNO_3 (trace b), and Acid Red 1 entrapped polypyrrole (trace c), polypyrrole-graphene oxide (trace d) and polypyrrole-reduced graphene oxide (trace e) composite films. The XRD pattern of graphene oxide only (trace a) exhibits a strong peak at $2\theta = 11.4°$, corresponding to the peak for graphene oxide. A 2θ peak at $11.4°$ was obtained by Bora and Dolui [21], and they attributed this to (001) reflection peak for graphene oxide. The spectrum of a polypyrrole film synthesised in the presence of KNO_3 (trace b) displays a broad diffraction peak at approximately $2\theta = 24.9°$. This is consistent with the peak obtained by Liu *et al.* [24] and Bora and Dolui [21], which arose from the amorphous nature of polypyrrole. After electropolymerisation of pyrrole in the presence of Acid Red 1 (trace c), in addition to the peak at $2\theta = 24.9°$ for polypyrrole, a peak at $2\theta = 8.7°$ was found for Acid Red 1, indicating the entrapment of Acid Red 1 in the polypyrrole film [12]. A polypyrrole film prepared in the presence of both Acid Red 1and graphene oxide (trace d) shows the same peaks at $2\theta = 8.7°$ for Acid Red 1 and $25.6°$ for polypyrrole, while the peak at $2\theta = 11.4°$ for graphene oxide in trace a has shifted to $13.8°$ with a significantly reduced peak intensity. This decrease in the peak intensity may be due to the exfoliation of graphene oxide layers upon ultrasonication and low graphene oxide concentration [21]. Moreover, the presence of these three peaks indicates the successful entrapment of Acid Red 1 in the polypyrrole-graphene oxide composite film. Thus the XRD results reveal that the graphene oxide sheets were well intercalated and uniformly dispersed in the polypyrrole matrix. On the other hand, the XRD pattern of polypyrrole-reduced graphene oxide composite film (trace e), which was prepared by electrochemical reduction of polypyrrole-graphene oxide film, shows a broader diffraction peak at approximately $2\theta = 24.4°$, which is almost similar to that in the XRD pattern of polypyrrole in trace b. Chandra and Kim [37] also reported a broad peak at $2\theta = 25°$ for polypyrrole-reduced graphene oxide and suggested that this peak arose from both the polypyrrole intermolecular spacing and reduced graphene oxide.

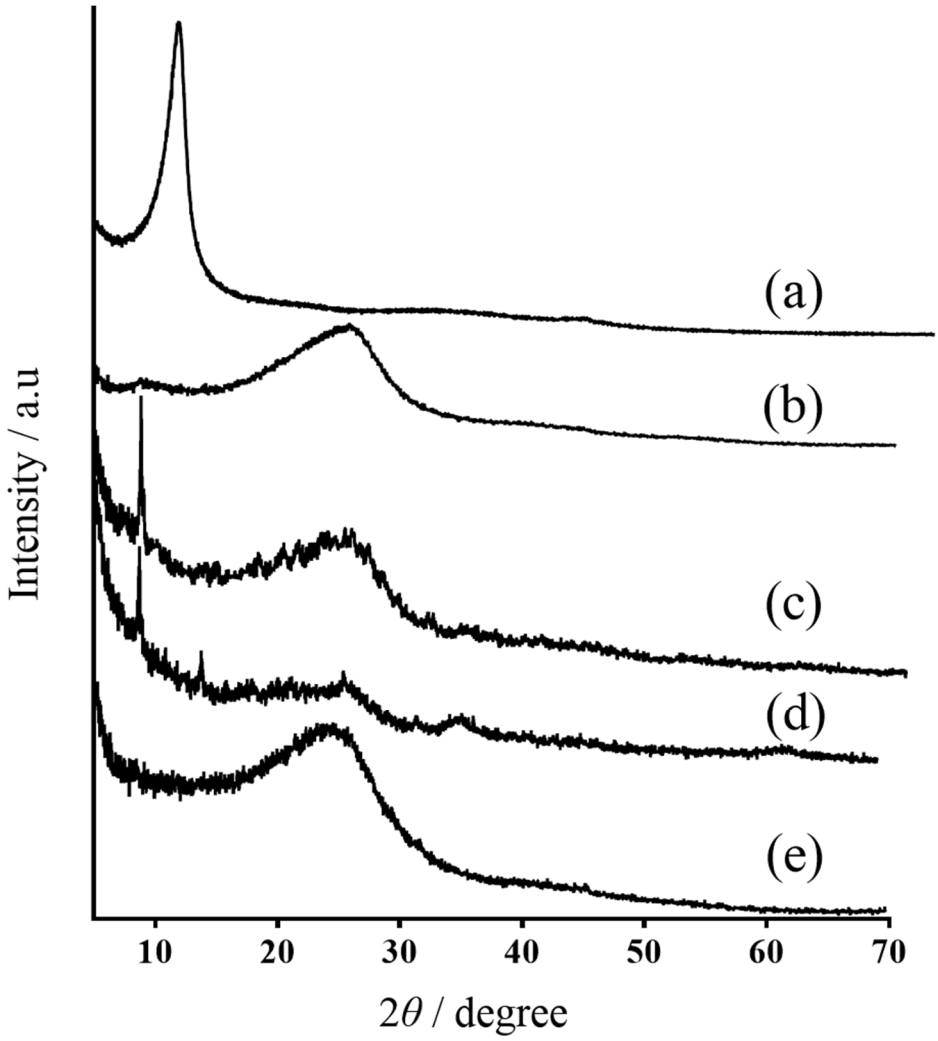

Figure 5.3 X-ray diffraction patterns of (a) graphene oxide alone, (b) polypyrrole in presence of KNO_3, (c) Acid Red 1 entrapped polypyrrole, (d) Acid Red 1 entrapped polypyrrole-graphene oxide and (e) polypyrrole-reduced graphene oxide composite films.

5.3.1.4 XPS analysis

XPS is a useful technique for characterising carbon-based materials. XPS can provide information about the actual composition and chemical state of surfaces of a materials. Figure 5.4 shows the C1s core-level spectra of Acid Red 1 entrapped in (a) polypyrrole, (b) polypyrrole-graphene oxide, and (c) polypyrrole-reduced graphene oxide composite films. The bands centered at 284.8 are known to be associated with C1s [45]. The C1s core-level spectra of all polypyrrole composite films (Figure 5.4 (a), (b) and (c)) show peaks at the binding energies of 284.7, 285, 286.7, and 288.3 eV, which correspond to the chemical bonds of

C-C/C=C, C-N/C=N, C-O and C=O/O-C=O, respectively by comparing to 284.7, 285.6, 286.7 and 288.3 eV reported by Si *et al.* [27]. The relative peak intensities of C-O and C=O/O-C=O are substantially decreased for polypyrrole-reduced graphene oxide (Figure 5.4(c)) after the electrochemical reduction polypyrrole-graphene oxide. Si *et al*. [27] and Feng *et al*. [29] observed similar results after electrochemical reduction of polypyrrole-graphene oxide film. They suggested that the decreased peak intensity was due to the removal of the oxygen functionalities on the surface of graphene oxide in the composite material during the electrochemical reduction (see Schematic in Figure 5.1(c)). The wide region scanning XPS spectra of Acid Red 1 entrapped polypyrrole, polypyrrole-graphene oxide and polypyrrole-reduced graphene oxide composite films are shown in Figure 5.4(d). The peaks at approximately 399-401 eV in the N1s spectra of Acid Red 1 entrapped polypyrrole, polypyrrole-graphene oxide and polypyrrole-reduced graphene oxide (Figure 5.4(d)) are associated with C-N and $C\text{-}N^{+}$, indicating the presence of polypyrrole in the composite films. These results are comparable to 399.6 and 401.7 eV observed by Feng *et al*. [29]. In Figure 5.4(d), the peaks at 531.1 eV for polypyrrole, polypyrrole-graphene oxide and polypyrrole reduced graphene oxide are associated with O1s. However the peak intensity decreased in polypyrrole reduced graphene oxide compared with polypyrrole-graphene oxide because of the removal of oxygen functionalities after electrochemical reduction. A small peak at approximately 168 eV in the S2p XPS spectra in Figure 5.4(d) correspond to the sulfur content of Acid Red 1 in polypyrrole, polypyrrole-graphene oxide and polypyrrole-reduced graphene oxide composite films.

The atomic percentage of a given chemical moiety in the near surface region of a film can be evaluated from the area under the peak of the XPS spectra, which is proportional to the number of atoms that contribute to a given intensity. Accordingly, the atomic percentages of carbon, nitrogen, oxygen and sulfur in the composite films were evaluated and data are summarised in Table 5.1.

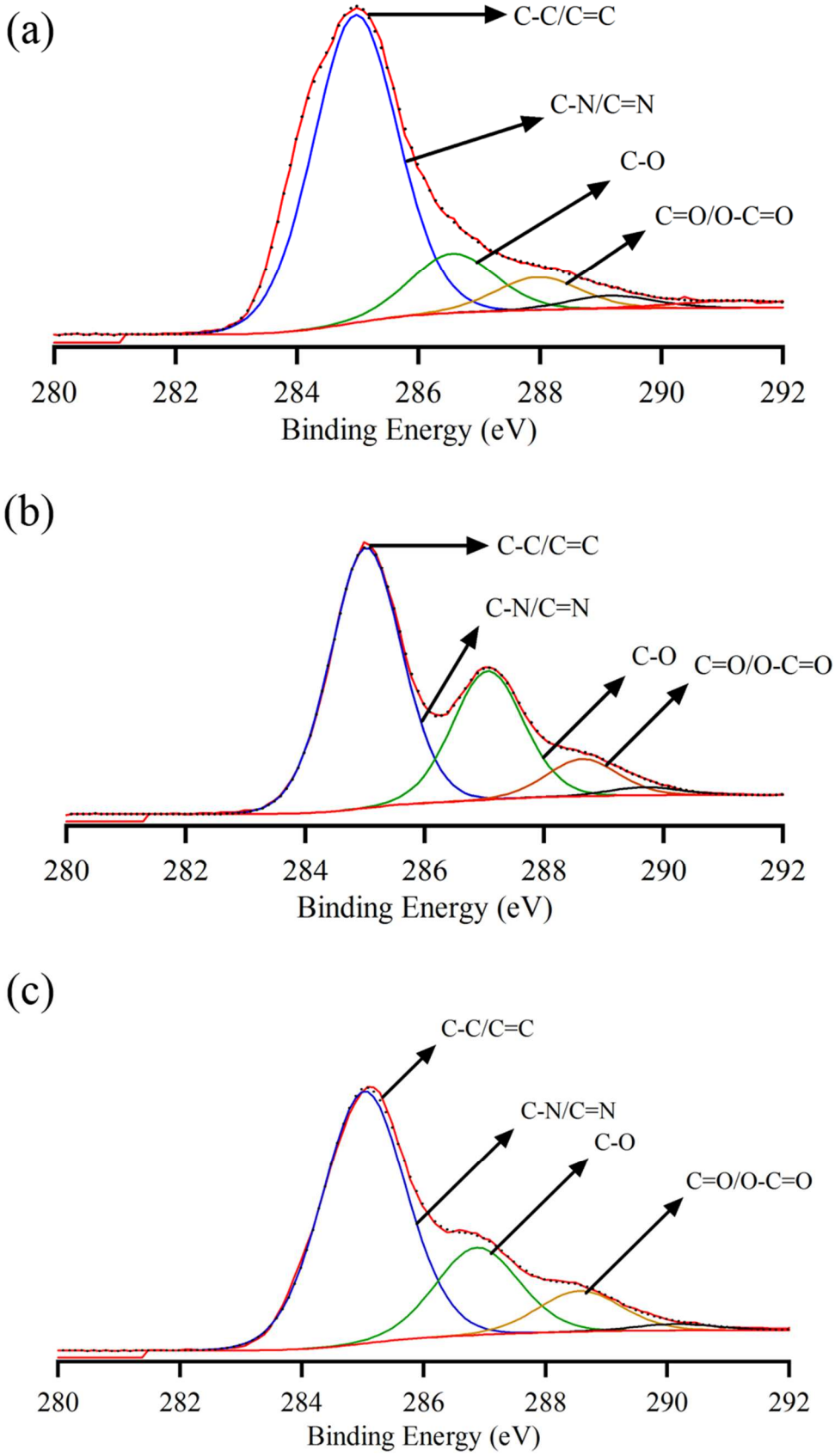
(a)
C-C/C=C
C-N/C=N
C-O
C=O/O-C=O
280
282
284
286
288
290
292
Binding Energy (eV)
(b)
C-C/C=C
C-N/C=N
C-O
C=O/O-C=O
280
282
284
286
288
290
292
Binding Energy (eV)
(c)
C-C/C=C
C-N/C=N
C-O
C=O/O-C=O
280
282
284
286
288
290
292
Binding Energy (eV)

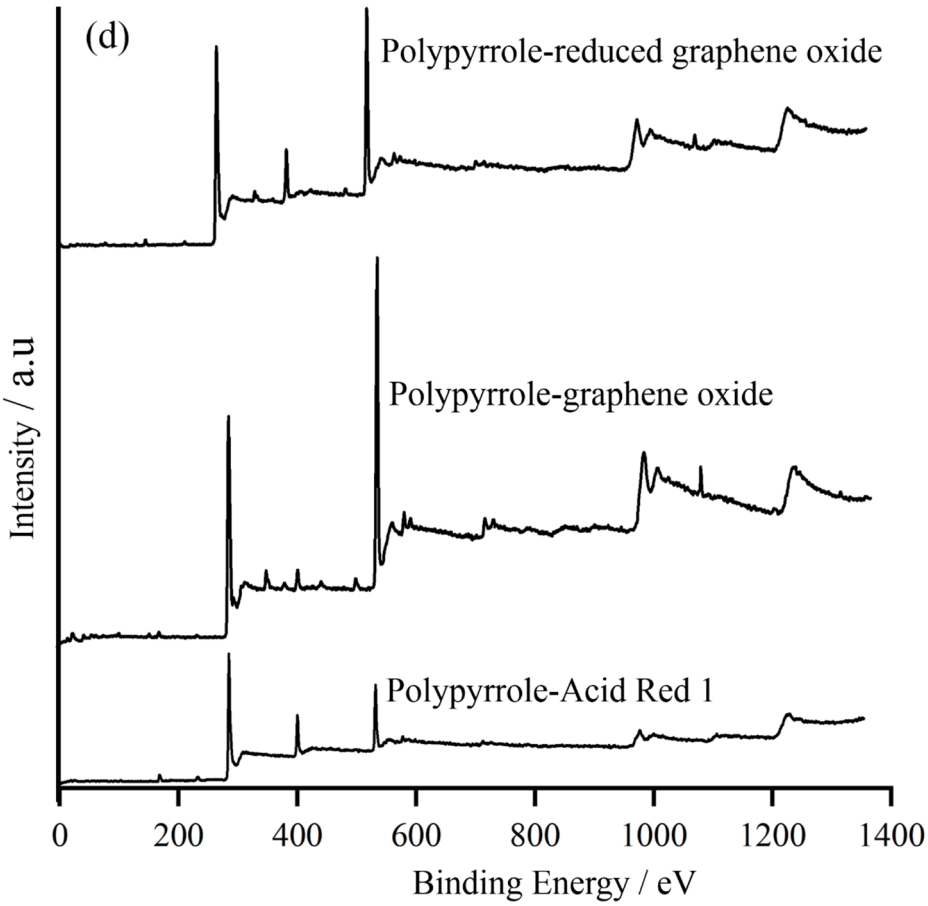

Figure 5.4 The C1s core-level spectra of Acid Red 1 entrapped (a) polypyrrole, (b) polypyrrole-graphene oxide, and (c) polypyrrole-reduced graphene oxide composite films and (d) the wide region canning XPS spectra Acid Red 1

Table 5.1 Relative atomic percentages of carbon, nitrogen, oxygen and sulphur in Acid Red 1 entrapped polypyrrole, polypyrrole-graphene oxide and polypyrrole-reduced graphene oxisde composite films.

Element	**Polypyrrole-Acid Red 1**	**Polypyrrole-graphene oxide**	**Polypyrrole-reduced graphene oxide**
	Atomic %		
C	71.75	63.21	66.16
N	12.41	2.84	8.72
O	12.72	28.85	21.12
S	1.91	0.69	0.86

5.3.1.5 SEM analysis

Figure 5.5 shows the scanning electron micrographs of (a) polypyrrole (in the presence of KNO_3), (b) Acid Red 1 entrapped polypyrrole, (c) polypyrrole-graphene oxide and (d) polypyrrole-reduced graphene oxide composite films. In Figure 5.5(a), the polypyrrole film prepared in presence of KNO_3 shows a rough surface morphology of polypyrrole, which is commonly observed on polypyrrole film synthesised in the presence of small anions (*e.g.*ClO_4^-, NO_3^-), and as previously reported by Chang *et al*. [28]. On the other hand, a polypyrrole film prepared in the presence of Acid Red 1 (Figure 5.5(b)) exhibits a typical cauliflower morphology composed of large nodules after the entrapment of Acid Red 1 in the polypyrrole film, similar to those previously observed in polypyrrole films polymerised in the presence of pTS$^-$ [46]. Scanning electron micrographs of polypyrrole-graphene oxide (Figure 5.5(c)) presents a similarly wrinkled or crumbled surface to that observed by Yang *et al.* [47] at the surface of electrodeposited polypyrrole-graphene oxide film, resulting from the formation of a thin layer of graphene oxide nanosheets within the polypyrrole film [47], that experienced an electrostatic repulsive interaction between the negatively charged adjacent graphene oxide nanosheets [27]. However, the surface of polypyrrole-reduced graphene oxide film appears cracked and porous microstructures. Pore and channel, resulting from the liberation of Acid Red 1 from the film during electrochemical reduction of polypyrrole-graphene oxide film to polypyrrole-reduced graphene oxide film. Similarly porous microstructures of polypyrrole-reduced graphene oxide film synthesised by electrochemical reduction of polypyrrole-graphene oxide was also observed in chemically synthesised polypyrrole-reduced graphene oxide by Chandra *et al*. [37] and in electrochemically synthesised polypyrrole-reduced graphene oxide by Yang *et al*. [47].

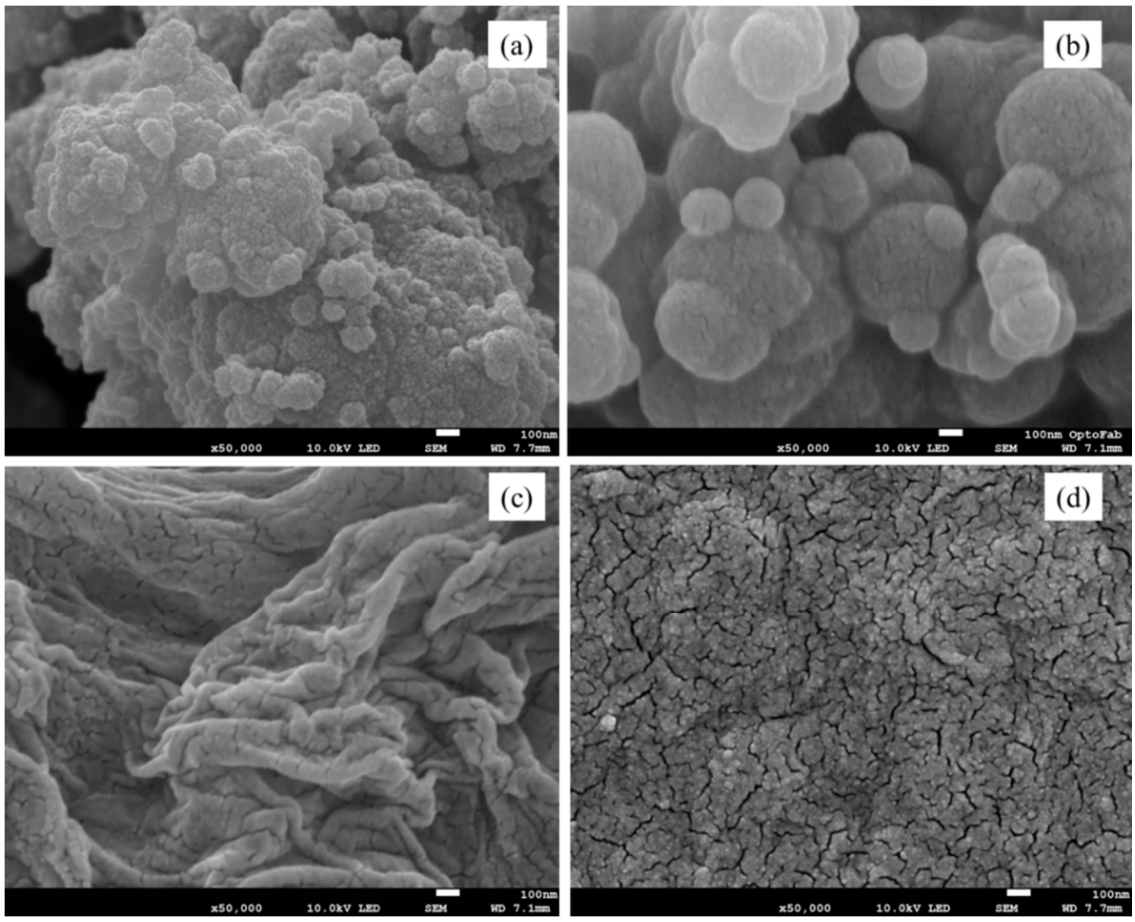

Figure 5.5 Scanning electron micrographs of (a) polypyrrole film in presence of KNO_3, and Acid Red 1 entrapped (b) polypyrrole, (c) polypyrrole-graphene oxide, and (d) polypyrrole-reduced graphene oxide composite films.

5.3.1.6 TGA

The thermal stability of polypyrrole and its composite films was studied by TGA. Figure 5.6 shows the TGA curves of graphene oxide, polypyrrole in the presence of KNO_3, Acid Red 1 entrapped polypyrrole, Acid Red 1 entrapped polypyrrole-graphene oxide and Acid Red 1 entrapped polypyrrole-reduced graphene oxide composite films, and the percentage of weight loss estimated from these TGA curves are tabulated in Table 5.2. In the TGA curves the weight loss of all samples at 100 °C was due to the removal of adsorbed water. As shown in Figure 5.6, graphene oxide exhibited a complete combustion at ~190 ºC, , which is comparable with the complete combustion of graphene oxide occur at around 150 ºC, due to the presence of large amount of oxygen containing groups as reported by Si *et al.* [27] and Lim *et al.* [48]. The polypyrrole and Acid Red 1 entrapped polypyrrole, polypyrrole-graphene oxide and polypyrrole-reduced graphene oxide films exhibited a dynamic mass loss in the temperature

range between 150 and 700 °C. The results in Figure 5.6 also show that polypyrrole is somewhat less thermally stable than the polypyrrole-composite films, with approximately 30% mass loss of polypyrrole occurred at 300 °C and then the weight decreased slowly up to 55% of the original weight at 700 °C. Above 300 °C, the polypyrrole-graphene oxide and polypyrrole-reduced graphene oxide films exhibited a weight loss trend similar to polypyrrole up to 700 °C. The initial weight loss between 100 and 250 °C for polypyrrole, polypyrrole-graphene oxide and polypyrrole-reduced graphene oxide films are probably due to the volatilization of oligomers and elimination of unreacted monomer, as well as the removal of the oxygen-containing functional groups. At higher temperatures, the protonic acid component of the polymer was then lost, and finally, at more extreme temperatures, cleavage of the polymer chain can lead to the production of volatile gases [49]. Approximately 57%, 56% and 57% of the weight remained for Acid Red 1 entrapped polypyrrole, polypyrrole-graphene oxide and polypyrrole-reduced graphene composite films at 700 °C, respectively (see Table 5.2). Despite the similar thermal degradation process, the major degradation in the composite films started at a higher temperature compared to polypyrrole. Thus, we have used these results to infer that the incorporation of graphene oxide in the polypyrrole matrix has enhanced the thermal stability of the polypyrrole composite films.

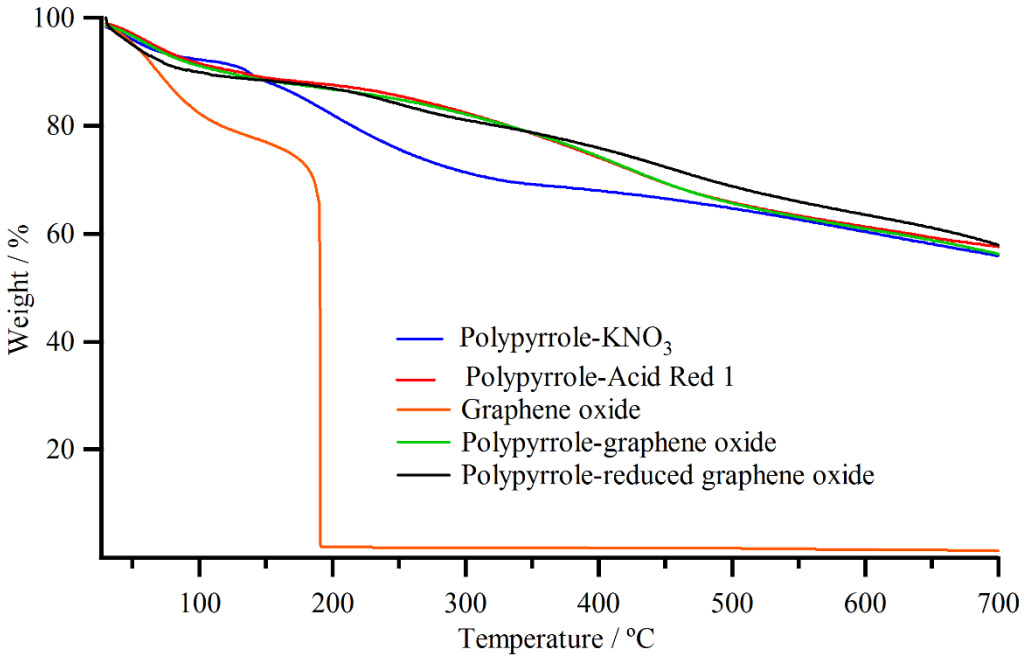

Figure 5.6 TGA of graphene oxide, polypyrrole in KNO_3, Acid Red 1 entrapped polypyrrole, polypyrrole-graphene oxide and polypyrrole-reduced graphene oxide composite films in a nitrogen atmosphere.

Table 5.2 TGA data of polypyrrole and polypyrrole composite films

Sample	Weight loss / % at temperature / °C							Weight retention /% at 700 °C
	100	200	300	400	500	600	700	
Polypyrrole-KNO_3	7.8	18.0	28.7	32.0	35.3	39.7	44.1	55.9
Polypyrrole-Acid Red 1	8.5	12.5	17.6	25.9	34.2	38.7	42.4	57.6
Graphene oxide	17.7	98.0	98.2	98.2	98.3	98.5	98.8	1.3
Polypyrrole-graphene oxide	8.9	13.3	17.9	25.7	34.4	39.1	43.8	56.2
Polypyrrole-reduced graphene oxide	10.1	13.1	18.9	24.2	31.2	36.5	42.1	57.9

5.3.1.7 BET Surface area analysis

In our work, BET surface area analysis was conducted in order to estimate the specific surface area of polypyrrole and its composite films. Figure 5.7(a) shows the nitrogen adsorption desorption plots (Volume adsorbed *versus* Relative pressure P/P_0) of (i) polypyrrole film in presence of KNO_3, (ii) Acid Red 1 entrapped polypyrrole, (iii) polypyrrole-graphene oxide and (iv) polypyrrole-reduced graphene oxide composite films at -196 ºC. The volume of gas adsorbed was observed to be greater for the Acid Red 1 entrapped polypyrrole-graphene oxide and polypyrrole-reduced graphene oxide composite films than the polypyrrole itself, suggesting a higher surface area or larger total pore volume. According to Equation (2.4) in Chapter 2, a plot of $1/[Q(P/P_0 - 1)]$ *versus* P/P_0 , which yields a straight line as shown in Figure 5.7(b) was obtained with a slope of $(C-1)/Q_mC$, and intercept, $1/Q_mC$. The value of Q_m can be estimated from the reciprocal of the sum of the slope and intercept. From the value of Q_m, the specific surface area, S_{BET}, can be evaluated using Equation (2.5) in Chapter. Using BET analysis, the specific surface area of polypyrrole (in the presence of KNO_3), and Acid Red 1 entrapped polypyrrole, polypyrrole-graphene oxide and polypyrrole-reduced graphene oxide composite films were estimated to be 4.72, 11.41, 21.33 and 34.73 $m^2 g^{-1}$, respectively. Our results are comparable to those observed by Bose *et al*.[50] and Chandra et al. [37], who found a high surface area for polypyrrole-graphene nanosheets and polypyrrole-reduced graphene oxide film, respectively, than polypyrrole itself. They suggested that the increased surface area is due to the incorporation of graphene oxide nanosheets with high surface area into the polypyrrole network. The increased surface area of the polypyrrole-composite films will thus increase the entrapment capacity of dye molecule in the polypyrrole-composite films.

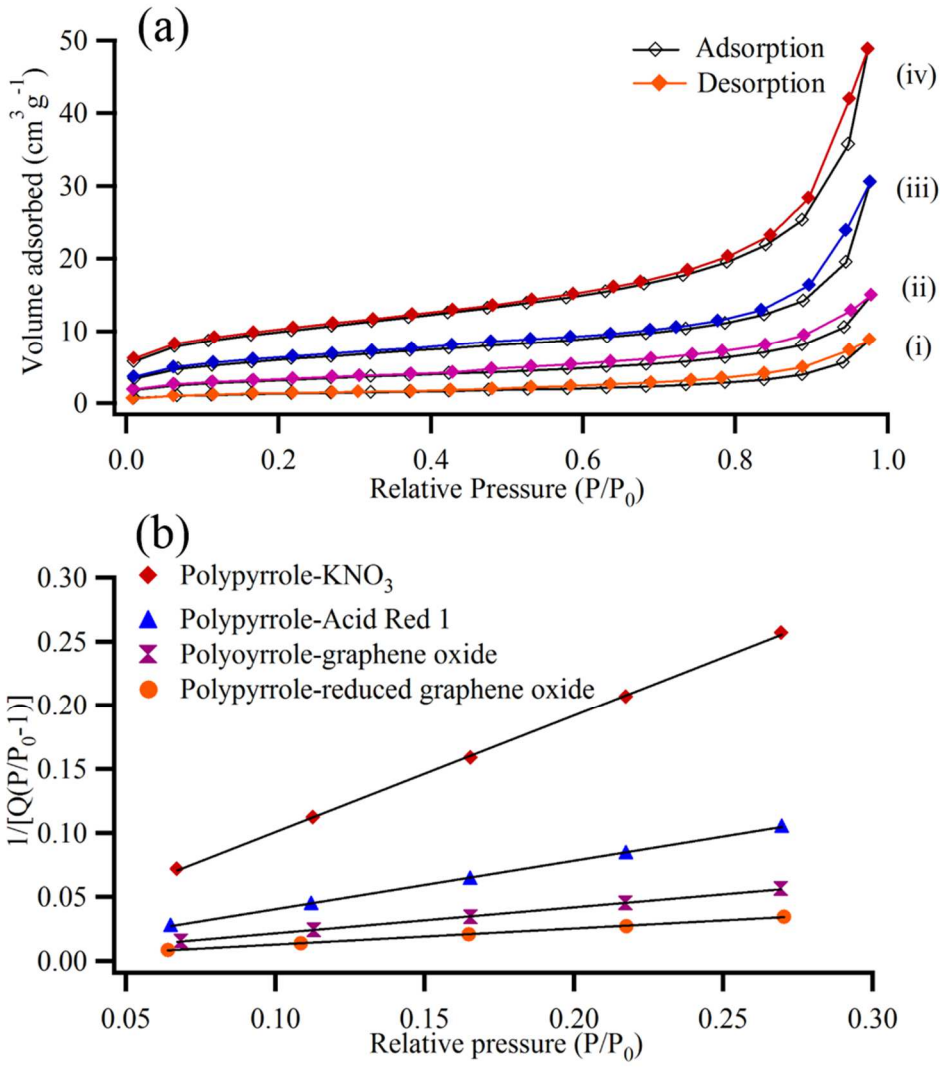

Figure 5.7 (a) Plots of the nitrogen adsorption desorption of (i) Polypyrrole in KNO_3, and Acid Red 1 entrapped (ii) polypyrrole, (iii) polypyrrole-graphene oxide and (iv) polypyrrole-reduced graphene oxide composite films at -196 °C. (b) BET surface area plot.

5.3.1.8 Mechanical properties of polypyrrole composite films

Mechanical stability of polypyrrole film is an important factor for consideration in repeated use of the film for Acid Red 1 entrapment and liberation process. Clearly, repeated use will aid in reducing the cost of treatment. The poor mechanical stability of polypyrrole films synthesised in the presence of Acid Red 1 is a major cause for the mechanical degradation of the polypyrrole films and weakening of the Acid Red 1 entrapment-liberation performance in repeated use of the film, as previously discussed in Section 3.3.6 in Chapter 3. To minimise polypyrrole film

degradation, we have prepared polypyrrole-graphene oxide and polypyrrole reduced graphene oxide films. In this work, we have evaluated the mechanical properties of NO_3^- entrapped polypyrrole films, Acid Red 1 entrapped polypyrrole films, Acid Red 1 entrapped polypyrrole-graphene oxide films and Acid Red 1 entrapped polypyrrole-reduced graphene oxide composite films by Instron 4302 tensile testing device according to ASTM D882-91. The results obtained are tabulated in Table 5.3. Polypyrrole-reduced graphene oxide film shows higher mechanical strength compared to NO_3^- entrapped polypyrrole film, Acid Red 1 entrapped polypyrrole and Acid Red 1 entrapped polypyrrole-graphene oxide film. The tensile strength of both polypyrrole-graphene oxide (14.5 MPa) and polypyrrole-reduced graphene oxide (15.2 MPa) composite films were found to be higher than those of polypyrrole alone (1.2 GPa) and Acid Red 1 entrapped polypyrrole film (1.5 GPa). The Young's modulus of polypyrrole-reduced graphene oxide film (7.5 GPa) was also found to be approximately 6 times higher than that of polypyrrole alone (1.1 GPa) and Acid Red 1 entrapped polypyrrole film (1.2 GPa). Zare *et al.* [51] reported that both the tensile strength and Young's modulus of polypyrrole graphene oxide were increased in comparison to the pure polypyrrole. The increase in the mechanical properties of polypyrrole-reduced graphene oxide is due to the superior mechanical strength and high aspect ratio of the graphene oxide sheets, the molecular-level dispersion of graphene sheets in the polypyrrole matrix, and the strong interfacial bonding between graphene oxide and polypyrrole [52], due to H-bonding and the π-π interaction between the graphene oxide layers and the aromatic polypyrrole rings [53].

5.3.1.9 Electrical properties of polypyrrole composite films

The average electrical conductivities of NO_3^- entrapped polypyrrole films and Acid Red 1^- entrapped polypyrrole, polypyrrole-graphene oxide and polypyrrole-reduced graphene oxide composite films are tabulated in Table 5.3. The NO_3^- entrapped polypyrrole film shows a relatively low conductivity of 8 S cm^{-1}, which lies between 12.3 S cm^{-1} reported by Si *et al.* [27] and 1.8 S cm^{-1} reported by Konwer *et al.* [15] for SO_4^{2-} entrapped and ClO_4^- entrapped polypyrrole films, respectively. The electrical conductivity of all polypyrrole composite films was found be increased dramatically in comparison to the polypyrrole film. For example, the average conductivity of Acid Red 1 entrapped polypyrrole, polypyrrole-graphene oxide and polypyrrole-reduced graphene oxide composite films was 16, 102 and 127 S cm^{-1}, respectively. Notably, a ratio of 20:1 (5% w/w) between pyrrole and graphene oxide was used in this experiment to obtain sufficiently highly conductive films that could be also easily removed

from the electrode. In this work, a conductivity of (~42 S cm^{-1}) was measured using films synthesised based on a 40:1 ratio (2.5% w/w). However, thick and fragile films were obtained using a ratio higher than 5% w/w and it was difficult to remove these films from the electrode. The increased conductivity of polypyrrole-graphene oxide was also observed as reported by Si *et al.* [27] and Konwer *et al.* [15]. Such enhancement of the conductivity of the composite films might be attributed to extended H-bonding between the polypyrrole and graphene oxide or Acid Red 1 that allows the π-π stacking between the graphene oxide layers and polypyrrole in the polymer chains for which the electron mobility inside the composite system increases [15, 21].

Table 5.3 Comparative study of mechanical and electrical property of polypyrrole composites. All uncertainties represent standard deviations of the measurements (N=5).

Materials	Tensile strength / MPa	Young's modulus / GPa	Conductivity / S cm^{-1}
Polypyrrole-KNO_3	1.2±0.2	1.1±0.4	8±0.2
Polypyrrole-Acid Red 1	1.5±0.3	1.2±0.2	16±0.5
Polypyrrole-graphene oxide	14.5±0.5	6.8±0.4	102±1.6
Polypyrrole-reduced graphene oxide	15.2±0.5	7.5±0.3	127±0.8

5.3.2 Evaluation of Acid Red 1 entrapment in polypyrrole and composite films

The polypyrrole, polypyrrole-graphene oxide and polypyrrole-reduced graphene oxide composite films characterised above were applied to the study of Acid Red 1 entrapment. In the study of the entrapment efficiency and stability of Acid Red 1 entrapped polypyrrole-graphene oxide and polypyrrole-reduced graphene oxide composite films, seven consecutive entrapment cycles for Acid Red 1 was performed at the same film after liberating Acid Red 1 by electrochemical reduction of the film. The results obtained were compared in terms of the entrapment efficiency of Acid Red in polypyrrole film. Figure 5.8 shows the Acid Red 1 entrapment percentage in polypyrrole, polypyrrole-graphene oxide and polypyrrole-reduced graphene oxide films for seven entrapment cycles. The maximum entrapment percentage of Acid Red 1 in polypyrrole-graphene oxide and polypyrrole-reduced graphene oxide was significantly higher than the polypyrrole film in all entrapment cycles. This can be explained by the large surface area in both the polypyrrole-graphene oxide and polypyrrole reduced graphene oxide films for Acid Red 1 entrapment than the polypyrrole film, as supported by the

BET surface area analysis results presented in Section 5.3.1.7. However, Acid Red 1 entrapment in polypyrrole-reduced graphene oxide is 13% higher than that in polypyrrole-graphene oxide. There may be steric hindering between negatively charged Acid Red 1 and negatively charged functional groups (such as -OH, -O-, -COOH) of graphene oxide in a polypyrrole-graphene oxide film. During the reduction of polypyrrole-graphene oxide to polypyrrole-reduced graphene oxide, many of the negative functional groups of graphene oxide were reduced and this would favour the entrapment of Acid Red 1 in the polypyrrole-reduced graphene oxide film.

Additionally, in Figure 5.8, the maximum entrapment percentage of Acid Red 1 in polypyrrole, polypyrrole-graphene oxide and polypyrrole-reduced graphene oxide films was estimated to be 56%, 82% and 95%, respectively. However, a lower entrapment percentage was obtained in all consecutive entrapment cycles. This decrease of the entrapment capacity may be attributed to the incomplete liberation of entrapped Acid Red 1 from the films, as, some dye molecules were firmly attached to the polymer network chain. Also, the degradation of polypyrrole during the oxidation- reduction cycles would reduce the Acid Red 1 re-entrapment in polypyrrole films with consecutive entrapment cycles. However, we observed in this work that, the mechanical strength of Acid Red 1 entrapped polypyrrole films was subsequently lowered after three repeated entrapment experiments, rendering the film not suitable for further entrapment-liberation experiment. On the other hand, polypyrrole-graphene oxide and polypyrrole-reduced graphene oxide films were observed to have significantly retained the Acid Red 1 entrapment capacity, 39% and 63%, respectively, even after five repeated entrapments (see Figure 5.8), indicating that the composite films exhibit excellent entrapment capacity and strong mechanical stability during oxidation-reduction cycle before the result decreased dramatically to 9% and 17%, respectively, after the seventh entrapment cycle. These results demonstrated that, under the laboratory conditions the polypyrrole-reduced graphene oxide films were capable of repeated good entrapment for up to 5 repetitions, which will reduce the cost of dye containing wastewater treatment process.

5.3.3 Liberation of Acid Red 1 from polypyrrole and composite films

UV-visible spectrophotometry was used to evaluate the liberation efficiency of Acid Red 1 in 0.5 mol L^{-1} NaOH after applying a reduction potential of -0.80 V for 300 min at Acid Red 1 entrapped polypyrrole films. This study was conducted using polypyrrole and its graphene oxide composites films synthesised in the presence of 1500 mg L^{-1} Acid Red 1. The results

obtained are shown in Figure 5.9. In this experiment, following a liberation duration of 300 min, a maximum Acid Red 1 liberation of 36%, 65% and 73% was estimated from polypyrrole, polypyrrole-graphene oxide and polypyrrole-reduced graphene oxide films, respectively. The enhanced liberation efficiency of polypyrrole-graphene oxide and polypyrrole reduced graphene oxide films was most likely due to the high surface area and mechanical stability of the films than the corresponding polypyrrole film.

In general, the liberation percentage of Acid Red 1 decreases in each subsequent liberation cycle for all film types. This is most likely because some dye molecules are firmly attached to the polymer chain network after each entrapment cycle and the dye molecule cannot escape from the film, as confirmed by XRD analysis reported in Section 3.3.1.8, resulting in low liberation efficiency. Moreover, the degradation of polypyrrole films caused by swelling and shrinkage of the film during their reuse (oxidation-reduction cycle), would reduce the Acid Red 1 re-entrapment in the polypyrrole film with consecutive entrapment cycle [13-15]. However, the maximum liberation efficiency was observed to dramatically decreased for polypyrrole during its repeated, due to its low surface area and weak mechanical stability during entrapment-liberation cycle and no more dye liberated after 3rd cycle. On the other hand, the polypyrrole-reduced graphene oxide composite film shows quite high liberation efficiency up to 4th liberation cycle (42%) compared to both polypyrrole and polypyrrole-graphene oxide composite film.

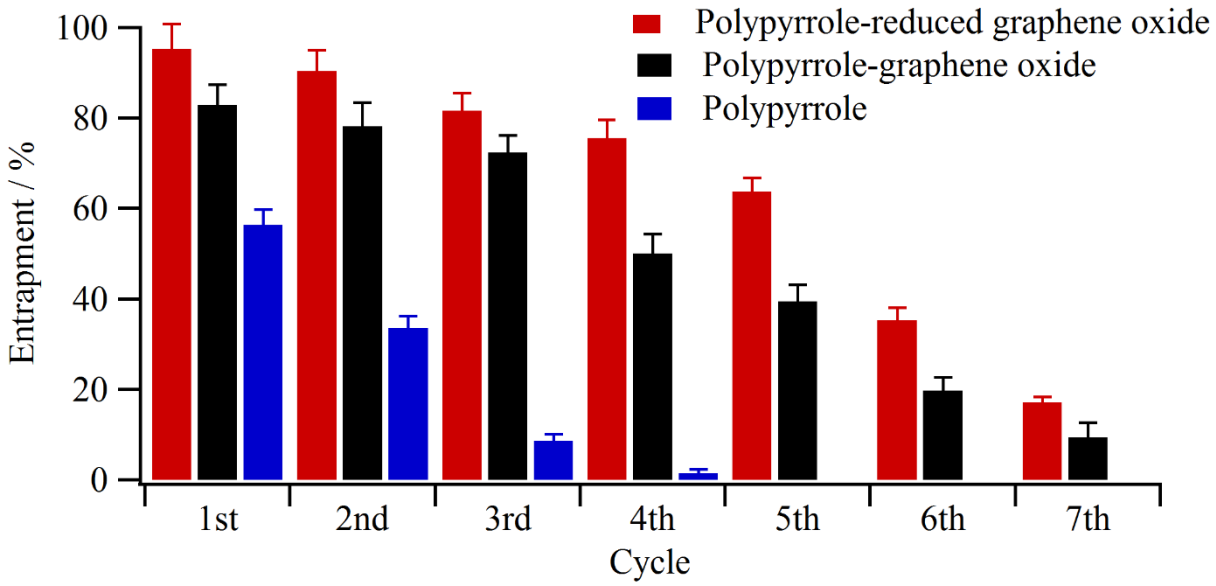

Figure 5.8 Entrapment percentage of Acid Red in polypyrrole, polypyrrole-graphene oxide and polypyrrole-reduced graphene oxide films

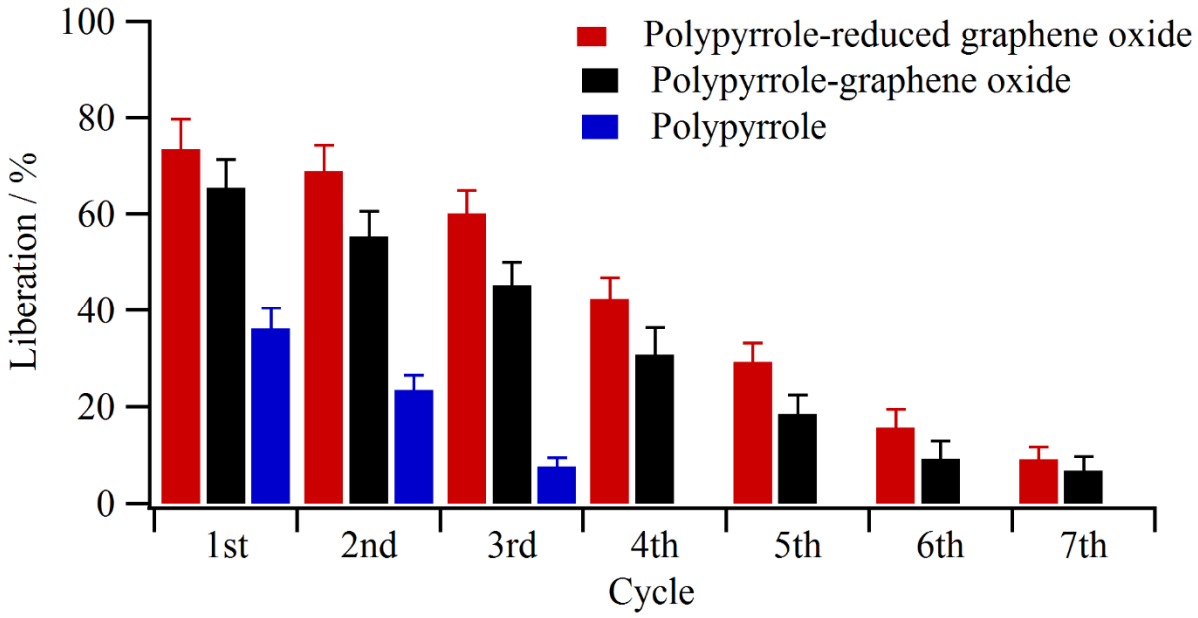

Figure 5.9 Acid Red 1 liberation efficiency of polypyrrole, polypyrrole-graphene oxide and polypyrrole-reduced graphene oxide films.

5.3.4 A preliminary study of Acid Red 1 entrapment in polypyrrole-reduced graphene oxide films in the presence of Indigo Carmine

This work has hitherto been focussed on the entrapment of a single dye of Acid Red 1 in a polypyrrole-reduced graphene oxide film. Clearly, real-life textile effluents are likely to be made up of a mixture of many dyes. Therefore, we have also devoted part of this work to the preliminary investigation of Acid Red 1 entrapment in a polypyrrole-reduced graphene oxide film in a dye mixture. However, to minimise the possible degree of complexity, we have limited this study to the entrapment of Acid Red 1 in the presence of a second azo dye, Indigo Carmine.

In this experiment, we have initially synthesised a polypyrrole-graphene oxide film in the presence of 1500 mg L^{-1} Acid Red 1 for a duration of 480 min as described in Section 2.5.2. After applying -1.3 V for 240 min to liberate Acid Red 1 and to reduce graphene oxide, an oxidation potential of 1.0 V was applied to the same film placed in a solution containing 1500 mg L^{-1} Acid Red 1 and 1500 mg L^{-1} Indigo Carmine to begin a re-entrapment experiment for a duration of 480 min. The entrapment percentages of both Acid Red 1 and Indigo Carmine estimated spectrophotometrically are presented in Figure 5.10.

In Figure 5.10, the respective entrapment of Acid Red 1 and Indigo Carmine was observed to increase with time. However, while there was an approximate maximum of 80% of

Acid Red 1 being entrapped, only 10% of Indigo Carmine was entrapped after 480 min. This difference in entrapment percentage may be rationalised by the selectivity of the polypyrrole-reduced graphene oxide film for Acid Red 1, which was originally synthesised in the presence of Acid Red 1 as a counter ion, and also by the different structure of the Acid Red 1 and Indigo Carmine molecules. During the polymerisation of pyrrole in the presence of Acid Red 1, channels were opened up within the polypyrrole film to allow the Acid Red 1 molecules to be incorporated into the film and to counter balance the positive charges present in the polypyrrole backbone. After applying the reduction potential of -1.3 V, Acid Red 1 was liberated from the film, leaving specific channels in the film that only fit Acid Red 1. As a result, when the film was placed in a solution of Acid Red 1 and Indigo Carmine, mainly Acid Red 1 was entrapped in the film. In addition, as shown in Figure 5.11, Indigo Carmine is a longitudinally larger molecule than Acid Red 1 molecule and is therefore not expected to fit into the channels but only non-specifically adsorb at the surface of the polypyrrole film. Notably, a similar degree of selectivity was reported by Beelen *et al.* [54], who investigated the electrochemical behaviour of polypyrrole films synthesised in the presence of small counter ions including NO_3^-, ClO_4^-, Cl^-, Br^-, F^- and toluene sulfonate. They observed that the polypyrrole films have high affinity for the specific anion that was initially doped during electropolymerisation of pyrrole.

The above explanation of selective entrapment of Acid Red 1 in polypyrrole-reduced graphene oxide film was further supported by XRD results. Figure 5.12 shows the XRD spectra of (a) polypyrrole in presence of KNO_3, (b) Indigo Carmine entrapped polypyrrole-reduced graphene oxide and (c) Acid Red 1 entrapped polypyrrole-reduced graphene oxide films. Based on a regular structure, the *d*-spacing between polypyrrole chains can be estimated from the Bragg's Law (details were described in Section 3.3.1.8 in Chapter 3). In Figure 5.12, a featureless spectrum, shown in trace a, was obtained with a NO_3^--entrapped polypyrrole film, but a sharp peak at $2\theta = 5.8°$ was clearly observable in the spectrum obtained at an Indigo carmine-entrapped polypyrrole-reduced graphene oxide film (trace b) and a peak at $2\theta = 8.7°$ (trace c) in the corresponding spectrum obtained at an Acid Red 1-entrapped-reduced graphene oxide film. The result at the Indigo Carmine-entrapped polypyrrole-reduced graphene oxide film was similar to that reported by Girotto *et al.* [55], who observed a signal at $2\theta = 5.8°$ for Indigo Carmine in the XRD spectra of electropolymerised polypyrrole-Indigo Carmine film. As shown in Section 3.3.1.8 in Chapter 3, by applying Bragg's Law, *d*-spacing of 10.2 Å and 15.3

Å were obtained for Acid Red 1 entrapped polypyrrole-graphene oxide and Indigo Carmine entrapped polypyrrole-graphene oxide films, respectively. These results are in good agreement with simulated results presented in Figure 5.11, estimated by a Chem 3D Plus calculation based on the MM2 (version 13.0.2.3021, Ultra ChemBio3D).

The above unique effects observed during the electrochemical oxidation-reduction of conducting polymers make their applications possible in the field of memory devices [56, 57]. During the electropolymerisation of pyrrole, the counter anions from the electrolyte solutions are incorporated in the polymeric film. This incorporation of the counter anions strongly modifies the electrochemical activity of the polymeric materials by inducing pores formation [54]. In other words, the size of the anion controls the microstructure and porosity of the polypyrrole film [58].

A possible mechanism of the memory effect of polypyrrole films involves the rearrangement of the chain configuration, which follows the incorporation and extraction of the counter ions upon oxidation and reduction. Just after discharging, opened channels are left by the counter ions in the polymeric network [57]. The dimension of these channels are dependent on the size and shape of the counter ions incorporated [54].

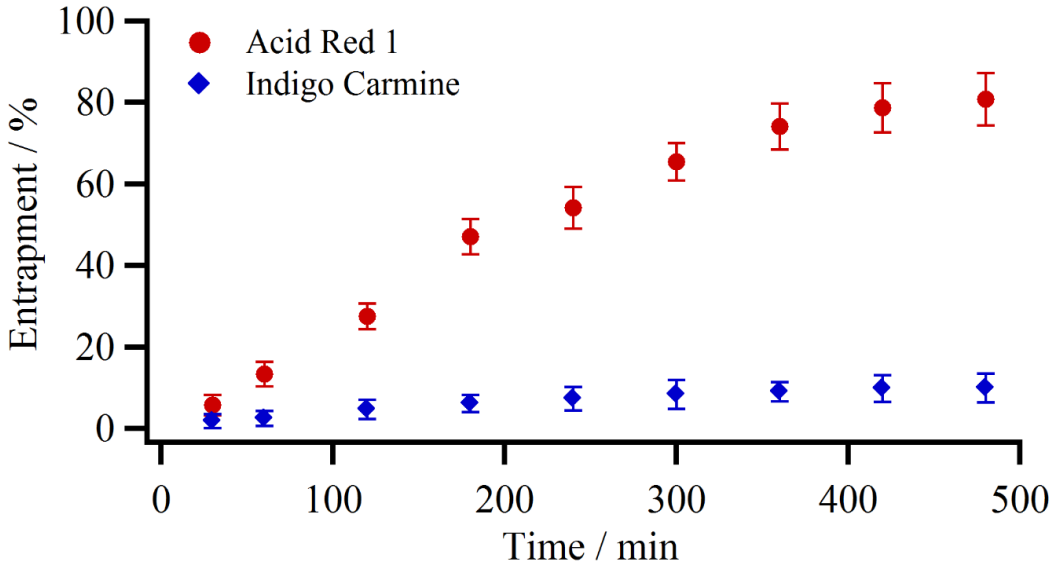

Figure 5 10 Re-entrapment of Acid Red 1 from a mixture of 1500 mg L^{-1} Acid Red 1 and 1500 mg L^{-1} Indigo Carmine solution at an Acid Red 1 liberated polypyrrole-reduced graphene oxide film

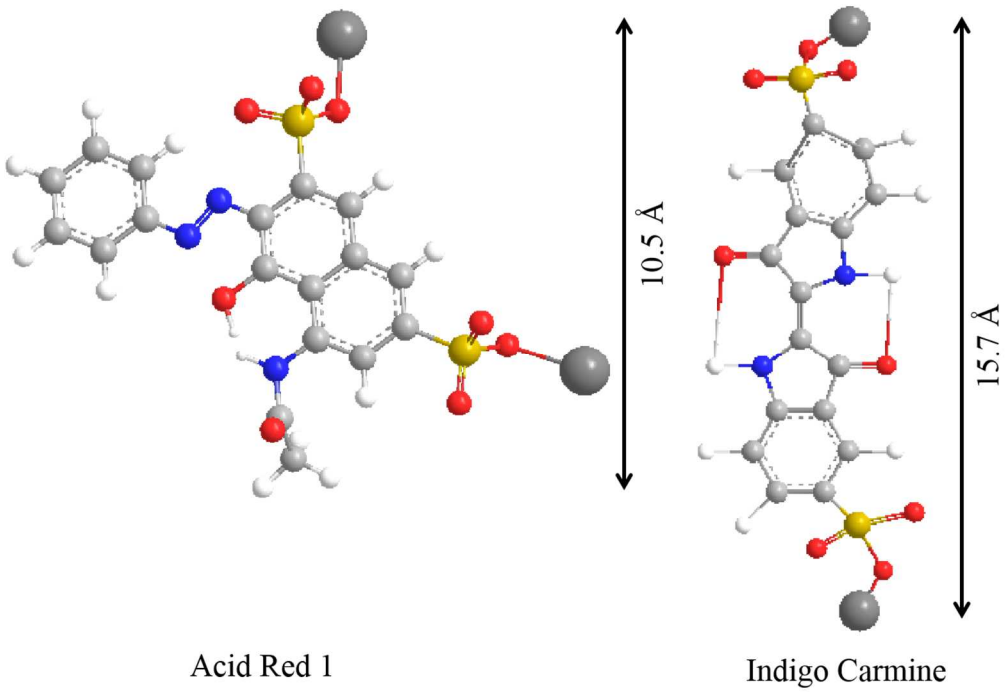

Figure 5.11 Molecular dimensions of Acid Red 1 and Indigo Carmine estimated by a Chem 3D Plus calculation based on the MM2 (version 13.0.2.3021, Ultra ChemBio3D)

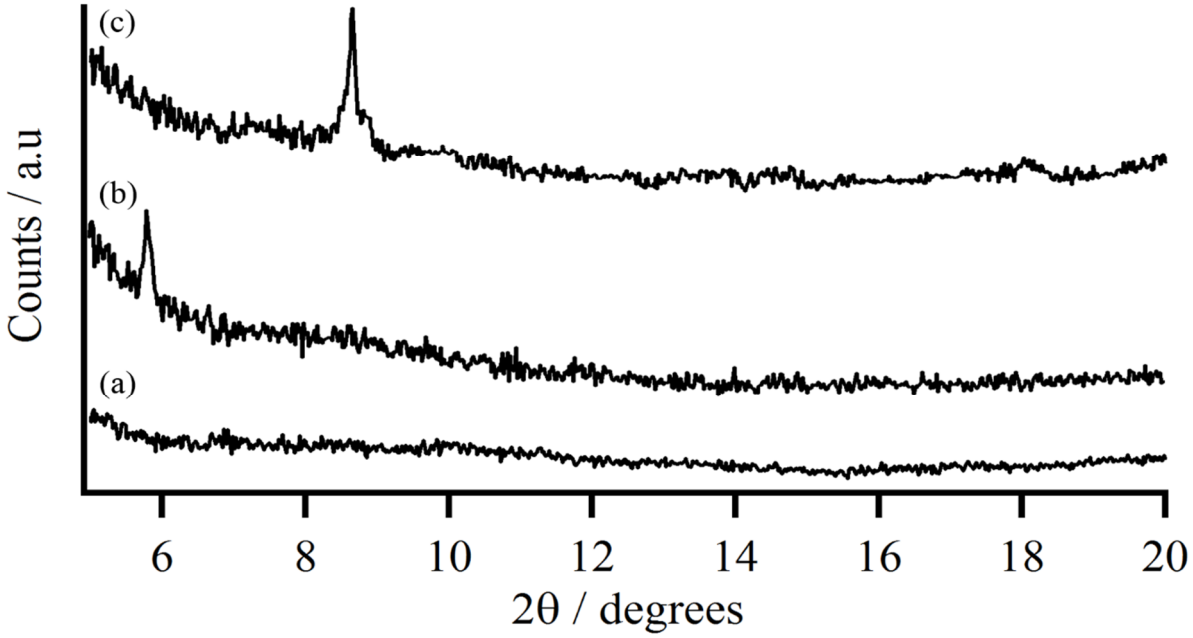

Figure 5.12 XRD spectra of (a) polypyrrole in the presence of KNO_3, (b) Indigo Carmine entrapped polypyrrole-reduced graphene oxide and (c) Acid Red 1 entrapped polypyrrole-reduced graphene oxide films.

5.4 Conclusion

In this chapter, we reported the synthesis, characterisation and evaluation of Acid Red 1 entrapment and liberation at mechanically stable polypyrrole-graphene oxide and polypyrrole-reduced graphene oxide composite films. Initially, we anodically synthesised polypyrrole-graphene oxide film by an *in situ* electropolymerisation of pyrrole and graphene oxide. A reduction potential was then applied to obtain a polypyrrole-reduced graphene oxide film from a polypyrrole-graphene oxide composite film. The synthesised composite films were then characterised by FTIR, XRD, XPS surface analysis, TGA and SEM. Brunauer, Emmett and Teller surface area analysis showed a 7.4-fold increase in surface area of a polypyrrole-reduced-graphene oxide film compared to that of a polypyrrole film. Also, mechanical testing results revealed that the tensile strength of polypyrrole-reduced graphene oxide films was enhanced by 12.7 folds compared to that of NO_3^- entrapped polypyrrole film. The conductivity of polypyrrole-reduced graphene oxide increased 15.9 folds than the corresponding NO_3^- entrapped polypyrrole film. We evaluated the entrapment-liberation efficiency of Acid Red 1 entrapped polypyrrole composite films and estimated that the entrapment percentage of Acid Red 1 in polypyrrole-reduced graphene oxide films was 95%, which is significantly higher than 58% in polypyrrole films. Similarly, the liberation efficiency for polypyrrole-graphene oxide was found to be higher (73%) than both polypyrrole-reduced graphene oxide (65%) and polypyrrole (36%) films. Finally, a preliminary study of Acid Red 1 entrapment in polypyrrole-reduced graphene oxide films in the presence of Indigo Carmine was also conducted to evaluate the selectivity towards Acid Red 1 of polypyrrole-reduced graphene oxide film. We observed that electropolymerised polypyrrole-reduced graphene oxide film showed excellent memory effect for selective entrapment of Acid Red 1.

5.5 References

1. Ayad, M.M. and El-Nasr, A.A. Adsorption of cationic dye (Methylene Blue) from water using polyaniline nanotubes base. *The Journal of Physical Chemistry C*, 2010. **114**(34): 14377-14383.
2. Wong, Y.C., Szeto, Y.S., Cheung, W.H. and McKay, G. Equilibrium studies for acid dye adsorption onto chitosan. *Langmuir*, 2003. **19**(19): 7888-7894.
3. Carmen, Z. and Daniela, S. Textile organic dyes–characteristics, polluting effects and separation/elimination procedures from industrial effluents–a critical overview. In

Organic pollutants ten years after the stockholm convention-environmental and analytical update. Puzyn, D.T., ed.2012, Intech: Croatia. p. 55-86.

4. Seshadri, S., Bishop, P.L. and Agha, A.M. Anaerobic/aerobic treatment of selected azo dyes in wastewater. *Waste Management*, 1994. **14**(2): 127-137.

5. Gong, R., Sun, Y., Chen, J., Liu, H. and Yang, C. Effect of chemical modification on dye adsorption capacity of peanut hull. *Dyes and Pigments*, 2005. **67**(3): 175-181.

6. Hameed, B.H. Removal of cationic dye from aqueous solution using jackfruit peel as non-conventional low-cost adsorbent. *Journal of Hazardous Materials*, 2009. **162**(1): 344-350.

7. Lin, R.-Y., Chen, B.-S., Chen, G.-L., Wu, J.-Y., Chiu, H.-C. and Suen, S.-Y. Preparation of porous PMMA/Na^+–montmorillonite cation-exchange membranes for cationic dye adsorption. *Journal of Membrane Science*, 2009. **326**(1): 117-129.

8. Bayramoğlu, G. and Arica, M.Y. Kinetics of mercury ions removal from synthetic aqueous solutions using by novel magnetic p(GMA-MMA-EGeDMA) beads. *Journal of Hazardous Materials*, 2007. **144**(1–2): 449-457.

9. Namasivayam, C. and Kavitha, D. Removal of congo red from water by adsorption onto activated carbon prepared from coir pith, an agricultural solid waste. *Dyes and Pigments*, 2002. **54**(1): 47-58.

10. Al-Bastaki, N. Removal of Methyl Orange dye and Na_2SO_4 salt from synthetic waste water using reverse osmosis. *Chemical Engineering and Processing: Process Intensification*, 2004. **43**(12): 1561-1567.

11. Golob, V., Vinder, A. and Simonič, M. Efficiency of the coagulation/flocculation method for the treatment of dyebath effluents. *Dyes and Pigments*, 2005. **67**(2): 93-97.

12. Haque, M.M., Smith, W.T. and Wong, D.K.Y. Conducting polypyrrole films as a potential tool for electrochemical treatment of azo dyes in textile wastewaters. *Journal of Hazardous Materials*, 2015. **283**(0): 164-170.

13. Fan, L.Z., Hu, Y.S., Maier, J., Adelhelm, P., Smarsly, B. and Antonietti, M. High electroactivity of polyaniline in supercapacitors by using a hierarchically porous carbon monolith as a support. *Advanced Functional Materials*, 2007. **17**(16): 3083-3087.

14. Li, L., Song, H., Zhang, Q., Yao, J. and Chen, X. Effect of compounding process on the structure and electrochemical properties of ordered mesoporous carbon/polyaniline composites as electrodes for supercapacitors. *Journal of Power Sources*, 2009. **187**(1): 268-274.

15. Konwer, S., Boruah, R. and Dolui, S. Studies on conducting polypyrrole/graphene oxide composites as supercapacitor electrode. *Journal of Electronic Materials*, 2011. **40**(11): 2248-2255.

16. Frackowiak, E., Khomenko, V., Jurewicz, K., Lota, K. and Beguin, F. Supercapacitors based on conducting polymers/nanotubes composites. *Journal of Power Sources*, 2006. **153**(2): 413-418.

17. Geim, A.K. and Novoselov, K.S. The rise of graphene. *Nature Materials*, 2007. **6**(3): 183-191.

18. Lee, C., Wei, X., Kysar, J.W. and Hone, J. Measurement of the elastic properties and intrinsic strength of monolayer graphene. *Science*, 2008. **321**(5887): 385-388.

19. Zhang, L. and Shi, G. Preparation of highly conductive graphene hydrogels for fabricating supercapacitors with high rate capability. *The Journal of Physical Chemistry C*, 2011. **115**(34): 17206-17212.

20. Stankovich, S., Dikin, D.A., Piner, R.D., Kohlhaas, K.A., Kleinhammes, A., Jia, Y., Wu, Y., Nguyen, S.T. and Ruoff, R.S. Synthesis of graphene-based nanosheets via chemical reduction of exfoliated graphite oxide. *Carbon*, 2007. **45**(7): 1558-1565.

21. Bora, C. and Dolui, S. Fabrication of polypyrrole/graphene oxide nanocomposites by liquid/liquid interfacial polymerization and evaluation of their optical, electrical and electrochemical properties. *Polymer*, 2012. **53**(4): 923-932.

22. Stankovich, S., Dikin, D.A., Dommett, G.H.B., Kohlhaas, K.M., Zimney, E.J., Stach, E.A., Piner, R.D., Nguyen, S.T. and Ruoff, R.S. Graphene-based composite materials. *Nature*, 2006. **442**(7100): 282-286.

23. Rudge, A., Davey, J., Raistrick, I., Gottesfeld, S. and Ferraris, J.P. Conducting polymers as active materials in electrochemical capacitors. *Journal of Power Sources*, 1994. **47**(1–2): 89-107.

24. Liu, A., Li, C., Bai, H. and Shi, G. Electrochemical deposition of polypyrrole/sulfonated graphene composite films. *The Journal of Physical Chemistry C*, 2010. **114**(51): 22783-22789.

25. Zhang, S., Shao, Y., Liu, J., Aksay, I.A. and Lin, Y. Graphene–polypyrrole nanocomposite as a highly efficient and low cost electrically switched ion exchanger for removing ClO_4^- from wastewater. *ACS Applied Materials & Interfaces*, 2011. **3**(9): 3633-3637.

26. Liu, J., Wang, Z., Xie, X., Cheng, H., Zhao, Y. and Qu, L. A rationally-designed synergetic polypyrrole/graphene bilayer actuator. *Journal of Materials Chemistry*, 2012. **22**(9): 4015-4020.

27. Si, P., Ding, S., Lou, X.-W. and Kim, D.-H. An electrochemically formed three-dimensional structure of polypyrrole/graphene nanoplatelets for high-performance supercapacitors. *RSC Advances*, 2011. **1**(7): 1271-1278.

28. Chang, H.-H., Chang, C.-K., Tsai, Y.-C. and Liao, C.-S. Electrochemically synthesized graphene/polypyrrole composites and their use in supercapacitor. *Carbon*, 2012. **50**(6): 2331-2336.

29. Feng, X., Li, R., Yan, Z., Liu, X., Chen, R., Ma, Y., Li, X.a., Fan, Q. and Huang, W. Preparation of graphene/polypyrrole composite film via electrodeposition for supercapacitors. *Nanotechnology, IEEE Transactions on*, 2012. **11**(6): 1080-1086.

30. Matsuo, Y., Tahara, K. and Sugie, Y. Structure and thermal properties of poly(ethylene oxide)-intercalated graphite oxide. *Carbon*, 1997. **35**(1): 113-120.

31. Liu, P., Gong, K., Xiao, P. and Xiao, M. Preparation and characterization of poly(vinyl acetate)-intercalated graphite oxide nanocomposite. *Journal of Materials Chemistry*, 2000. **10**(4): 933-935.

32. Kotov, N.A., Dékány, I. and Fendler, J.H. Ultrathin graphite oxide–polyelectrolyte composites prepared by self-assembly: Transition between conductive and non-conductive states. *Advanced Materials*, 1996. **8**(8): 637-641.

33. Cassagneau, T. and Fendler, J.H. High density rechargeable lithium-ion batteries self-assembled from graphite oxide nanoplatelets and polyelectrolytes. *Advanced Materials*, 1998. **10**(11): 877-881.

34. Zhang, L.L., Zhao, S., Tian, X.N. and Zhao, X. Layered graphene oxide nanostructures with sandwiched conducting polymers as supercapacitor electrodes. *Langmuir*, 2010. **26**(22): 17624-17628.

35. Zhang, K., Zhang, L.L., Zhao, X.S. and Wu, J. Graphene/polyaniline nanofiber composites as supercapacitor electrodes. *Chemistry of Materials*, 2010. **22**(4): 1392-1401.

36. Li, S., Lu, X., Xue, Y., Lei, J., Zheng, T. and Wang, C. Fabrication of polypyrrole/graphene oxide composite nanosheets and their applications for Cr (VI) removal in aqueous solution. 2012.

37. Chandra, V. and Kim, K.S. Highly selective adsorption of Hg^{2+} by a polypyrrole-reduced graphene oxide composite. *Chemical Communications*, 2011. **47**(13): 3942-3944.

38. Hummers Jr, W.S. and Offeman, R.E. Preparation of graphitic oxide. *Journal of the American Chemical Society*, 1958. **80**(6): 1339-1339.

39. Witkowski, A., Freund, M.S. and Brajter-Toth, A. Effect of electrode substrate on the morphology and selectivity of overoxidized polypyrrole films. *Analytical Chemistry*, 1991. **63**(6): 622-626.

40. Schlenoff, J.B. and Xu, H. Evolution of physical and electrochemical properties of polypyrrole during extended oxidation. *Journal of the Electrochemical Society*, 1992. **139**(9): 2397-2401.

41. Beck, F., Braun, P. and Oberst, M. Organic electrochemistry in the solid state-overoxidation of polypyrrole. *Berichte Der Bunsen-Gesellschaft-Physical Chemistry Chemical Physics*, 1987. **91**(9): 967-974.

42. Guo, H.-L., Wang, X.-F., Qian, Q.-Y., Wang, F.-B. and Xia, X.-H. A green approach to the synthesis of graphene nanosheets. *ACS Nano*, 2009. **3**(9): 2653-2659.

43. Zhang, G., Yang, F., Gao, M., Fang, X. and Liu, L. Electro-Fenton degradation of azo dye using polypyrrole/anthraquinonedisulphonate composite film modified graphite cathode in acidic aqueous solutions. *Electrochimica Acta*, 2008. **53**(16): 5155-5161.

44. Zhang, D., Luo, L., Liao, Q., Wang, H., Fu, H. and Yao, J. Polypyrrole/ZnS core/shell coaxial nanowires prepared by anodic aluminum oxide template methods. *The Journal of Physical Chemistry C*, 2011. **115**(5): 2360-2365.

45. Xiaomiao, F., Ruimei, L., Zhenzhen, Y., Xingfen, L., Runfeng, C., Yanwen, M., Xing'ao, L., Quli, F. and Wei, H. Preparation of graphene/polypyrrole composite film via electrodeposition for supercapacitors. *Nanotechnology, IEEE Transactions on*, 2012. **11**(6): 1080-1086.

46. Liu, A.S., Bezerra, M.C. and Cho, L.Y. Electrodeposition of polypyrrole films on aluminum surfaces from a *p*-toluene sulfonic acid medium. *Materials Research*, 2009. **12**(4): 503-507.

47. Yang, Y., Wang, C., Yue, B., Gambhir, S., Too, C.O. and Wallace, G.G. Electrochemically synthesized polypyrrole/graphene composite film for lithium batteries. *Advanced Energy Materials*, 2012. **2**(2): 266-272.

48. Lim, Y., Tan, Y.P., Lim, H.N., Tan, W.T., Mahnaz, M., Talib, Z.A., Huang, N.M., Kassim, A. and Yarmo, M.A. Polypyrrole/graphene composite films synthesized via potentiostatic deposition. *Journal of Applied Polymer Science*, 2013. **128**(1): 224-229.

49. Basavaraja, C., Kim, N.R., Jo, E.A., Pierson, R., Huh, D.S. and Venkataraman, A. Transport properties of polypyrrole films doped with sulphonic acids. *Bulletin of the Korean Chemical Society*, 2009. **30**(11): 2701-2706.

50. Bose, S., Kim, N.H., Kuila, T., Lau, K.-t. and Lee, J.H. Electrochemical performance of a graphene–polypyrrole nanocomposite as a supercapacitor electrode. *Nanotechnology*, 2011. **22**(29): 295202.

51. Zare, M., Sharif, M. and Kashkooli, A. Study on the effect of polypyrrole and polypyrrole/graphene oxide nanoparticles on the microstructure, electrical and tensile properties of polypropylene nanocomposites. *Polymer-Plastics Technology and Engineering*, 2014. **53**(13): 1392-1401.

52. Kuilla, T., Bhadra, S., Yao, D., Kim, N.H., Bose, S. and Lee, J.H. Recent advances in graphene based polymer composites. *Progress in Polymer Science*, 2010. **35**(11): 1350-1375.

53. Bissessur, R., Liu, P.K.Y. and Scully, S.F. Intercalation of polypyrrole into graphite oxide. *Synthetic Metals*, 2006. **156**(16–17): 1023-1027.

54. Beelen, E., Riga, J. and Verbist, J.J. Electrochemical doping of polypyrrole: XPS study. *Synthetic Metals*, 1991. **41**(1–2): 449-454

55. Girotto, E.M., Gazotti, W.A., Tormena, C.F. and De Paoli, M.A. Photoelectronic and transport properties of polypyrrole doped with a dianionic dye. *Electrochimica Acta*, 2002. **47**(9): 1351-1357

56. Yamaura, M., Sato, K., Hagiwara, T. and Iwata, K. Memory effect of electrical conductivity upon the counteranion exchange of polypyrrole films. *Synthetic Metals*, 1992. **48**(3): 337-354.

57. Villeret, B. and Nechtschein, M. Memory effects in conducting polymers. *Physical review letters*, 1989. **63**(12): 1285.

58. Dong, S., Sun, Z. and Lu, Z. A new kind of chemical sensor based on a conducting polymer film. *Journal of the Chemical Society, Chemical Communications*, 1988. **1988**(15): 993-995.

CHAPTER 6

CONCLUSION

6.1 Concluding remarks

Industrial wastewater pollution is an ever growing global environmental problem, which needs to be promptly and effectively addressed. Hence, appropriate treatment processes must be recommended to treat polluted effluents, especially dye containing effluents.

Dye containing effluents have been shown to cause detrimental effects upon the overall health of waterways through their potential toxicity, carcinogenetic and intense colouring capabilities. In order to remove these dyes from effluents and to ensure adequate environmental protection, there is a real need for the development of an efficient, applicable, inexpensive, and environmentally friendly system of treatment.

The main aim of this project was to develop an environmentally friendly electrochemical technique to not only remove dye, but also to recover dye from dye containing effluents. To fulfil this aim, the conducting polymer, polypyrrole, was employed as an alternative electrode substrate. The unique feature of polypyrrole acting as an anion exchanging membrane can be directly applied to an electrode surface by electropolymerisation. This then encourage the anionic dye of Acid Red 1 to be readily entrapped. The dye could also be easily liberated from the polypyrrole film by applying a reduction potential. In this way, the polypyrrole film was successfully used to entrap (remove) the Acid Red 1 from a laboratory solution, and then liberate (recover) it from the polypyrrole film. In conjunction with spectroscopic techniques including FTIR and XRD, our results have confirmed that Acid Red 1 was entrapped during oxidation of pyrrole to form polypyrrole films and then liberated during reduction of polypyrrole. This entrapment-liberation was found to be reversible. This was then exploited to develop a cost effective treatment method in which the films can be repeatedly used.

Attentively, the film can also be applied as a single use. In addition, based on a two level-factorial design, the entrapment process was found to be dependent on pH, Acid Red 1 concentration in solution and polymerisation time. Moreover, the kinetic study revealed that Acid Red 1 entrapment in polypyrrole films follows a pseudosecond order model involving an intra-particle diffusion. The thermodynamic study also suggested that the Acid Red 1 entrapment in a polypyrrole film is a spontaneous process, endothermic and physical in nature. However, problems such as the mechanical strength of the films and possible irreversible oxidation resulted in films having limited life times. To minimise the limitation of using conducting polypyrrole films as an electrochemical treatment tool for entrapment-liberation cycle of Acid Red 1, it was necessary to improve the mechanical strength of polypyrrole films. In order to improve the stability and entrapment efficiency of polypyrrole films, a combination of polypyrrole and reduced graphene oxide to form a composite film has also been studied. We observed a significantly higher entrapment (95%) and liberation (73%) efficiency of Acid Red 1 in polypyrrole-reduced graphene composite films. Mechanical testing and surface area analysis revealed that enhanced entrapment-liberation efficiency of Acid Red 1 in polypyrrole-composite film is most likely due to the increased mechanical stability and higher surface area of the film. All these factors contributed to the increased life times of the film up to several entrapment-liberation cycles.

Very significantly, some of the advantages in the use of polypyrrole composite films in the treatment of dye containing effluents include the ability to remove and recover the dye from the solution without the formation of toxic dye degradation by-products, the simplicity and inexpensive procedure in fabricating the electrodes, and the ability to easily replace the electrode.

6.2. Limitations

In the present work, a relatively low Acid Red 1 liberation efficiency was achieved mainly because dye molecules can be firmly trapped in the polypyrrole chain network, giving rise to a multiple layered dense sandwich structure. Additionally, unlike small doping anions which can move freely into and out of the polymer film, the bulky Acid Red 1 is less mobile and showed only slow liberation over time. Moreover, over oxidation of polypyrrole film was likely to have occurred during dye entrapment–liberation cycle. During overoxidation, the polypyrrole film would lose their conductivity as well as electrochemical entrapment-liberation performance.

Therefore, in applying a polypyrrole-Acid Red 1 film for anion exchanging, problems concerning the spontaneous or gradual overoxidation of the film and the mobility of Acid Red 1 in and out of the film may be encountered. This will be one of the determining factors that will define the success and application of this polypyrrole electrode as an anion exchanging membrane for the removal of Acid Red 1 from effluents.

6.3 Future directions

A possible direction in this work is the application of the system to much larger vessels by increasing the size of the polypyrrole composite films. This can be achieved by using large stainless steel electrodes for polymerisation of pyrrole in the presence of a dye molecule. A large surface area contained polypyrrole film may be achieved with the use of stainless steel supports that have column or fibular like structure on their surface. In addition, the surface area of the electrode can be increased using highly porous carbon fibre cloth-polymer composite or nanoparticle embedded polymer composite. Carbon fibre cloth is available and inexpensive material, thus can be used on a commercial scale. This direction needs to be considered so that the next step in applying this electrodes to a real-life system may be achieved. The simple entrapment-liberation of azo dye molecules in polypyrrole film may lead to applications where polymerisation is performed in the presence of more than a single dye, enabling the removal of a large proportion of multiple dyes in a dye vat by a single film. Also, studies need to be performed on the large range of possible reagents used in different dying process (*e.g.*, NaCl, Na_2SO_4, NaOH, $NaHCO_3$, Na_2CO_3, NaOCl and H_2O_2), which may act as interfering anions on degradative agents of the films.

Additional improvements to the polypyrrole electrode lifetime may be possible by applying porous coatings such as Nafion, which may increase the mechanical strength and may also act as a coating to inhibit the incorporation of other unwanted anions.

In summary, further studies on the use of these electrodes will need to increase surface area and mechanical strength as well as highly porous polypyrrole film, explore the possibility of employing the films to remove multiple dyes with one film, to explore the effect of other chemicals on the film behaviour, and to increase the mechanical strength of the film via the application of some porous coating.

APPENDIX

Isotherm studies

The equilibrium data obtained for entrapment of Acid Red 1 in polypyrrole films with an initial concentration from 60 to 2000 mg L^{-1} was examined based on the Langmuir and the Freundlich isotherm models. The Langmuir adsorption is based on a monolayer adsorbate coverage on a structurally homogeneous substrate surface with no interaction between–adjacent adsorbate molecules, while the Freundlich isotherm model is an empirical equation employed to describe a heterogeneous surface coverage system and not restricted to the formation of a monolayer. The Langmuir and Freundlich models can be described by Equation 1 and Equation 2, respectively.

$$\frac{1}{q_e} = \frac{1}{x_m b C_e} + \frac{1}{x_m} \qquad \text{Equation 1}$$

$$\log q_e = \log k_f + \frac{1}{n} \log C_e \qquad \text{Equation 2}$$

where x_m (mg g^{-1}) denotes the Langmuir constant related to maximum entrapment capacity, b (L mg^{-1}) the energy of entrapment, C_e (mg L^{-1}) the equilibrium concentration of Acid Red 1, q_e (mg g^{-1}) the equilibrium entrapment of Acid Red 1 in polypyrrole film, n the intensity of entrapment, and k_f (L g^{-1}) the Freundlich constants. From Equation 1, a plot $1/q_e$ *versus* $1/C_e$ will give a straight line. However, using the equilibrium data obtained for entrapment of Acid Red 1 in polypyrrole films, the corresponding plot did not yield a straight line (Figure 1). Similarly, from Equation 2, a linear $\log q_e$ *versus* $\log C_e$ plot is expected but the corresponding experimental plot displayed nonlinearity (Figure 2). The experimental data thus did not obey any of the adsorption model, indicating Acid Red 1 was not adsorbed, but was entrapped in a polypyrrole film. In this way, we expect a higher entrapment of Acid Red 1 possible in a polypyrrole film compared to adsorption methods that required diffusion of a dye towards an adsorbate. This will in turn make the entrapment method in polypyrrole films a more effective

and efficient treatment method compared to those relying on adsorption. Similarly, the entrapment method may also aid in preventing dye leakage from polypyrrole films back to a sample matrix.

Therefore, we are of the view that it is unnecessary to consider other isotherms, such as Temkin, Dubinin-Radushkevich, Redlich-Peterson, Flory-Huggins, Hill, Sips, Toth, Koble-Corrigan models, which are often derived based on the Langmuir isotherm (for homogeneous surface adsorption) and Freundlich isotherm (for heterogeneous surface adsorption).

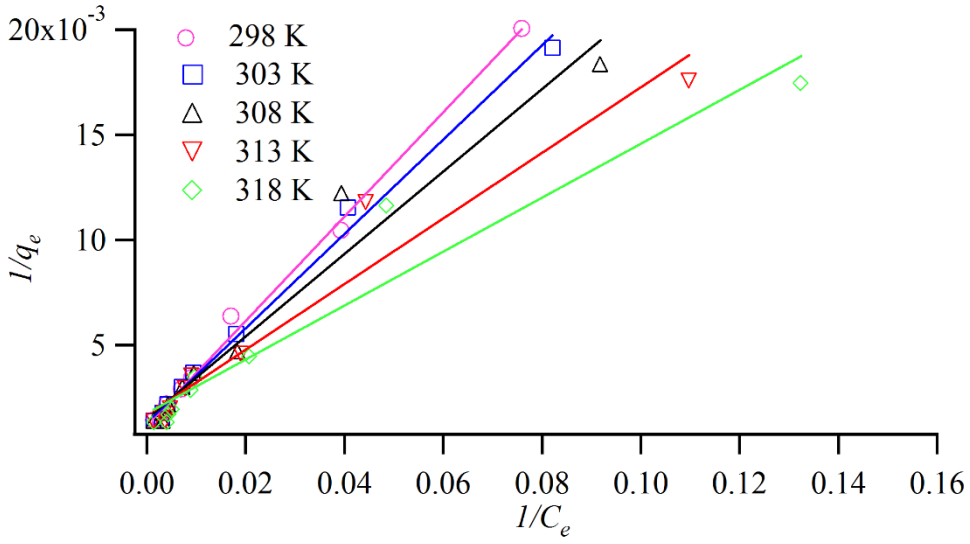

Figure 1 Langmuir isotherm model for entrapment of Acid Red 1 in polypyrrole films.

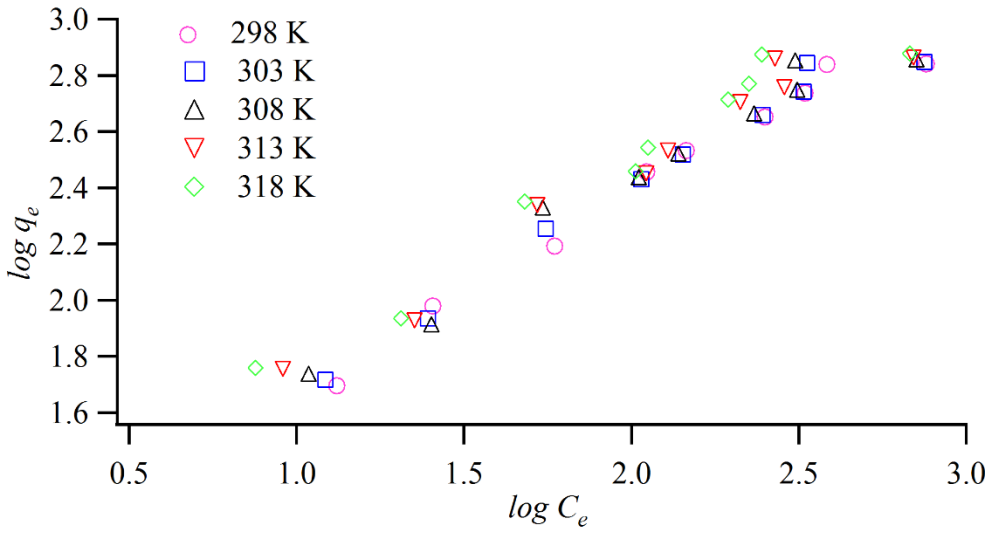

Figure 2 Freundlich isotherm model for entrapment of Acid Red 1 in polypyrrole films.